THE ELECTRON CAPTURE DETECTOR

A thesis submitted for the degree of

DOCTOR OF PHILOSOPHY

by

SURENDRA PUNAMBHAI PATEL

in

THE UNIVERSITY OF ASTON IN BIRMINGHAM

JULY 1976

SUMMARY

Practical problems encountered in the use of the electron capture detector have been investigated. A theoretical model is also proposed for the instrument.

Detector characteristics and operating parameters are discussed and an experimental study investigated their influence on the detector response. The two principal processes occurring within the cell, electron attachment and recombination are also discussed and partly based on the consideration of these processes, a kinetic model is proposed for the ECD. An attempt has been made to verify experimentally some of the assumptions made in the present theory and in other previous models (which have been discussed as well). The experiments included the use of electrostatic probes to determine the positive ion density in the cell, oscilloscope traces of the current pulse and current measurements on the gas outlet to observe the effect of carrier gas flow.

The proposed model has shown an improvement in the prediction of the detector response observed when only pure carrier gas is flowing through the cell. It is further used to determine the electron-ion recombination coefficient for the most likely positive ion (H_3O^+) present when moist helium is used as carrier gas.

PREFACE

This thesis, which is being submitted for the Degree of Doctor of Philosophy in the University of Aston in Birmingham, is an account of the work done under the supervision of Professor F. M. Page, B.A., Ph.D, Sc.D., in the Department of Chemistry of the University of Aston in Birmingham from October 1972 to May 1976. Except where references have been given in the text, the work described herein is original and has not been submitted for any other award.

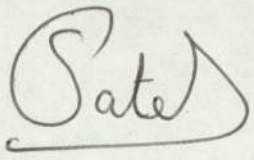

"To climb steep hills
requires a slow pace at first."

Shakespeare, Henry VIII Act I, Sc.I

ACKNOWLEDGEMENTS

I wish to express my gratitude to Professor F. M. Page for his continued guidance and encouragement throughout the course of this work.

Thanks are due to other members of the University of Aston in Birmingham for their helpful discussions and suggestions on particular aspects of the work. I also wish to thank two great friends, Mehmet Konuray and Fikret Ateş, with whom three most enjoyable and rewarding years were shared.

Finally, I am grateful to the University of Zambia, Lusaka, for financial support and to Mrs L. Perkins for typing this thesis.

To my mother
and father

CONTENTS

LIST OF FIGURES

FIG.16

CURRENT AT VARIOUS ELECTRODE SPACINGS (SOURCE ^{63}Ni)

FIG.17

CURRENT-ELECTRODE SEPARATION RELATION FOR d.c. MODE

FIG.18

THE INVERSE OF CURRENT VERSUS ELECTRON TRANSIT TIME

FIG.19

CURRENT-SEPARATION PLOTS FOR He AND Ar + CH_4

FIG.20

CURRENT VARIATION IN AN ASSYMMETRICAL CELL - ANODE FIXED

FIG.21

CURRENT VARIATION IN AN ASSYMMETRICAL CELL - CATHODE FIXED

FIG.22

THE EFFECT OF REVERSAL OF CELL POLARITY - SOURCE ON ANODE

FIG.23

CURRENT VARIATION WITH INTER-ELECTRODE SEPARATION - SOURCE ON ANODE

FIG.24

CURRENT VARIATION WITH GAS PRESSURE (BELOW ATMOSPHERIC)

FIG.25

CURRENT VARIATION WITH GAS PRESSURE (ABOVE ATMOSPHERIC)

FIG.26

CURRENT - CELL LENGTH RELATION AT VARIOUS PRESSURES

FIG.27

PULSE INTERVAL VERSUS PRESSURE CORRESPONDING TO MAXIMUM CURRENT

FIG.28

THE EFFECT OF CARRIER GAS (N_2) FLOW ON CURRENT IN d.c. MODE

FIG.29

CURRENT VARIATION WITH GAS FLOW IN THE PULSED MODE

FIG.30

CURRENT VARIATION WITH GAS (Ar + CH_4)

FIG.31

CURRENT VARIATION WITH GAS FLOW IN A SYSTEM SUSPECTED OF LEAKAGE

FIG.32

THE EFFECT OF CONTAMINANTS ON OBSERVED CURRENT

FIG.33

CURRENT-VOLTAGE PLOTS FOR DIFFERENT/FLOW RATES AT SMALL ELECTRODE SEPARATION

FIG.34

CURRENT-VOLTAGE RELATIONSHIP IN d.c MODE AT HIGH GAS FLOW RATE

FIG.35

VARIATION OF CURRENT WITH VOLTAGE IN d.c. MODE

FIG.36

CURRENT-VOLTAGE RELATIONSHIP AT LOW GAS FLOW RATE

FIG.37

ONSET VOLTAGE FOR SATURATION CURRENT AT DIFFERENT ELECTRODE SPACINGS (d.c. MODE)

FIG.38

ONSET VOLTAGE FOR SATURATION CURRENT UNDER THE PULSED MODE ($Ar + CH_4$)

FIG.39

CURRENT VARIATION WITH PULSE AMPLITUDE AT VARIOUS ELECTRODE SEPARATION

FIG.40

CURRENT-PULSE INTERVAL RELATION FOR VARIOUS GASES

FIG.41

COMPARISION OF RESULTS BETWEEN THEORY AND EXPERIMENT

FIG.42

PREDICTION OF THE PROPOSED MODEL COMPARED WITH EXPERIMENTAL DATA FOR ARGON

FIG.43

SATURATOR USED FOR INTRODUCING SAMPLE IN CARRIER GAS

FIG.44

CURRENT VARIATION WITH PULSE INTERVAL FOR HELIUM AND HELIUM + UF_6

FIG.45

Ne - PULSE INTERVAL RELATION FOR HELIUM AND He + UF_6

FIG.46

VARIATION OF Ne WITH GAS FLOW RATE THROUGH SATURATOR CONTAINING UF_6

FIG.47

Ne - PULSE INTERVAL RELATION FOR HELIUM AND He + H_2O

LIST OF TABLES

LIST OF FIGURES

Symbol	Representation
$\bar{a}$	Radius of sheath around an electrostatic probe.
A	Area.
C_o	Concentration of contaminant.
d	Distance.
D_a	Ambipolar diffusion coefficient.
e	Electron concentration; electronic charge.
E_a	Electron Affinity
F	Gas flow rate
G	Ion-pairs formed by a β^- particle.
I	Current.
k, K	Boltzmann constant.
k_1 A	Rate of production of electrons.
k_2	Electron-ion recombination rate coefficient.
k_3	Electron capture rate coefficient.
k_4	Ion-ion recombination rate coefficient.
ℓ	Length of cell.
m	Concentration of sample molecules.
n	Negative ion concentration.
N_e	Number of electrons per pulse.
p	Positive ion concentration
P	Gas pressure
r_p	Probe radius
R	'Gaines' factor.
s	Field free interval between pulses.
t	Time
t_p	Pulse interval
T	Temperature

V	Applied potential; Volume.
V_a	Ambipolar speed.
w	Pulse width.
X	Electric field strength.
λ	Debye length
ν_x	Drift velocity of species x.

The conductivity of gases in an ionisation chamber is exquisitely sensitive to small changes in gas composition. Several detectors, based on this observation, have been constructed for use in gas chromatographic systems. The recent emphasis on analysis of environmental pollutants present in trace amounts has brought one of these detectors, namely, the electron capture detector (ECD), to the forefront.

The ECD, since its inception in 1960 by Lovelock and Lipsky[1] has been extensively used in investigations of biological, physical and chemical importance. Its contribution to topics of scientific interest can be chiefly attributed to its extreme sensitivity, and the ease with which it can be operated. Its design is also relatively simple and has only been slightly modified since it was originally devised. The ECD still is a two-electrode ion chamber with an internal radiation source.

Physiochemical aspects of free electron reactions have been studied with the aid of the ECD. The toxicity or biological activity of compounds such as dinitrophenol and thyroid hormones has been suggested[2] to be due to their ability to function as irreversible electron traps. Carcinogenic activity of compounds such as polycyclic aromatic hydrocarbons, halogenated aliphatic hydrocarbons, azo dyes and quinolinol N- oxides has been loosely linked[3] to the ability of these compounds to extract electrons from their normal path in a living cell.

Characteristic 'spectra' based on the measurement of cross-section for electron attachment at different electron energies have been obtained[4] by applying radio-frequency potentials to the ECD.

Dissociative electron capture or attachment has also been the subject of many investigations in which the ECD has played a

paramount role. Studies[5] have attempted to distinguish between two mechanisms by which attachment of thermal electrons to aliphatic and aromatic halogen compounds proceeds :

a) electron attachment to a thermally excited molecule followed by direct dissociation into a halide ion and a radical

$$AB^{*} + e^{-} \longrightarrow A^{-} + B^{\bullet}$$

b) electron attachment to form a stable negative ion of the molecule which in turn becomes thermally activated to undergo dissociation into the halide ion and a radical

$$AB + e^{-} \longrightarrow (AB^{-})^{*} \longrightarrow A^{-} + B^{\bullet}$$

The electron capture detector has been most widely used however, for analytical purposes. It has provided reliable results in analysis of pesticide traces in materials of biological origin. This is but one example of its use in this field; others are its use in the determination of a vast array of suitably derivatised biochemicals and drugs, chelated metals, meteorological tracers, air pollutants and lead alkyls. The literature, consequently is voluminous. An extensively comprehensive review on the application of the ECD to various fields, but primarily concerned with its function under various analytical circumstances, has been published by R. V. Smith[6].

It is the detector's use as an analytical tool that has attracted attention and aroused controversy. Aue and Kapila[7] point out that entirely due to the ECD, terms such as polychlorinated biphenyls' have ascended to household prominence and it is partly responsible for the discontinued use of DDT in countries around the world.

The instrument's controversial nature arises largely from a lack of understanding of its mode of action. This becomes

apparent from the difficulties and problems faced by GC operators : the ECD is or is not disturbed by water; its standing current is or is not dependent on either gas flow rate or temperature; it is or it is not a mass-sensing device. Negative excursions below the baseline after the emergence of a peak and shifting baseline are phenomena experienced regularly.

Besides these practical problems there exists theoretical deficiencies. Models, explaining numerically the signals it generates, are often inadequate for various reasons outlined later in this work when they are more fully discussed. The ECD's response is a complicated function arising from the interaction of several physiochemical parameters. This has made the task of predicting the signals it generates difficult.

A programme of fundamental study has therefore been undertaken to resolve some of the practical problems faced and a theoretical model is proposed for the ECD. The model makes use of carrier gas parameters, such as positive ion mobilities and electron-ion recombination coefficients (which have been well established by other techniques) to calculate empirical factors introduced in the theory.

CHAPTER TWO - DETECTOR AND OPERATION CHARACTERISTICS

2.1 DETECTOR CLASSIFICATION

A gas chromatographic detector senses the variation in the amount of sample passing through it. The response can be classified as concentration dependent, mass flow-rate dependent, or as a mixed function. The concentration detector produces a signal that is proportional to the amount of solute per unit volume of carrier gas passing through the cell. A mass flow-rate detector gives a signal that is proportional to the amount of solute passing through it in unit time, but is independent of the volume of carrier gas required for elution. The flame ionisation detector is an example of this latter class while the electron capture detector has been classified as a concentration detector for certain classes of compounds.

Qualitative gas chromatographic analysis involves separation of the sample into its constituents. Quantitative evaluation of the resulting chromatogram consists of determining the absolute or relative quantities of individual components. This necessitates the determination of peak areas, ie. integration of the detector signal with time. With detectors of the first category, the signal is proportional to the sample concentration, C, in the carrier gas. The peak area, A is expressed as

$$A = q \int C \, dt = q \int \frac{f_1}{f_1 + f_2} \, dt \qquad [1]$$

where q is a constant of proportionality and f_1 and f_2 are the flow-rates (moles per second) of the sample and the carrier gas respectively. A proportionality between peak area, A, and the quantity of the sample holds true only for constant flow-rate $(f_1 + f_2)$, as can be seen from Equn. [2].

$$A = \frac{q}{f_1 + f_2} \int f_1 \, dt \qquad [2]$$

at a given temperature and pressure.

The signal produced by detectors of category two is proportional to the mass flow-rate of the sample. In this case, the peak area is proportional to the size of the component, even if the flow-rate of the gas mixture, $(f_1 + f_2)$, changes during the measurement.

Fluctuations in the carrier gas flow-rate give erroneous results for the concentration-sensitive detectors. Halász[8] has pointed out that this adverse effect can be minimised by the addition of a scavenger gas though at the expense of some loss in sensitivity.

2.2 CELL CONFIGURATIONS

The ECD is basically a two-electrode chamber through which gas can flow and which contains a source of ionising radiation. There are three principal forms in use today and these are illustrated in Fig.(1) Early ECD's were generally converted argon ionisation detectors operated at low applied potentials. Such detectors have coaxial geometry with the anode located along the axis of the cell and surrounded by a cylindrical cathode to which is attached the radioactive source. In the plane parallel configuration, the anode and the cathode are arranged parallel to one another at the end of an electrically insulated chamber. In the concentric cylinder ECD[9], the cathode houses the radioactive foil but the anode is removed and isolated by a Kovar glass union. The third version is really only useful when a continuous d.c. voltage is applied across the electrodes.

These detectors function satisfactorily if due attention is paid to the peculiarities of each, and care is taken to optimise

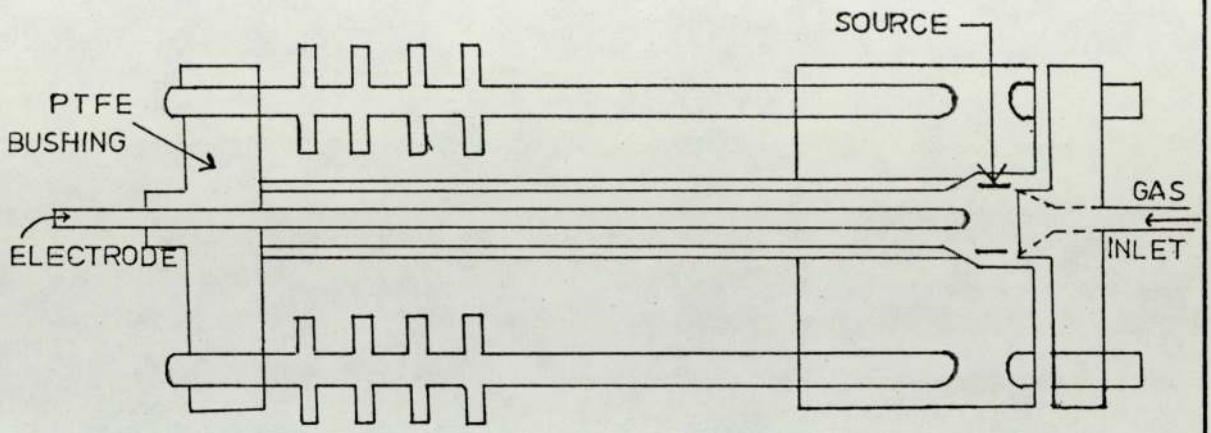

COAXIAL ECD

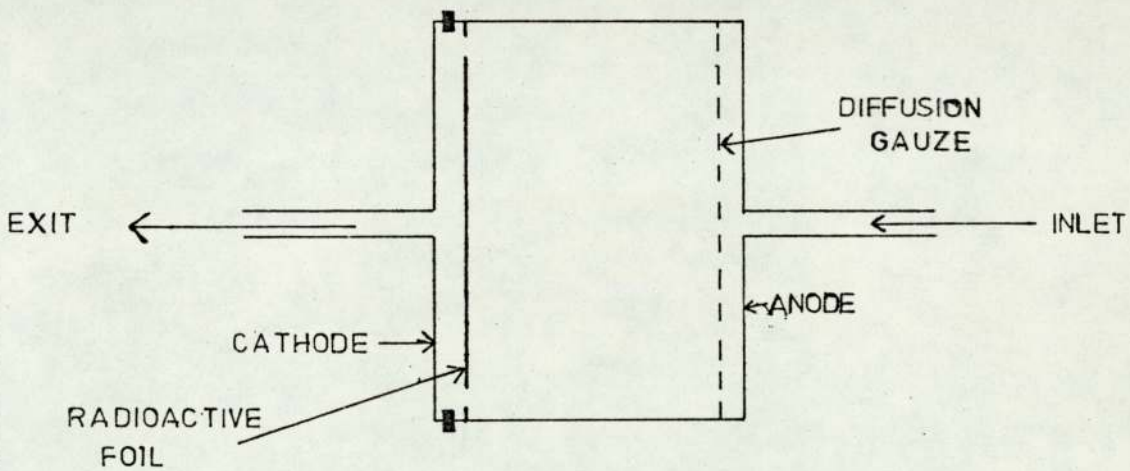

PLANE PARALLEL ECD

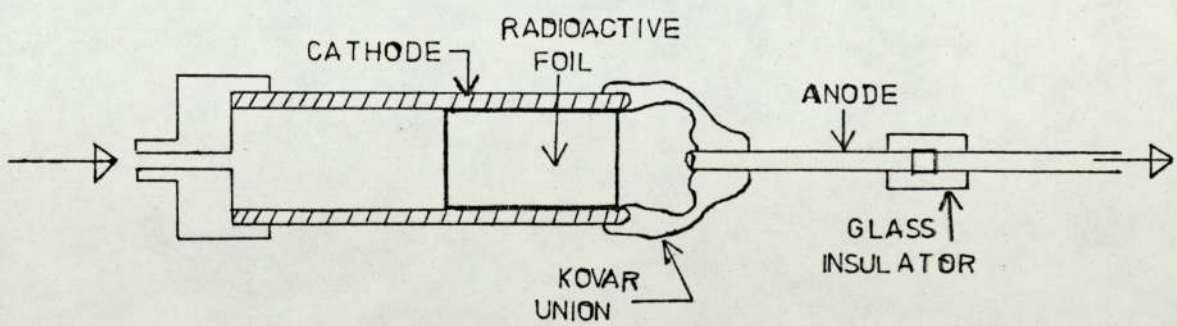

CONCENTRIC CYLINDER ECD

FIG. 1

ELECTRON CAPTURE CELL CONFIGURATIONS

the operating parameters. A comparison between these geometrical types has been reported[10] but they are difficult to evaluate because a large number of experimental variables affect their overall performance. In the design of a practical detector, the dimensions are certainly more important and these are considered in the experimental section where a plane parallel cell used in the present studies is fully described.

2.3 BASIC PRINCIPLES OF OPERATION

At normal temperatures and pressures a gas behaves as a perfect insulator; if however, electrically charged atoms, molecules or free electrons are present, their motion in the direction of an electrical field renders the gas conducting. The radio-active source emits energetic β^- particles which undergo ionising collisions with carrier gas molecules. The application of a voltage across the two electrodes creates a potential difference, allowing the collection of charged species present in the cell. The resulting current is measured on an electrometer connected in series with the ECD.

At atmospheric pressure, the principal process causing the loss of ions at low field strengths is the recombination of negative and positive ions to regenerate neutral molecules. The probability of recombination between a free electron and a positive molecular ion is between 10^5 and 10^8 less than between oppositely charged molecular ions. The formation of negative ions through electron capture results in a rapid disappearance of charged species in the cell at low applied fields. Consequently, the presence of an electron capturing gas or vapour reduces the observed signal of the ECD corresponding to a decrease in the standing current (ie. current when only

pure carrier gas is flowing).

2.4 SPACE CHARGE DEVELOPMENT

The current-voltage relationship of a gas filled insulated vessel containing two plane parallel electrodes is well established[11]; as the voltage increases the current tends towards a constant level, the saturation current, corresponding to the collection of all ions and electrons generated within the chamber (Fig. 2). At higher voltages the current increases again and tends to infinity at some finite applied potential. This is because the electrons originally formed by irradiation (or by any other ionising source) in the gas, gain energy from the field and reach velocities which enable them to ionise gas molecules. The length of the saturation current plateau depends upon the nature of the gas and on the density of ionisation. Practical ionisation detectors need to be operated at some voltage in the plateau region so as to provide a current directly related to the concentration of the sample present.

J. E. Lovelock[12] has pointed out that in an ion chamber where the applied potential is low and ion density is high, the current flow is strongly affected by the development of space charges. The situation is similar to one that exists in gas filled electronic diodes[13]. So many electrons are emitted from the thermionic cathode that only a fraction of them are collected by the anode at the working potential. The remainder form a 'cloud' of negative charges, known as a 'space charge', near the cathode. In the ECD, the positive ion concentration may be several thousand times greater than the free electron concentration. This is simply due to the fact that the free electrons are collected very soon after their formation whereas the positive ions with their lower drift velocity

FIG. 2

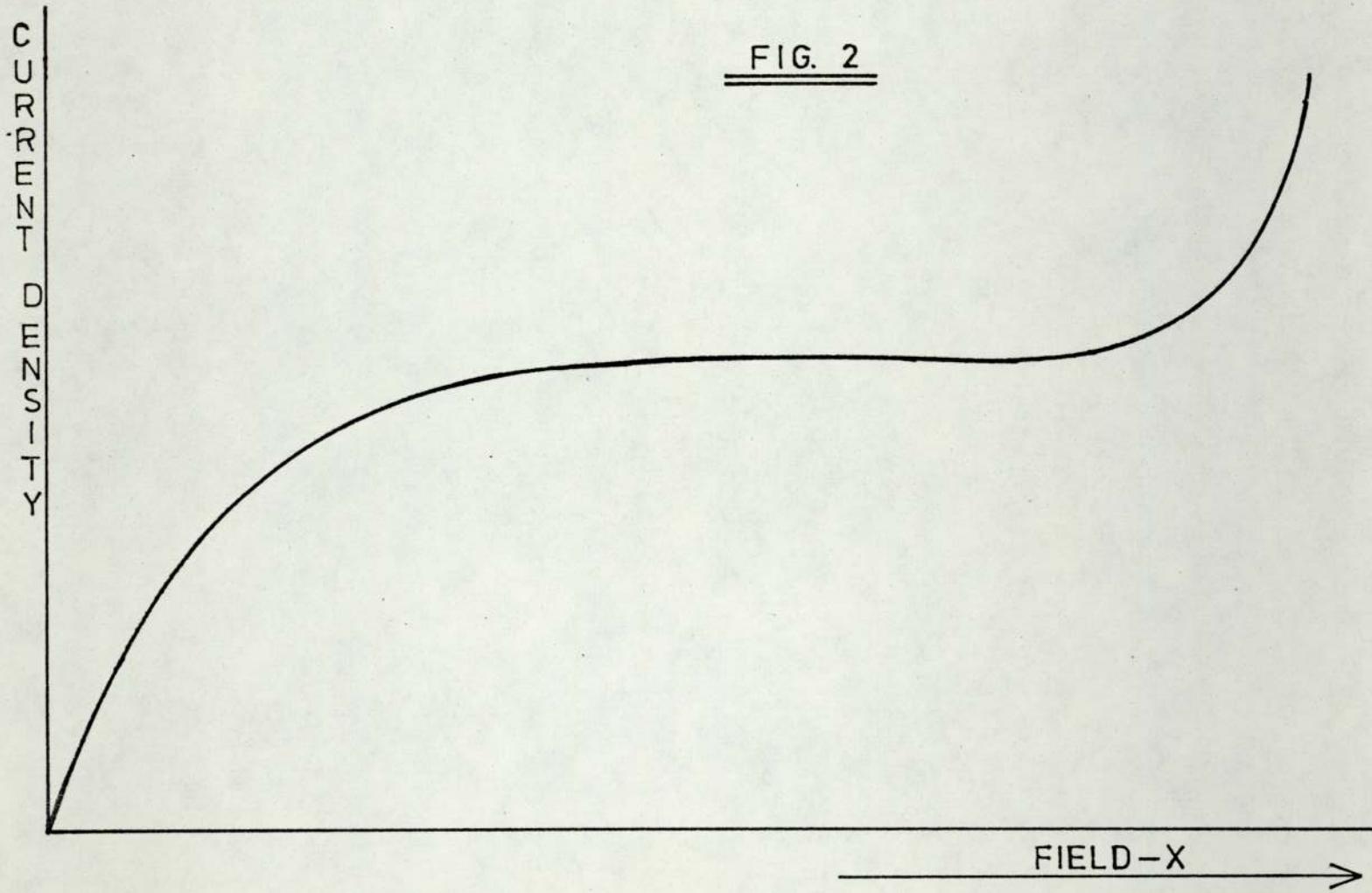

RELATION BETWEEN CURRENT DENSITY, j, AND FIELD X IN A GAP WITH PLANE ELECTRODES

move only slowly to the cathode and accumulate there as a space-charge cloud. In general, electrons have a mobility a thousand times greater than the positive ions in their own gas. For a plane parallel geometry chamber, Sharpe's[14] equation derived for space charge limitation is

$$N = \frac{k^- V^2}{\pi d^4} \qquad [3]$$

where N is the rate of ion production; k^-, is the electron mobility; V, is the applied potential and d is the electrode separation. N is that at which the space charge reduces the field at the anode to zero. The equation suggests that the extent of space charge limitation is reduced by using small chamber dimensions and a high potential.

2.5 PRODUCTION OF THERMAL ELECTRONS

Secondary electron production in the cell occurs through inelastic and elastic collisions between the primary electrons, ie. the β^- particles and molecules of the carrier gas. Beta-particles released from a ^3H source have a maximum energy of 17.6 - 18.9 keV, while those from ^{63}Ni are about 67 keV[15]. However, these particles rapidly lose their energy in ionising collisions until their energy is less than that necessary for formation of an ion pair. Approximately 36 eV are expended in forming a nitrogen ion pair, while 28 eV are necessary in argon-methane[15]. The electrons produced by the β's will initially have an energy in excess of thermal energies but they rapidly lose energy in collisions until their average energy is thermal (about 0.03 eV). With nitrogen as carrier gas, the reactions are as follows :

$$\beta^- + N_2 \longrightarrow N_2^+ + e^- + e^*$$

$$N_2^+ + N_2 \longrightarrow N_4^+$$

In pure argon, only elastic collisions can take place once the energy is below the excitation level of argon. However, if argon containing a quench gas (eg. methane) is employed, then the energetic electrons produced are thermalised during collision with the quench gas. The decay of argon metastables via the quench gas is also facilitated. The reactions can be stated as follows:

$$\beta^- + Ar^o \longrightarrow Ar^{\pm} + e^- + e^*$$

$$Ar^{\circ} + e^- \xrightarrow[\text{potential}]{\text{Applied}} (Ar^-)^* \quad (11.6\ eV)$$

$$(Ar^-)^* + CH_4 \longrightarrow Ar^o + e^- + CH_4 \pm \text{energy}.$$

Possible modes for the loss of energy in the presence of methane are through excitation of low-level vibrational and rotational states of the gas. Thus, a reduction in temperature and deceleration of the fast electrons results.

An estimation of thermalisation times has been made by Warman and Sauer[17]. They demonstrated that thermalisation of electrons occurred in fractions of a microsecond when n-hexane is used with monatomic or diatomic gases; in the absence of a quench gas, the electrons were not completely thermalised even after 50 ms. Wentworth et al.,[18] estimated that an electron with an energy of 10 keV is cooled to 10% above thermal energies in 0.076 μs. As the energy of activation or electron affinity for a solute molecule may be 0 - 4 eV, it is apparent that the thermalisation of electrons occurring from highly energetic β^- particles is necessary in order to allow or enhance the capturing process while minimising solute ionisation.

2.6 MODES OF OPERATION

The ECD has basically three modes of operation :

a) d.c. continuous mode

b) pulsed mode

c) constant current mode.

In the first mode, a constant potential is applied and this produces a migration of charged species towards electrodes of opposite polarity[19]. As a result, a composite current of electrons and ions results, rather than a pure electron current. Detector configuration and the species to be measured determine the choice of the d.c. potential as well as carrier gas composition and detector contamination[20]. This requires an initial determination of the detector output current versus voltage for a set of analytical conditions.

There are some inherent errors in this mode of operation. Application of a direct potential prevents the electrons from reaching thermal equilibrium with the carrier gas molecules and therefore decreases the probability for capture. The problem is acute in the noble gases and to a lesser extent in nitrogen, since the energy gained by the electrons from the applied field is not easily lost during their elastic collisions with the gas molecules[12]. Besides the electron energy, the probability of electron absorption depends also on the half-life of the electron in the cell. Changes in this quantity leads to a non-linear response to varying sample concentration[12].

The space charge of positive ions in the vicinity of the cathode sets up a potential in opposition to that applied to the ECD and it may hinder the collection of free electrons. The presence of a polyatomic vapour in the cell changes the electron mobility and as a result, the extent of the space charge cloud and the observed current.

The temporary absorption of a trace of an eluted component upon one of the electrode surfaces can give rise to a contact potential which may either enhance or oppose the applied potential.

Lovelock[12] has pointed out that where the contact potential opposes the applied potential, the chromatogram peak has an erroneously large area and frequently shows severe tailing; where the potential enhances that applied to the detector, there is a diminished response and the peak may show a drift below the base line at the tailing edge. There is also the additional effect of reducing the number of Beta particles emitted if the absorption has occurred on the electrode with the radiation source.

In the d.c. mode, the ECD could respond to other parameters of the sample introduced in the carrier gas stream besides electron attachment[12]: ionisation cross-section, electron mobility and metastable atom ionisation processes ("argon" detection). The extent to which these other detection processes predominate in the d.c. mode, depends upon the gas composition in the cell, the intensity of the radiation source, the geometry of the detector and the magnitude of the applied potential.

When the ECD is responding as an argon or as a cross-section detector, in addition to its function by electron absorption, peaks below the base-line have appeared together with a reduction in peak height.

It is difficult to avoid these and other possible sources of error inherent in the d.c. mode. There are however, alternative methods in which electron absorption takes precedence over the other detection methods outlined and anomalous effects of space charge limitation, contact potentials and changes in electron energy can be avoided.

In the pulse mode of operation, square wave voltage pulses (Fig. 3) are applied across the electrodes for a very short time - 1 to 5 μ s depending on the carrier gas and the geometry of the cell. The pulse amplitude (V) and width (W) is sufficient to

FIG. 3

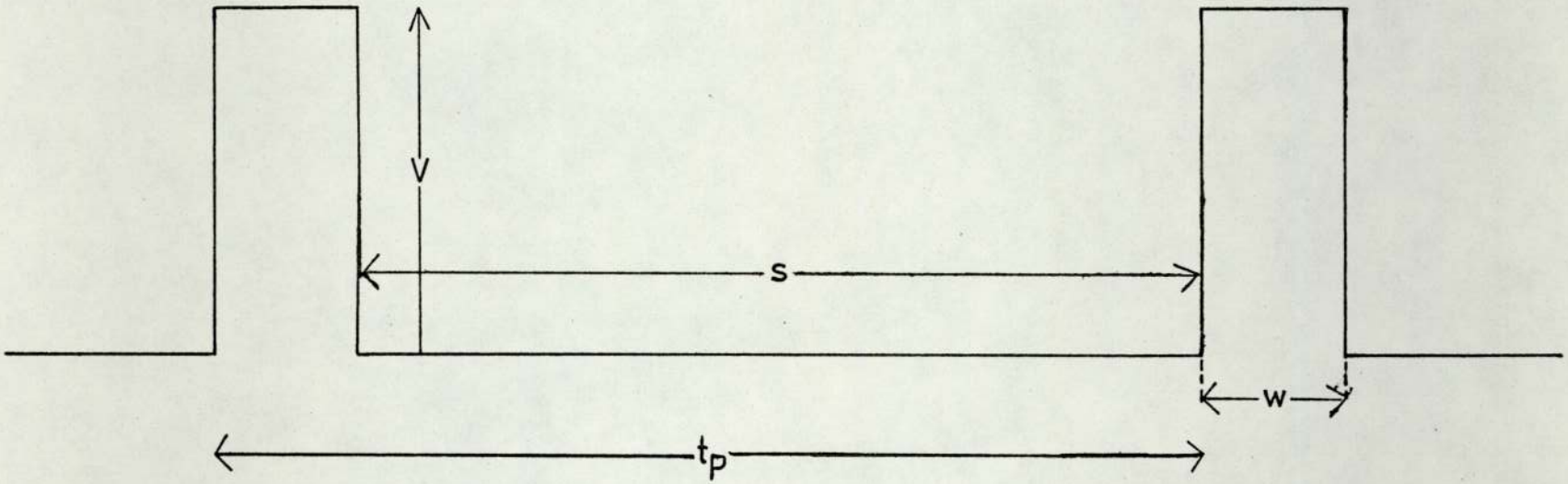

APPLIED PULSE CHARACTERISTICS

collect all electrons and it is generally stated that the contribution of ions to the current is negligible. When the applied potential is zero, ie. during the pulse interval (s), the electrons in the cell are in thermal equilibrium and there is no drift of charged species in either direction; consequently, space charge effects are minimised. It is also generally[12] believed that with the pulse sampling technique, contact potential effects are rarely encountered as the pulse amplitude (about 50 Volts) is sufficiently large to counteract the contact potential and yet collect all electrons present in the cell. With argon + methane as carrier gas and the cell operated in the pulse mode, the detector cannot function either as an argon detector or an electron mobility detector, as the electron energy is maintained at a constant thermal level. Hence, many anomalous responses are avoided and the highest sensitivity and stability is usually obtained by operating in this mode.

The third mode of operation is where the detector current is held constant while the frequency of the applied pulses is varied.[21] Briefly, a reference current, I_r, is compared with the average current, I_D, and the applied pulsed frequency, maintains via feedback the relationship $(I_D - I_r) = 0$

As I_D begins to decrease due to an electron capturing species entering the detector a ΔI is produced. The magnitude of ΔI is amplified and the amplifier output voltage proportionally changes the applied pulse frequency so as to maintain the above relationship.

Thus, the magnitude of change in pulse frequency becomes a measure of the concentration of the electron capturing vapour. The linear dynamic range has been reported[21] to be 5×10^4 for a 10 mCi ^{63}Ni detector operated in this mode.

Some of the notions generally accepted regarding the ECD's operation are illfounded; these will be discussed in the experimental

section. It is to be noted here that they relate to the possible effects of the space charge and the interpretation of the observed current in various modes of operation.

CHAPTER THREE - THEORY

3.1 ELECTRON ATTACHMENT

When an "electron capturing" solute enters the detector, a large number of low-energy free electrons are available, providing an ideal environment for electron attachment. The solute molecule may attach an electron to form either a negative molecular ion,

$$e^- + AB \longrightarrow AB^- + \text{energy}$$

or a neutral radical and a negative ion

$$e^- + AB \longrightarrow A^{\cdot} + B^- \pm \text{energy}$$

The collisions in which electrons attach to atoms to form stable negative ions involve a release of energy, since a stable negative ion has an energy somewhat below that of its parent atom and free electron. The binding energy of the extra electron is known as the electron affinity, EA. In the case of a molecular negative ion its 'adiabatic electron affinity' is defined as the difference between the electronic energies of the molecule and the negative ion state and thus different from the vertical attachment energy[22].

Only for a few organic compounds has the electron affinity been measured. Thermodynamic techniques are more suited to investigations of molecular electron affinities than other techniques such as photodetachment and electron impact thresholds. In the magnetron device[23], a very pure metal filament is surrounded by two grids and a cylindrical anode. A magnetic field is applied parallel to the filament. The first grid is held several hundred volts positive to the filament to minimise space charge current limitation. The second grid suppresses secondary emission from the anode. The total electron-plus-negative ion current is measured in the absence of the

magnetic field and the negative ion current is measured on its own when the field is applied. From a measurement of the temperature dependence of the relative abundances of electrons and negative ions, the electron affinity is calculated using Boltzmann statistics.

Electron affinities, measured with the aid of the ECD, have been reported for several aromatic compounds[18, 24, 25]. They are presented in Table One; their derivation is based on the kinetic theory developed by Wentworth and his co-workers[18]. The theory is discussed in section (3.3). The electron affinities need to be used with caution as most of them have not been confirmed by other techniques; in cases where they have been measured by other methods, a serious discrepancy exists. For example, Page and Goode[26] measured EA for azulene by the magnetron technique and found it to be 2.66 eV.

It has been shown[27] that the problem of negative ion stability can only be approached by using the nuclear kinetic operator. For stability of a negative ion, the wave function must contain at least as many molecular spin orbitals of given spin symmetry as does that of the neutral molecule.

TABLE ONE

ELECTRON AFFINITIES FOR SELECTED AROMATIC COMPOUNDS

COMPOUND	ELECTRON AFFINITY (eV)
Naphthalene	0.152
Triphenylene	0.284
Phenanthrene	0.308
Anthracene	0.552
Pyrene	0.579
Azulene	0.587
Nitrobenzene	0.850
Chlorobenzene	0.860
O-Chlorotoluene	1.100
m-Dinitrobenzene	1.430

There is also an additional factor affecting the existence of stable molecular negative ions. The lowest stable state of a given system of nuclei and electrons must always posses a certain geometrical configuration. Should the addition of a single electron to a system imply a change in the geometrical configuration, then it is difficult, if not impossible, to form the negative ion by collisions of the molecule with electrons[28]. When the formation of a negative ion requires deformation, a significant 'activation energy' of attachment may arise, even though the adiabatic electron affinity is positive (ie. stable negative ion).

The molecular attachment process, yielding the negative ion of the parent molecule, can only proceed via an excited state, since it is a resonance process and the molecule has a real electron affinity. The excited state, which may be purely vibrational, may either be deactivated collisionally (three-body attachment) or pass radiatively to the ground state. A third possibility is that the negative ion exists for periods of the order of a few microseconds, detaching spontaneously after this time.

The rate of formation of stable AB^- by electron capture followed by collision stabilization is proportional to the pressure at low pressures but, owing to saturation, becomes independent of it at higher pressures. Massey[29] showed that the total probability, ρ', of the ion being stabilised by collision before it breaks up is

$$\rho = \int_0^\infty \exp\left\{-t\left(\frac{1}{\tau} + \frac{1}{\theta}\right)\right\} dt/\tau$$

$$= \theta / (\theta + \tau)$$

$$\rho = P/(P + P')$$

where P is the gas pressure and P' a critical pressure for which $\theta = \tau$. The average time taken for a vibrationally excited ion

$(AB^-)^*$ to lose its excess energy through collision with a gas molecule is τ ; the time before spontaneous dissociation occurs is θ. The above equation suggests that if P is large enough then ρ becomes independent of it.

Dissociative attachment proceeds by resonance capture of an electron by the molecule AB, into an antibonding quasi-stationary state AB^-. There is then competition between dissociation and the autodetachment process $AB^- \longrightarrow AB + e$. Fig. (4) illustrates the potential energy curves for both the dissociative and non-dissociative capture processes. In all three cases (a), (b) and (c) curve I is the potential energy curve of the initial state of the neutral molecule AB while the second curve in each case represents that for the state of the negative molecular ion into which the electron is captured. Briefly, the three possibilities are:

Case (a)

Electrons with energies between E_1 and E_2 are captured and molecular dissociation results, giving atoms A and ions B^- with kinetic energies lying between E_3 and E_4.

Case (b)

Electrons with energies between E_1 and E_3 are captured and lead to molecular dissociation while electrons with energies between E_2 and E_3 give rise to a vibrationally excited molecular ion $(AB^-)^*$.

Case (c)

Electrons with energies of about E_6 are captured giving rise to an excited molecular ion which at higher pressures is stabilised.

Negative ions formed by the capture of very slow electrons (with thermal energy) will normally be molecular ions AB^- formed as described above. The reverse process, ie. detachment proceeds through collisions with gas molecules

$$AB^- + X \longrightarrow AB + X + e^-$$

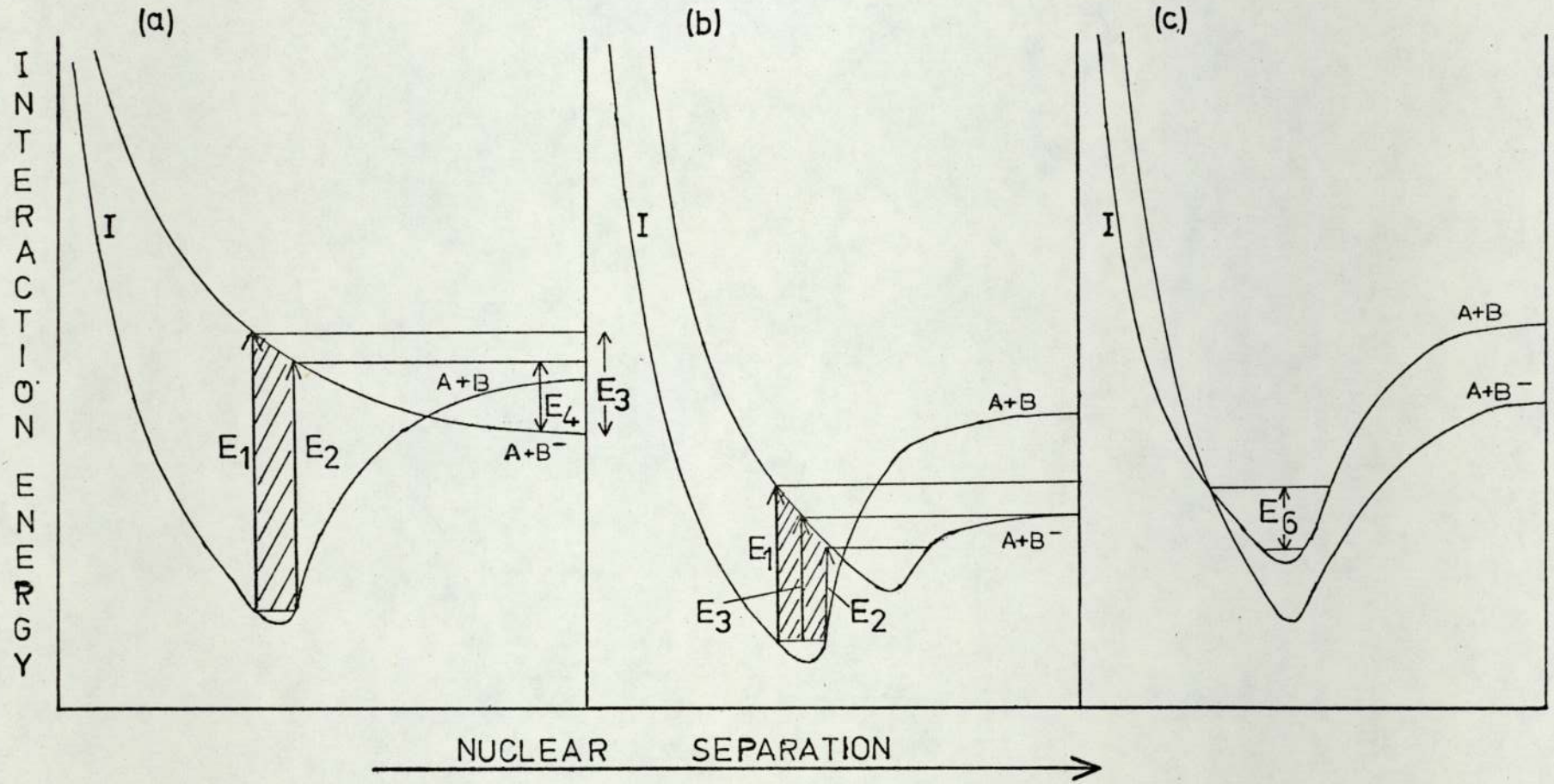

FIG. 4

POTENTIAL ENERGY CURVES ILLUSTRATING 3 POSSIBLE WAYS IN WHICH NEGATIVE IONS MAY BE FORMED BY ELECTRON CAPTURE

and the energy required to detach the electron is obtained by transfer from kinetic energy of relative motion[30]. At ordinary temperatures, T, the fraction of gas molecules possessing sufficient translational energy will be small, unless the electron affinity of X is comparable with 3/2 kT or the electric field accelerating the ions is large enough for them to acquire that energy.

The electron affinity for a parent molecule which forms a stable negative ion will determine the overall parent ion stability but not necessarily its "electron attachment capacity". The probability of electron attachment can be interpreted in terms of the capture cross-section. For dissociative capturing molecules, the process may occur with a high capture cross-section and with almost zero energy electrons if the molecules contain electrophores whose electron affinity exceeds the bond dissociation energy[31]. This suggests that an absolute measurement of the electron attachment capacity of a sample molecule is its capture cross-section and not its electron affinity. Hence, the probability of electron attachment is related to electron affinity, energy of activation, cross-section for collision and consideration of bond stability versus dissociation into stable ions. The electron capture coefficient, K, is the net result of all these processes.

Burdett[32] concluded that the response of the ECD does not vary directly with the electron affinity of the molecules which are introduced in the gas stream but rather with their electron capture cross-section. As indicated above, this depends on the nature of the molecules besides the energy of the attaching electrons. Hence, it is necessary to investigate the relationship of molecular structure to sensitivity in electron capture detection.

It is generally recognised by investigators who employ electron attachment techniques that only relatively few organic compounds

readily accommodate thermal electrons. The probability of electron attachment for different solute species, as shown in Table 2, cover a wide range of at least a million fold.[19,33] The relative attachment coefficient, K', for thermal electrons by compounds is generally made with respect to chlorobenzene, which is assigned a value of one.

For halogen-containing compounds, the magnitude of K' is inversely related to electronegativity and bonding energy. A decrease in K' is observed for the series I > Br > Cl > F.

Studies have been made on the relative contribution of chloro, nitro and amino substituents and their influence through aromatic ring substitution on overall sensitivity[34]. Observations can be rationalised on the basis of increased or diminished electron density in the aromatic ring via resonance and the electron-withdrawing and releasing character of the function groups.

Examples of good electron capturing compounds are alkyl di- and trisulphides and organometallics. In alkyl-lead compounds, some correlation exists between increasing alkyl chain length (possibly electron-releasing effect of ethyl) and overall sensitivity.

Predicting coefficients for attachment becomes more complicated as the complexity of the molecule increases. In general, knowledge of the structure of negative ions formed is seriously lacking, making it difficult to predict the effect of functional groups when present in large molecules.

3.2. RECOMBINATION PROCESSES

In the d.c. mode, at low applied potentials, the major process causing the loss of ions and electrons is recombination. It also occurs in the pulsed mode at long pulse interval. Hence, an understanding of the recombination phenomenon is necessary if a kinetic study of the processes taking place in the ECD is to be

TABLE TWO

RELATIVE ATTACHMENT COEFFICIENTS FOR VARIOUS COMPOUNDS

CHEMICAL CLASSES	K^1	SELECTED EXAMPLES
Alkanes, alkenes, alkynes, aliphatic ethers, esters.	0.01	Hexane Benzene Cholesterol Naphthalene
	0.10	
Aliphatic alcohols, ketones, aldehydes, amines, nitriles		Vinyl chloride Chlorobenzene
	1.0	
Barbiturates, thalidomide, alkyl-leads	300	
Pesticides, dibromo and trichloro compounds	1000	
Polychloro, quinones, dinitro compounds	10,000	

undertaken.

When an electron and a positive ion recombine, energy must be released in some form. The different mechanisms for carrying off this surplus energy give rise to the possible processes of recombination. They may be summarised as follows:

a) Radiative recombination

$$A^+ + e^- \longrightarrow A + h\nu$$

b) Dielectronic recombination

$$A^+ + e^- \longrightarrow A''$$

$$A'' \longrightarrow A' + h\nu$$

or $$A'' + B \longrightarrow A' + B + \text{kinetic energy.}$$

Here, the surplus energy is given to a second electron in the positive ion so that a doubly excited atom or molecule is formed. It may then be stabilised by emission of radiation or by collision.

c) Dissociative recombination

$$AB^+ + e^- \longrightarrow A' + B'$$

d) Three-body recombination

$$A^+ + e^- + B \longrightarrow A' + B + \text{kinetic energy.}$$

At high neutral gas pressures, the latter process is certainly the most important for removing surplus energy. The process is amenable to classical treatment; in the original analysis by Thomson[35], recombination took place if a collision with a third body is suffered by either ion or electron when its distance, d, from the third body is $d \leqslant \frac{2e^2}{3kT}$

where e is the electronic charge; k, the Boltzmann constant, and T is the temperature.

This assumption leads to the following expression for the recombination coefficient, α_T, in terms of the electron momentum

transfer cross-section σ_d :

$$\alpha_T = \frac{64\,(3\pi^2)^{1/2}}{81} \quad \frac{e^2\,Me\,\sigma_d\,No}{Mo(kT)^{5/2}}$$

where the subscript zero refers to the neutral species and No is Loschmidt's number.

Besides 'volume' electron-ion recombination, there is the possibility of losing charged particles through recombination at the walls of the cell. The electrons, which travel the fastest, tend to diffuse outwards and stick to the cell walls, where they remain until neutralised by an incident positive ion. In the steady state, the number of electrons crossing unit area in unit time at any point is equal to the number of ions and the 'ambipolar speed', V_a , is given by

$$Va = - Da \frac{1}{N} \frac{dN}{dx}$$

where N is the charge density and Da is the ambipolar diffusion coefficient. It is normally expressed in terms of the diffusion and mobility coefficients (D and k respectively) of the charged particles:

$$Da = \frac{D+\,k-\, + D-\,k+}{(k+\, + \,k-)}$$

Operation of the ECD in the pulse mode minimises wall recombination as a result of ambipolar diffusion, since the applied field lasts a very short time only. Loeb[36] has pointed out that in a time of 10^{-5} second, the amount of diffusion is negligible.

Collisions between a positive ion A^+ and a negative ion B^-, which can lead to neutralisation of charge may be summarised as follows:

a) two body process,

$A^+ + B^- \longrightarrow A + B$ in which the excess energy is distributed as kinetic energy among the collision products.

b) three body process,

$A^+ + B^- + C \longrightarrow A + B + C$ where excess internal energy is removed by another atom or molecule.

Thomson's[35] three body recombination theory has proved very successful for gas pressures less than 10^3 torr. The recombination coefficient, α_T, in terms of the masses of the two ions, M1 and M2 is expressed by

$$\alpha_T = \frac{8\,(3\pi^2)^{1/2}}{9} \frac{e^4}{(kT)^{3/2}} \left(\frac{M1 + M2}{M1 \cdot M2}\right)^{1/2}$$

for pressures in air between 700 and 1000 torr.

Langevin[83] based his calculation of the recombination coefficient, α_E, at pressures greater than two atmospheres on the mobilities of the ions :

$$\alpha_E = 4\pi e^2 (k_+ + k_-)$$

In the presence of sample molecules, the recombination of negative ions (formed by electron attachment) with positive ions resulting from ionisation of carrier gas molecules, will dominate that involving electrons as the negative species. At long pulse periods, it may be possible to calculate recombination coefficients for certain species (eg. H_3O^+) from the response of the ECD as recombination is certainly the principal process occurring under these conditions.

3.3. PRESENT KINETIC MODELS

The earliest attempt to describe quantitatively the ECD's response is the Beer's Law interpretation due to Lovelock[37]. This model is based on electron attachment phenomena, as discussed in the text by Healey and Reed[38]. The detector response, S, is related to the concentration of electron capturing species according to the following equation :

$$S/Io = 1 - \exp(-KxC) \qquad [4]$$

where Io is the detector current in the absence of electron acceptors

and S is the loss in current due to the presence of the capturing species whose concentration is C. x is a characteristic dimension of the detector. The constant K is related to the electric field strength and the electron capture cross-section of the sample. As a first approximation, the above equation serves well to predict the observed current but is not meant to represent all the processes occurring in the cell. Moreover, it is only applicable when the ECD is operated in the d.c. mode.

A kinetic model for the mechanism leading to stable negative ion formation has been developed by Wentworth, Chen and Lovelock[18]. Differential equations describing the processes occurring in the ECD when operated in the pulse-sampling mode are solved using the steady state approximation.

Several assumptions are made in the model:

a) The rate of production of thermal electrons is constant and not affected by the presence of the added capturing species.

b) The reaction zone is localised in the region about 1 to 2 mm. from the tritium foil.

c) The reaction zone includes a cloud of ions, electrons and radicals in addition to the argon-methane mixture and the electron capturing species.

d) The 'cloud' is not neutral but has an excess of positive ions and radicals.

e) The reaction zone is homogeneous and can be treated as a static system with respect to the electron concentration.

f) There is slow removal of material from the cell by flow of the carrier gas.

g) Recombination is the principal process by which electrons are lost in the presence of the carrier gas alone. Diffusion losses are minor.

h) If the negative ions are stable, then detachment of the

electrons can occur or they can recombine with positive ions. A host of subsequent reactions are possible when the negative ions dissociate.

i) The amount of material which undergoes electron capture is small in comparison to the total amount of material present. The process taking place in the cloud and their respective rate constants are described as :

$$\beta^- + Ar + CH_4 \xrightarrow{k_{pR}} \oplus + e^- + \beta^{-*}$$

$$\oplus + e^- \xrightarrow{kN'} \text{neutrals}$$

$$R^\bullet + e^- \xrightarrow{kR'} R^-$$

$$AB + e^- \underset{k_{-1}}{\overset{k_1}{\rightleftharpoons}} AB^-$$

$$AB^- + \oplus \xrightarrow{kN1} \begin{cases} A^\bullet + B^\bullet + R^\bullet \\ AB + R^\bullet \end{cases}$$

$$AB^- + R^\bullet \xrightarrow{kR1} \begin{cases} ABR^- \\ AB + R^- \\ AR + B^- \end{cases} + \oplus \longrightarrow \text{neutrals}$$

where

$\oplus$ = concentration of positive ions

k_{pR} = rate for thermal electron production

a = concentration of capturing species, AB

b = electron conc . in the absence of a capturing species.

In the absence of an electron capturing species,

$$\frac{d[e^-]}{dt} = kpR - kN' [\oplus][e^-] - kR' [R^\bullet][e^-] \quad [5]$$

which when solved gives

$$b = \frac{kpR}{k_D} \left[1 - \exp(-k_D t) \right] \quad [6]$$

where $k_D = kN' [\oplus] + kR' [R^\bullet]$

In the presence of a capturing species, the electron concent-

ration is given by

$$[e^-] = \frac{k_p R}{k_D \left(\frac{k_L k_1 a}{k_D (k_L + k_{-1})} + 1 \right)} \qquad [7]$$

where $kL = \left(k_{N1} [\oplus] + k_{R1} [R^\cdot] \right)$

At time infinity,

$$b^\infty = \frac{k_p R}{k_D}$$

so that,

$$\frac{b^\infty - [e^-]}{[e^-]} = \frac{k_L k_1 a}{k_D (k_L + k_{-1})} \qquad [8]$$

$$= k a$$

where k is the capture coefficient.

Since the capture coefficient contains the term $(kL + k_{-1})$, it is convenient to consider the case where $kL \gg k_{-1}$ and $k_{-1} \gg kL$ in order to examine the type of temperature dependence. If the temperature variation for the forward reaction is small, corresponding to no energy of activation for the addition of an electron, and if the electron affinity of the molecule is appreciable then the backward rate constant k_{-1} must have a significant temperature variation.

For $k_{-1} \gg kL$ Eq.[8] becomes,

$$\frac{b - [e^-]}{[e^-]} = \frac{kL}{k_D} k_{eq} a \qquad [9]$$

and since

$$k = \frac{kL}{k_D} k_{eq.} = \frac{kL}{k_D} A T^{-3/2} \exp (Ea/kT)$$

$$\text{Ln. } k T^{3/2} = \text{ln. } \frac{kL}{k_D} + \text{ln } A + Ea/kT \qquad [10]$$

By plotting ln. $k T^{3/2}$ against 1/T, Wentworth et al.[18] calculated the electron affinities of several aromatic hydrocarbons from the slope of the graphs.

For $k_{-1} \gg kL$, Eq.[8] becomes,

$$\frac{b - [e^-]}{[e^-]} = ka = \frac{k_1}{k_D} a \qquad [11]$$

If there is no energy barrier to the addition of an electron, k should be insensitive to temperature.

The capture coefficient, k, is obtained by integration with respect to the volume of gas passing through the detector during the residence time of a peak.

$$\int_0^v \frac{Ib - Ie}{Ie} dv = k \int_0^v a \, dv \qquad [12]$$

where Ib is the maximum standing current in the absence of the capturing species and Ie is the current in its presence.

$$v = \frac{Fr}{Cs} \cdot W$$

where W is the peak width; Fr, the gas flow rate and Cs is the chart speed.

Therefore,

$$\frac{Fr}{Cs} \int_0^W \frac{Ib - Ie}{Ie} dW = \frac{Fr}{Cs} \cdot A = k n$$

and $$k = \frac{Ib - Ie}{Ie} \cdot W\,1/2 \cdot \frac{Fr}{sM} \qquad [13]$$

where W 1/2 is the peak width at half height; s is sample size (μl); M is the molar concentration; A is the peak area and n is the number of moles.

The Wentworth model allowed for the first time the study of

electron attachment phenomena under conditions of atmospheric pressure, low fields and with low energy electrons in the presence of complex organic molecules. Most of the assumptions made in the model are justifiable though for some experimental evidence is lacking, eg. the dimensions of the reaction zone, the excess of positive ions and the removal of material by carrier gas flow.

Some of the arguments in the model become obscure when unknown and probably unknowable reaction steps are considered. There is as yet little experimental evidence of any of the species assumed to be present in the cell. Also, the system of rate equations is solved using the steady state approximation, ie. on the basis that the reduction in detector current is due to an equilibrium between electrons, capturing molecules, ions and molecules. The rate constant for the processes by which electrons are lost, k_D, is calculated from the initial slope of the graph of the number of electrons per pulse versus the pulse interval (gives kpR) and the saturation current ($bt \longrightarrow \infty$). Equation [6] is then used to predict the above described graph, having obtained the initial increase and also the plateau value from it. A satisfactory fit is to be expected, since a circular argument is presented for an equation describing an exponential increase to a constant level.

A few other models of the ECD based on the steady state approximation are to be found in literature. Lyons et al[39] proposed reaction steps, similar to Wentworth's for ethylene as the carrier gas, based on the observation of positive ions and radicals by Meisels[40] when ethylene undergoes primary irradiation. Equilibrium electron concentrations are calculated from kinetic schemes for three situations : before any pulses are applied, during the application of a voltage pulse and after a large number of pulses. Diffusion of charges to the cell walls is considered together with loss of

positive ions by flow. An error is made in the calculation of the rate of production of electrons; the Y-axis intercept of the straight line obtained when log $\left[Ne - (Ne)_b \right]$ is plotted against log tw, is regarded as the number of electrons produced at zero pulse width (tw).

Burdett[32] attempted to measure electron affinities using Wentworth's model; however, the values calculated were not in agreement with those obtained by other methods. A possible mechanism for electron capture proportional to the cross-sectional area of the molecules has been suggested as an alternative. The approach assumes a steady state situation for the electrons in the cell.

Scolnick[9] obtained empirical equations relating the observed current to the applied voltage and to functions of gas pressure and temperature. A concentric cylinder ECD with an isolated anode was used for the purpose and as such the equations are likely to be applicable only to detectors having that configuration.

Recently, Sullivan and Burgett[41] presented a theoretical model for the detector when used in the d.c. mode. The processes removing electrons, ie. ambipolar diffusion, mass transport out of cell, recombination and capture by bleed and impurities are collectively expressed by one rate constant which is assumed to be first order. This simplification leads to an erroneous conclusion: linearity of response is predicted to be better if the separation column has high bleed.

Lovelock[42] has also recently described the performance characteristics of the ECD. The stirred reactor model describes the processes causing the removal of electrons and molecules from the cell as follows :

$$e^- + AB \xrightarrow{k_1} \left.\begin{matrix} \\ \\ \end{matrix}\right\} \text{Inert products} \qquad [14]$$

$$e^- + \oplus \xrightarrow{k_d} \qquad [15]$$

$$AB + X \xrightarrow{k_x} \qquad [16]$$

$$AB \xrightarrow{U/V} \text{Ventilation} \qquad [17]$$

Reaction 14 is an irreversible second-order reaction with rate constant k_1. Reactions 16 and 17 concern the removal of sample molecules by processes other than in reaction in the gas phase with electrons. The detector volume is V and the gas flow rate U, the rate of injection of electrons A and of sample molecules B. The steady state electron concentration in the absence of sample molecules is

$$e^- = \frac{A\left\{1 - \exp(-kdt)\right\}}{k_d} \qquad [18]$$

which is the same as that derived by Wentworth et al.(Eq. 6). The theory is based on similar assumptions; excess of positive ions in the cell, uniform mixing and the removal of all electrons by a sampling pulse. However, the sample molecule is assumed to have a high capture rate constant unlike in the Wentworth model. After simplification, the sample concentration, C is expressed by

$$C = B/\ (k_1 e^- + kx + U/V) \qquad [19]$$

Conditions under which sample molecules are removed by processes other than by reaction with charged species have not been fully explained. The removal of sample molecules (with high capture rate constant) by ventilation during the flow of the carrier gas is considered to be the most important process yet the sample molecules remain for a sufficiently long time in the cell under conditions whereby the electron capture process is enhanced. It is uncertain which of these processes is dominant.

The presence of the positive ions and the effects of the

space charge need further consideration. The density of the ions continues to increase as electrons are collected but a limit must exist maximising their concentration. The assumption that the gas molecules and the electrons are uniformly mixed would imply that the space charge is no longer confined to the neighbourhood of the cathode. Also, the possible loss of electrons as they traverse the cell is not estimated.

An approach based on treating the ECD as a chamber containing two plane parallel electrodes and an internal ionisation source, with diffusion and recombination responsible for loss of charged particles, has been attempted. Ramey[43] has treated the case where volume recombination in a gas can be neglected, but in the ECD it has to be taken into consideration.

The current density at any point in space in the reaction volume is equal to the net production or loss of ion-pairs at that point.

$$\frac{dJ}{dx} = eNo - eknp$$

where:

J - current density

N_o - rate of production of ion-pairs

n - electron concentration

p - positive ion concentration

k - recombination coefficient

$$J = \int_0^x eNo\, dx - \int_0^x eKnp\, dx$$

$$= eNox - eknpx \qquad \text{where } No \neq f(x)$$

The current due to electrons only can also be expressed as:

$$J = -en\, \nu_d - eD^- \, dn/dx$$

ν_d is the electron drift velocity and D^- is the electron diffusion coefficient.

$$eNox - e\,knpx = -en\,\mathcal{V}d - e\,D^{-}\,dn/dx$$

$$\frac{dn}{dx} + \left(\frac{\mathcal{V}d}{D} - \frac{kpx}{D}\right)\cdot n = \frac{-No}{D}\,x$$

This is of the form,

$$\frac{dy}{dx} + p(x)\cdot y = Q\,(x)$$

Let $A = \mathcal{V}d/D$, $B = kp/D$ and $C = -No/D$

The integrating factor, I is

$$I = \exp \int (A - Bx)\,dx = \exp\,(Ax - 0.5Bx^2)$$

$$\frac{d}{dx}\left[\exp\,(Ax - 0.5\,Bx^2)\cdot n\right] = C\,x\,\exp\,(Ax - 0.5\,Bx^2)$$

$$\exp\,(Ax - 0.5\,Bx^2)\cdot n = C\int^{x} \exp\,(Ax - 0.5\,dx^2)\,dx$$

The solution of the integral on the R.H.S is

$$-\frac{1}{B}\,\exp\,(Ax - 0.5\,Bx^2) + \frac{A}{B}\int \exp\,(Ax - 0.5\,Bx^2)\,dx$$

The resulting integral has to be solved numerically and using both the Trapezium and Simpson's Rules, the values obtained were 4.12 and 4.20 for the low and high applied voltage cases respectively. The electron diffusion coefficient for nitrogen is calculated from the mean free path and the average velocity ($De = \bar{C}\ \lambda e/3$).

The electron concentration is then given by,

$$n = \frac{No}{kp}\left[\frac{4.2\,\mathcal{V}d}{D}\ \exp - (Ax - {}^{1}/_{2}\ Bx^2) - 1\right]$$

The measured current, I, is

$$I = \left(eNo\,V - es^{-}\cdot \mathcal{V}d^{-}\cdot n - es^{+}\cdot \mathcal{V}d^{+}\cdot p\right)$$

where V is cell volume and s is the electrode surface area.

The first term on the R.H.S. represents the saturation current. The second and third terms should reduce the current with decreasing applied voltage. With nitrogen as the carrier gas, the saturation

current term is 4.9 nA. Considering the average electron and positive ion concentrations ($\simeq 10^6$ cm^{-3} and 10^{10} respectively), the contribution of both the second and third terms (5.8×10^{-8}A and 4.6×10^{-7}A) is greater than the saturation current. Analysis of the ECD response on the basis of this approach is obviously not possible. The theory would probably be applicable in cases where the electron and positive ion concentrations are similar (ie. negligible space charge effects) and losses by recombination are very small.

In the section following, a theory for the ECD is proposed to overcome some of the deficiencies outlined in the discussion of various kinetic models. The theory is partly based on experimental observations made and these are fully described in chapters four and five.

3.4. PROPOSED MODEL FOR THE ECD

The basic approach to the problem is kinetic, ie. the detector is described by a system of rate processes[44]. A 'plasma' is created by energetic β^- particles emitted by the radio-active source. It contains Ve electrons Vp positive ions and Vn negative ions in a volume V. A given species, x, is removed from this 'plasma' by diffusion and volume flow rate F and has a mobility of μx under the appropriate conditions during a pulse. The cell has a cross-sectional area A and length l and the rate at which β^- particles leave the foil is $k_1 A$, each particle yielding G ion-pairs. The formation of one secondary electron and a positive ion by ionisation of a carrier gas molecule is referred to as an ion-pair.

A given species x may undergo a charge transfer process to yield a new species xj,

$$x + \text{neutral 1} \longrightarrow xj + \text{neutral 2}$$

or it may undergo attachment to yield xk,

$$x + \text{neutral} \longrightarrow xk.$$

Recombination processes involving positive ions and electrons or negative ions can be regarded as being of the first type together with reactions such as,

$$x^+ + Y \longrightarrow x + Y^+ + \Delta E \quad \text{and}$$

$$x^+ + x \longrightarrow x + x^+$$

It is a truly formidable task to list all X_i while the rates of none of these processes are known. Even if they were, the only actual measurement is that of total charge so that no detailed analysis would be possible. The discussion, therefore, is confined to the total species x while noting the fact that the rate constants used are weighted average rate constants, eg. for the recombination of electrons and positive ions,

$$\text{Total rate} = \sum_{P_i} k_i e p_i = ep \left[\frac{\sum k_i P_i}{\sum P_i}\right] = kep$$

where

$$p = \sum P_i \quad \text{and} \quad k = \frac{\sum k_i P_i}{\sum P_i}$$

As ki is not strongly dependent on the species P_i, little inaccuracy is introduced. Recombination coefficients for common molecular ions (except He_2^+) are in the range 10^{-7} to 10^{-6} $cm^3 s^{-1}$ [22].

The rates of removal of various species can be expressed as follows:

(Rate of formation) - (Rate of attachment) - (Rate of recombination) - (Rate of mass transport) - (Rate of migration)

Between pulses, the rates are :

$$V\frac{de}{dt} = k_1 AG - k_2 Vep - k_3 Vem - Fe \cdot e \qquad [20]$$

$$V\frac{dp}{dt} = k_1 AG - k_2 Vep - k_4 Vnp - Fp \cdot P \qquad [21]$$

$$V\frac{dn}{dt} = k_3 em - k_4 Vnp - Fn \cdot n \qquad [22]$$

where

e = electron concentration

p = positive ion concentration

n = negative ion concentration

m = concentration of sample molecules

Fe, Fp and Fn correspond to diffusion and volume flow rate for electrons, positive and negative ions respectively. The concentrations have units of particles cm^{-3}

During application of a pulsed voltage, a term ($- V_x . A . x$) has to be added to each equation; V_x is the drift velocity of the species x. The charged particles are said to be contained within a 'plasma' occupying a volume V, which may be different from that of the detector. A plasma is defined[45] as a system of charged particles with a nett charge equal to zero and in which the space scale for charge separation is much smaller than the dimensions of the plasma. The space scale for charge separation, called the Debye length, λ refers to the radius of the sphere of oppositely charged particles around a charge necessary to screen the electrostatic force of the central charge.

The Debye length is expressed by:

$$\lambda = \left(\frac{kT}{4\pi e^2 Ne} \right)^{1/2} \qquad [23]$$

where k is the Boltzmann constant; T is the electron temperature (298K); e is the electron charge and Ne is the average electron density.

In the ECD, a typical average electron density is about 5×10^6 cm^{-3} and the value of λ is then 0.05 cm. The charge density in the cell is sufficiently large and consequently the Debye length is much smaller than the dimensions of the plasma volume (the reaction zone is said to be confined within a distance of 0.25 cm. from the cathode).

The removal of electrons from the plasma by the applied field, creates a space charge of positive ions as explained in section 2.4. This space charge clearly cannot continue to build up and some mechanism must exist to limit its growth.

It is helpful to consider the situation under the pulse mode of operation. A β^- particle forms p' and e' positive ions and electrons respectively. If it is assumed that a constant fraction, r, of positive ions is removed during each cycle, then the number of ions remaining in the cell at the end of the first pulse is $p_{+1} = p' (1-r)$. During the following pulse interval, p' positive ions again form and after losing the fraction r, the number remaining after the application of the second pulse is $p_{+2} = (1 - r) (p_{+1} + p')$. This process continues as more pulses are applied :

$$p_{+1} = (1 - r)\, p'$$

$$p_{+2} = (1 - r)\ (p_{+1} + p')$$

$$p_{+n} = (1 - r)\ (p_{+(n-1)} + p')$$

Subsitution gives,

$$p_{+2} = (1 - r) \left[(1 - r) \cdot p' + p'\right]$$

$$= p' (1 - r)^2 + p' (1 - r)$$

and at the end of n pulses,

$$p_{+n} = p' \sum_{n=1}^{n} (1 - r)^n$$

After a large number of pulses, the density of the positive ions converges to a limiting value,

$$p = \lim_{n \to \infty} \frac{p' \left[1 - (1 - r)^n\right]}{\left[1 - (1 - r)\right]}$$

$$= p' \ / \ r = e' \ / \ r \quad \text{(ion-pair formation)} \qquad [24]$$

As pointed out by A. F. Gaines, the term $R = r^{-1}$ expresses the ratio of positive ion to electron density at the beginning of

the applied pulse. The magnitude of the 'Gaines factor' approaches close to infinity after collection of electrons during the pulse. As the electron concentration in the cell builds up again during the following pulse interval, the 'Gaines factor' approaches its limiting value, R. The pulse interval would have to be sufficiently long for this to occur and factors governing the electron concentration would determine its magnitude. The continuous variation in the 'Gaines factor' during the pulse interval leads to an integration over the pulse period to obtain its average value.

The first point in the development of the model is to evaluate R from the rate equations already stated.

Once the space charge of positive ions has formed, no accumulation of charge occurs over a complete cycle, so that

$$\sum \int_0^s \frac{dX}{dt} + \sum \int_0^w \frac{dX}{dt} = 0 \qquad [25]$$

where s denotes the field free interval and w is the pulse width. Assuming that,

$$\frac{de}{dt} + \frac{dn}{dt} = \frac{dp}{dt}$$

and substituting equations [20] [21] and [22] in the above equation gives,

$$\left(Fe.e + Fn.n - Fp.p\right) = 0 \qquad [26]$$

During application of the pulse, the addition of the drift velocity term results in,

$$e\,(Fe + \nabla e.A) + n\,(Fn + \nabla n.A) - p\,(Fp + \nabla p.A) = 0 \qquad [27]$$

Substitution of equations [26] and [27] in [25] gives,

$$\int_0^s (Fe\cdot e + Fn\cdot n - Fp\cdot P)dt + \int_0^w \left[e\,(Fe + \nabla e.A) + n(Fn + \nabla nA) - p(Fp + \nabla p\cdot A)\right]dt = 0 \qquad [28]$$

Solution of equation [28] involves solving integrals for e, p and n over the field free interval and the pulse width.

The positive ion concentration can also be expressed as the sum of the ions remaining in the cell after a pulse has been applied and those generated as ion-pairs during the preceeding pulse interval, ie. $p = (p_o + e)$. If p and e are thus linked and negative ions are neglected, equation [20] becomes,

$$V \frac{de}{dt} = K_1 AG - K_2 Ve (p_o + e) - Fe \cdot e$$

$$= K_1 AG - e (K_2 VP_o + Fe) - K_2 Ve^2$$

$$V \frac{de}{dt} = a + be + Ce^2$$

where, $a = K_1 AG$, $b = -(K_2 VP_o + Fe)$ and $C = -K_2 V$.

Integrating the above equation with the boundary conditions $e = 0$ at $t = 0$ (beginning of the field free interval) gives :

$$\frac{1}{V} \int_0^t dt = \int_0^e \frac{de}{(a + be + Ce^2)}$$

$$\frac{t}{V} = \left[\frac{1}{\lambda} \ln. \frac{2Ce + b - \lambda}{2Ce + b + \lambda} \right] \Bigg|_0^e \qquad [29]$$

where $\lambda = (b^2 - 4aC)^{1/2}$

$$\frac{1}{\lambda} \left[\ln \frac{2Ce + b - \lambda}{2Ce + b + \lambda} - \ln \frac{b - \lambda}{b + \lambda} \right] = \frac{t}{V}$$

$$\frac{2Ce + b - \lambda}{2Ce + b + \lambda} \cdot \frac{(b + \lambda)}{(b - \lambda)} = \exp (\lambda t/V)$$

$$\frac{\left[\frac{2Ce + b - \lambda}{b - \lambda} \right]}{\left[\frac{2Ce + b + \lambda}{b - \lambda} \right]} \cdot \frac{(b + \lambda)}{(b - \lambda)} = \exp (\lambda t/V)$$

Let $X = \frac{2Ce}{b - \lambda}$ and $Y = \frac{b + \lambda}{b - \lambda}$

$$X - \frac{X}{Y} \cdot \exp(\lambda t/V) = \exp(\lambda t/V) - 1$$

$$X = \frac{\exp(\lambda t/V) - 1}{1 - \exp(\lambda t/V)/Y}$$

$$\frac{2Ce}{b-\lambda} = \frac{[\exp(\lambda t/V) - 1](b+\lambda)}{(b+\lambda) - (b-\lambda)\cdot\exp(\lambda t/V)}$$

$$2Ce = \frac{[\exp(\lambda t/V) - 1](b^2 - \lambda^2)}{(b+\lambda) - \{(b-\lambda)\cdot\exp(\lambda t/V)\}}$$

$$e = \frac{1}{2C} \frac{(b^2 - \lambda^2)[\exp(\lambda t/V) - 1]}{\lambda[\exp(\lambda t/V) + 1] - b[\exp(\lambda t/V) - 1]}$$

$$e = \frac{2a[\exp(\lambda t/V) - 1]}{\lambda[\exp(\lambda t/V) + 1] - b[\exp(\lambda t/V) - 1]} \qquad [30]$$

The above equation describes the build up of electron concentration during the field free interval. However, its use is limited; further integration over the pulse width leads to an overwhelmingly complicated solution. Consider the case where p is constant.

$$V\frac{de}{dt} = K_1 AG - K_2 \cdot Vep - Fe.e$$

$$= K_1 AG - e(K_2 \cdot Vp + Fe.e)$$

Let $a = K_1 AG$ and $b = (K_2 \cdot Vp + Fe.e)$

Integration over the field free interval leads to,

$$\int_0^e \frac{de}{(a - be)} = \frac{1}{V} \int_0^t dt$$

$$\frac{t}{V} = -\frac{1}{b}\left[\ln.(a - be) - \log a\right]$$

$$1 - \frac{be}{a} = \exp(-bt/V)$$

$$e = \frac{a}{b}\left[1 - \exp(-bt/V)\right] \qquad [31]$$

Equation [31] can be used to determine the decrease in electron concentration during the pulse width (w). The boundary conditions now are $e = e_t$ at $t = o$ and $e = e$ at $t = w$. Considering the drift velocity term and in the absence of sample molecules, Equation [20] becomes :

$$V \frac{de}{dt} = K_1 AG - K_2 Vep - Fe.e - \mathcal{V}e .Ae$$

$$= K_1 AG - e (K_2 Vp + Fe.e + \mathcal{V}e.A)$$

Let $a = K_1 AG$ and $b' = (K_2 Vp + Fe.e + \mathcal{V}e.A)$

$$\int_{e_t}^{e} \frac{de}{(a - b' e)} = \frac{1}{V} \int_{o}^{t} dt$$

The integral is of the same form as the previous one and its solution is,

$$- \frac{b't}{V} = \ln \left(\frac{a - b'e}{a - b'e_t}\right)$$

$$(a - b'e) = (a - b' e_t) \exp (-b't/V)$$

$$e = \frac{a}{b'} \left[1 - \exp (-b't/V)\right] + e_T \exp (-b't/V) \qquad [32]$$

It is now necessary to evaluate the total charge in the cell during the field free interval. This is done for the case where p is constant, since where $p = p_o + e$, the integrals are again very unwieldy. Using equation [31] ,

$$\int_{o}^{t} e \, dt = \int_{o}^{t} \frac{a}{b} \left[1 - \exp (-bt/V)\right] dt$$

$$= \frac{a}{b} \left[t + \frac{V}{b} \exp (-bt/V) - \frac{V}{b}\right]$$

$$= \frac{a}{b}\left[t - \frac{V}{b}\left(1 - \exp(-bt/V)\right)\right] \qquad [33]$$

Similarly, the total charge lost during the application of the pulse is obtained by integrating equation [32].

$$\int_0^t e\,dt = \frac{a}{b'}\int_0^t \left[1 - \exp(-b't/V)\right] dt + \int_0^t e_T \exp(-b't/V)dt$$

$$= \frac{a}{b'}\left[t - \frac{V}{b'}\left(1 - \exp(b't/V)\right)\right] + \frac{e_t V}{b'}\left[1 - \exp(-b't/V)\right] \qquad [34]$$

Graphical representation of the equations derived is shown in Figure(5). Having obtained integrals for the electron concentration equation [28] can now be considered. Without the negative ion terms it is :

$$\int_0^s (Fe.e - Fp.p)\,dt + \int_0^w \left[e(Fe + \mathcal{V}eA) - p\,(Fp + \mathcal{V}pA)\right] dt = 0$$

Making the substitution $p = (p_o + e)$ gives,

$$\int_0^s (Fe - Fp)\,e\,dt + \int_0^w (Fe + \mathcal{V}eA)\,e\,dt = Fp\,p_o\,s + \int_0^w (Fp + \mathcal{V}pA)pdt$$

Inserting the various integrals involved, the left-hand-side (L.H.S) of the above equation becomes,

$$(Fe - Fp)\frac{a}{b}\left[s - \frac{V}{b}\left(1 - E^{-bs/V}\right)\right] + (Fe + \mathcal{V}eA)\left\{\frac{a}{b'}\left[w - \frac{V}{b'}\left(1 - E^{-b'w/V}\right)\right] + \frac{e_t V}{b'}\left(1 - E^{-b'w/V}\right)\right\}$$

and the R.H.S. is,

$$Fp\,p_o s + (Fp + \mathcal{V}pA)\left\{\frac{a}{b''}\left[w - \frac{V}{b''}\left(1 - E^{-b''w/V}\right)\right] + \frac{(p_o + e_t)V}{b''}\cdot\left(1 - E^{-b''w/V}\right)\right.$$

[35]

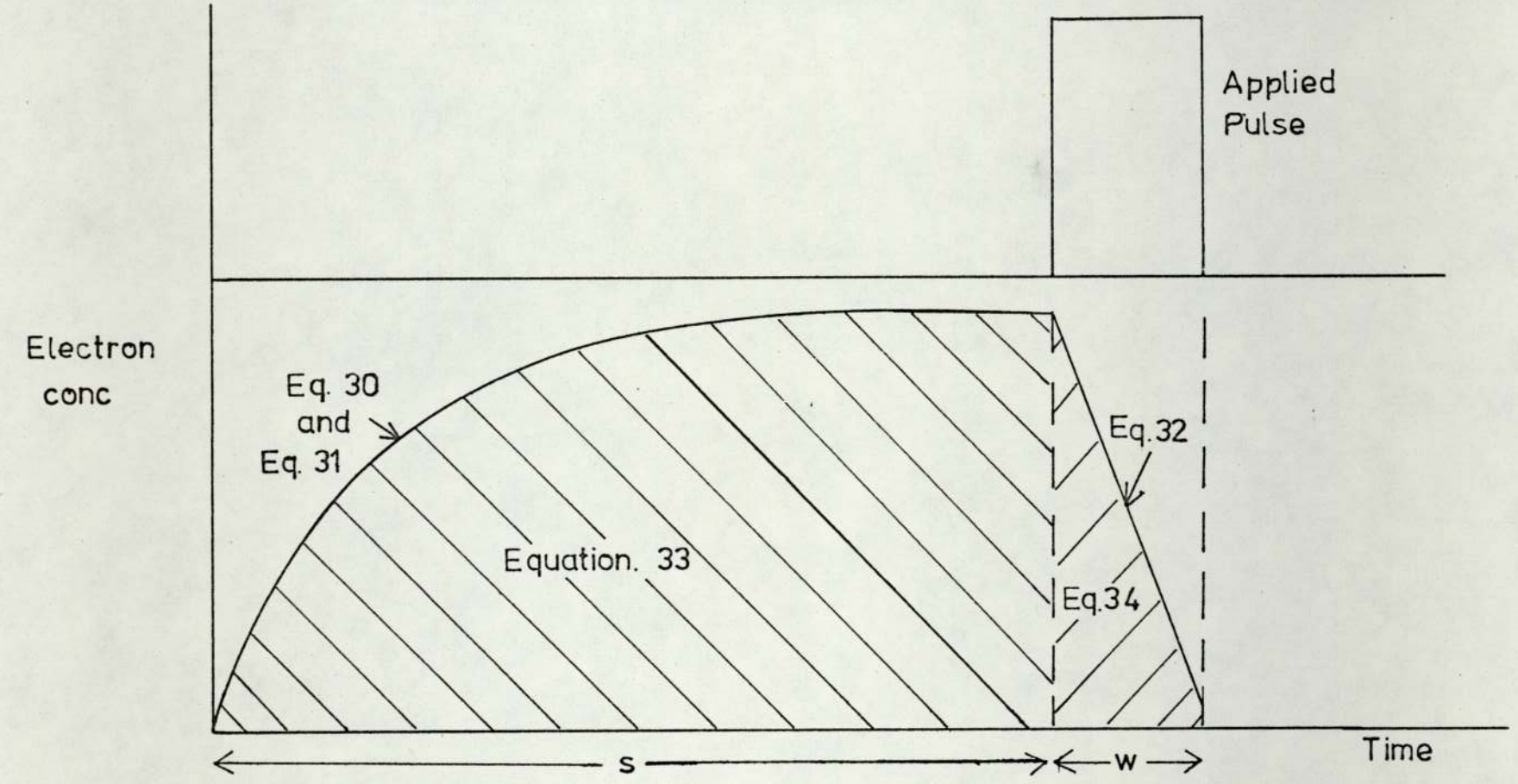

FIG. 5

GRAPHICAL REPRESENTATION OF EQUATIONS DERIVED IN THE PROPOSED MODEL

The integral expressing the positive ion concentration is of the same form as that for the electron density and the constant $b'' = (K_2 Ve + Fp + \nu pA)$.

The term $(Fe + \nu e.A)$ can be replaced by $(b' - K_2 Vp)$ and similarly for $(Fp + \nu pA) = (b'' - K_2 Ve)$. As the number of electrons removed, through collection at the anode, is small in comparision to the positive ion density, $p = p_o + e \simeq po$. Further simplification of equation [35] is achieved by making approximations under real conditions. An order of magnitude analysis of various terms is given below :

$$b' = (K_2 Vpo + Fe + \nu eA) \simeq (10^3 + 3 + 10^5) \simeq 10^5 \quad cm^3 \; s^{-1}$$

$$b'' = (K_2 Ve + Fp + \nu pA) \simeq (10^{-1} + 3 + 10^3) \simeq 10^3 \quad cm^3 \; s^{-1}$$

$$\frac{V}{b}\left[1 - \exp\,(-bs/V)\right] \simeq 10^{-4} \quad s^{-1}$$

$$\frac{V}{b'}\left[1 - \exp\,(-b'\,w/V)\right] \simeq 10^{-6} \quad s^{-1}$$

$$\frac{e_t V}{b'}\left[1 - \exp\,(-b'\,w/V)\right] \simeq 1 \; scm^{-3}$$

$$Fp\; P_o s \simeq 10^6$$

$$\frac{V}{b''}\left[1 - \exp\,(-b''\,w/V)\right] \simeq 10^{-4} \; s^{-1}$$

$$\frac{(Po + et)\; V}{b''} \simeq 10^7 \; scm^{-3}$$

The L.H.S. of equation [35] simplifies to,

$$\frac{(b' - K_2\, Vpo)\; e_t}{b'}$$

while the R.H.S. becomes,

$$Fp\; pos + (b'' - K_2\, Ve)\left[w\,(po + e_t)\right]$$

Substituting $a = be_t$ and $p_o = (R-1)e_t \simeq Re_t$ gives,

$$\frac{(b' - K_2 V p_o)\, e_t}{b'} = Fps\,(R-1)e_t + (b'' - K_2 Ve)\,(Re_t\omega)$$

$$= R\left[Fps + \omega\,(b'' - K_2 Ve)\right] - Fps$$

Hence,

$$R = \frac{1 - \frac{K_2 V p_o}{b'} + Fps}{(b'' - K_2 Ve)\,\omega + Fps}$$

Since, $b' \gg K_2 V p_o$, the 'Gaines factor' is expressed by,

$$R = \frac{1 + Fps}{(Fp + \sqrt{pA})\,\omega + Fps}$$

$$R = \frac{1 + Fps}{\sqrt{p \cdot A}\,\omega + Fp\,(\omega + s)} \qquad [36]$$

It is to be noted that the above expression is merely an approximation for R; its value is dependent on gas parameters and also on pulse characteristics, ie. a function of time. The average value of R is obtained by integrating over the pulse interval and dividing by the period.

$$\int_0^t R\,dt = \frac{1}{s}\int_0^t \frac{1 + Fpt}{(Fp + \sqrt{p.A})\,\omega + Fpt}\,dt$$

Let $(Fp + \sqrt{pA})\,\omega = Q$

$$\int_0^t R\,dt = \frac{1}{T}\left[\int_0^t \frac{dt}{(Q + Fpt)} + \int_0^t \frac{Fpt}{Q + Fpt}\right]dt$$

$$\int_0^t \frac{dt}{(Q + Fpt)} = \frac{1}{Fp} \ln (Q + Fpt) \Big/_0^t$$

$$= \frac{1}{Fp} \left[\ln \left(1 + \frac{Fpt}{Q}\right) \right]$$

$$\int_0^t \frac{Fpt}{Q + Fpt} dt = t - \frac{Q}{Fp} \left[\ln Q (Q + Fpt) \right]$$

In real terms, the magnitude of the latter integral is very much smaller than that of the former and hence,

$$\int_0^s Rds = \frac{1}{Fps} \ln \left[1 + \frac{Fps}{(Fp + VpA)W} \right] \qquad [37]$$

Having obtained the 'Gaines factor', it can now be used to determine the positive ion density in the cell. As a first approximation, the rate of production of ion-pairs can be equated to the product of the electron concentration and the rates of loss by recombination and volume flow.

$$a = be = e (K_2 Vpo + Fe)$$

If Fe is small,

$$Po = eR = \frac{R\,a}{(K_2 Vp_o)}$$

The positive ion concentration is therefore given by

$$P_o = \left(\frac{Ra}{K_2 V} \right)^{1/2} \qquad [38]$$

It is axiomatic in the present work that mixing within the plasma is sufficiently rapid for the concentration to be uniform. A single criterion may be used to test the degree of mixing - if the electron drift velocity is much less than the gas kinetic velocity, mixing can be held to be complete but if the converse is

then there is very little.

The drift velocity for electrons is about 7×10^6 cms^{-1} at 100 Volts cm^{-1} in argon + methane, while the gas kinetic velocity at STP is $(RT/M)^{1/2} = 1.2 \times 10^7$ cms^{-1}. The criterion is indecisive and mixing cannot be held complete but is certainly significant. This point is further discussed in the experimental section where the effect of carrier gas flow is considered.

Experimental verification of the model is now possible for the case where only the pure carrier gas response is observed under the pulse mode of operation.

CHAPTER FOUR - AN EXPERIMENTAL STUDY OF THE ECD

4.1 DETECTOR DESIGN AND CONSTRUCTION

For the purpose of the present study, a cell had to be constructed since the commercially available detectors do not offer the necessary flexibility needed to investigate the various characteristics of the instrument. The design was kept as simple as possible to avoid any complexities arising from the detector's geometry yet was comparable to that of commercial detectors.

Scolnick[46] showed that if the ECD were to function as a concentration detector, the volume of the chamber has to be about 0.5 cm^3. The ratio of the detector time constant to the chromatogram peak width at 60.6% of the maximum sample concentration, has to be small to minimise loss in peak resolution. Another point which requires consideration is the choice of the inter-electrode insulator. At high temperature Scolnick found that the conductivity of glass insulators used in many concentric ECDs, is not small in comparision to the conductivity of the ionised gas.

Figure (6) illustrates the ECD constructed. It is of the normal parallel plane configuration except for the gas flow arrangement - the inlet and exit were perpendicular rather than parallel to the electrodes. This allowed the electrode separation to be varied and the vortices in such a flow system would probably provide better mixing. The main cell body was of PTFE; the wall thickness being 1.27 cm. The gas inlet and outlet were 0.635 cm. brass tubing threaded half way through the cell body. The electrodes consisted of a brass disc (1.27 cm. in diameter) and a stainless steel rod (0.3175 cm. in thickness). They were locked into the desired position by PTFE nuts pressing onto an 'O' ring. The cell was

FIG. 6

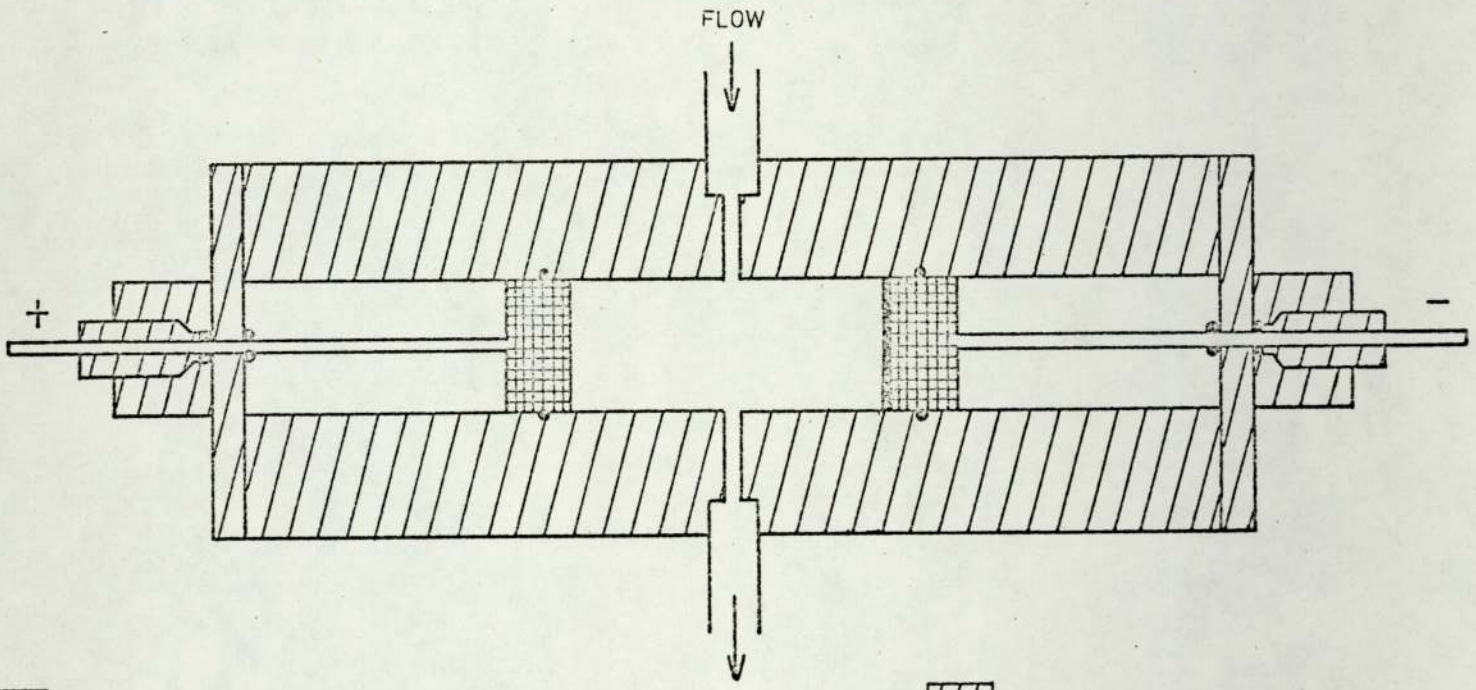

THE ELECTRON CAPTURE DETECTOR.

made leak proof by having rubber 'O' rings both on the electrodes and at either ends of the cylindrical body. The radioactive foil consisted of ^{3}H occluded on a titanium surface with a copper backing. The foil was soldered on to the brass disc to form the cathode of the cell. This was done using a low melting solder (85°C) so as to avoid any loss of radioactivity.

The ECD was housed in an aluminium box with its own separate gas supply to prevent back diffusion of atmospheric oxygen[46]. A loose fitting lid provided access to the detector while permitting the vented gas finally to escape into the atmosphere. The metal container also prevented possible interference from stray capacitance and other outside electrical disturbances.

4.2 ELECTRICAL CIRCUIT

Figure (7) shows the electrical circuit used for normal operation of the cell. The voltage source was a Hewlett Packard model 214A pulse generator providing a maximum pulse amplitude of 100 volts and had continuously variable pulse width and interval. The applied pulses were monitored on an oscilloscope. The current flowing through the cell was measured as a voltage drop across the high input resistance of a vibrating reed electrometer. The instrument used was an E.I.L model 33C Vibron with two additional resistances of 10^{7} and 10^{8} ohms fitted in the convertor unit. The full scale deflection of the meter was 1000 mV and the input resistance was variable from 10^{7} to 10^{12} ohms in powers of 10. At 10^{12} ohms, the time constant is stated to be about 30 seconds and is much less with lower resistances. Since the currents measured were in the nano- to pico A region, it was necessary to eliminate local leakage current loops set up as a result of slight potential differences existing between various earth points. Care had to be taken to

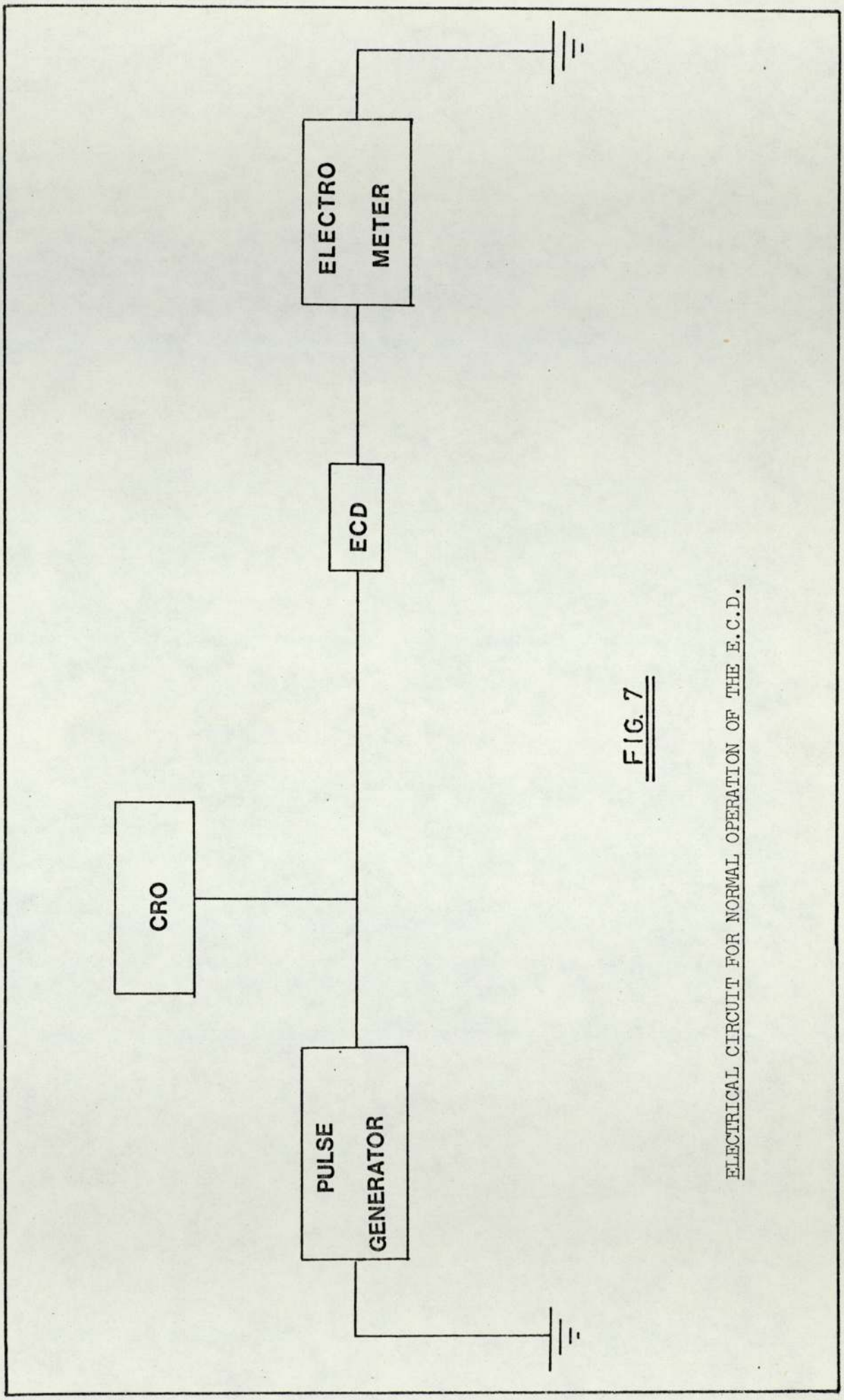

FIG. 7

ELECTRICAL CIRCUIT FOR NORMAL OPERATION OF THE E.C.D.

avoid inefficient shielding of cables and also of the ECD.

4.3 GAS PURIFICATION

To study various parameters of the detector, nitrogen was mainly used as the carrier gas. The 'white spot' nitrogen supplied by the British Oxygen Company was exclusively used. The flow rate was regulated by rubber diaphragm type of valves and was measured on flowmeters supplied by the Rotameter Manufacturing Company. These were calibrated by means of a bubble flow meter. 0.25 in. O.D. copper tubing and thick-walled nylon tubing were used for gas transport. Diffusion through the walls of the latter did not seem to occur as the current was not affected when the length of tubing was changed. All connections were made with 'Enot' fittings. The gas after monitoring passed through a molecular sieve, supplied by Kenmore Incorporated, for the removal of moisture. Before entering the cell, the gas also passed through an 'Oxy Trap' which was supplied by Allteck Associates. All joints were thoroughly tested for leaks with soap solution and the line was evacuated to about 10^{-2} torr. Precautions for good performance, as laid down by Lovelock[42], were taken as far as it was practically possible. These included the use of metal diaphragm pressure regulators, clean short tubing for all gas connections and the avoidance of flow regulators at the head of the gas line.

To check on the presence of oxygen in the carrier gas, a chemical test was carried out. A solution of Co $(dipy)_3$ $(ClO_4)\cdot 3H_2O$ in dimethyl sulphoxide (DMSO) was reduced by an aqueous solution of sodium borohydride. Nitrogen from the ECD was bubbled through the solution. The product of the reduction remains deep blue in the absence of any oxygen and turns colourless to yellowish in the presence of the smallest amount[47]. The carrier gas was found to

be oxygen free. The whole apparatus had to be removed because the solvents were back-diffusing through the gas line to the detector.

Another simple check of the cleanliness of the carrier gas is to determine the electron half-life within the chamber[48]. This is done by finding the pulse period at which the detector standing current falls to half of that measured at the shortest pulse interval. Under ideal conditions with really clean gas, it may be as much as 1 ms and has to be greater than 300 μs. With nitrogen as carrier gas, the electron half-life was about 750 μs.

4.4 CHARACTERISATION OF THE DETECTOR

Under the pulsed mode of operation, the detector current depends partly upon the pulse amplitude, width and interval. Preliminary experiments were carried out to determine the optimum operating conditions necessary for the detector regarding pulse characteristics.

Figure (8) shows the current variation with applied voltage. The current rises steeply and reaches a steady level at about 20 volts. At low applied voltages, electrons and ions are lost through recombination as the field strength is not sufficiently high to allow their collection at the respective electrodes. At constant pulse amplitude and width and temperature and pressure, the number of electrons per pulse, N_e, is expressed by,

$$N_e = \frac{I \times s}{1.6 \times 10^{-19}}$$

where I is the observed current and s is the pulse interval. The voltage corresponding to the onset of theplateau in Fig. (8) is independent of the pulse interval but depends on the pulse width.

It is desirable to have the pulse width (w) as short as possible so that the number of ion-pairs formed during the pulse is

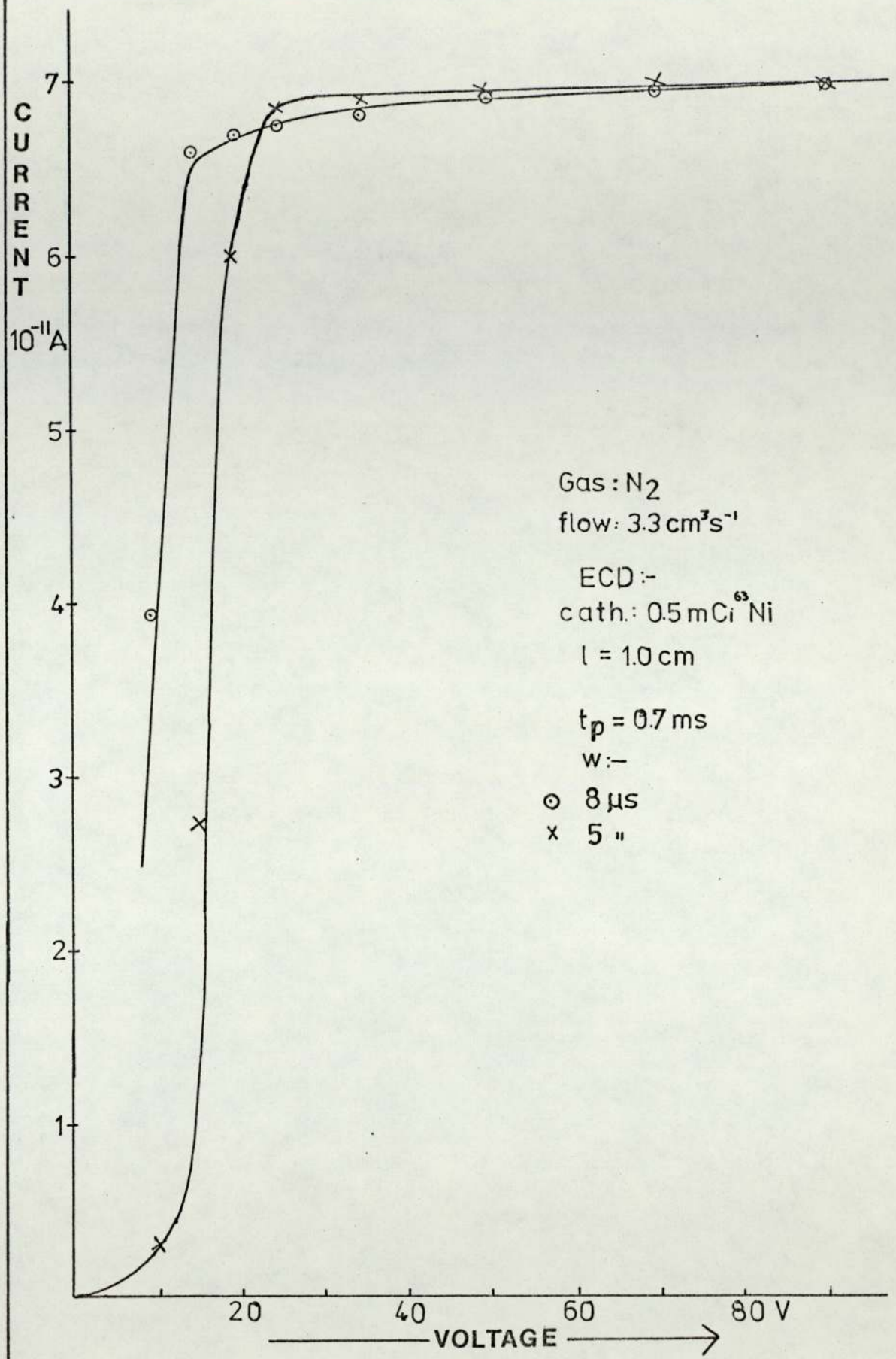

FIG. 8

CURRENT (I) VARIATION WITH PULSE AMPLITUDE (V)

not appreciable and the electrons have the maximum possible time to reach thermal equilibrium. If the duration is too short however, there is not sufficient time to collect all electrons and hence the saturation current is not reached. From Fig. (9) it can be seen that a pulse width of about 3.5μs is sufficient to remove all electrons. Normally pulses of 5 μ s duration were employed. The critical pulse width at which the curve effectively flattens off is said to correspond to the electron transit time between the two electrodes. Electron drift velocities have been calculated from this data[18,39].

Besides the amplitude of the voltage and the length of time for which it is applied, the interval between pulses also affects the current flowing through the cell. The current is proportional to the number of pulses per second, that is, inversely proportional to the period (Fig. 10). This relation does not work at small pulse interval as an 'equilibrium' has not been established between the process of production of ion-pairs and those processes responsible for their loss. The relationship between the number of electrons per pulse (Ne) and the pulse interval is more difficult to explain as often a maximum is observed (Figs. 11 and 12). A good test for the kinetic models outlined in the previous chapter is to predict the above relationship. This point is discussed more fully in section 4.7 this chapter.

4.5 RADIATION SOURCES AND INTER-ELECTRODE SPACING

The nature of the ionisation source has been found to be of primary importance. The dimensions of the ionisation zone are determined by the cross-sectional area of the radiation source and the range of the emitted β^- particles. The two most commonly used sources are ^{3}H and ^{63}Ni. As stated earlier, β^- particles released from a ^{3}H source have a maximum energy distribution between 17.6 and 18.9 KeV, while those from ^{63}Ni are about 67 KeV[15]. The

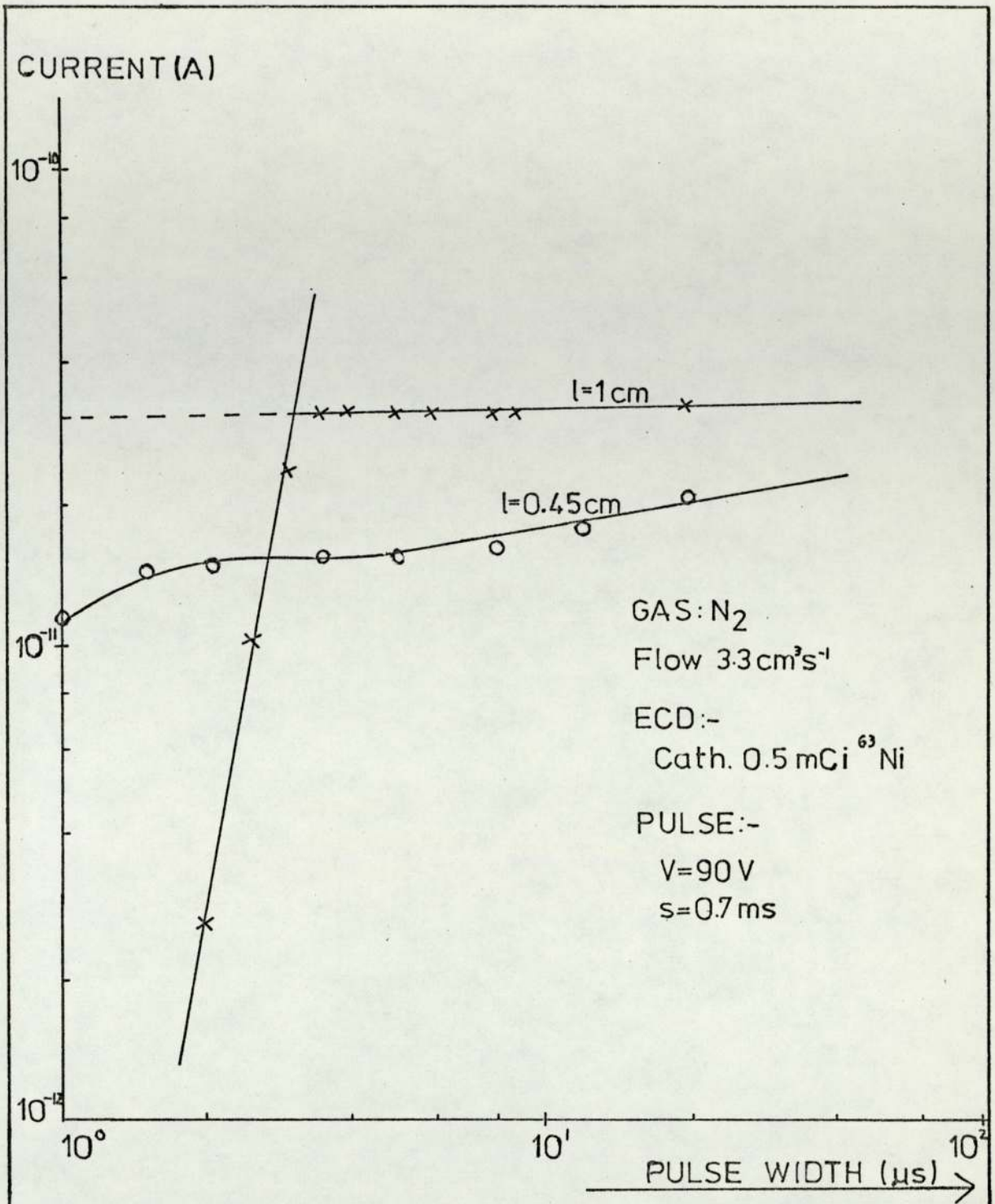

FIG. 9

CURRENT VARIATION WITH PULSE WIDTH (W)

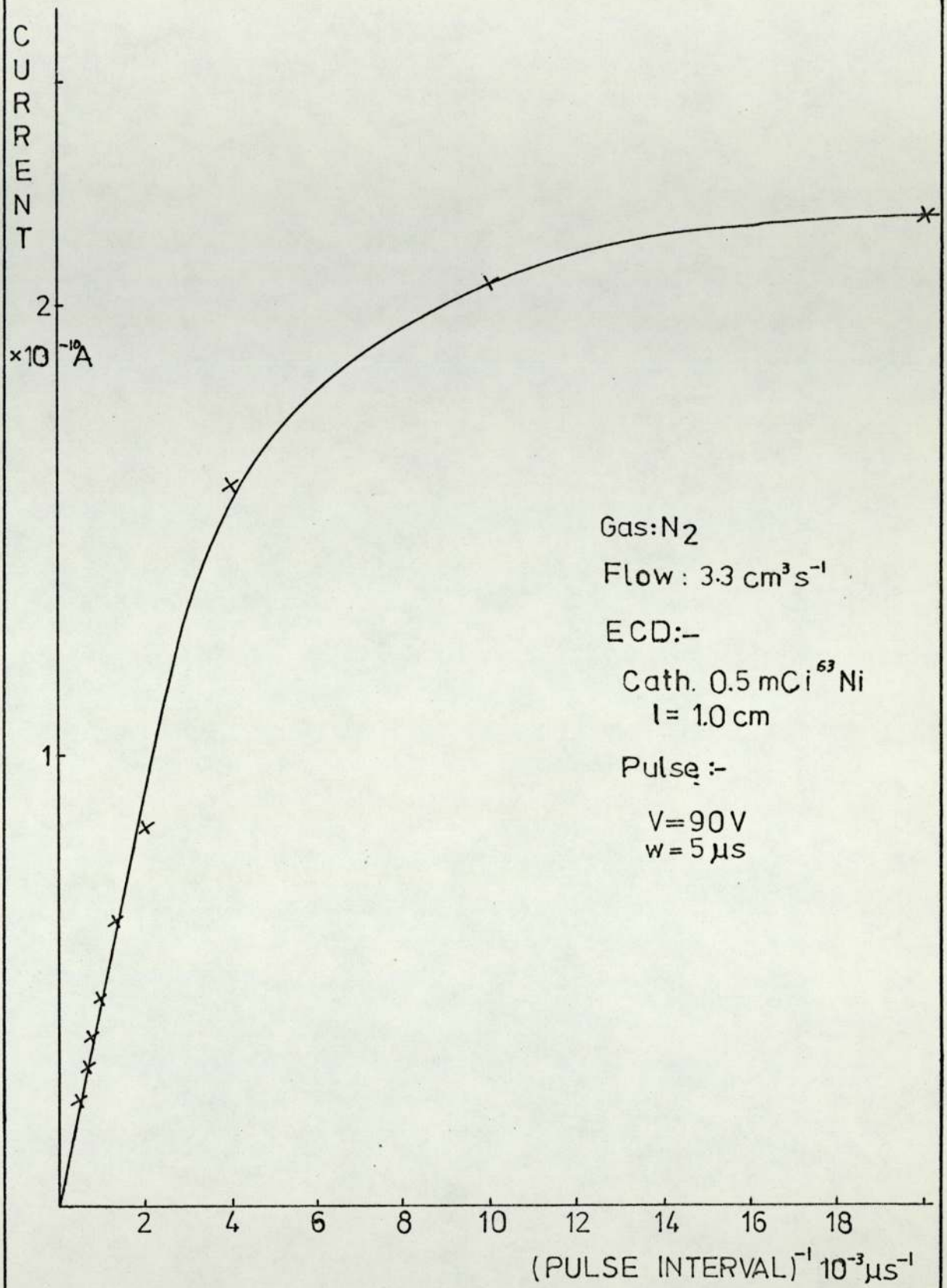

FIG. 10

CURRENT VARIATION WITH PULSE INTERVAL $(s)^{-1}$

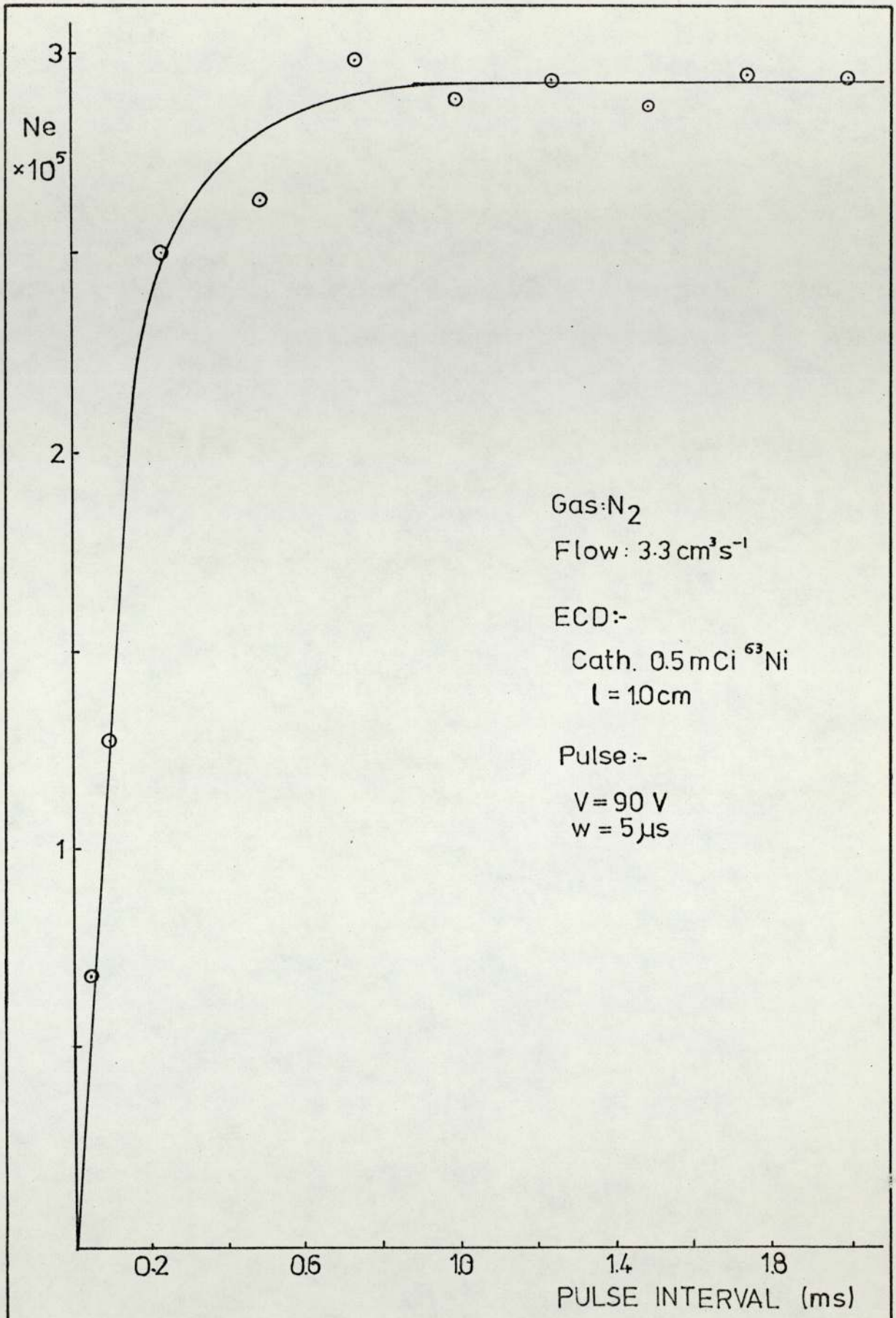

FIG. 11

Ne VERSUS s PLOT FOR ^{63}Ni SOURCE

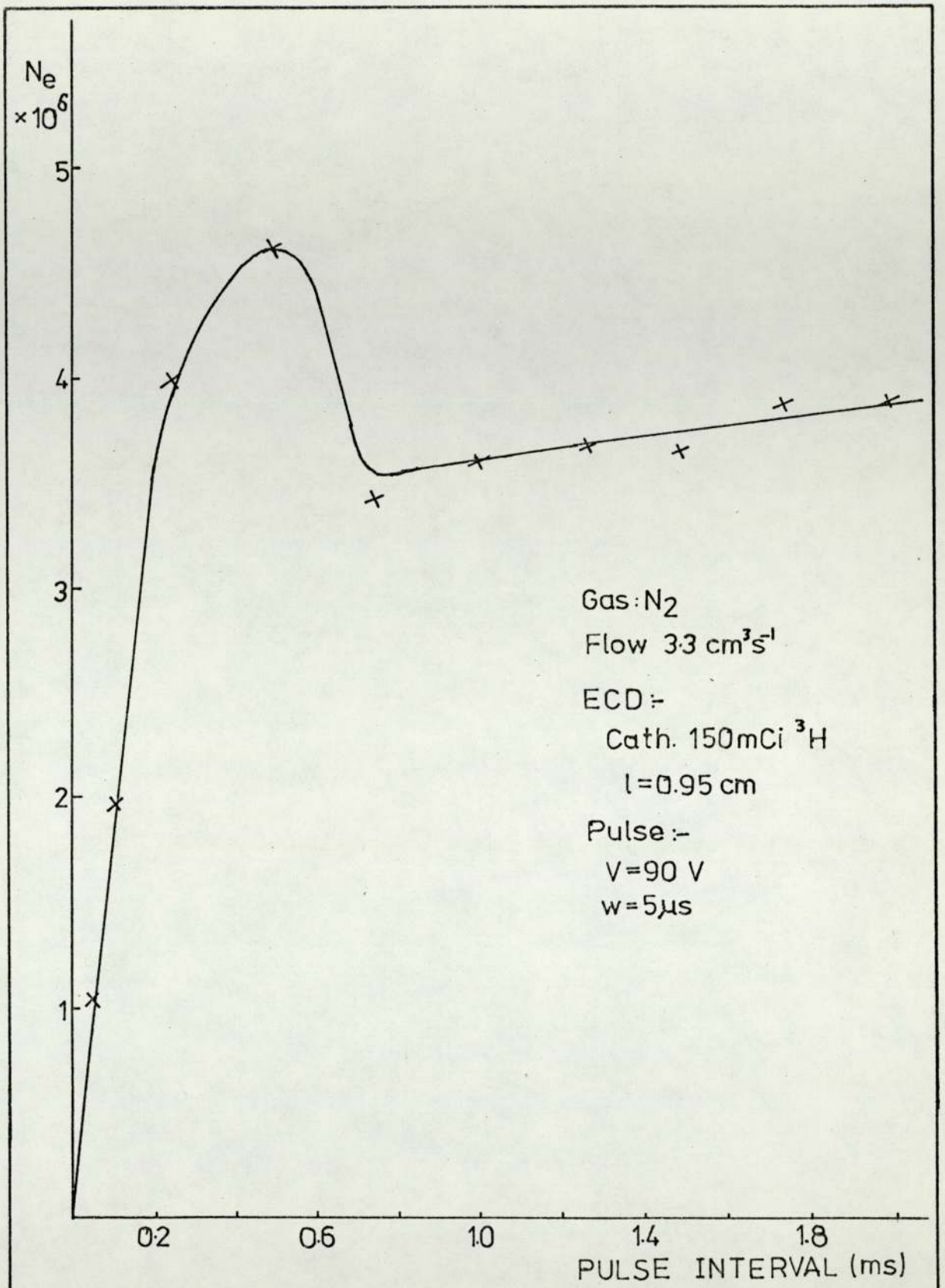

FIG. 12

Ne VERSUS s PLOT FOR 150 mCi SOURCE

average energy is about one third the maximum energy. The number of ion-pairs formed decreases with increasing energy of β^- particles (Fig.13), since the time in which energy can be transferred from the particle to the gas molecule upon collision decreases with increasing velocity. When low energy β^- particles are being considered, the range has been found to be almost independent of absorber material. The graph of specific ionisation, ie. the rate at which β^- particles lose energy in passing through air, versus range (Fig. 14) shows a very steep increase in the number of ion-pairs formed at a distance of about 2 mm. from the ^3H source[49]. There is then an exponential decrease in the number of pairs formed with increasing distance.

The range of the β^- particles, R, can be calculated from an empirical relationship,

$$\text{Ln. } E = 6.63 - 3.2376\ (10.2146 - \ln R)^{1/2}$$

where E is the maximum energy in MeV. The equation is valid for $0.01 \leqslant E \leqslant 2.5$ M eV. Weakly energetic β^- particles from a ^3H source travel about 2 mm. in air. Wentworth et al.[18] and the Radiochemical Centre[50] quote similar values. β^- particles of maximum energy travel about 6 mm. while those from the ^{63}Ni source have a range of about 9 mm. The combined effects of continuum spectra and scattering lead to an approximately exponential absorption law for β^- particles of a given maximum energy. The nearly exponential decrease applies both to numbers and specific ionisation of β^- particles. Hence, the energy and number distribution lead to the conclusion that there are many more β^- particles close to the source and because of their low energy, a large number of ion-pairs could be formed in this region.

Loss through self-absorption and scattering is much more pronounced with electrons than with heavy particles. Self absorp-

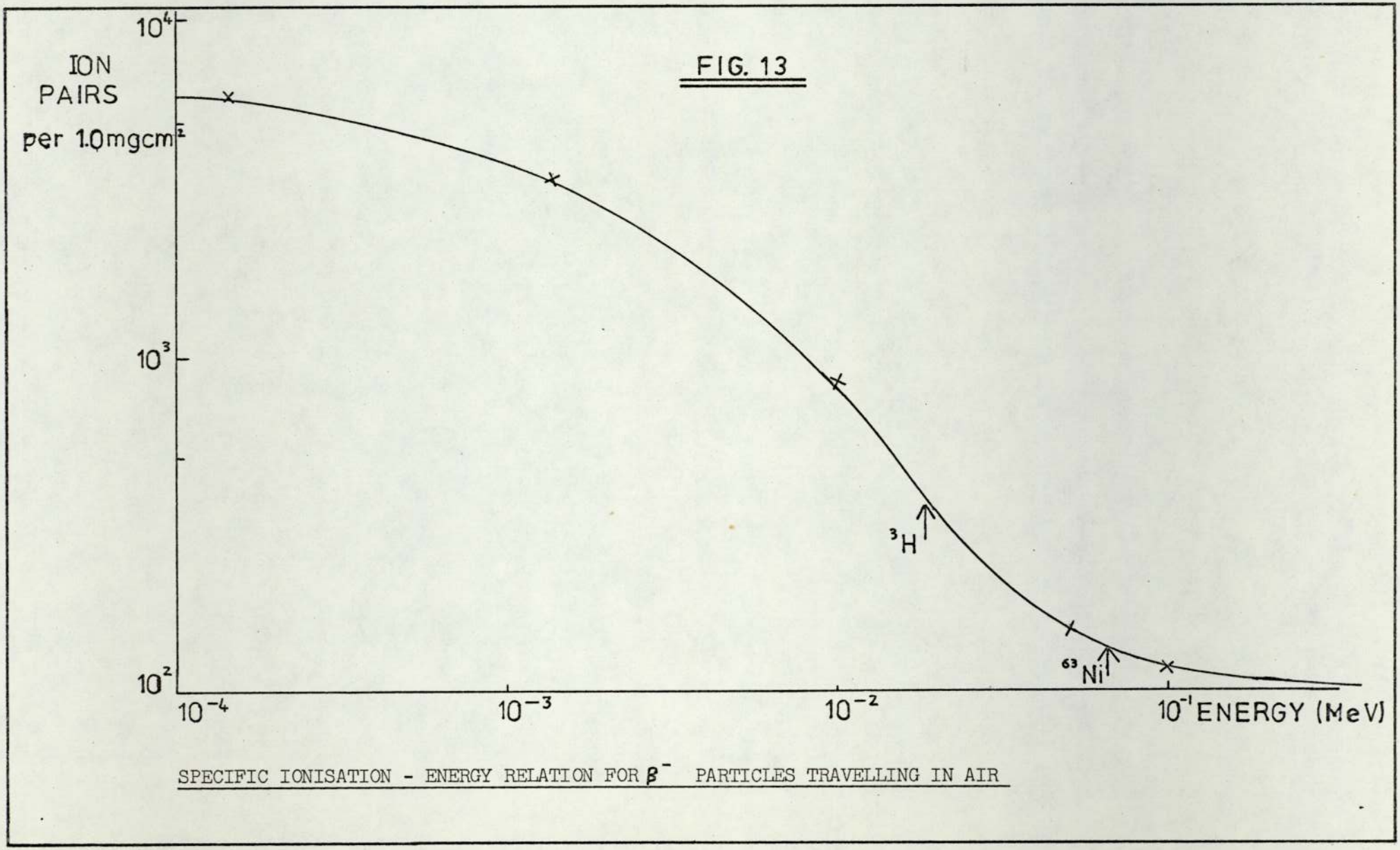

SPECIFIC IONISATION - ENERGY RELATION FOR β^- PARTICLES TRAVELLING IN AIR

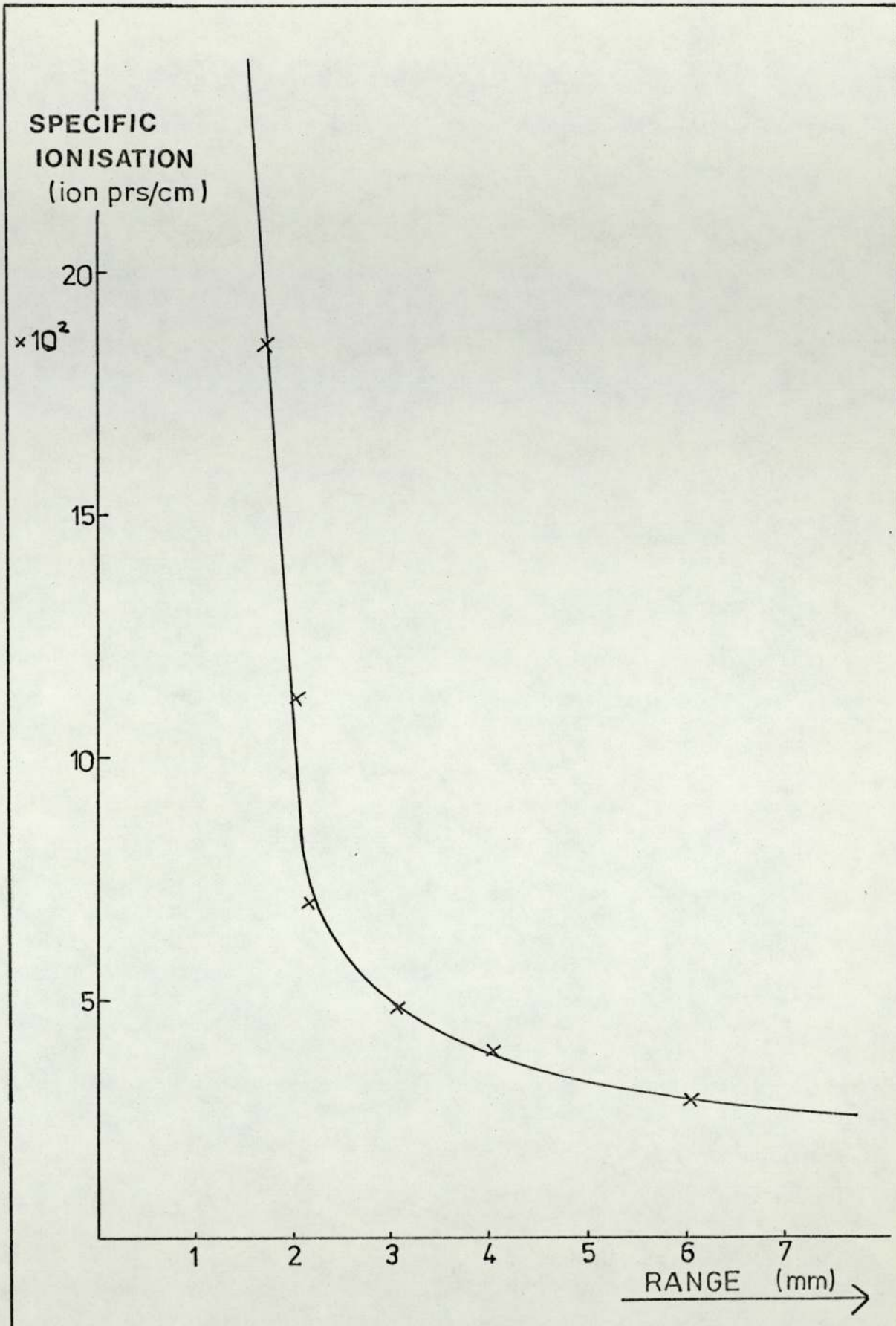

FIG. 14

SPECIFIC IONISATION - RANGE RELATION FOR β^- PARTICLES

tion can be calculated from the foil thickness (x) and the absorption coefficient (m),

$$\frac{R_o}{R} = \frac{1}{mx} \left[\exp (- mx) \right]$$

where R_o and R are the measured and true counting rate respectively. The foil thickness can be estimated as follows :

$$\beta^-\text{s emitted by foil} : (0.15\text{Ci cm}^{-2} \times 3.7 \times 10^{10}\ \text{s}^{-1}$$

$$= 5.55 \times 10^9\ \text{cm}^{-2}\ \text{s}^{-1}$$

The decay rate constant is $(0.6933/3.87 \times 10^8\ \text{s}) = 1.792 \times 10^{-9}\ \text{s}^{-1}$ and hence there are $3.097 \times 10^{18}\ \beta^-\ \text{cm}^{-2}$. Assuming one atom of tritium per atom of titanium, the foil thickness is,

$$\frac{3.097 \times 10^{18}}{6.02 \times 10^{23}} \times 50.92\text{g} = 0.26\ \text{mg cm}^{-2}$$

With a typical absorption coefficient of approximately 3.0 $\text{cm}^2\ \text{mg}^{-1}$, this gives a self absorption of 59%. Loss in emitted radiation through self-scattering is likely to be of the same magnitude.

An estimation of the current arising from ionisation of carrier gas molecules can now be made. Assuming that β^- particles emitted from the top 0.13 mg/cm^2 manage to escape, and considering losses through self absorption and scattering, a 150 mCi source is effectively about $0.15 \times 3\ (1/2) = 0.02\ \text{Ci cm}^{-2}$ which corresponds to $7 \times 10^8\ \beta^-$ particles $\text{cm}^{-2}\ \text{s}^{-1}$. Considering energetic electrons from a tritium source, the number of ion-pairs formed by each β^- particle is about 2.9×10^2. Hence, the number of electrons produced may be calculated to be 2.0×10^{11} electrons per second which corresponds to a current of 3.3×10^{-8} A. The measured current (3.4×10^{-9}) compares well with this, considering the assumptions made.

A radiochemical examination of the tritium foil[51] revealed the presence of two other radioactive species of 0.33 and 0.7 MeV. They were present in neglible amounts and considering their high energy, they could not contribute significantly to the ionisation of carrier gas molecules.

Figures (15) and (16) show the variation in current as a function of electrode spacing. At short separations the β^- particles emitted from the source (on the cathode) hit the anode and are lost through surface recombination. As the spacing is increased, more of them undergo ionising collisions with carrier gas molecules and hence the observed increase in current. However, when the electrode spacing exceeds the maximum range of the β^- particles, electrons formed in the plasma are lost through recombination as they traverse the cell. In the pulse mode of operation at large electrode spacings, the time the pulse is normally applied for (5 μs) is also too short for most of the electrons to be collected. In nitrogen the electron drift velocity is estimated to be 3.0×10^5 cms^{-1} (60). Hence, to travel a distance of 2.50 cm would require 8.33 μs — much longer than the applied pulse duration.

It is generally accepted that the range of β^- particles emitted by a ^{63}Ni source is about 8 - 9 mm. at NTP and this is borne out by Fig. (16). However, the results obtained with the ^3H source do not support the normally assumed value of about 2.5 mm. The maximumappears at about 6.5 mm. which is in agreement with the calculated maximum range of β^- particles from a tritium source. The result points towards a much larger reaction zone in ECD's equipped with this source.

Varying electrode separation while operating the cell in the d.c. mode (Fig. 17) also supports the above conclusion. The current reaches its peak value at about 6.0 mm. The graph also shows that at high field strength (40 Volts cm^{-1}) and flow, the

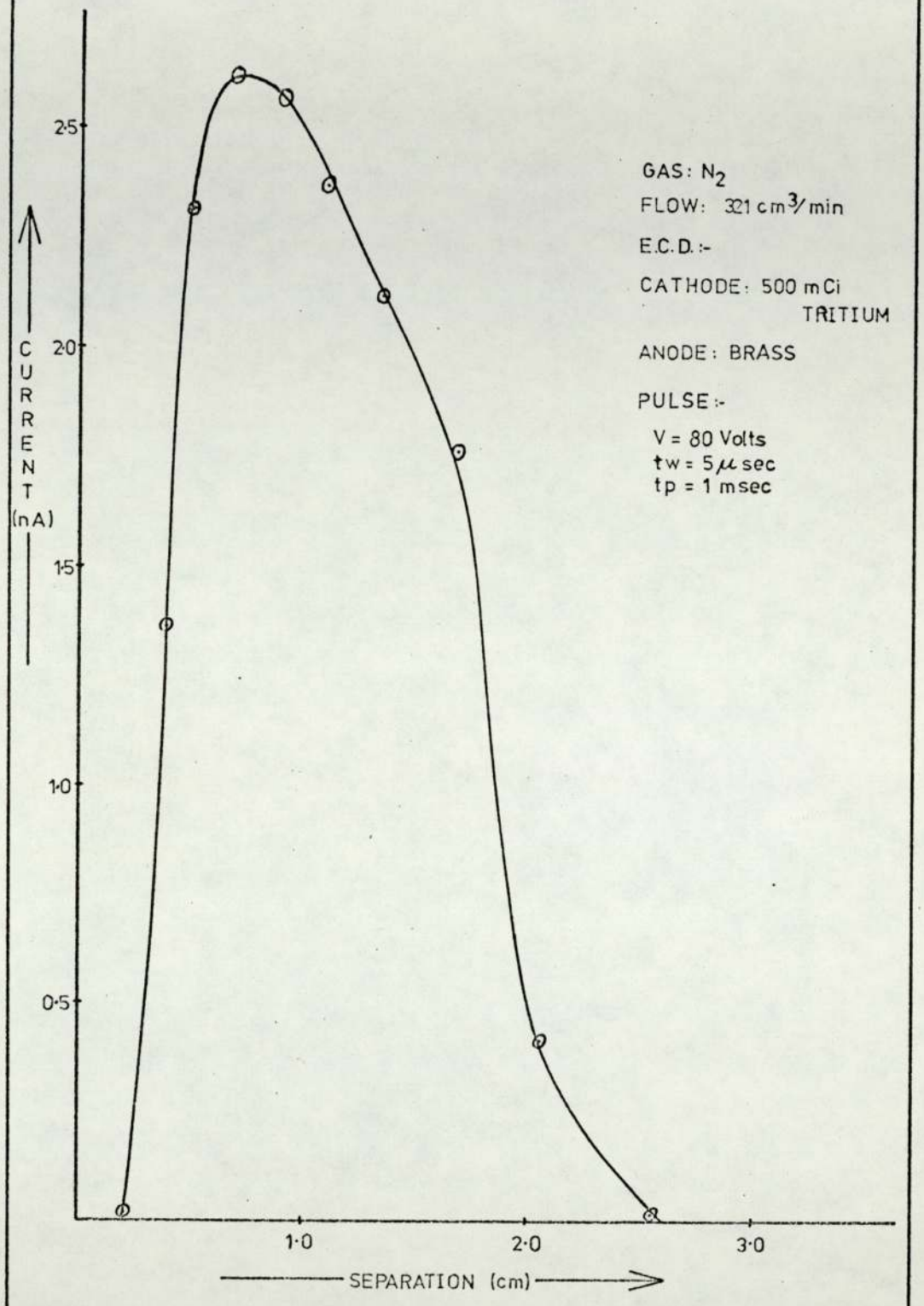

FIG. 15

CURRENT AT VARIOUS ELECTRODE SPACINGS
(SOURCE: ^3H)

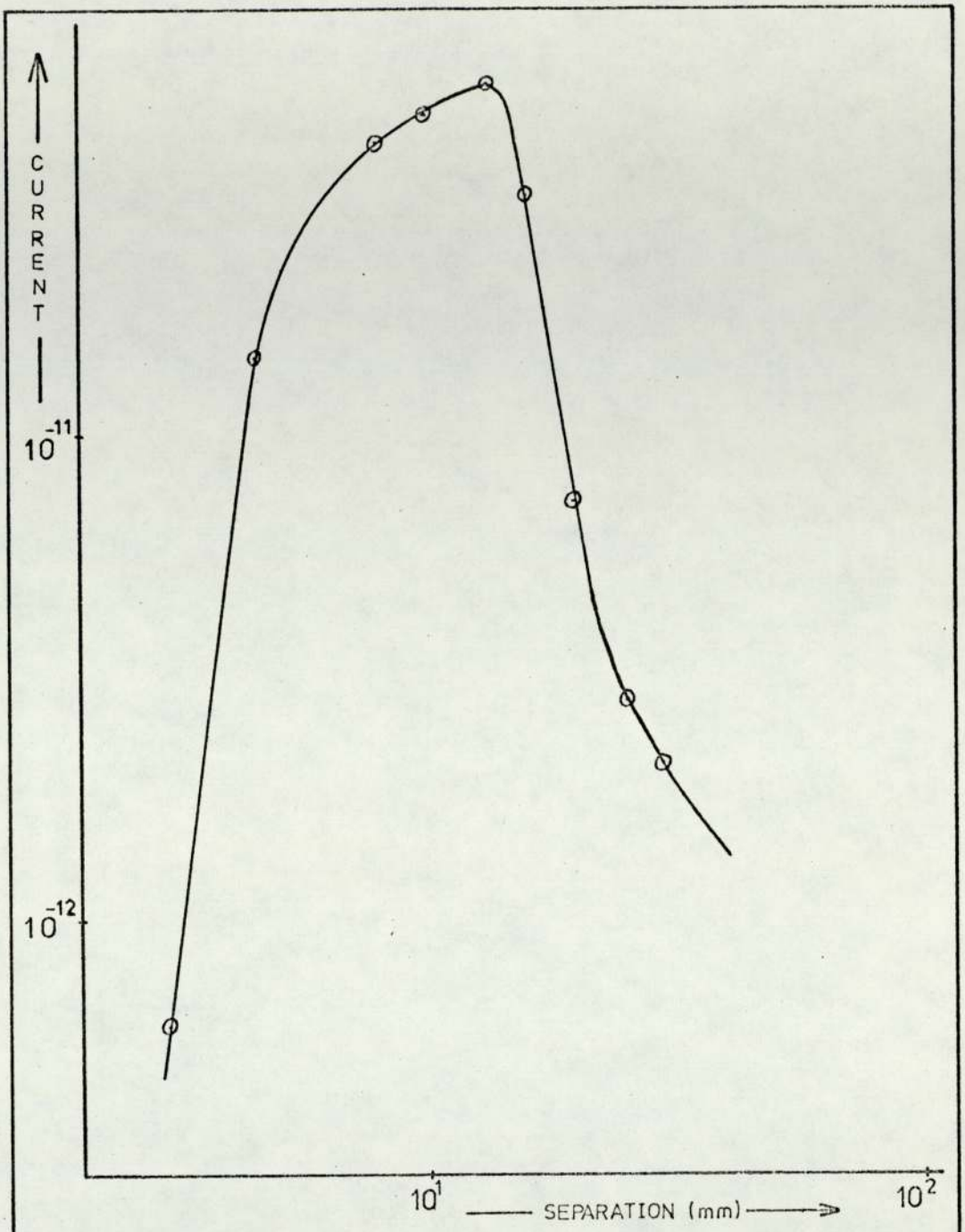

PULSE CONDITIONS:-

V = 90 Volts
tw = 5μsec
tp = 1 ms

GAS: N_2
FLOW: 135 (228 cm^3/min)
E.C.D. :-
CATHODE: 0.5mCi Ni^{63}
ANODE: BRASS

FIG. 16

CURRENT AT VARIOUS ELECTRODE SPACINGS (SOURCE: ^{63}Ni)

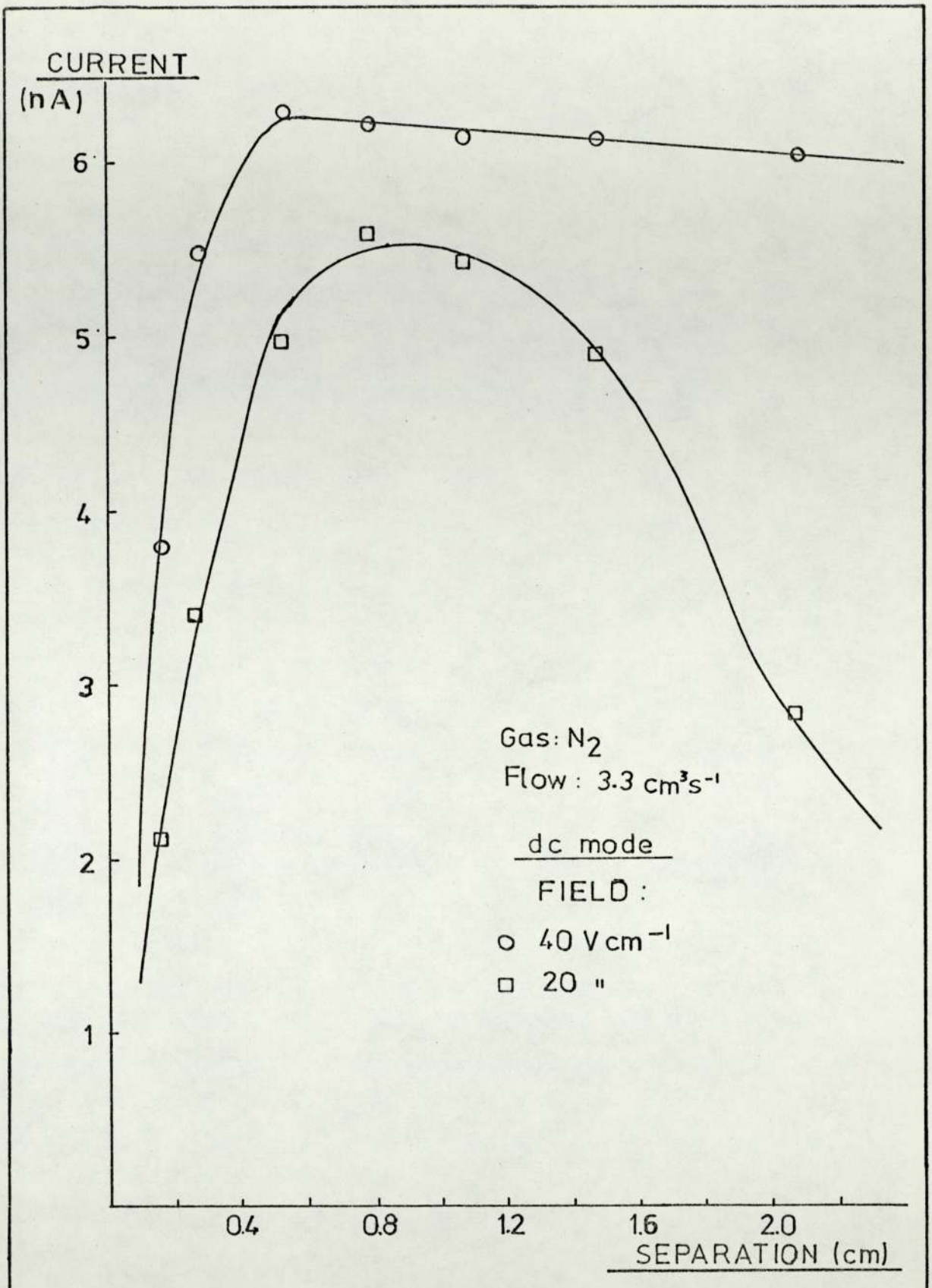

FIG. 17

CURRENT - ELECTRODE SEPARATION RELATION FOR d.c. MODE

current decreases very gradually with increasing separation indicating that almost all charged particles present in the cell are being collected at the electrodes. However, at low field strength (20 Volts cm^{-1}) the decrease in current is very steep, similar to that observed under the pulsed mode. As recombination seems to be the dominant process of loss under these conditions, an attempt was made to calculate the electron-ion recombination coefficient.

As a first approximation, the time rate of change of electron concentration is

$$\frac{de}{dt} = -ke^2$$

assuming that the electron and positive ion concentrations are equal. The solution of the above equation is

$$\frac{1}{e} = kt + \frac{1}{e_o}$$

where e_o is the initial concentration of ion-pairs. At a field strength of 20 Volts cm^{-1}, the electron drift velocity is 2.25×10^5 cms^{-1}. Hence, the time taken to cross the cell at various cell distances can be calculated. Fig. (18) shows the variation of the inverse of the current with time. The slope of the graph is 5.49×10^{13} A^{-1} s^{-1}, and the recombination coefficient for nitrogen is then 1.62×10^{-5} cm^3 s^{-1} which is about an order of magnitude too large. This is to be expected considering the simplifications and assumptions made.

Another approach explaining the decrease in current with increasing separation can be based on the consideration of Eq.(20) (without the negative ion term) at steady state.

$$V\frac{de}{dt} = k_1 AG - k_2 Vep - Fe.e = 0$$

The electron concentration is,

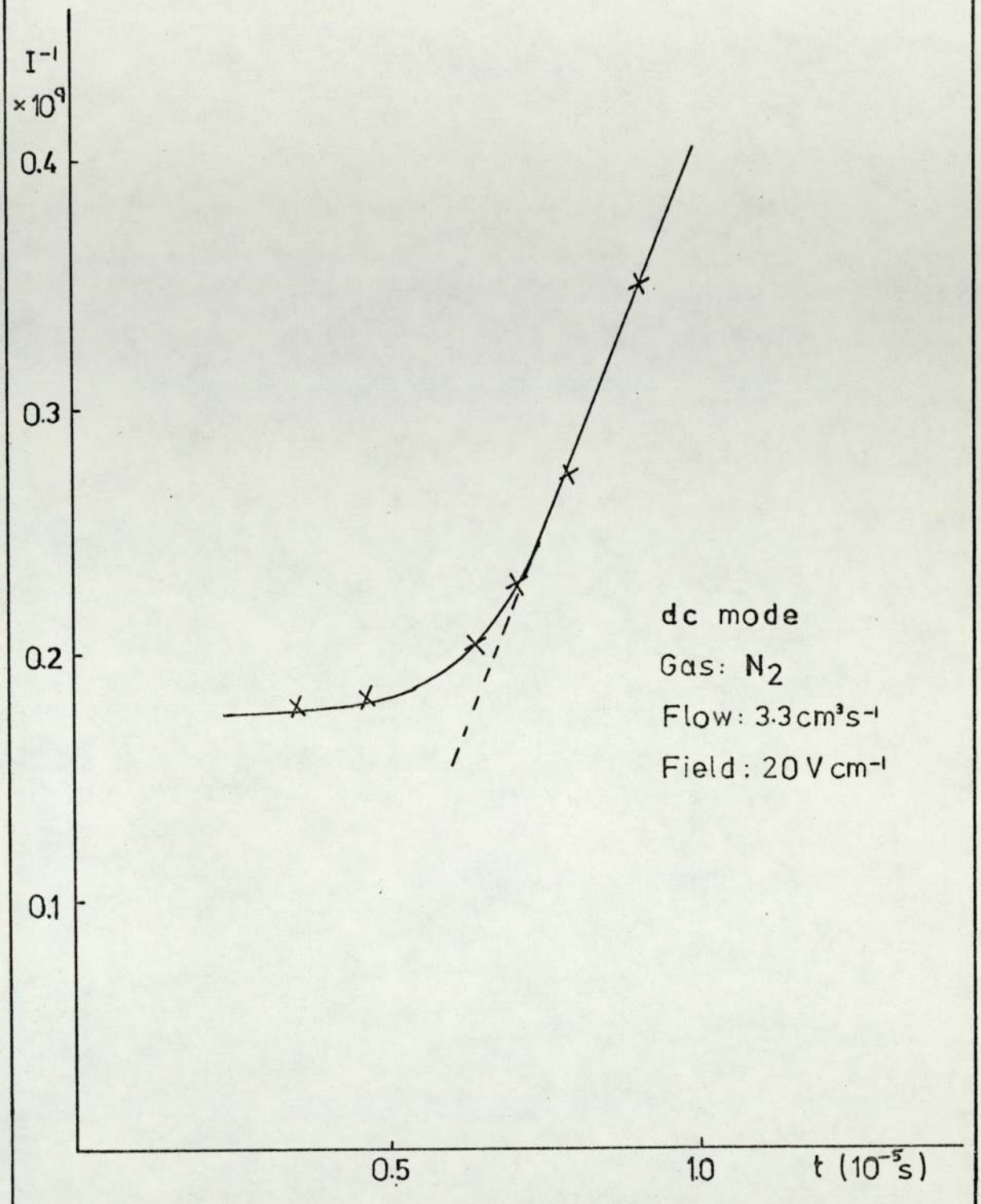

FIG. 18

THE INVERSE OF CURRENT VERSUS ELECTRON TRANSIT TIME

$$e = \frac{k_1 G}{(k_2 lp + Fe/A}$$

where l is the inter-electrode separation. Assuming an order of magnitude value for p ($\simeq 10^9$), the value of e at l = 1.8 cm. is 2.22×10^6 cm^{-3} which gives a current of 0.36 nA. This compares well with the experimental value of 0.72 nA, considering the approximate value of p.

Since the density of the medium has an effect on the range of the β^- particles, electrode spacing studies were carried out at constant pressure using various carrier gases. The density decreases in the following order :

$$Ar > Ar + CH_4 > C_2H_4 > N_2 > He$$

Fig. (19) compares the range of β^- particles in Ar + 5% CH_4 and He. The former has a density ($\simeq 0.1786$ gl^{-1}) which is about ten times greater than that of the latter. The graph shows that in helium the current reaches its peak value at about 1.25 cm. while in Ar + CH_4, the corresponding separation is about 0.6 cm. The behaviour is as expected and it appears that a ten fold increase in density of carrier gas corresponds to a reduction in range of β^- particles by one half.

As stated earlier, when the radiation source is considered on its own, a large number of ion-pairs form in close vicinity of the source. However, as part of the detector, it appears that most ion-pairs are formed some distance away from the source, indicating that high energy β^- particles are responsible for ionisation of carrier gas molecules. Scolnick[46] arrived at a similar conclusion.

Emission of bremsstrahlung radiation by the β^- particles has been suggested to be partly responsible for ionisation. The radiation in question arises from the acceleration of an electron

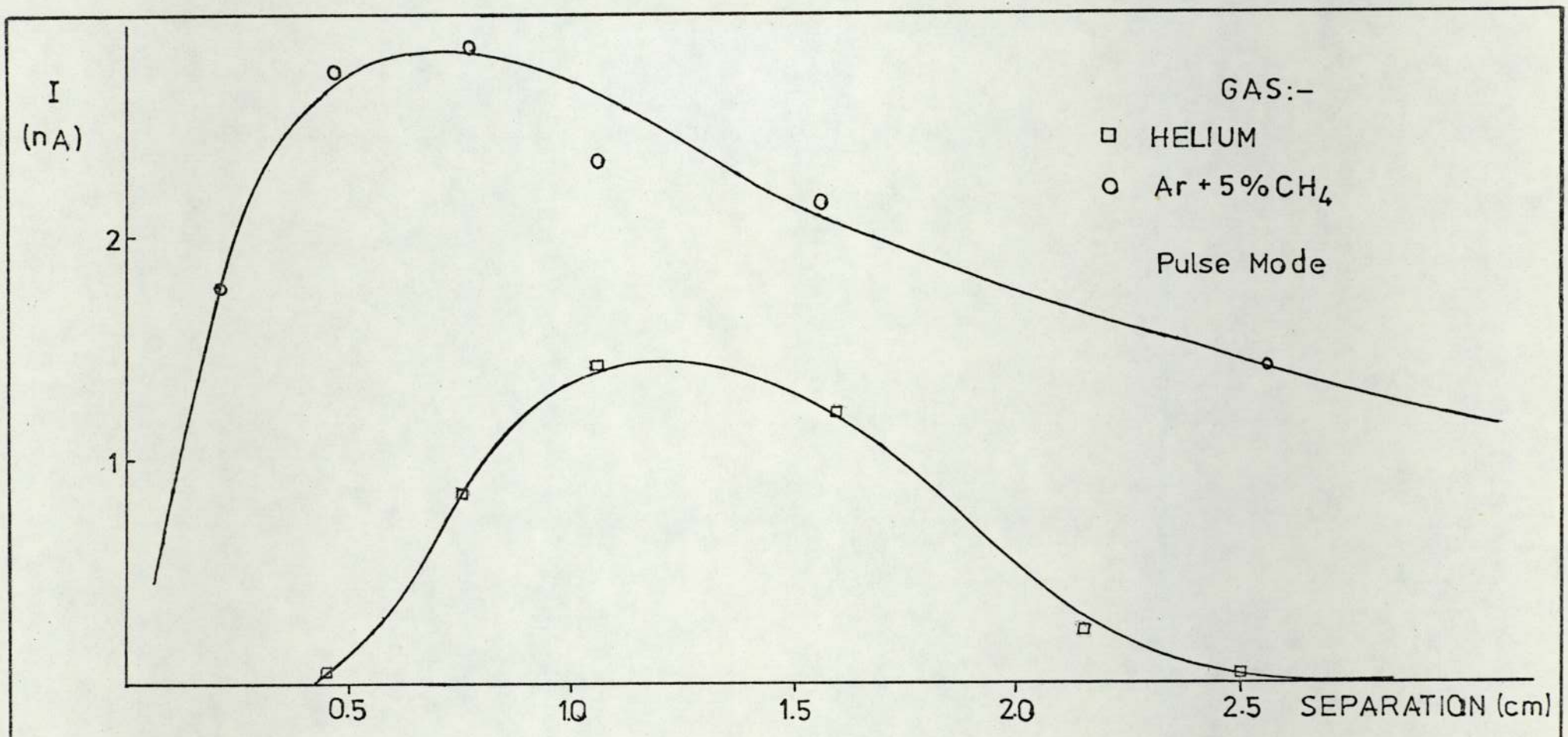

FIG. 19

CURRENT - SEPARATION PLOTS FOR **He** AND **Ar** + CH_4

by an atomic or ionic field. The ratio of energy loss by bremsstrahlung radiation to energy loss by ionisation in an element of atomic number Z is approximately equal to EZ/800, where E is the electron energy in MeV.[15] In the case of nitrogen, this energy loss is 0.016% for β^- particles from ^3H source and 0.058% for ^{63}Ni source. Ionisation arising from bremsstrahlung radiation appears to be unimportant for the sources normally used.

The effect on current flow in an assymmetrical cell was investigated. One electrode in turn was fixed very close to the gas inlet and the separation was varied by changing the position of the other. There was no significant difference between the two (Figs. 20 and 21) except for a slightly higher current for the case where the cathode was fixed. The effect of flow on the plasma may be responsible for this observation.

In comparison to the symmetrical cell, the plasma seems to be more diffused in both cases of the assymmetrical cell. In the latter configuration the current is either increasing or at its plateau value until the separation is about 1.4 cm; this is unlike the former configuration where the current is on the decline only after about 0.7 cm. The vortices in the flow pattern could enhance diffusion of the plasma contained in the assymmetric chamber since the electrode fixed close to the gas inlet behaves as a reflecting surface.

Two ^3H sources of different activities and of almost the same area were investigated. The activities were approximately 150 and 500 mCi. Assuming that the two foils had similar characteristics, such as the presence of other radiation sources, the theoretical ratio of their activities is 3.33. Currents measured for the two sources, under both the d.c. and pulsed modes, are given in Table 3. At long pulse interval the mean ratio of currents measured under similar conditions for the two sources is 2.84 while

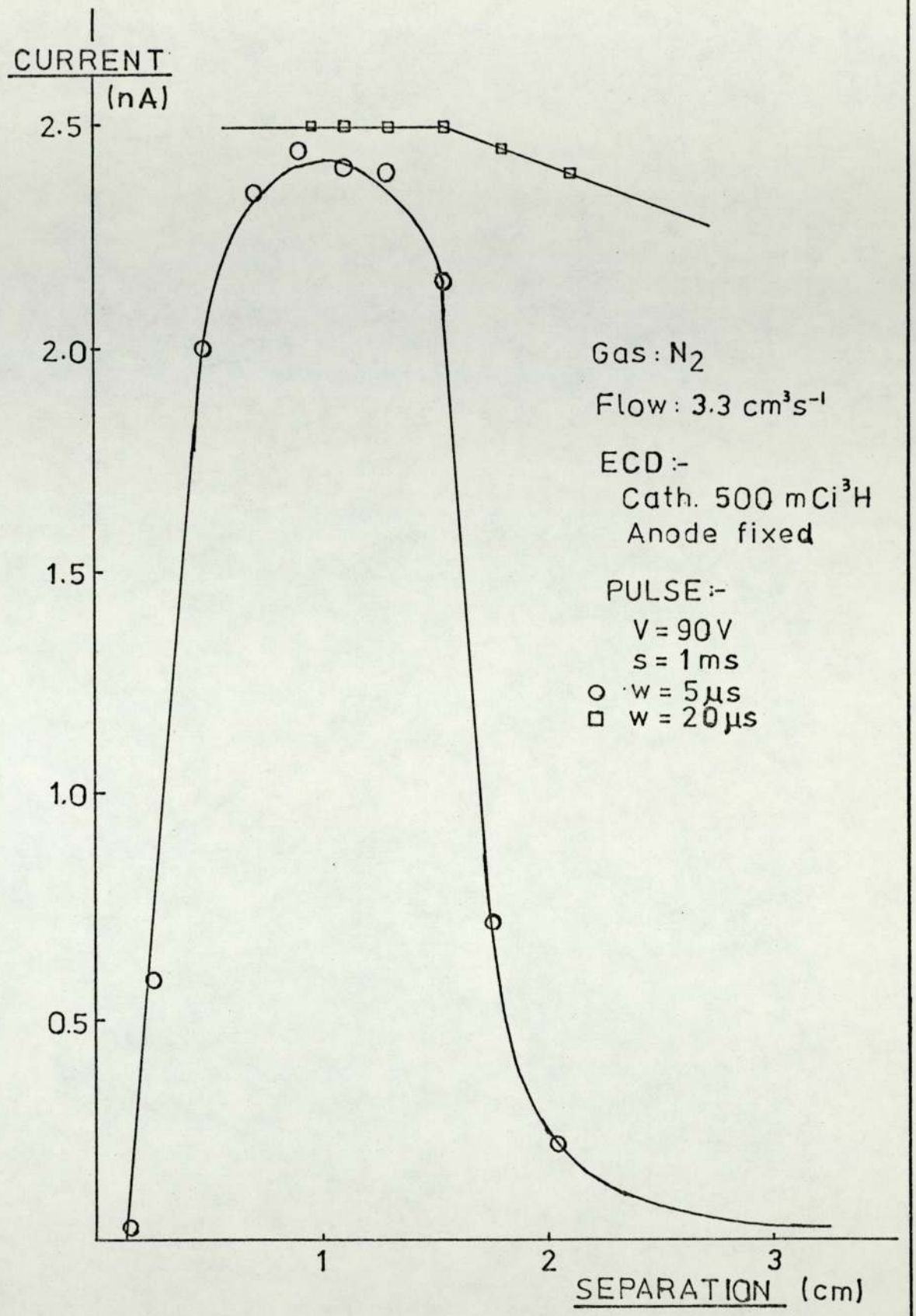

FIG. 20

CURRENT VARIATION IN AN ASSYMMETRICAL CELL - ANODE FIXED

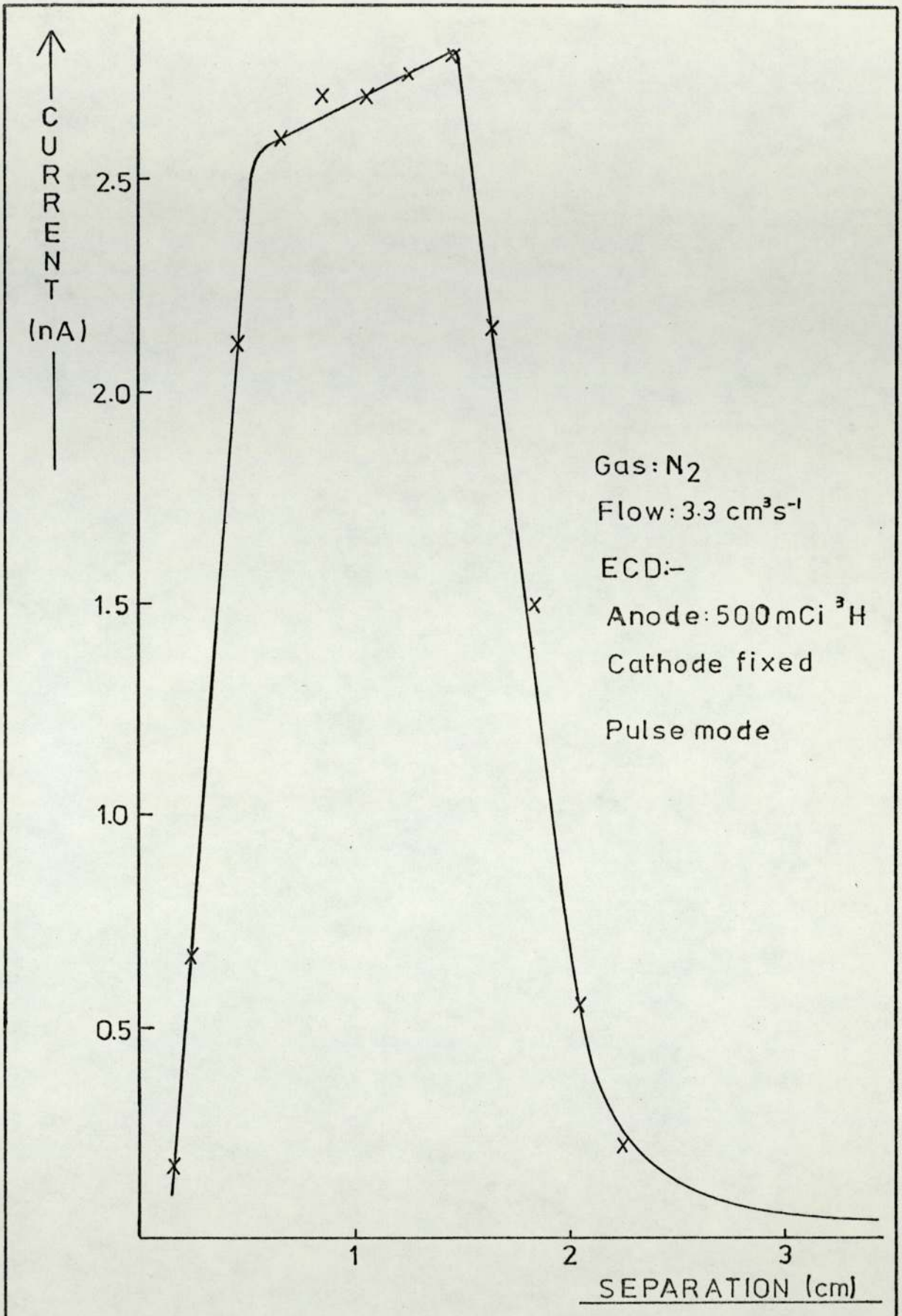

FIG. 21

CURRENT VARIATION IN AN ASSYMMETRICAL CELL - CATHODE FIXED

TABLE 3

COMPARISION OF CURRENTS FROM ^{3}H SOURCES OF DIFFERENT ACTIVITIES

gas : N_2 ECD :- Pulse:

Flow: 3.2 cm^3 s^{-1} Anode: Brass V = 90 Volts

Separation: 1.0cm. W = 5 μ s

SOURCE ^{3}H	d.c. SATURATION CURRENT I	PULSE INTERVAL, S					
		50μs	100 μ s	250 μ s	1 ms	1.5 ms	2.0 ms
500 mCi	6.50 nA	6.10nA	5.85nA	5.0 nA	2.40nA	1.65nA	0.87nA
150 mCi	3.40 nA	3.33nA	3.15nA	2.55nA	0.82nA	0.59nA	0.31nA
I0.5/0.15	1.91	1.85	1.86	1.96	2.93	2.80	2.81

short pulse interval and under the d.c. mode, the ratio is 1.90. Considering that the two activities are not precisely known (especially the lower one) it seems reasonable to conclude that the current at long pulse interval varies by the same ratio as that of the activities of the sources. However, at short pulse interval, the current ratio of the two foils is about one half of the theoretical ratio. Space charge effects may be responsible for the observed difference in the mean ratios. At short pulse periods, for the current ratio to be close to the theoretical, the 500 mCi currents need to be much higher. However, this in practice is not possible as relatively denser space charge exists since loss through recombination is minimal under these pulse conditions.

Comparison of detector currents arising from sources providing β^- particles of different energies is much more difficult as sources tend to have different activities as well. Considering a 500 mCi ^{3}H source and a 0.5 mCi ^{63}Ni source, the average current ratio was found to beabout ten times larger than the ratio of their energies, ie.

$$^{63}Ni\ /\ ^{3}H = 67\ KeV/18.6\ KeV = 3.60$$

Other sources which have recently come into use are ^{90}Sr, ^{147}Pm and ^{241}Am. Alternative sources are necessary mainly because of the need to work at higher detector temperatures. The generally acceptable temperature limit for the ^{3}H source is 225°C while that for the ^{63}Ni source is 350°C. Detectors equipped with ^{147}Pm can be heated to 400°C [52] and the maximum operating temperature for ^{241}Am is 500°C.[53] At elevated temperatures a considerable loss in activity results and this leads to large variations in day-to-day standing currents. The emanation of radio-active material into the atmosphere of the room however, is a more serious consequence. A low level contamination of the environment (constituting a health

hazard) occurs with ^{3}H sources when the detector temperature exceeds 230°C.[54] A comprehensive study of possible radiation hazards arising from radioactive sources in ECDs has been made by Taylor.[55]

In normal operation, the radiation source is placed on the cathode and hence the electrons present in the plasma are drawn across the cell to the anode. Their greater mobility ($\simeq 10^{3} cm^{2} V^{-1} s^{-1}$) ensures that a relatively small applied voltage (about 25 Volts) gives saturation current. However, when the polarity of the cell is reversed, a considerably larger voltage is necessary for current saturation (Fig. 22). This is to be expected as the heavier positive ions with their lower mobility ($\simeq 2.5 cm^{2} V^{-1} s^{-1}$) need to be drawn across the cell to the cathode. The β^{-} particles from the source on the anode recoil to the source forming few ion-pairs. Fig. (23) shows the current variation with inter-electrode separation. Maximum current is observed at very small spacing since β^{-} particles of average energy have been shown to have a range of about 2mm. The current gradually decreases until a separation of about 6 mm, corresponding to the distance travelled by particles of maximum energy. Thereafter, the current declines steeply as ion-pairs are no longer generated and also losses through recombination are considerable. The initial decrease in current substantiates the explanation given (that ionisation zone extends to about 6 mm. from the source) for the increase in current observed when the source is on the cathode (Fig. 17).

4.6 PRESSURE AND FLOW RATE OF CARRIER GAS

Since the range of β^{-} particles depends on the number of molecules in their path, a shorter range is to be expected at higher pressures. The plasma volume would consequently decline. Figs. (24) and (25) show the current variation at pressures below and above atmospheric. The term G, the ion pair yield, is potentially

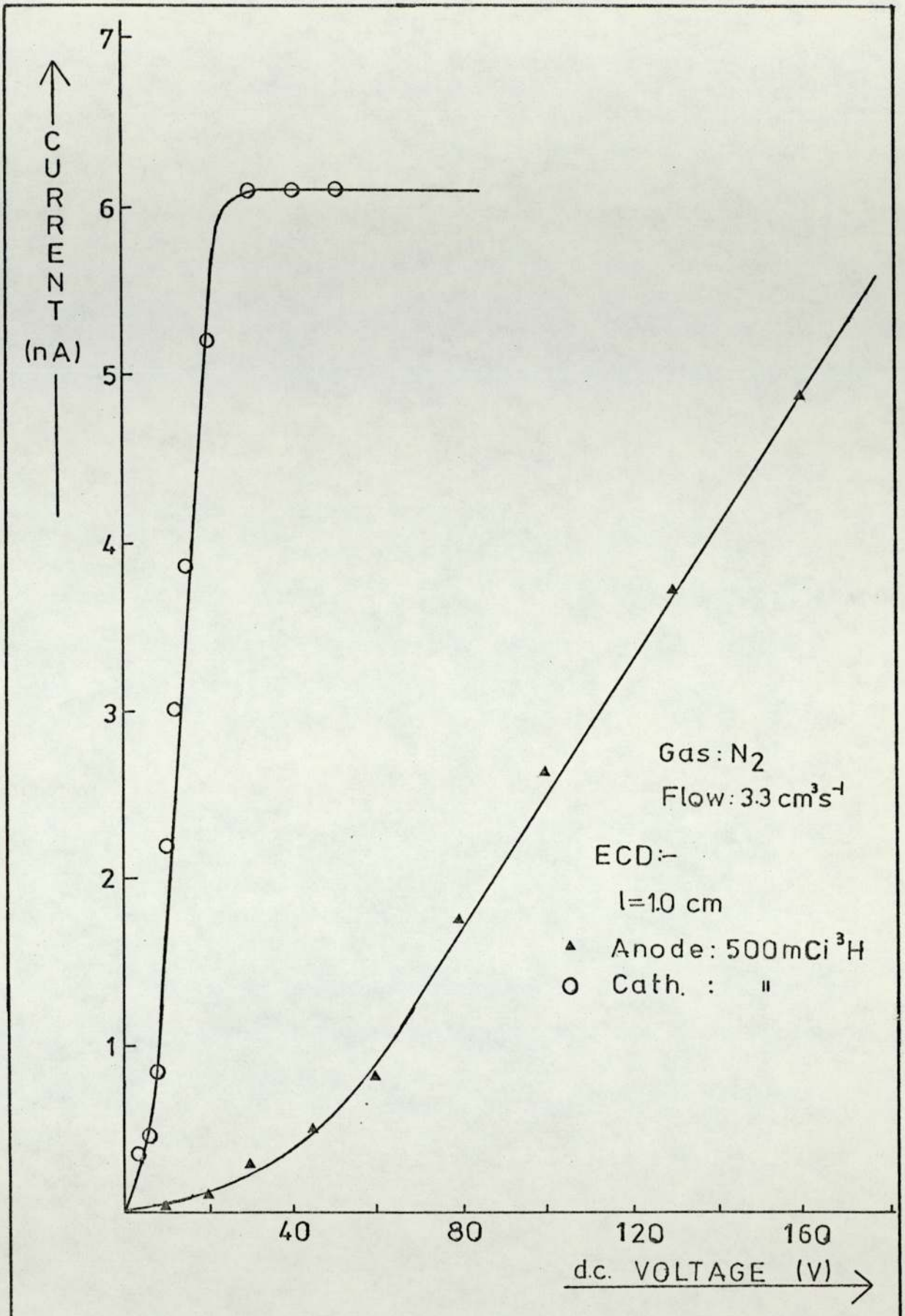

FIG. 22

THE EFFECT OF REVERSAL OF CELL POLARITY-SOURCE ON ANODE

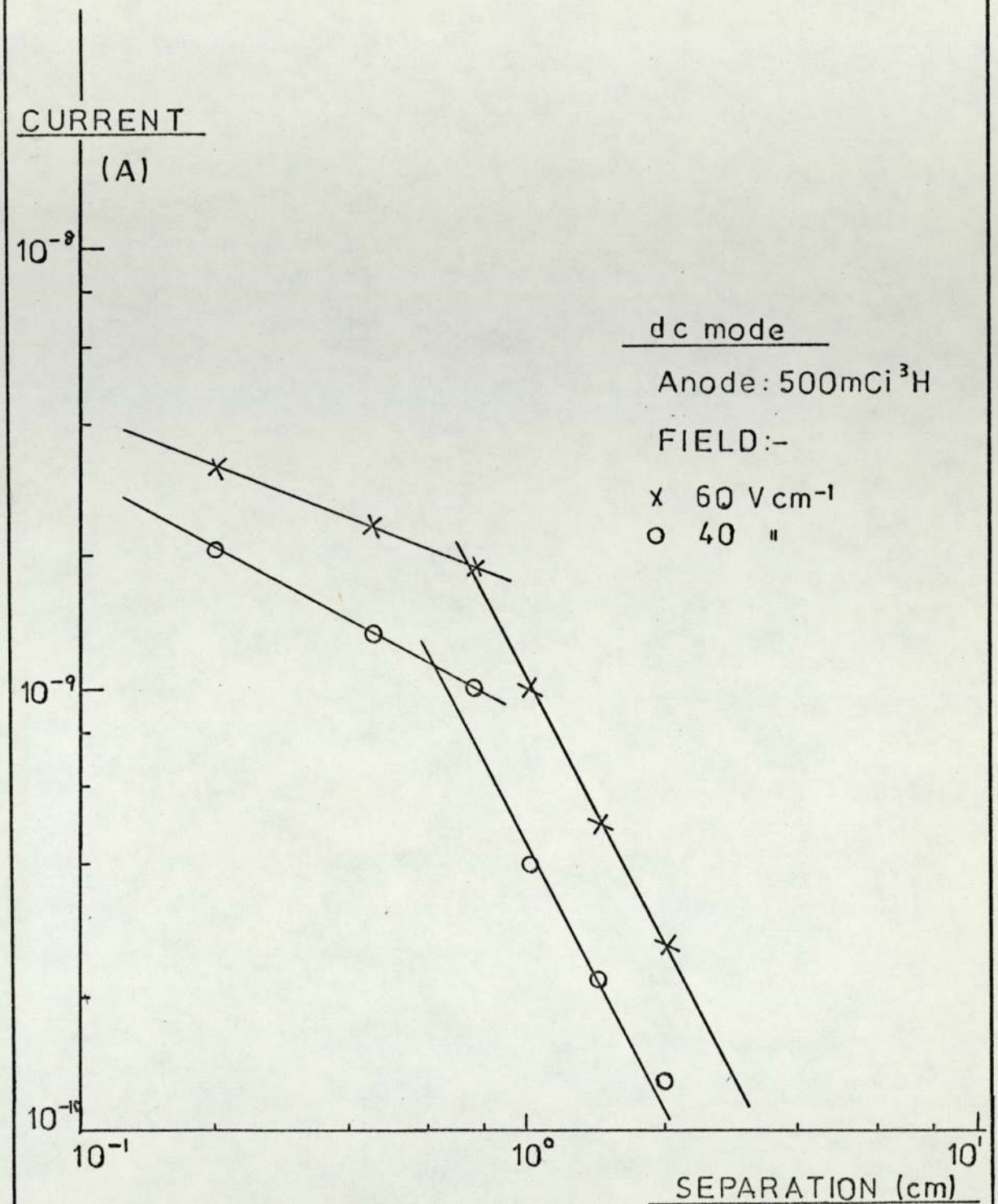

FIG. 23

CURRENT VARIATION WITH INTER-ELECTRODE SEPARATION - SOURCE ON ANODE

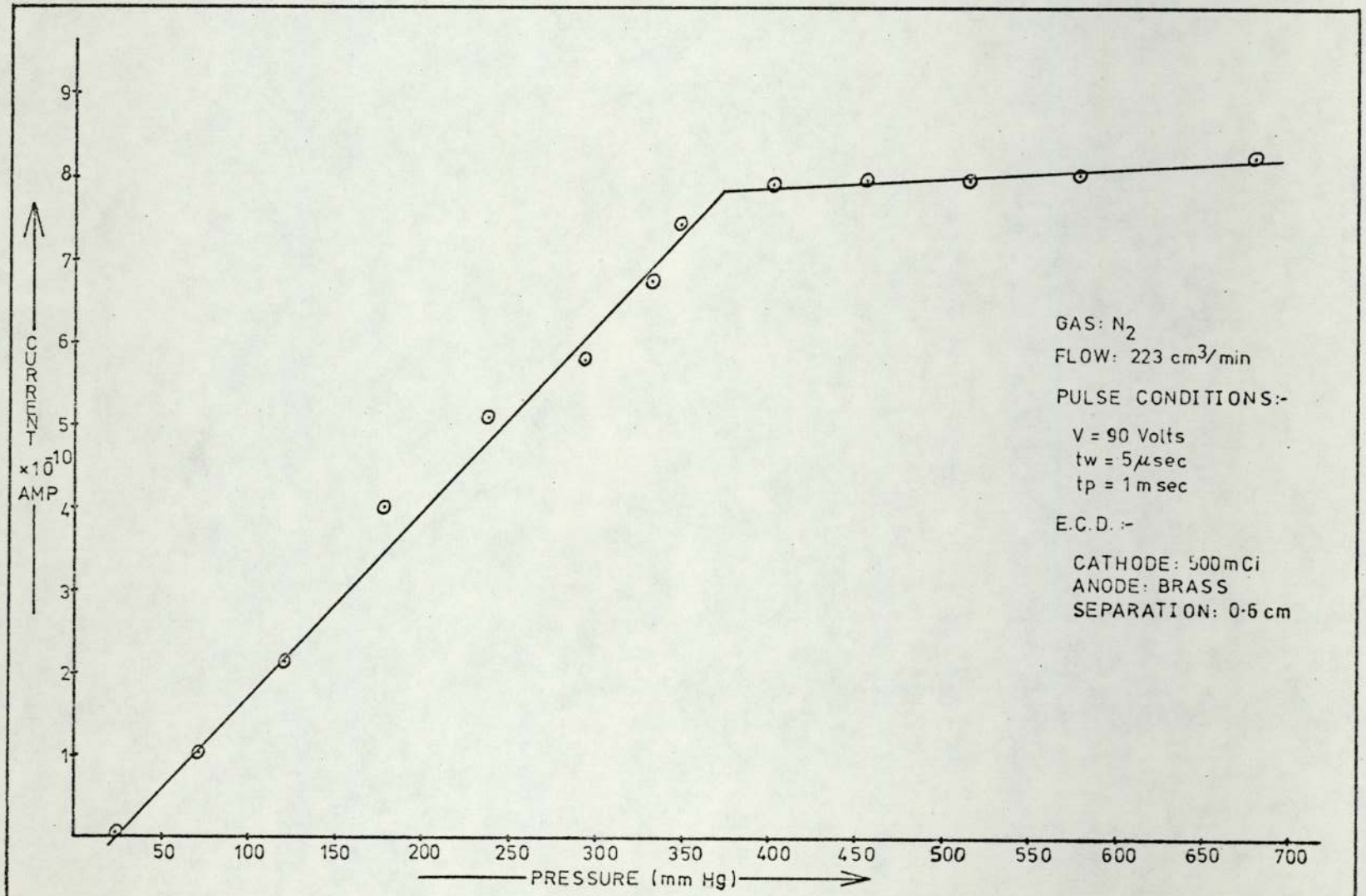

FIG. 24

CURRENT VARIATION WITH GAS PRESSURE (BELOW ATMOSPHERIC)

FIG. 25

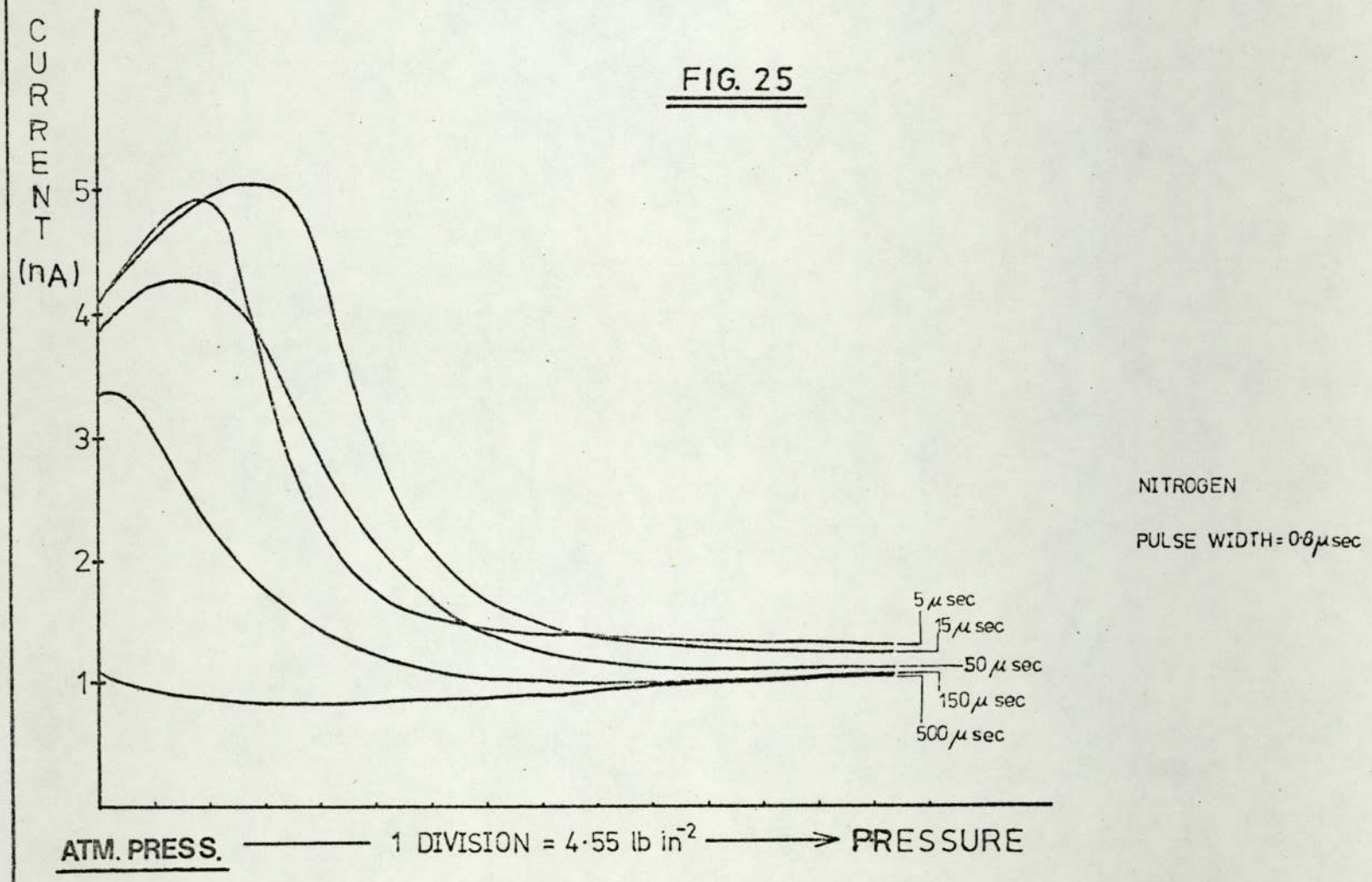

CURRENT VARIATION WITH GAS PRESSURE (ABOVE ATMOSPHERIC)

pressure dependent. The number of ion pairs formed, is equal to the product of the number of ion pairs per unit length and the path length. While the path (whose length is inversely proportional to the pressure) lies within the cell, this product is constant, but when the path length exceeds the inter-electrode spacing, the number of pairs will fall.

In terms of the proposed model,

$$a = be = e\,(k_2\, V p_o + Fe)$$

or $$\frac{a}{eV} = k_2\ p_o + \frac{Fe}{V}$$

If Fe/V is small and $p_o = eR$, then

$$e = \left(\frac{a}{k_2\, V\, R}\right)^{1/2}$$

The observed current, I, is to a close approximation, eV electrons per pulse. Hence,

$$I = V\left(\frac{a}{k_2\, V\, R}\right)^{1/2} = \left(\frac{k_1\, A\, G\, V}{k_2\, R}\right)^{1/2} \qquad [39]$$

The 'Gaines' factor, R depends partly on the relative drift velocities of electrons and positive ions and hence is a function of (X / P) where X is the applied field and P is the pressure. Since R is inversely proportional to the pressure and the volume of the plasma varies in a similar way, the current I, in accordance with Eq. [39], should be independent of the pressure as long as the path length is within the cell (ie. G is constant). This is the case at large pressures and the current is very nearly constant as shown in Fig. (24). At lower pressures, where G is proportional to the pressure, the current does exhibit a linear increase with pressure.

Changing electrode spacing at various pressures below atmospheric (Fig. 26) show that the range of β^- particles is considerably extended; for the tritium source, the range of particles

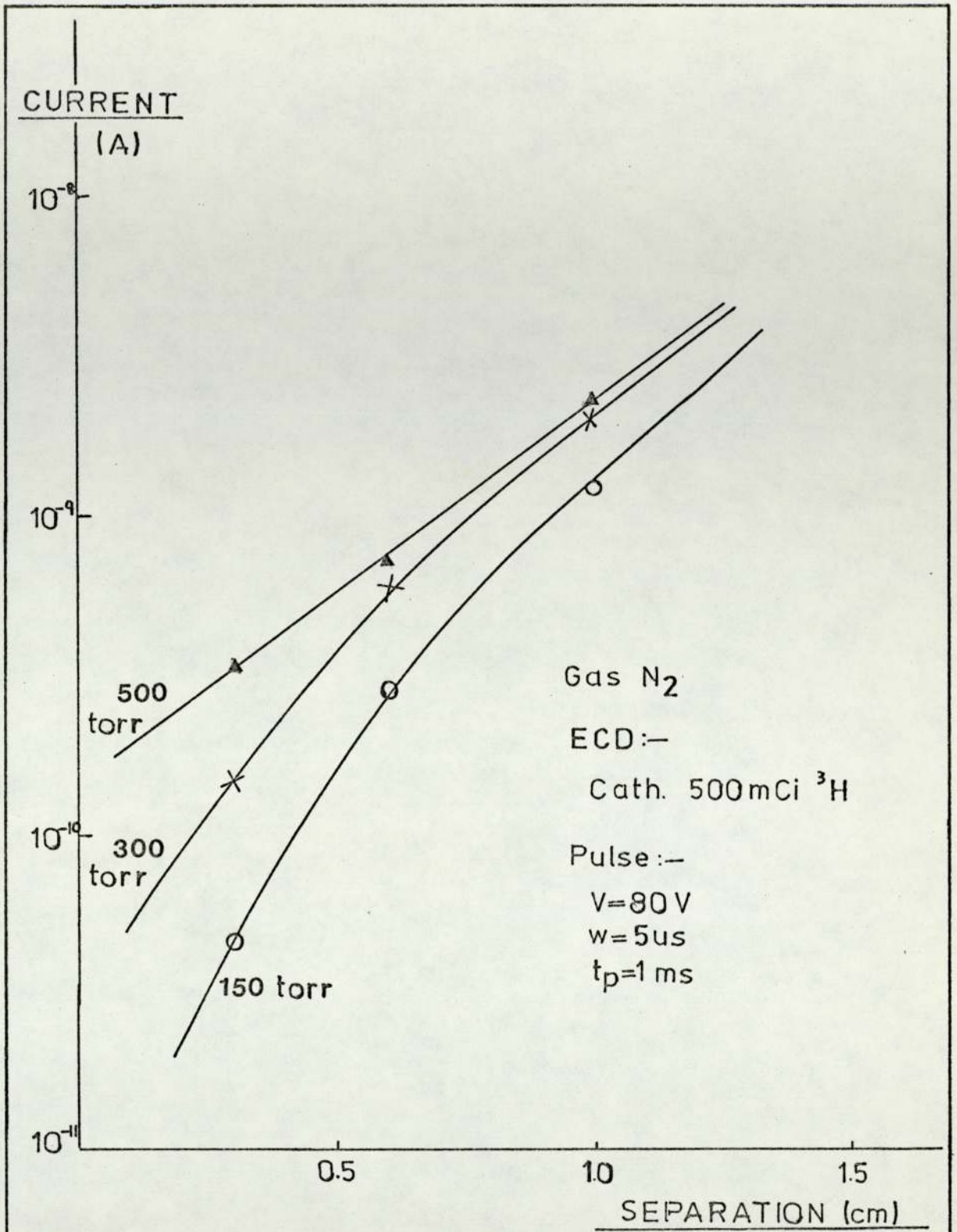

FIG. 26

CURRENT - CELL LENGTH RELATION AT VARIOUS PRESSURES

with high energy is greater than 1.0 cm even at pressures of about 500 mm Hg. Since studies were confined to a maximum cell length of 1.0 cm, it is not possible to determine exactly the dimension of the plasma at various pressures.

At pressures above atmospheric[56] the current declines steeply with increasing pressure. The high density of neutral molecules hinders collection of charges and also enhances volume recombination. Plotting the pulse interval against the magnitude of the pressure corresponding to the maximum current (Fig. 27) suggests that at atmospheric pressure, high electron concentrations (for coulometric response) are obtainable at long pulse periods (about 0.5 ms).

The effect of carrier gas flow rate on the response of the ECD has generated considerable controversy. As stated earlier, any detector whose response is concentration dependent would be affected by gas flow but only in the presence of sample molecules or varying pressure. However, in the ECD, the presence of a large excess of positive ions and the detector's extreme sensitivity has complicated the situation. Devaux and Guiochon[57] noted a decrease in standing current with decreasing flow rate. Burdett[32] concluded similarly. However, Lovelock[58] and Tommassen[59] have both found that the two parameters are not related in the pure carrier gas. Aue and Kapila[7] rightly pointed out there exists much confusion in the literature on this issue.

The present studies show that when the usual precautions are taken (as stated in 4.2) to obtain a 'clean' carrier gas in the normal ECD set up, there is a dependency on flow but only at very low flow rates. This was found to be the case in two different E.C. systems using metal and nylon tubing respectively. The variation in current was observed under both the d.c. (Fig. 28) and pulsed

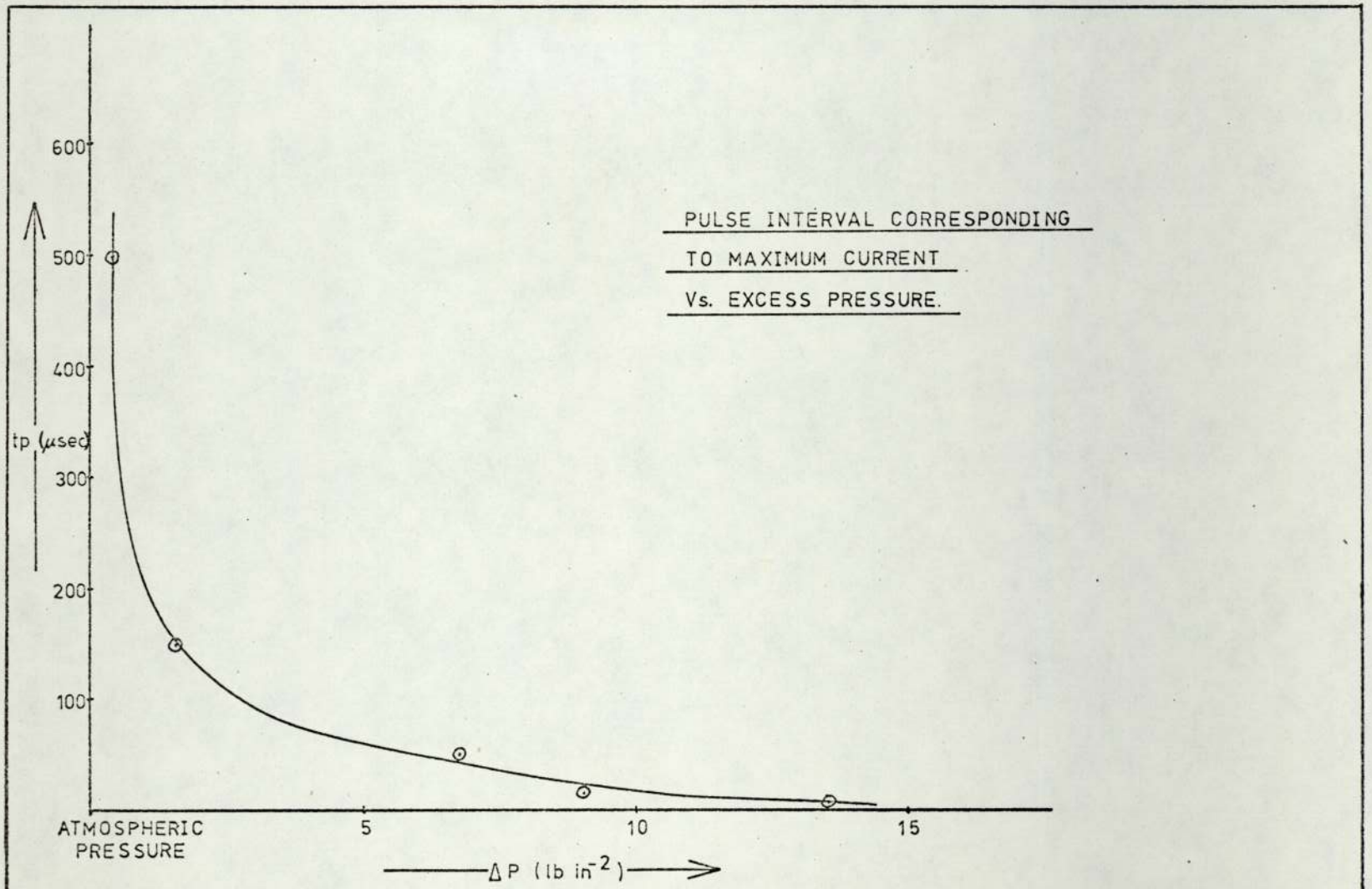
PULSE INTERVAL CORRESPONDING
TO MAXIMUM CURRENT
Vs. EXCESS PRESSURE.
600
500
400
300
200
100
tp (μsec)
ATMOSPHERIC
PRESSURE
5
10
15
ΔP (lb in⁻²)

FIG. 27

modes (Fig. 29) of operation. It is clear from these two graphs, that G.C. operators could have either observed a dependency on flow or not depending on the particular conditions under which results were obtained. In the continuous d.c. mode, the effect of flow is more apparent at lower voltages than at and above the critical voltage giving saturation current. In the pulsed mode, flow has a negligible effect on the standing current at shorter pulse interval and is magnified as the pulse period becomes longer. However, it seems that over a considerable range, above 20 cm^3 min^{-1}, there is almost no dependency, irrespective of the magnitude of the pulse interval. Similar results were obtained with 95% argon + 5% CH_4 as carrier gas (Fig. 30).

The presence of electron capturing contaminants in the carrier gas stream, whether originating from the gas itself or diffusing through the tubing and various joints, has been held responsible for the observed variation in standing current with gas flow rate.(59)

An analysis of the effects of a capturing impurity is briefly presented. Two possible situations could arise :

1) The concentration of the contaminant is constant, Co, and is entering the cell at the same flow rate as the carrier gas (U). This would be the case if it is present in the gas supply. At steady state,

Rate of entry of impurity = Co U/V

Rate of outflow = Co U/V

Rate of formation of negative ions = kC e

where k is the capture coefficient and e is the electron concentration in the cell.

Hence, $Co = C\,(1 + kVe / U)$

The rate of loss of electrons = $kCe = \frac{k\,Co\,e}{1 + (kVe/U)}$ [40]

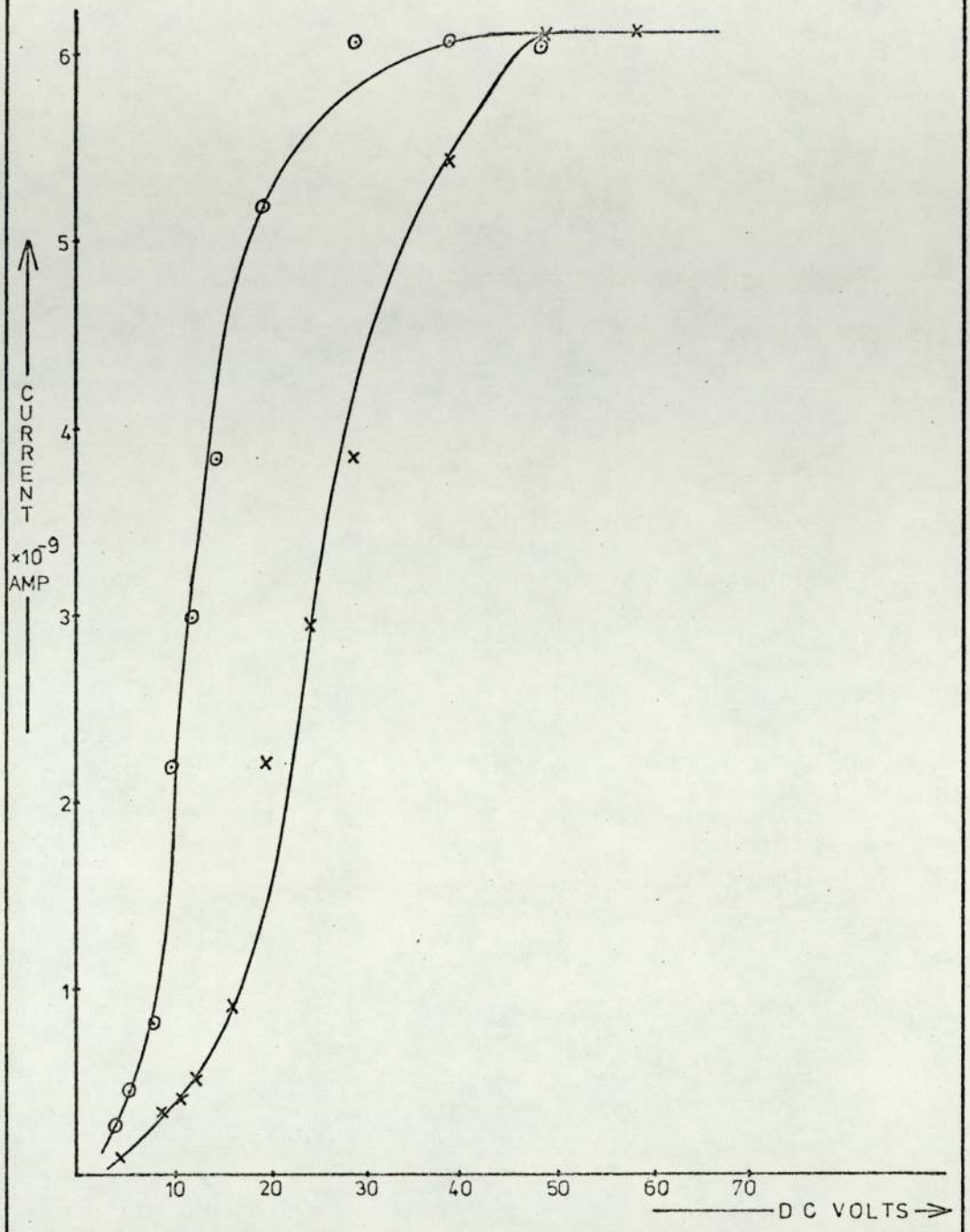

GAS: N_2

FLOW:-

× 6 cm^3/min

⊙ 230 cm^3/min

E.C.D. :-

CATHODE: 500 mCi TRITIUM

ANODE: BRASS

SEPARATION: 1·05 cm

FIG. 28

THE EFFECT OF CARRIER GAS (N_2) FLOW ON CURRENT IN d.c. MODE

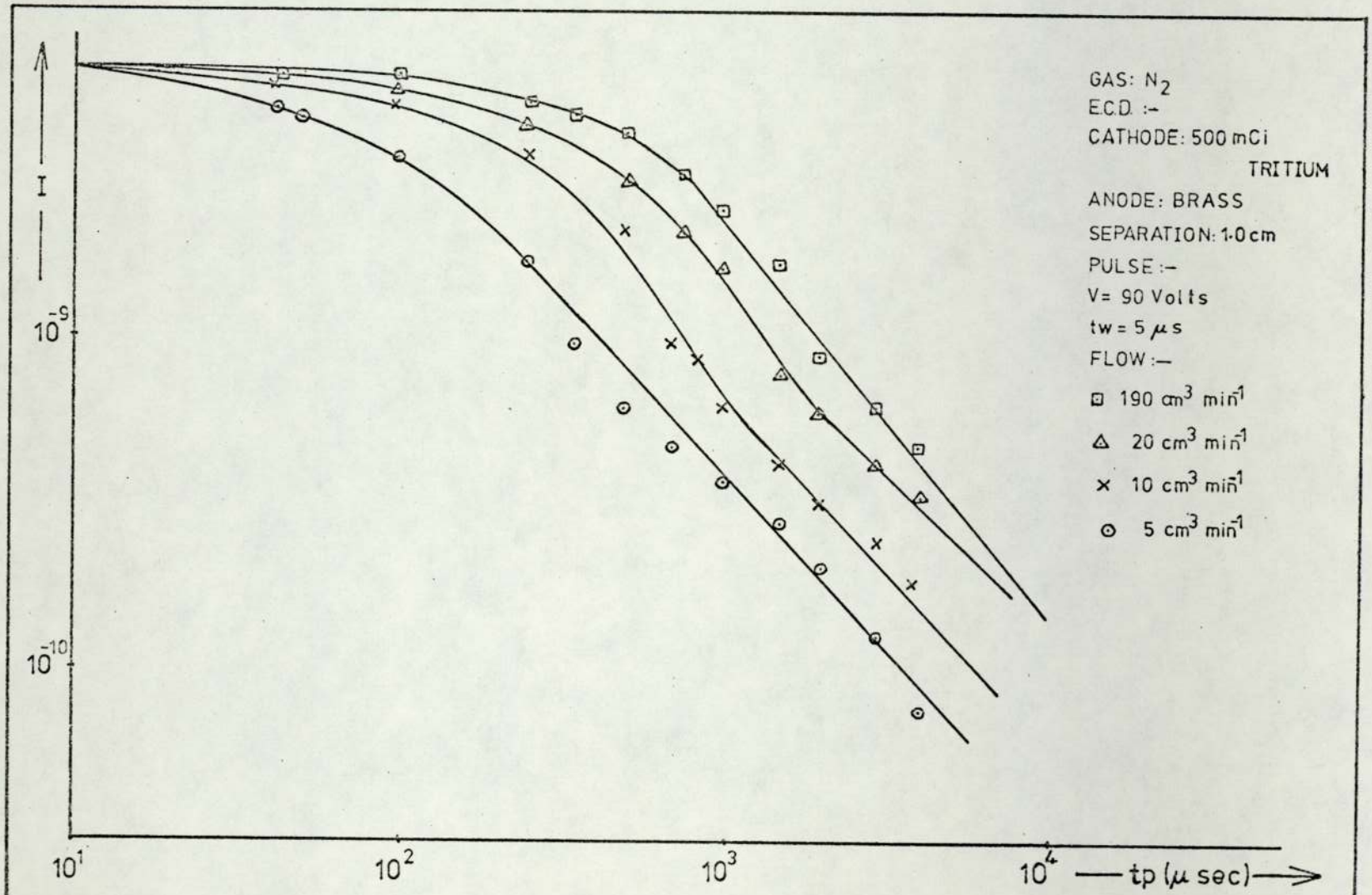

FIG. 29

CURRENT VARIATION WITH GAS FLOW IN THE PULSED MODE

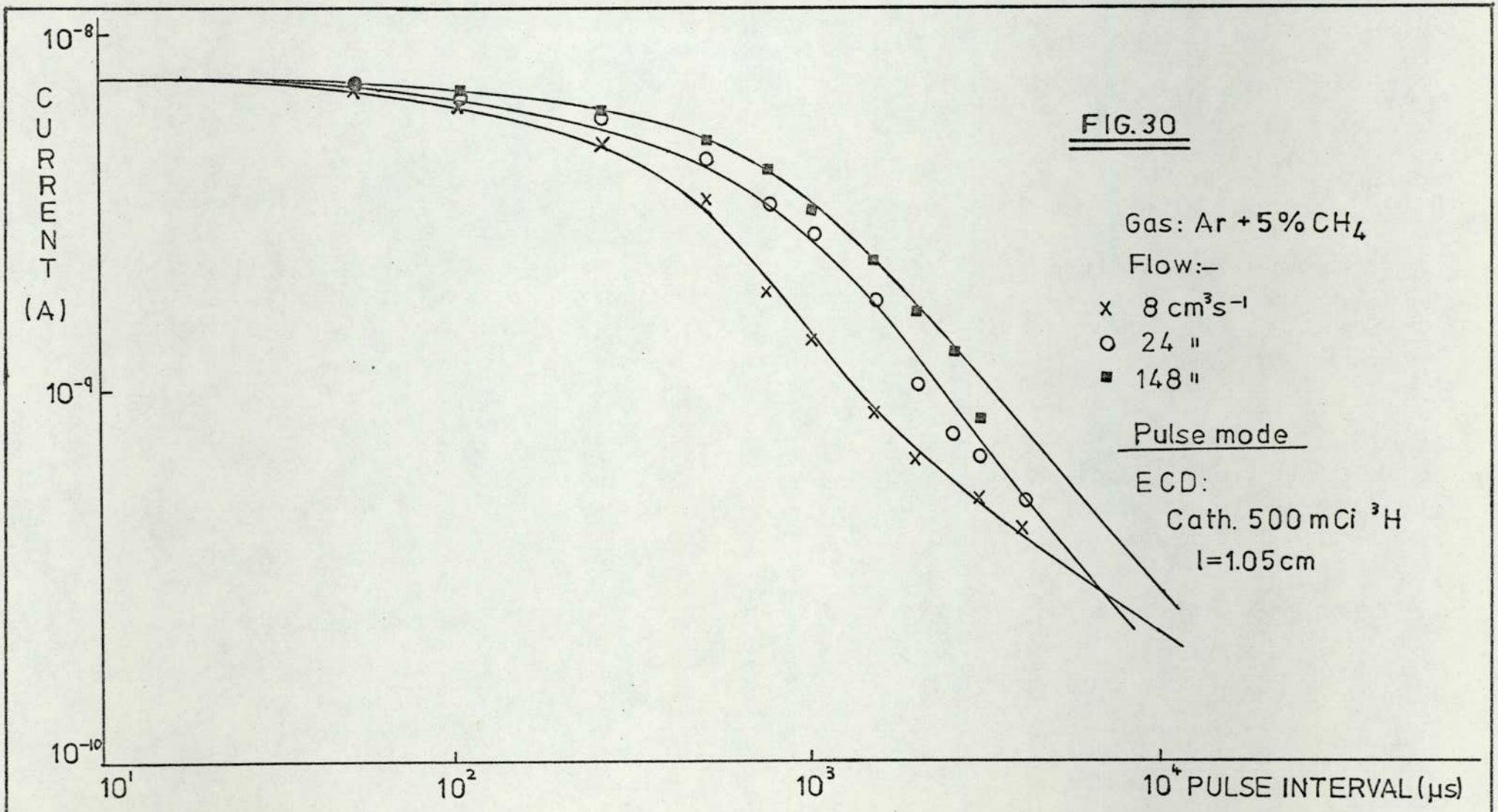

CURRENT VARIATION WITH GAS (Ar + CH_4) FLOW

which increases as U increases (as a first approximation) and consequently the standing current decreases. However, in practice the current is found to increase with carrier gas flow rate.

2. The contaminant is diffusing, bleeding or leaking into the carrier gas stream at some constant rate, Q, independent of the gas flow rate. Similar rate terms to those presented in case one can now be considered.

Rate of entry of impurity = Co Ux/V where Ux is the rate of flow of impurity.

Rate of outflow = C (Ux + U) /V

At steady state,

$Ux \cdot Co = k\,VCe + C\,(Ux + U)$

Hence,

$$C = \frac{Ux\ Co}{k\,Ve + (Ux + U)} \qquad [41]$$

Eq. [41] predicts that as the flow rate of carrier gas increases, the concentration of the impurity in the cell decreases and thus accounting for the observed increase in standing current.

Readings taken with a gas line suspected of leakage showed considerable dependency on flow as shown in Fig. (31). The difference between the asymptotic current value (Io) and that at a lower flow rate (I) is proportional to C in Eq. [41]. A linear relationship between $(Io - I)^{-1}$ and U is predicted by that equation. Fig. (32) shows that this is the case. As the gas line is made increasingly contaminant free, the slope becomes steeper and this parameter can be regarded as a measure of the concentration of impurity in the cell.

The earlier explanation for the variation of standing current with carrier gas flow was the dispersion and eventual removal of

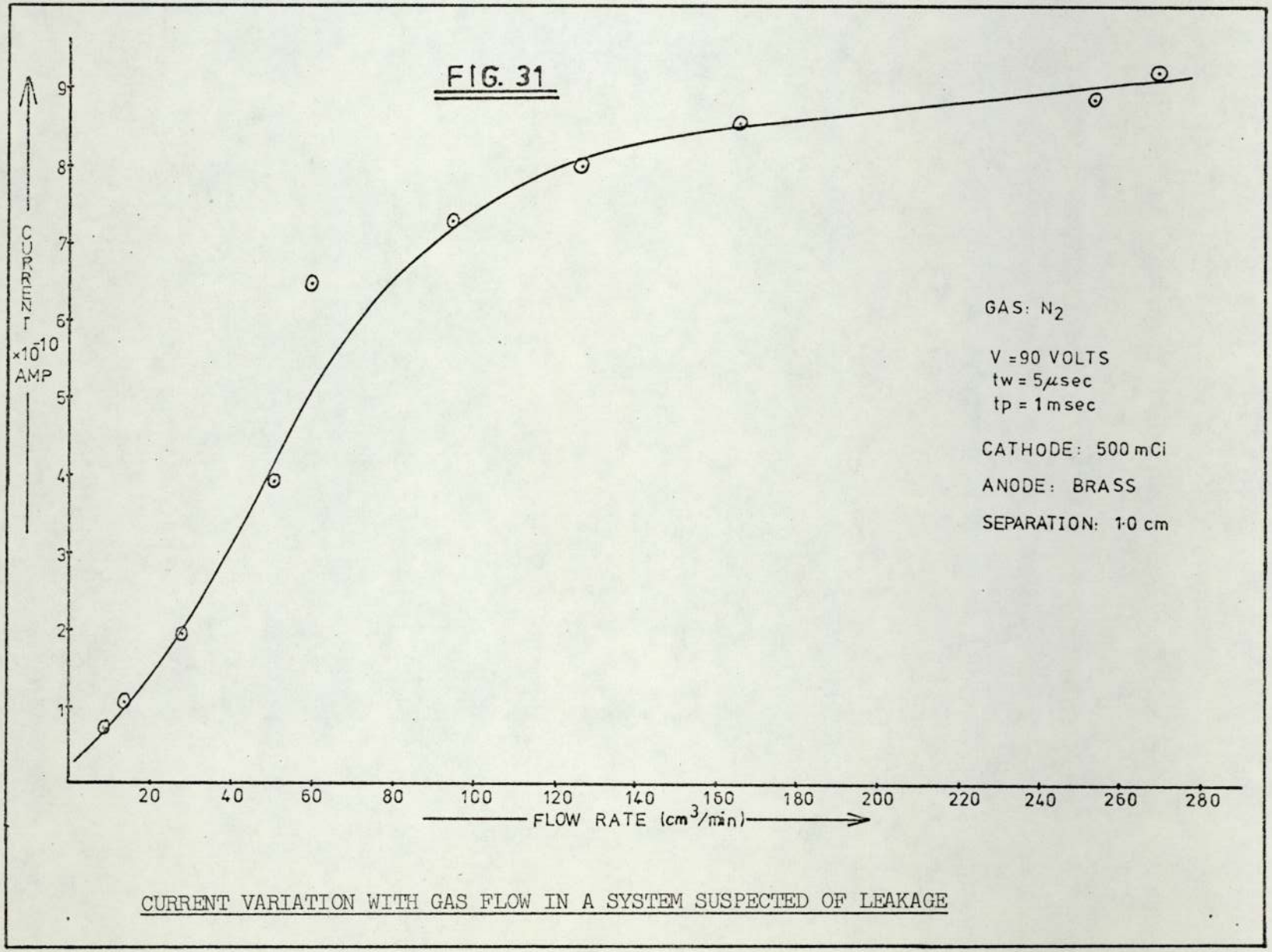

CURRENT VARIATION WITH GAS FLOW IN A SYSTEM SUSPECTED OF LEAKAGE

FIG. 32

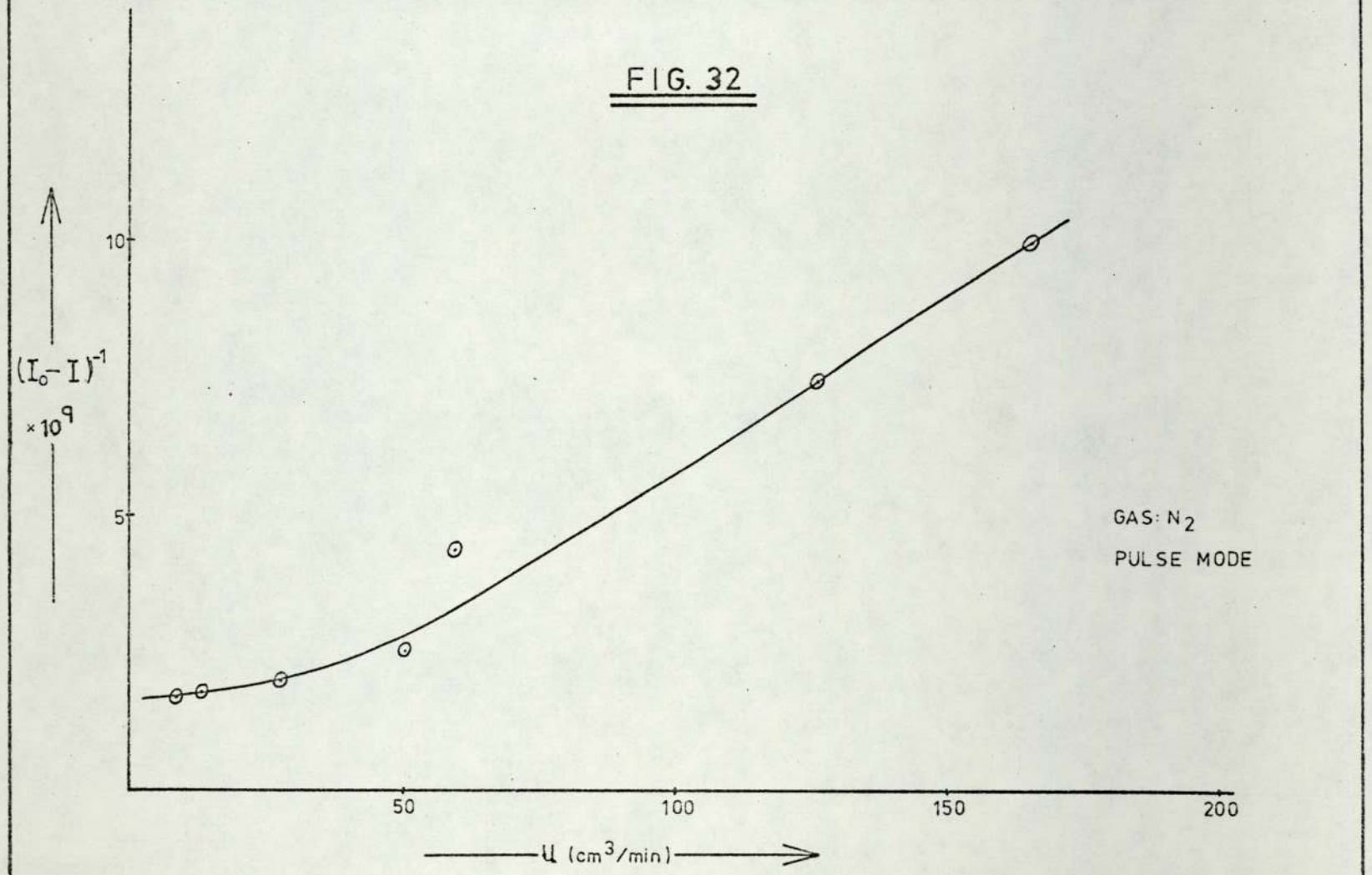

THE EFFECT OF CONTAMINANTS ON OBSERVED CURRENT

positive ions in the gas stream. Wentworth et al.,[18] noted that in the pulsed mode, loss of positive species may occur through flow out of the cell at longer pulse periods. Lyons et al.,[39] have suggested that two processes are involved. In the low flow region ($\simeq$ 100 cm^3 min^{-1}) the positive space charge around the cathode is dispersed by increasing the gas flow. In the high flow region positive ions are removed in the gas stream so that the concentration of positive ions in the chamber is inversely proportional to the flow rate.

The rather large variation in current with carrier gas flow rate observed by Lyons et. al., is almost certainly due to the presence of a capturing impurity, as the results obtained from a system suspected of leakage have shown.

A possible effect of flow would be to influence the degree of mixing in the cell. As shown earlier, the electron drift velocity is comparable to the gas kinetic velocity, indicating that mixing is occurring in the cell but it is not sufficient to assume complete mixing. In the assymmetrical cell, the gas flow does seem to diffuse the space charge of positive ions as the current - electrode separation plots showed. Also, in the case where the cathode was fixed close to the gas outlet, the maximum current was higher than that measured when the position of anode remained fixed. This is possibly an indication of loss of positive species from the space charge in the vicinity of the cathode.

Lovelock[37] has pointed out that ionisation detectors are not usually sensitive to changes in gas flow rate. This is because the drift velocity of the ions is large compared with the linear velocity of the gas flowing through the detector. If, however, the drift velocity of either the positive or negative ions becomes comparable with the linear gas velocity, gas flow can affect the

detector current.

If flow out of the cell is to be a plausible mode of loss for positive ions, then the time constant for this process has to be comparable to that of recombination which is by far, the most important process by which the ions are lost. For a cell with an electrode spacing of 2.0 cm and assuming a high gas flow (3.67 cm^3 s^{-1}), the residence time for gas molecules is 3.45×10^{-1} s. Assuming an average positive ion density of 1×10^9 cm^{-3} and a recombination coefficient of about 1×10^{-7} cm^{-3} s^{-1}, the time constant is 1×10^{-2}s. The two values do not differ significantly.

Besides volume recombination, the positive ions can also be lost by surface recombination at the cathode. At low field strengths (10 Vcm^{-1}), the positive ion drift velocity in nitrogen is 2.55×10^1 cm s^{-1} and the time to cross the cell of spacing 2.0 cm. would be about 7.8×10^{-2} s. This value too, is comparable with the residence time for molecules at high gas flow. Hence, it seems that positive ions could be lost through flow out of the cell, when cell volumes are big and the flow rate is high.

At small electrode separations, flow was found to have no effect on the current (Fig. 33) but as the spacing was increased, a higher current was observed for a particular voltage when the gas flow rate was high (Fig. 28)

4.7 d.c. MODE OF OPERATION

Though this mode of operation has inherent sources of error, it is still quite widely used in analytical work. Hence, an attempt was made to analyse the typical response characteristic of the detector - a parabolic rise in current with applied voltage.

Several theories have been formulated for a discharge in a gas between two parallel plate electrodes. One approach based on calculating the current density at any point in space in the reaction volume, has already been outlined in section 3.3. Another

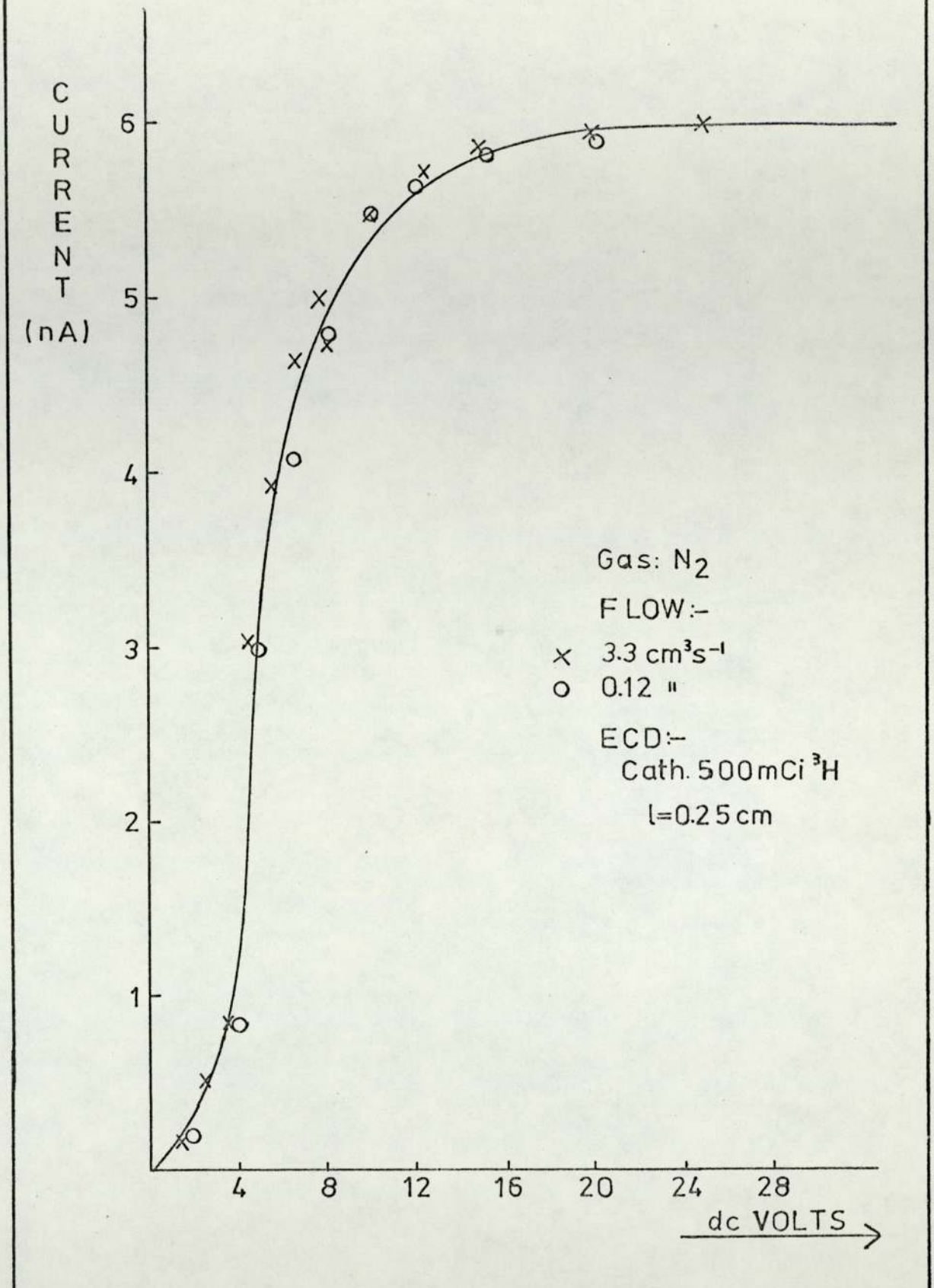

FIG. 33

CURRENT - VOLTAGE PLOTS FOR DIFFERENT FLOW RATES AT SMALL ELECTRODE SEPARATION

approach, based on Poisson's equation and applicable at high gas pressure and in the presence of a space-charge leads to the following relationship between the current density and voltage[13] :

$$j = \frac{2.95 \times 10^{-12} \mu V^2}{d^3} \qquad [42]$$

where μ is the mobility of the species responsible for the current and d is the electrode spacing. The electron current density calculated from the above equation for nitrogen is 5.8 nA m^{-2} while the measured current density (for the 500 mCi ^3H source) is 4.9×10^{-5} Am^{-2}. Several factors contribute towards the inadequacy of these theories in predicting the ECD current. It is assumed that ionisation is uniform throughout the cell; that the space charge is very dense and either electrons or positive ions are to be considered and not mixtures.

In terms of the proposed model, the electron density under the d.c. mode would be expressed by

$$e = (a / b')^{1/2}$$

$$= \left[\frac{k_1 AG}{(k_2 Vp + \sqrt{pA} + Fe)} \right]^{1/2}$$

The equation predicts an electron density several orders of magnitude smaller than that calculated from the observed current density. The inclusion of a diffusion term however improves the prediction. Since the latter process leads to surface recombination of the ion-pairs generated, the equation can be modified to :

$$e = \frac{k_1 AG (De + Dp) \; l}{(k_2 Vp + \sqrt{pA} + Fe)} \qquad [43]$$

Considering the case where the applied voltage is 20 volts, l = 1.0 cm and the source is500 mCi ^3H, the measured electron density in nitrogen is 2.58×10^{10} cm^{-3}. The density calculated from Eq. [43] is 6.2×10^{8} cm^{-3}.

As theoretical analysis has failed to explain satisfactorily the current-voltage behaviour, an empirical relationship was sought. The standing current is proportional to V^2 and inversely proportional to l^3 at high gas flow rates (Fig. 34 and 35) and in the low flow region, the relationships appear to be : $I \propto V^{3/2}$ and $I \propto d^{-2}$ (Fig. 36). Similar relationships are expressed by Child's law describing space-charge limited currents in vacuum and gas-filled electronic devices such as thermionic diodes.

The graph of the onset voltage for saturation current at different inter-electrode spacing (Fig. 37) shows the effect of space charge — a potential trough near the cathode. The intensity of the space charge is determined by the parabolic character of the curves; it appears that a denser space charge exists at very low gas flow rates. This would be the case if positive ions were being removed from the cell by flow. Similar results were obtained with 95% Ar + 5% CH_4 (Fig. 38).

4.8 PULSED MODE OF OPERATION

To overcome many of the problems faced when the detector is operated in the d.c. mode, Lovelock[12] suggested the use of square wave voltage pulses as the source of potential. Pulse variables - voltage, V, width, w and interval, s, were defined in section 2.6 and the detector used was characterised in terms of these parameters in section (4.4).

When the ECD operates in the pulsed mode, its response over a voltage range shows a plateau (Fig. 8); the particular voltage at which this plateau occurs depends upon the pulse width and the detector design. It is also indicative of cell and carrier gas purity. With nitrogen and 95% Ar + 5% CH_4 as carrier gases, the onset voltage for saturation current is about 20-30 volts under normal operating conditions. In the presence of electron

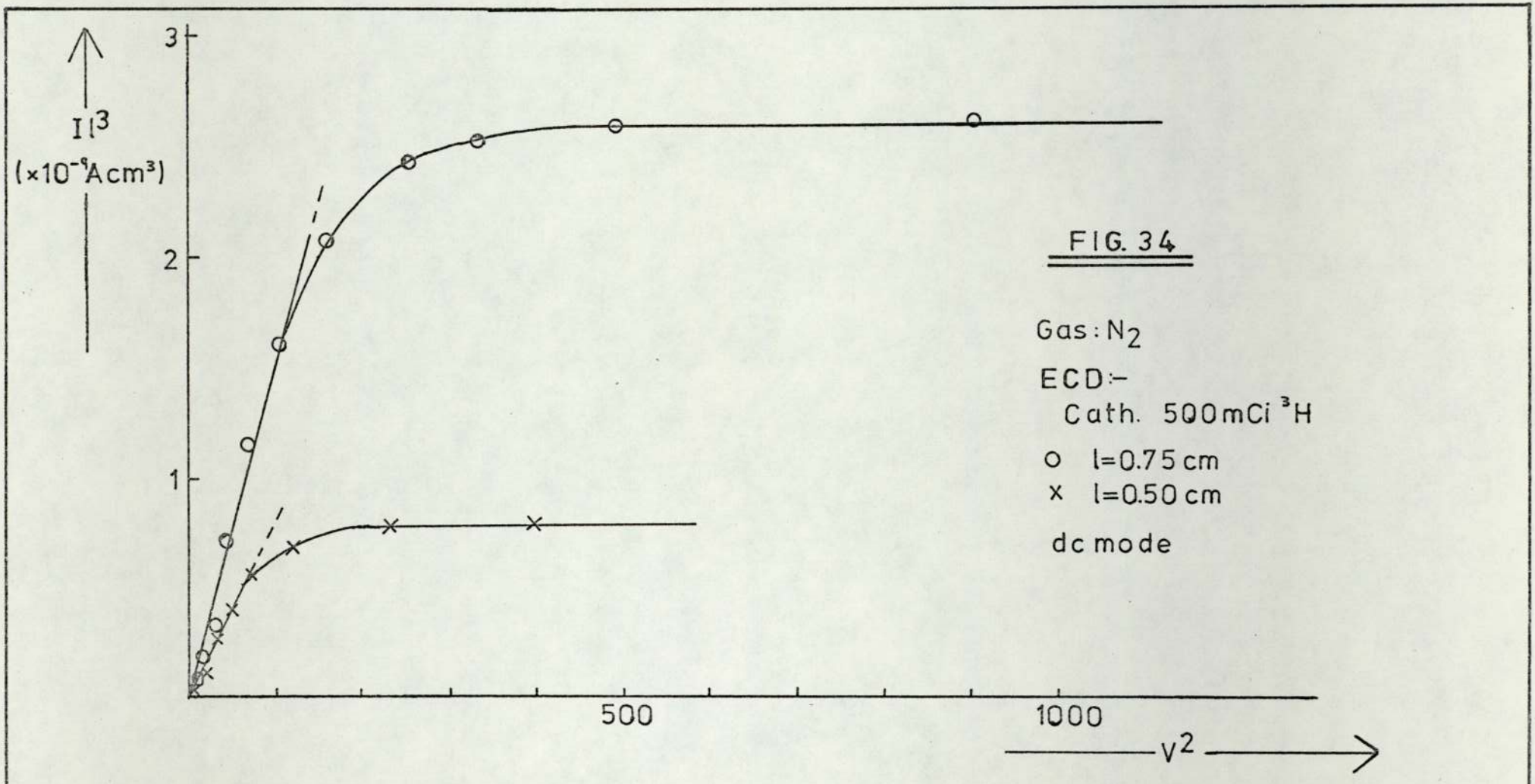

CURRENT - VOLTAGE RELATIONSHIP IN d.c. MODE AT HIGH GAS FLOW RATE

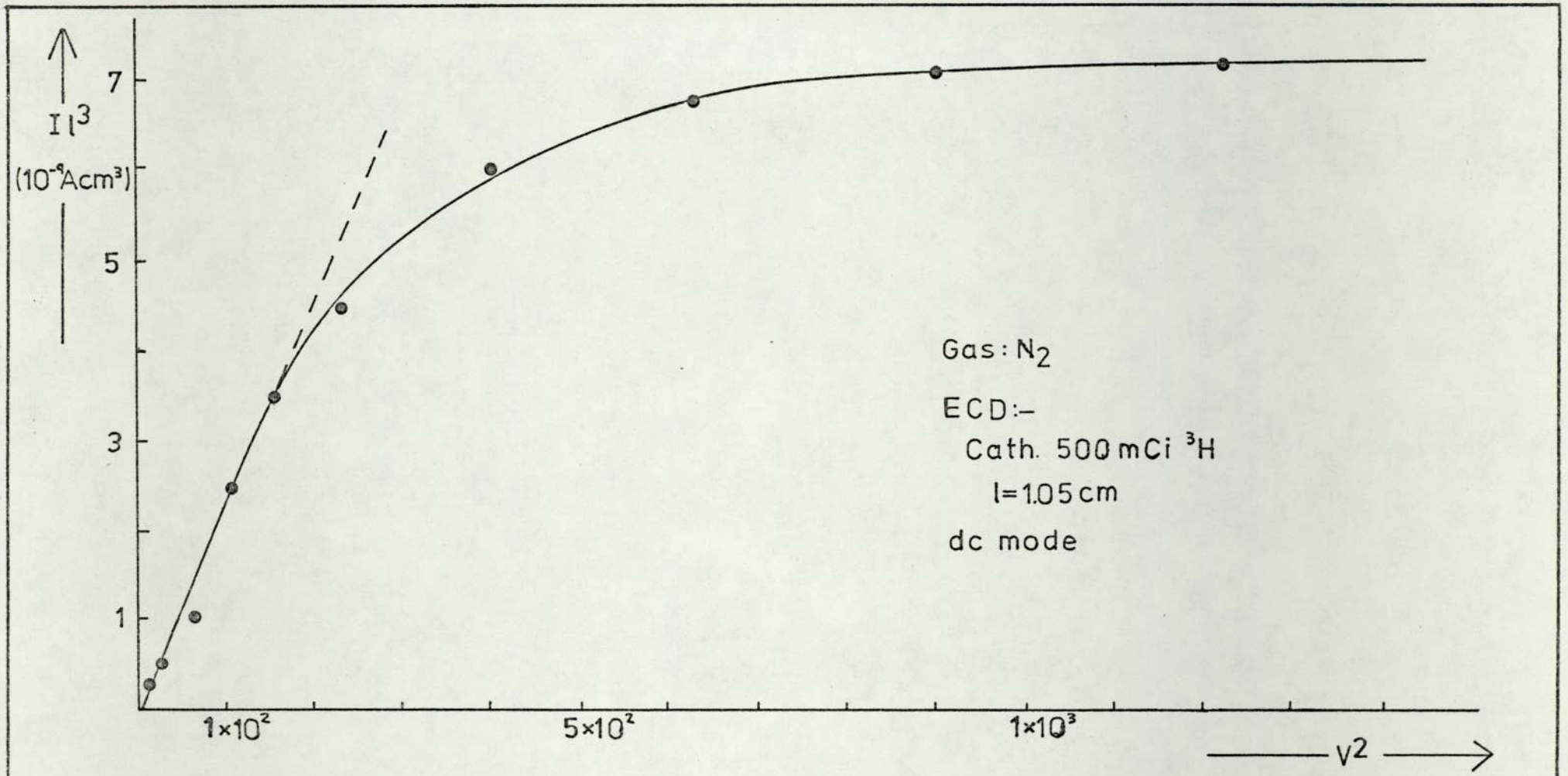

FIG. 35

VARIATION OF CURRENT WITH VOLTAGE IN d.c. MODE

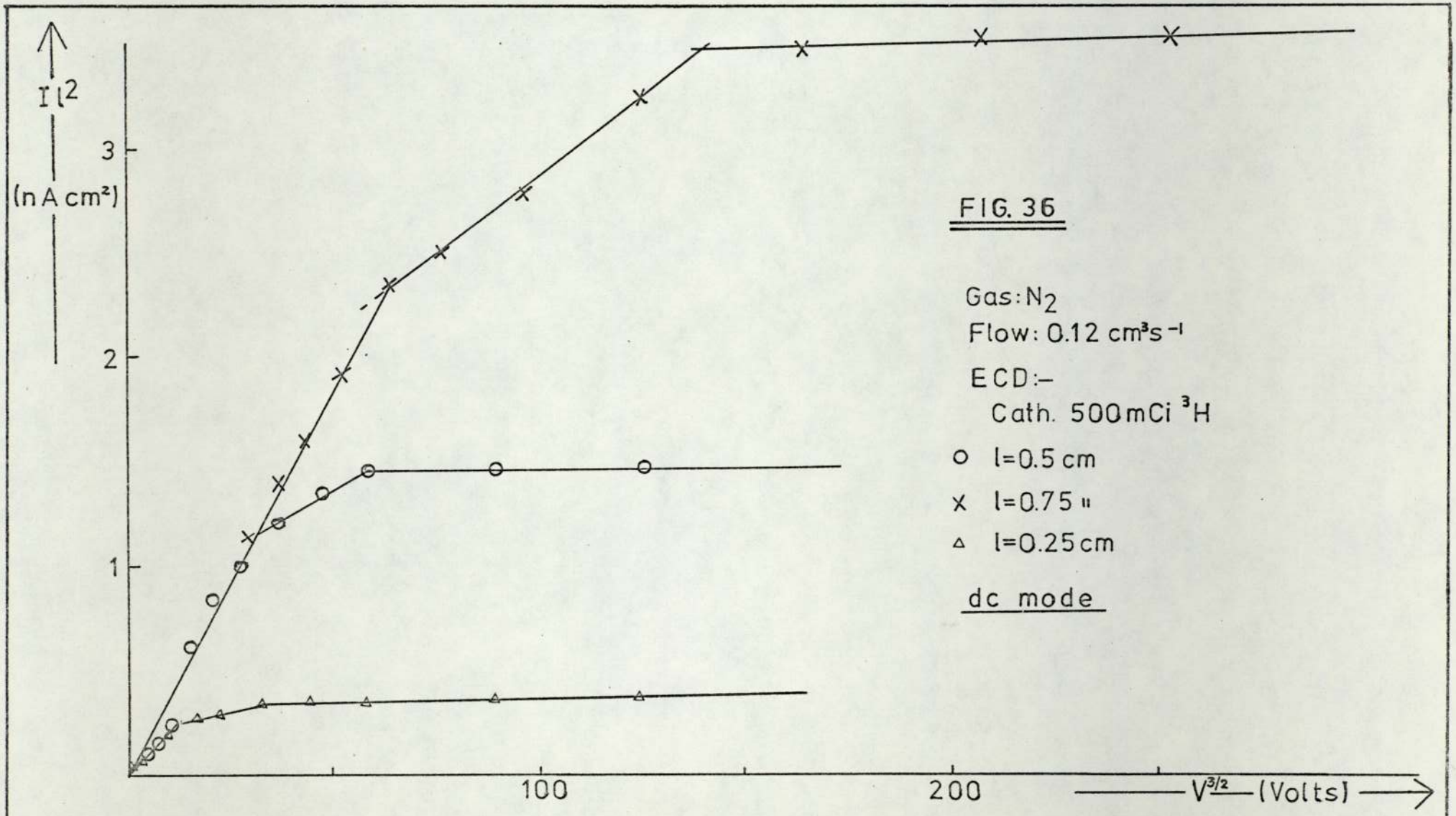

CURRENT-VOLTAGE RELATIONSHIP AT LOW GAS FLOW RATE

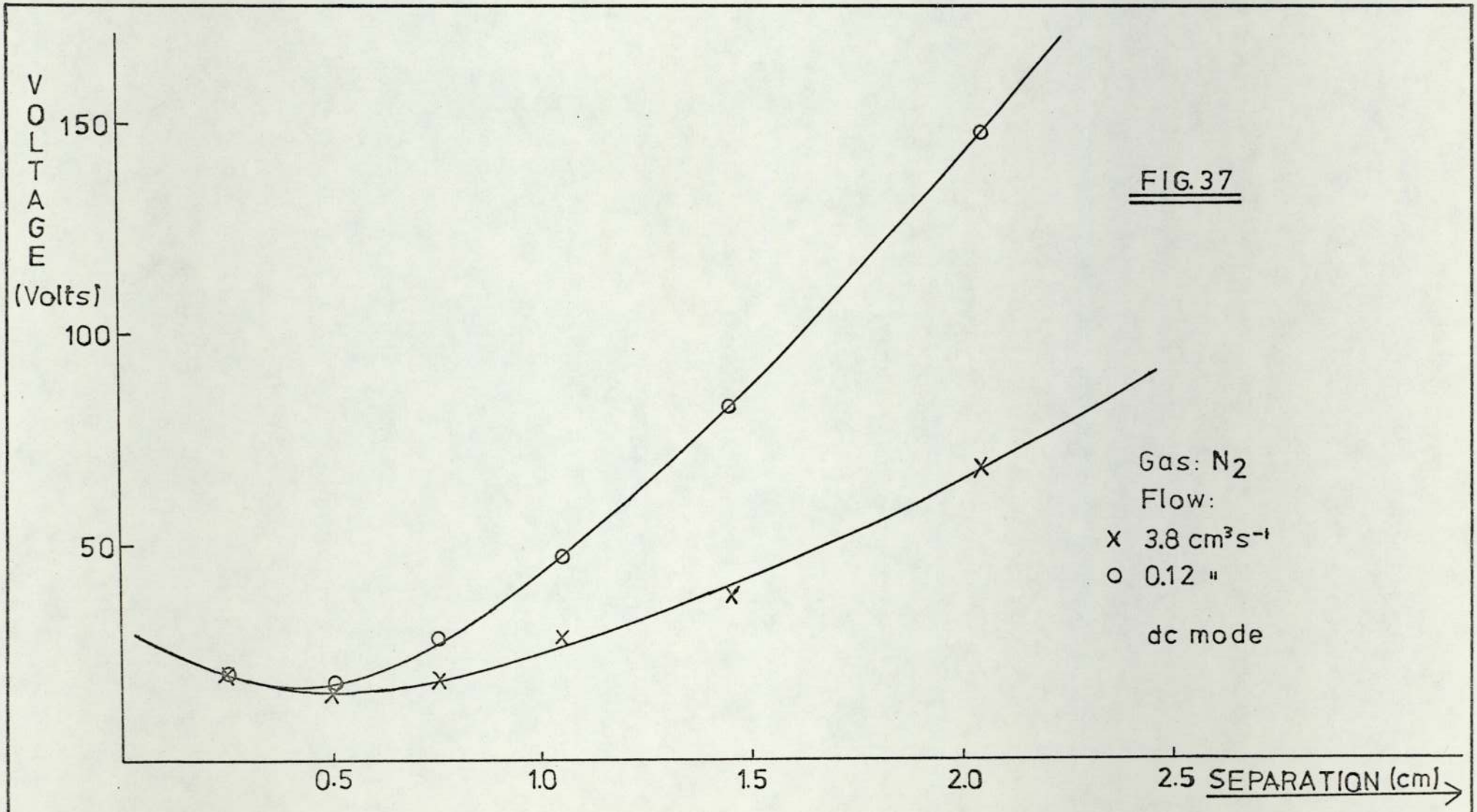

ONSET VOLTAGE FOR SATURATION CURRENT AT DIFFERENT ELECTRODE SPACING (d.c. MODE)

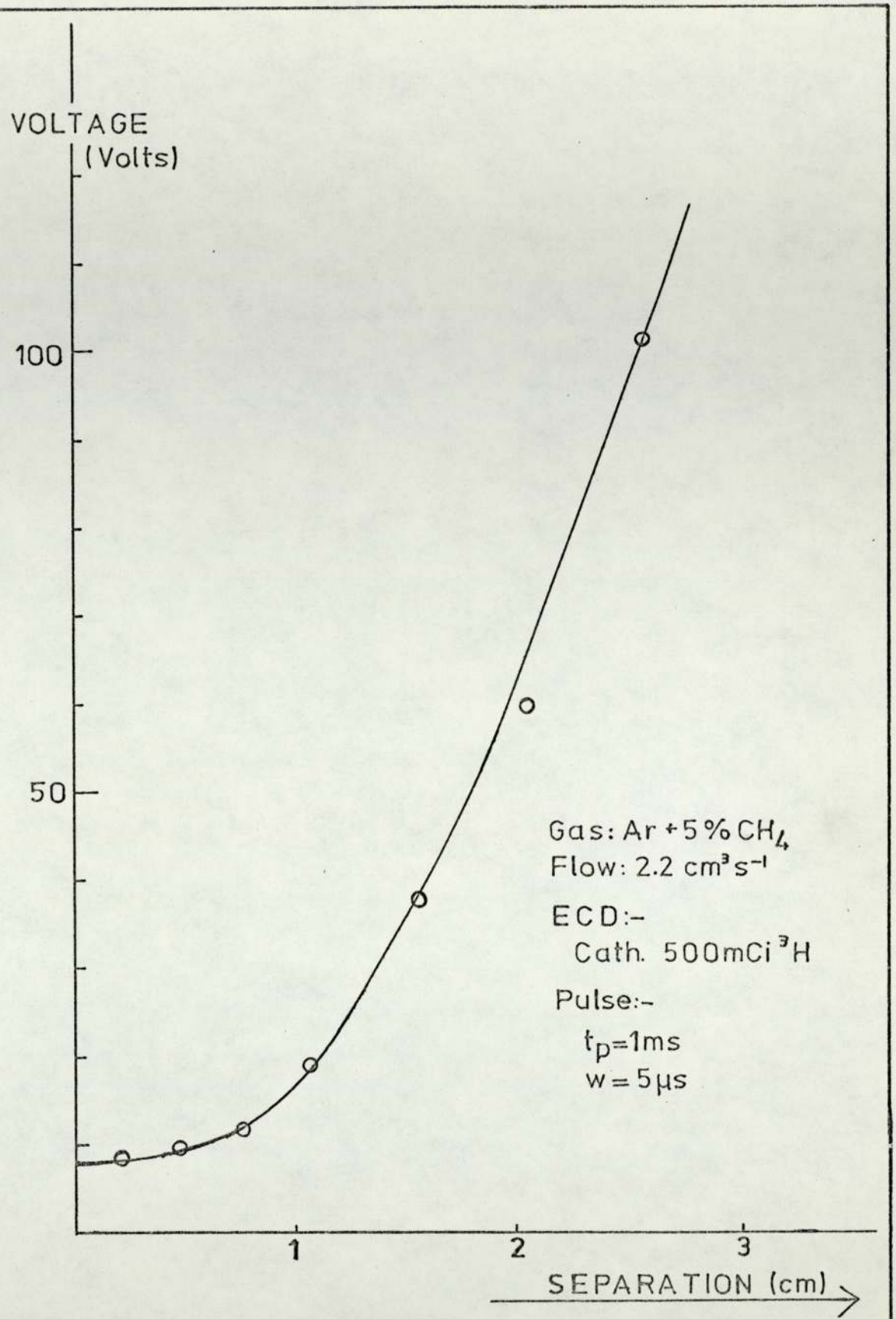

FIG. 38

ONSET VOLTAGE FOR SATURATION CURRENT UNDER THE PULSED MODE ($Ar+CH_4$)

capturing impurities, a larger voltage is necessary since the negative species formed upon capture are being collected as well.

In explaining the decrease in current at long inter-electrode spacings, it was shown that the normal pulse width of 5 μs is too short to allow collection of all electrons. This would imply that if the field intensity (which is proportional to V) were to be increased, the drift velocities of the charged species would increase as well and hence the saturation current be reached. Fig. (39) shows that this is the case.

As with the d.c. mode, if the onset voltages giving saturation current at various electrode separations were to be plotted against the separation (Fig. 38), a potential trough is observed. This would imply that a space charge of positive ions also exists under the pulsed mode of operation, contrary to what is normally stated.[18]

The current variation with pulse width is similar to that observed for the pulse amplitude — a steep increase initially, followed by saturation (Fig. 9). The slight increase in the saturation region is thought to be due to the collection of charges produced during the application of the pulse. As stated in section 4.4, the pulse width at which the current ceases to increase linearly denotes the electron transit time. If this is the case, then it should be possible to calculate the electron drift velocity from that time and the cell length. At $(X/P) = 0.07$ V cm^{-1} torr^{-1}, Brown[60] gives the electron drift velocity in nitrogen as 2.7×10^5 cm s^{-1}. Table 4 shows the drift velocities calculated with different ionisation sources and cell lengths. The electron transit time is denoted by Wc and the field strength (X) is assumed to be uniform in the cell. The average electron drift velocity in nitrogen calculated from the results given in Table 4 is 2.83×10^5

FIG. 39

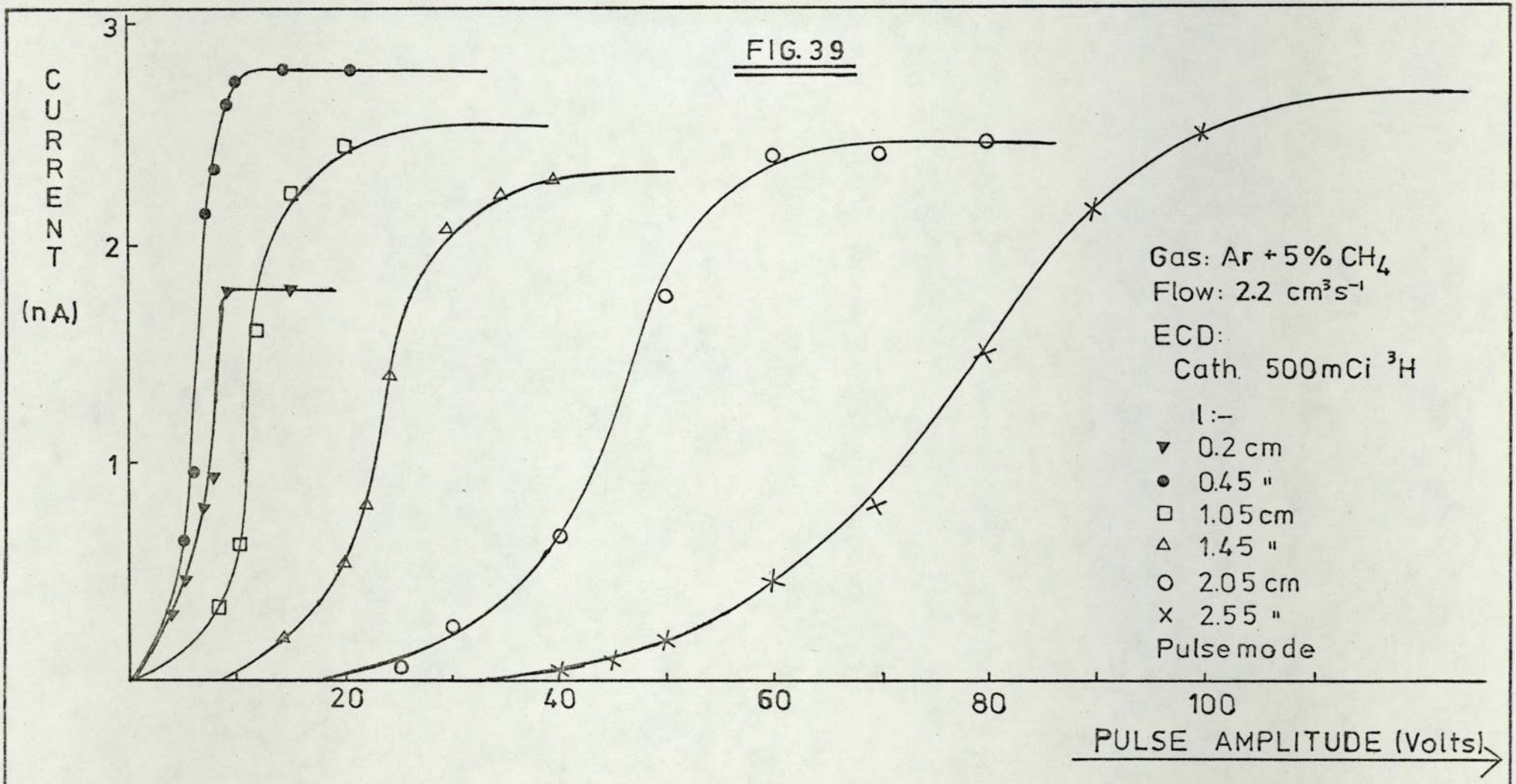

CURRENT VARIATION WITH PULSE AMPLITUDE AT VARIOUS ELECTRODE SEPARATIONS

TABLE 4

ELECTRON DRIFT VELOCITY (V_d) IN NITROGEN

SOURCE	CELL LENGTH	FIELD	Wc	V_d cms^{-1}
500 mCi ^3H	1.0 cm	50.0 Vcm^{-1}	3.50 μs	2.86×10^5
150 mCi ^3H	1.6 cm	56.25 Vcm^{-1}	6.30 μs	2.54×10^5
150 mCi ^3H	0.95 cm	52.6 Vcm^{-1}	3.40 μs	2.79×10^5
0.5mCi ^{63}Ni	1.0 cm	50.0 Vcm^{-1}	3.20 μs	3.12×10^5
0.5mCi ^{63}Ni	1.55 cm	58.1 Vcm^{-1}	5.50 μs	2.82×10^5

TABLE 5

ELECTRON DRIFT VELOCITIES IN VARIOUS GASES AT LOW (X/P)

GAS	PRESENT STUDY V_d	LITERATURE VALUES V_d
Nitrogen	2.83×10^5 cms^{-1}	2.7×10^5 cms^{-1} (60)
Ar + 5% CH_4	2.65×10^6 cms^{-1}	3.5×10^6 cms^{-1} (18)
Argon	3.05×10^5 cms^{-1}	2.0×10^5 cms^{-1} (18)
Helium	3.22×10^5 cms^{-1}	3.5×10^5 cms^{-1} (60)
Ethylene	8.65×10^5 cms^{-1}	—

cm s^{-1}. The distance travelled by the electrons has been taken to be the entire cell length even though it appears that ionisation occurs some distance away from the source. This seems reasonable since most β^- particles are confined very close to the source as was pointed out in section 4.5.

Electron drift velocities in various gases have been calculated and are presented in Table 5 together with literature values (60) where available. Small changes in (X/P) in the range considered (at atmospheric pressure) have negligible effect on the drift velocity(29). The results obtained are in agreement with those acquired using other techniques for measuring electron mobility. The potential use of the ECD to measure electron mobilities at very low (X/P) values is amply demonstrated.

The experimental parameters expressing kinetic control of the reactions occurring in the detector are the number of electrons collected per pulse (Ne) and the pulse interval (s). Fig. (29) shows a typical current variation with pulse interval — gradual levelling off at short periods giving maximum current and a steep decrease with increasing s. The extrapolated current value at zero pulse period corresponds to the maximum current observed under the d.c. mode. In the case of nitrogen this is about 6.3 nA. However, with 95% Ar + 5% CH_4 the current at short pulse interval (50 μ s) was slightly higher (by 0.3 nA) than the d.c. saturation current (6.85 nA). With argon and ethylene, the latter was found to be slightly higher. These small fluctuations are within experimental error and it can generally be said that at short pulse periods, the current does approach the d.c. saturation current. This would imply the collection of positive ions under the pulsed mode, contrary to what is generally accepted (that only electrons are collected)(61).

Fig. (40) shows the current variation with pulse interval for different gases studied-argon, 95% Ar + 5% CH_4, ethylene, helium

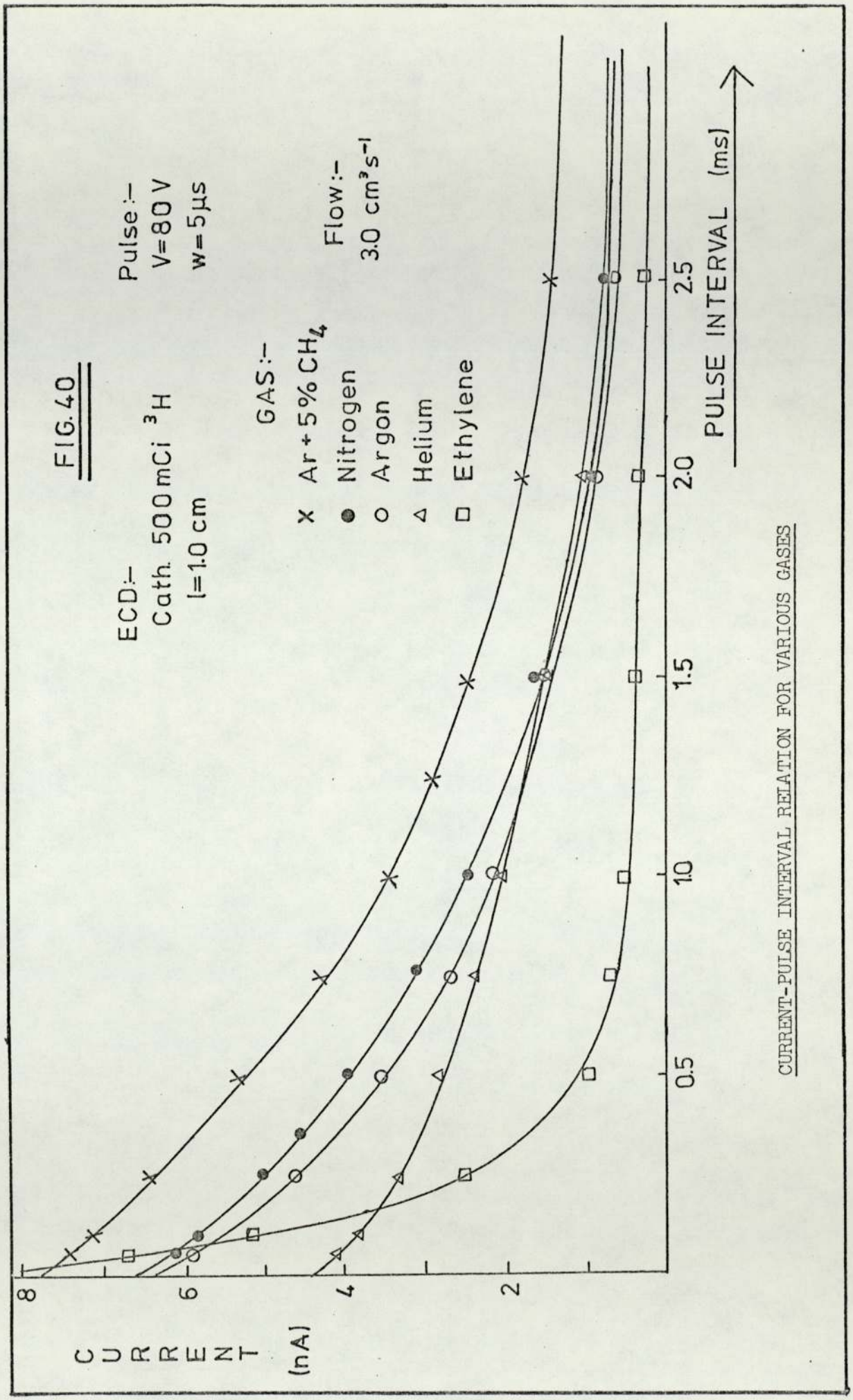

CURRENT-PULSE INTERVAL RELATION FOR VARIOUS GASES

and nitrogen. The addition of small amount of methane to argon maintains the electron energy at a constant thermal level and the quenching gas molecules also remove argon metastables in deactivating and ionising collisions. In pure argon, electrons are not completely thermalised during the applied pulse times and this probably accounts for the lower current observed in argon since the ionisation cross-section decreases with increasing electron energy. The metastable potential of helium is relatively high (20.7 eV)[11] and since ionisation of rare gas molecules occurs only via the excited state, the measured current is expected to be much smaller in comparison to that of argon. The reactions are :

$$He + e^- \longrightarrow He^* + e^-$$

$$He^* + He \longrightarrow He_2^+ + e^-$$

Fig. (40) also illustrates the loss of electrons and positive ions through recombination processes. Assuming that the rate of decrease in average current (as measured by the electrometer) with increasing pulse period is unaffected by the nature of the gas in the detector, the effect of different rates of recombination is clearly exhibited at long pulse interval. Helium, with its lower rate of recombination gave almost the same current as nitrogen and argon at long pulse periods. With ethylene as carrier gas, a very steep decline in current is observed. The formation of several positive species upon irradiation have been reported[40] : $C_2H_2^+$, $C_2H_3^+$, $C_2H_4^+$, and $C_4H_7^+$. Though an overall recombination coefficient is not known for the gas, it is expected to be large ($\simeq 10^{-6}$ cm^3 s^{-1}).

Equation [30] predicts the build up of electron concentration during the field free interval. The rate of production of ion-pairs, k_1 AG, is given by the initial slope of (Ne versus s) graph. For the 500 mCi ^{3}H source and nitrogen as carrier gas, k_1 AG = 2.41 x 10^{10} cm^{-3} s^{-1}. The mobility and electron ion recombination coefficient (for N_4^+) is 2.5 cm^2 V^{-1} s^{-1} and 1.50 x 10^{-6} cm^3

s^{-1} respectively.[22, 30] Fp is taken to be the flow rate of the gas. The 'Gaines factor', R, is calculated from Eq. [36] for several values of s and this allowed the positive ion concentration, Po, to be evaluated from Eq. [38]. Table 6 shows the values of these two parameters for nitrogen. All the factors involved in Eq. [30] are now known and hence the electron concentration can be calculated. Fig. (41) shows the prediction of the present theory together with that made by Lovelock's 'stirred reactor' model[42] and these are compared with the experimentally observed variation of Ne versus s. Eq. [33] giving the average electron concentration and the corresponding equation in Lovelock's model both fail to saturate at long pulse periods. This probably indicates that the current measured does not correspond to the electron concentration per pulse integrated over the pulse period but rather to the actual concentration of electrons at the end of thepulse period, as expressed by Eq. [30].

Expressing R as the ratio of positive ions to electrons in the cell simplifies Eq. [30] to :

$$e = \frac{a^{1/2}\,[\exp(q\,t) - 1]}{c^{1/2}\,[\exp(q\,t) + 1]} \qquad [44]$$

where $a = k_1\,AG$ $C = k_2 R$ and $q = 2\,(ac)^{1/2}$

The recombination coefficient, k_2, for Ar_2^+ is 6.7×10^{-7} $cm^3\,s^{-1}$ as calculated by Oskam and Middlestadt.[62] The drift velocity for the ion is 1.52×10^2 cms^{-1} at a field strength of 80 Vcm^{-1}. The mean value of R is 3.66×10^2. Fig. (42) shows the theoretical prediction according to Eq. [44] and also the experimental variation of Ne with the pulse interval.

An equation can easily be derived for the recombination coefficient from the proposed model,

$$k_2 = \frac{k_1 V^2}{n_e^2 R} - \frac{2V}{n_e R s} + \frac{1}{k_1 R s^2} \qquad [45]$$

TABLE 6

THE 'GAINES FACTOR' AND POSITIVE ION CONCENTRATION IN NITROGEN AT VARIOUS PULSE PERIODS

S $\langle \mu s \rangle$	R x 10^2	p_o x 10^9
43	6.33	3.97
100	5.68	3.76
250	4.46	3.33
500	3.29	2.86
750	2.63	2.56
1000	2.17	2.32
1500	1.62	2.01
2000	1.30	1.80

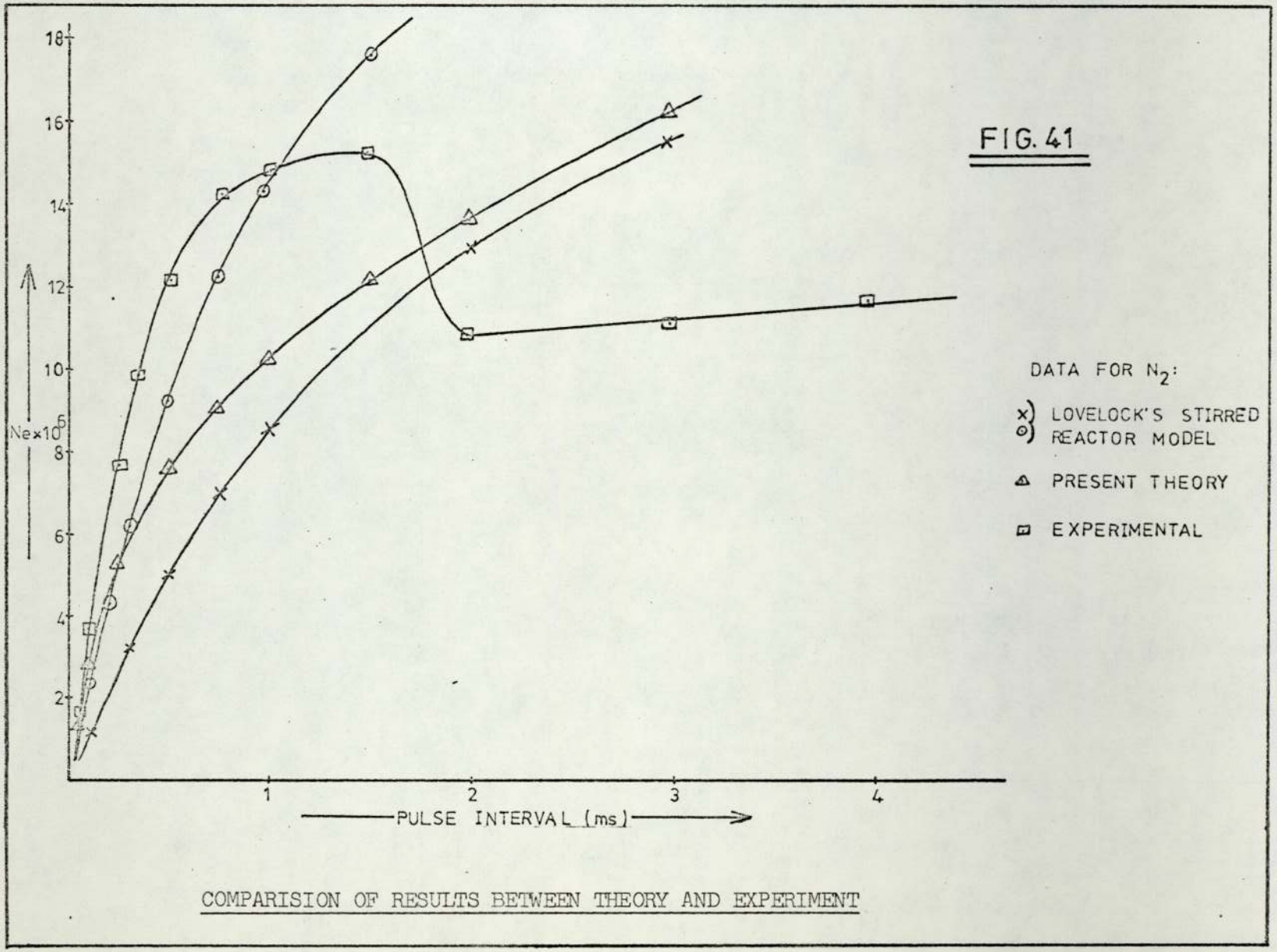
FIG. 41
DATA FOR N_2:
LOVELOCK'S STIRRED REACTOR MODEL
PRESENT THEORY
EXPERIMENTAL
Ne×10^6
PULSE INTERVAL (ms)
COMPARISION OF RESULTS BETWEEN THEORY AND EXPERIMENT

FIG. 42

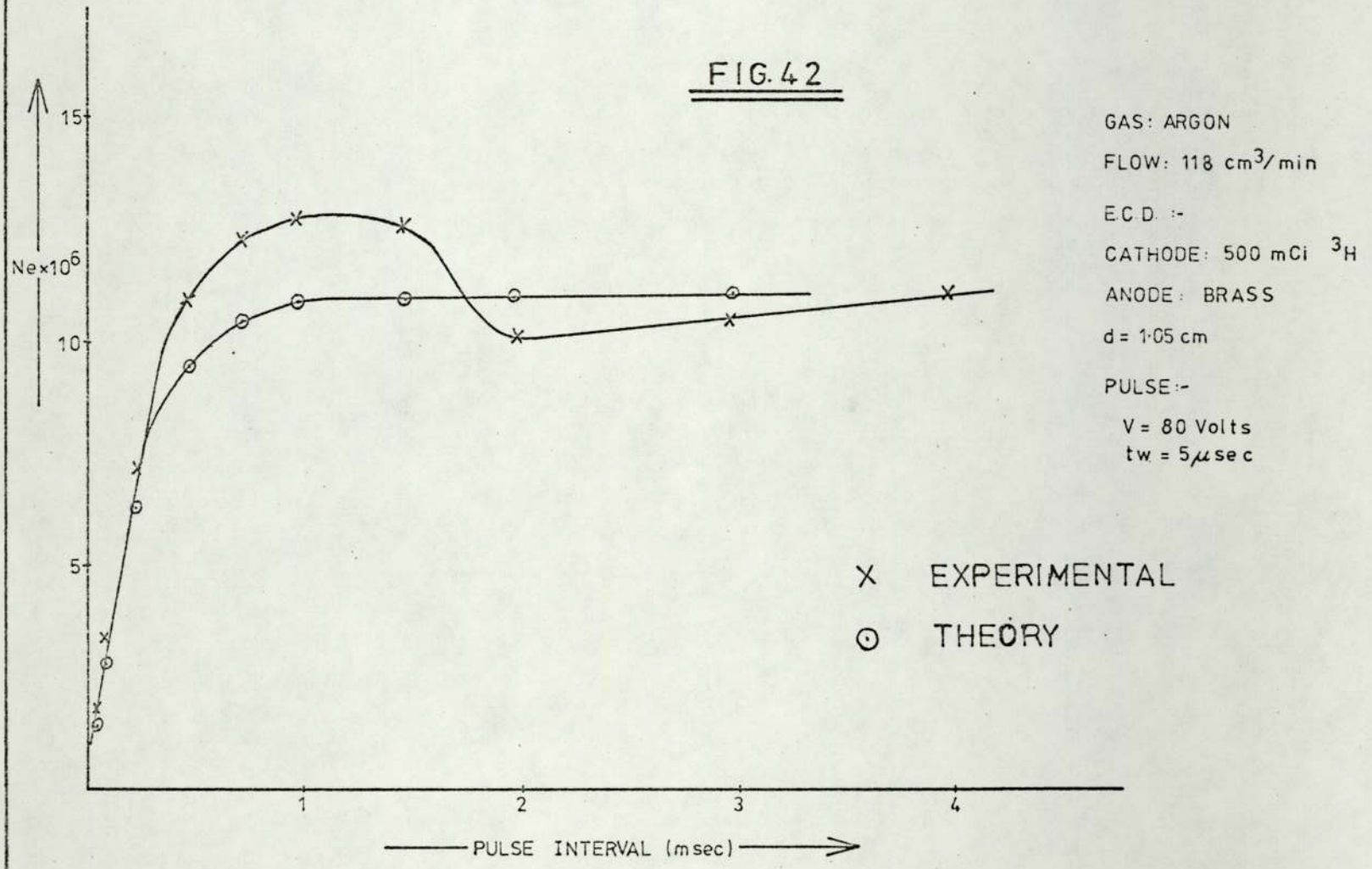

PREDICTION OF THE PROPOSED MODEL COMPARED WITH EXPERIMENTAL DATA FOR ARGON

The positive ion mobility in ethylene is approximately 2.5 $cm^2\ V^{-1}\ s^{-1}$ giving a drift velocity of 2.0×10^2 cm s^{-1} at a field strength of 80 V cm^{-1}.(39) The mean value of R is 4.66×10^2 and $k_1 = 2.84 \times 10^{10}\ cm^{-3}\ s^{-1}$ when the cell volume is 1.27 cm^3. As recombination is a dominant process at long pulse periods, the value of $Ne = 3.15 \times 10^6$ is taken at s = 1 ms. The electron-ion recombination coefficient for ethylene, calculated from Eq. [45], is then equal to $8.95 \times 10^{-6}\ cm^3\ s^{-1}$.

For helium, when the 'Gaines factor' is calculated from Eq. [36], the recombination coefficient, $k_2 = 1.35 \times 10^{-6}\ cm^3\ s^{-1}$ which is considerably larger than the reported values.(22) An alternative way of obtaining the 'Gaines factor' is to consider it as a function of the ratio of the mobilities of positive ions and electrons in the gas under study. Thus,

$$R = G \left(\frac{\mu p}{\mu e} + \frac{u s}{V}\right)^{-1} \qquad [46]$$

where G is the number ofion-pairs formed per number of β^- particles actually emitted; μp and μe refer to the mobility of positive ions and electrons respectively and u is the gas flow rate. R calculated in this way gives a value of 6.22×10^4 for helium. The rate of production of ion-pairs, $k_1 = 1.58 \times 10^{10}\ cm^{-3}\ s^{-1}$ and $Ne = 1.3 \times 10^7$ at s = 1 ms. Eq. [45] then gives the recombination coefficient for helium and is equal to $2.3 \times 10^{-9}\ cm^3\ s^{-1}$ which agrees very well with the values quoted by Hasted(22).

The use of known values of recombination coefficients and positive ion mobilities has made it possible to check the predictions of the proposed theory. Accounting for the positive ion space charge, through the 'Gaines factor', shows that the charge concentration in pure argon is about $4.0 \times 10^9\ cm^{-3}$ at s = 1 ms. Wentworth et al.,(18) estimated the value to be $1.1 \times 10^{11}\ cm^{-3}$.

Theory, however, failsto explain the observed maxima and

the subsequent sharp decline. The peak appeared in all the gases studied and it seems that a process with a reaction time of about 0.5 ms is responsible in almost all the cases. Wentworth et al.,[18] observed a similar peak in their studies and attributed it to a different process of loss for the positive ions in the cell. At short pulse periods the ions are collected at the cathode but at long pulse interval, they are lost through flow out of the cell. A different electron concentration would hence be reached at steady state and the curve would exhibit a distinct 'jump' from one level to another. The maxima has been observed mainly when less efficient ionisation sources have been used; Wiel and Tommassen[59] using a 10 mCi ^{63}Ni source did not observe such a peak. It seems that loss of ions through flow out of the cell becomes significant only with lesser electron input sources.

4.9 PRESENCE OF UF_6 AND H_2O IN CARRIER GAS

The ECD response to a capturing species depends upon the physico-chemical properties of the sample molecules. For a weakly electron capturing compound, the response is linear when the electron - molecule reaction takes place under conditions which ensure that the detector is operating in the pseudo-first order region[42]. This is the case when the sample concentration greatly exceeds that of the electrons, ie. with a less efficient ionisation source giving a low saturation current. For strongly electron capturing compounds a linear response is observed when the electron concentration within the detector exceeds that of the sample molecule concentration. Nearly all of the sample input is ionised; a high d.c. saturation current (10^{-8} A) is necessary for this to occur.

A considerable body of information on molecular electron affinities indicate that the negative ions formed are often far too stable for the reverse reaction to occur (ie. electron detach-

ment).[26] As stated in section 3.1, at ordinary temperatures, a very small fraction of gas molecules possess sufficient translational energy necessary to detach an electron from a negative ion. Thus the formation of negative ions can be considered to be proceeding only in one direction, ie. as a rate process. This point was further considered by Burdett[32] who showed that the detector does respond to the geometrical cross section of sample molecules when a group of organic compounds of the same type is considered. The electron detachment rate, depending on the electron affinity and activation energy has a much smaller effect in comparison.

In order to check these conclusions, the effect of small concentrations of UF_6 in helium was investigated. The sample was placed in a saturator - a U - shaped glass vessel (Fig. 43) with a sintered glass disc in the wider, gas outlet side to support the compound and effect better mixing of the carrier gas with the vapour of the compound. The saturator was placed in a flask containing dry ice. A known variable fraction of the carrier gas passed through the saturator and was pre-mixed with the main stream before entering the detector.

Fig. (44) shows the current variation with pulse interval for pure helium and helium containing different concentrations of UF_6. At short pulse periods, the current approaches the same d.c. saturation current in all cases - an indication that all charged species present in the cell are collected. The presence of different concentrations of sample in the carrier gas is consequently more apparent at long pulse periods, ie. between 0.5 and 1.5 ms. The graphs of Ne versus t_p (Fig. 45) exhibit an anomalous behaviour; the number of electrons collected per pulse decreases very steeply at long pulse interval instead of reaching a steady level as in the pure gas. Dissociative electron attachment ($UF_6 + e^- \longrightarrow UF_5^- + F$)

FIG. 43

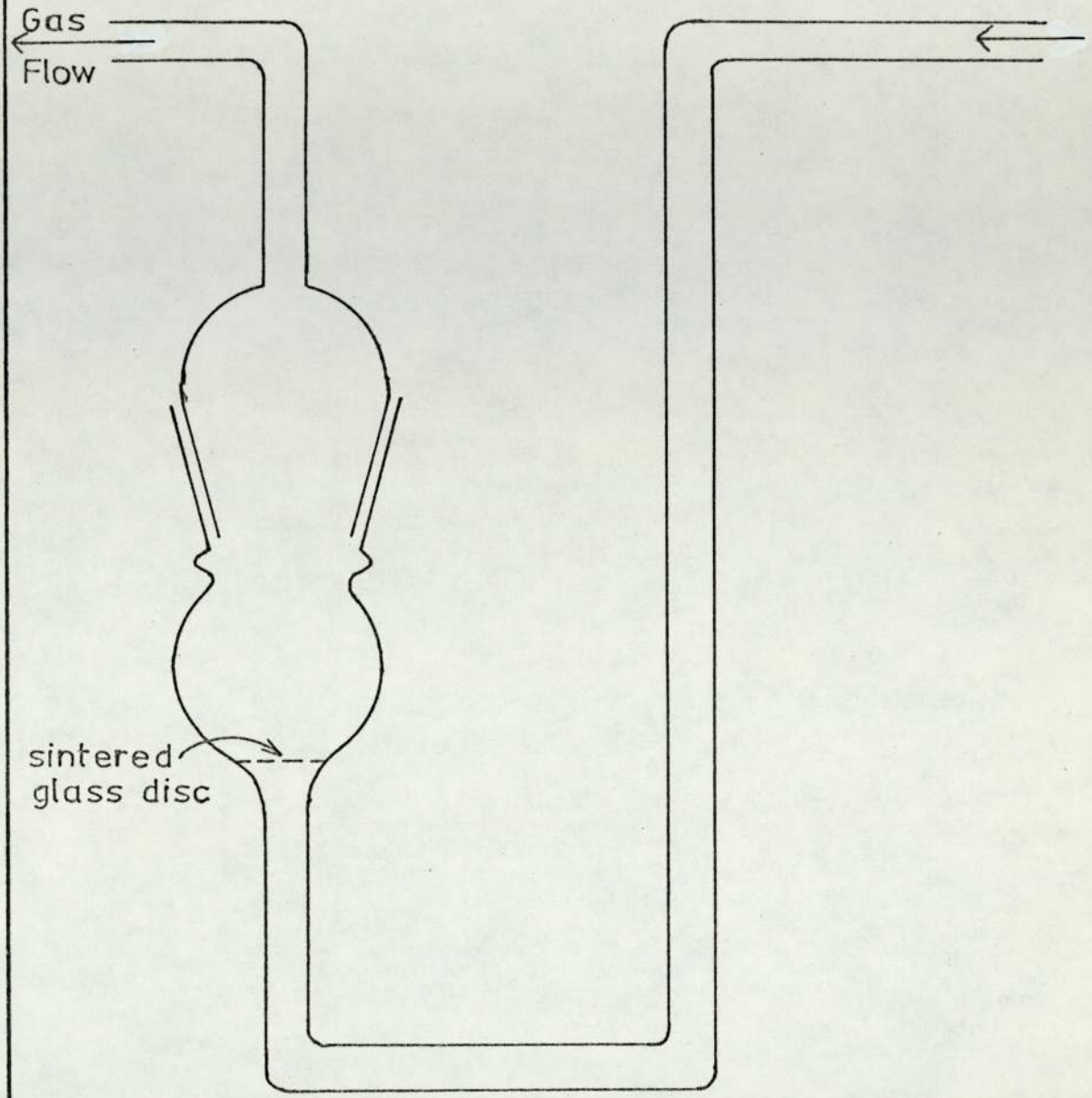

SATURATOR USED FOR INTRODUCING SAMPLE IN CARRIER GAS

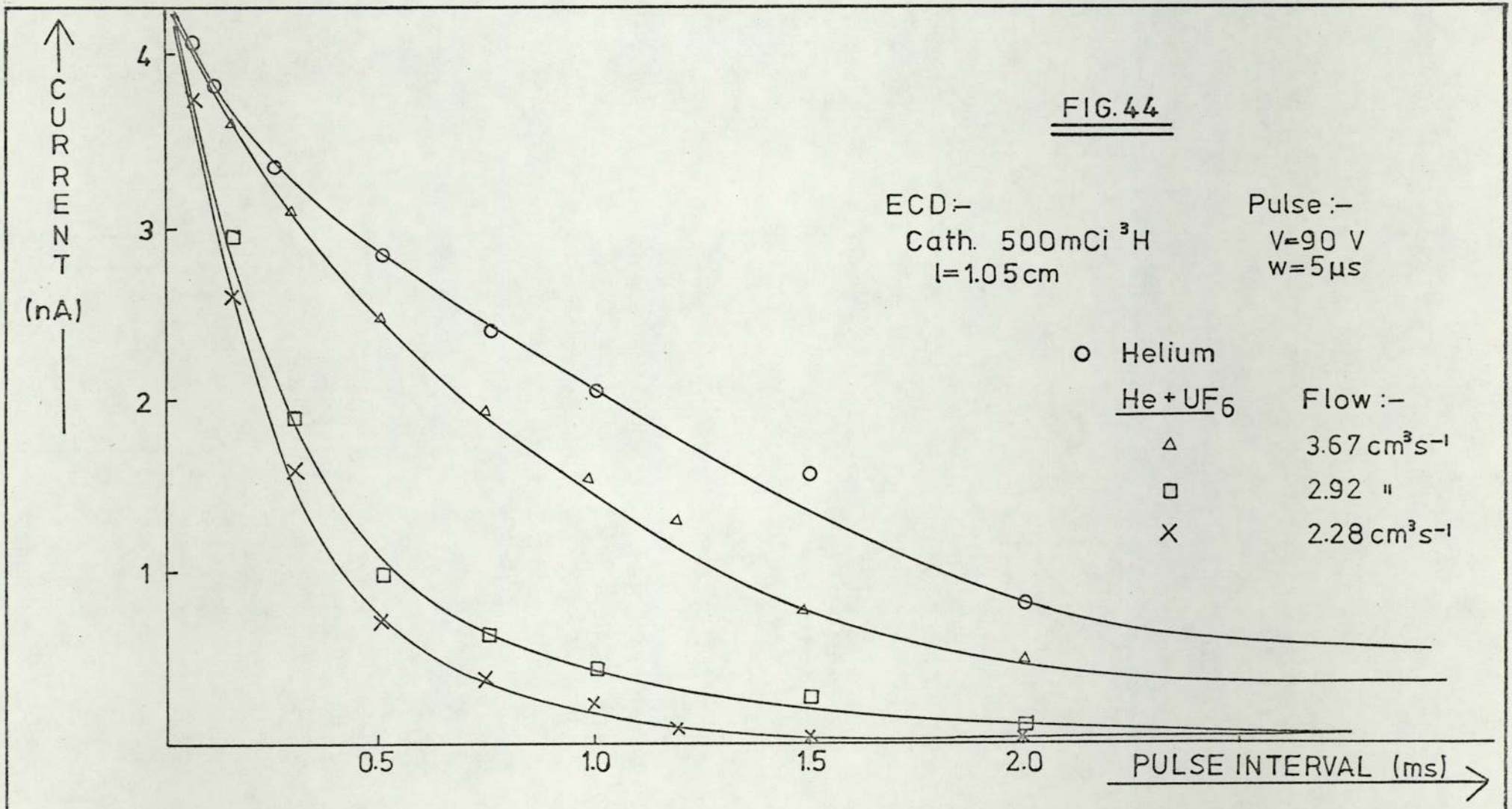

CURRENT VARIATION WITH PULSE INTERVAL FOR HELIUM AND HELIUM + UF_6

FIG. 45

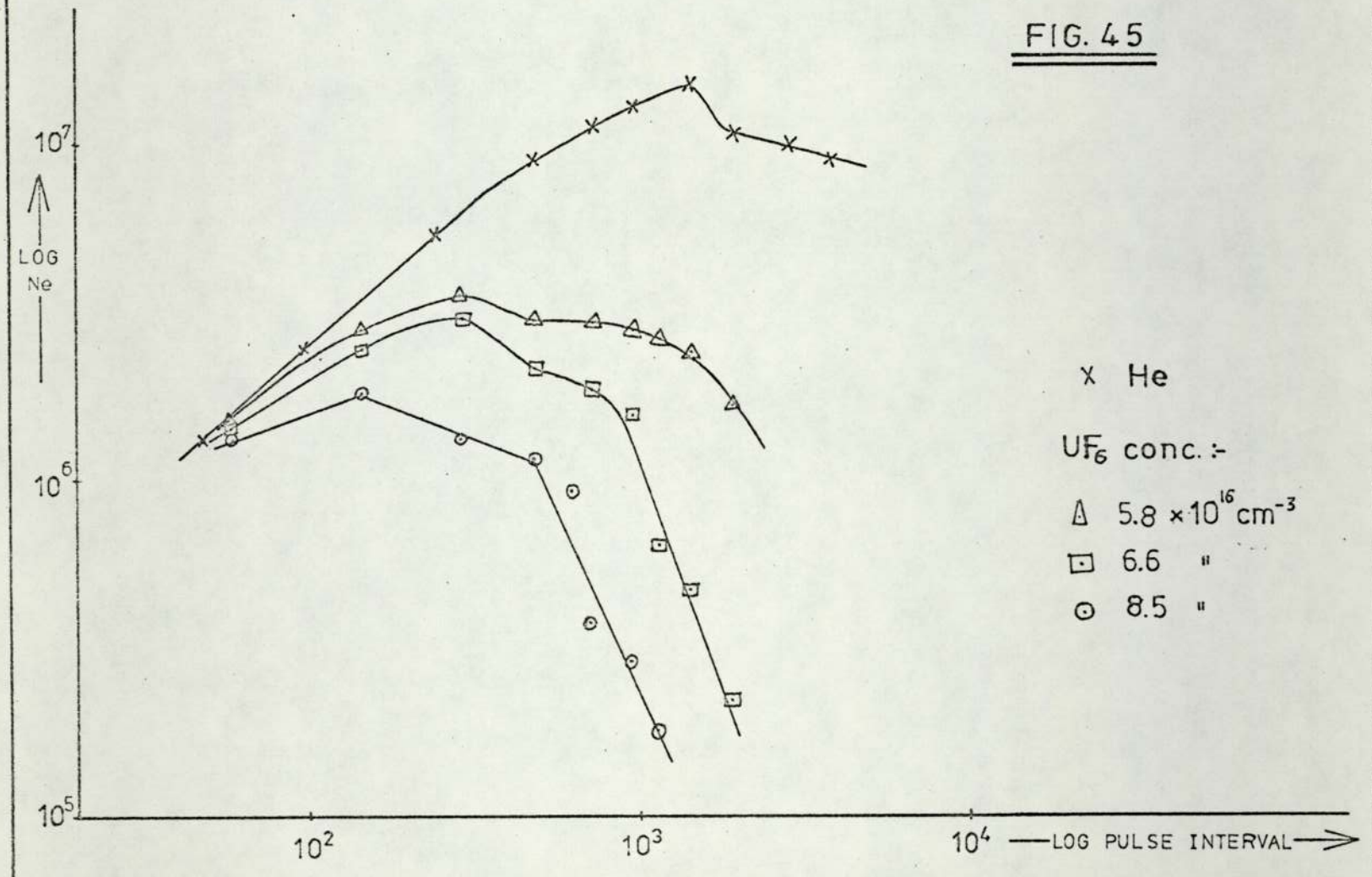

Ne - PULSE INTERVAL RELATION FOR HELIUM AND He + UF_6

leading to an highly capturing species as a product may well be responsible for this observation.

The flow rate which is inversely proportional to the concentration of UF_6 introduced, varies linearly with Ne (Fig. 46). Hence, a linear relationship exists between detector response and sample concentration. Basing the calculation on Lovelock's 'stirred reactor model', the capture rate constant for UF_6 is about 5.1×10^{-14} cm^3 $molecules^{-1}$ sec^{-1}. Table 7 shows the values obtained with two different sample concentrations. In comparision to the capture rate constant for SF_6 (approximately 2.5×10^{-7} cm^3 s^{-1}) the value obtained for UF_6 is very small. Stockdale and Compton[63] have shown that direct electron attachment in UF_6 is absent and this probably explains the low capture rate constant.

The need for a carrier gas free of electron capturing impurities has always been recognised. The presence of trace levels of oxygen in the carrier have been shown (59) to reduce the standing current to less than half its maximum value. However, the presence of water has been a controversial issue as both its effects and non-effects have been reported[7]. It is of practical importance to know its effect on the ECD response as many GLC samples are either prepared or present in an aqueous media. The presence of small quantities of water vapour in the detector may also facilitate the determination of the electron-ion recombination coefficient for H_3O^+ ion.

The apparatus used for the purpose was the same as that described for the introduction of UF_6 in the carrier gas stream. The saturator was filled with 10 cm^3 of boiled distilled water and a fraction of the gas stream was bubbled through it. With the saturator at a temperature of $0.5^{\circ}C$, the amount of water vapour present ($\simeq$ 4.75 mm. Hg. pressure) reduced the standing current by 25%. To

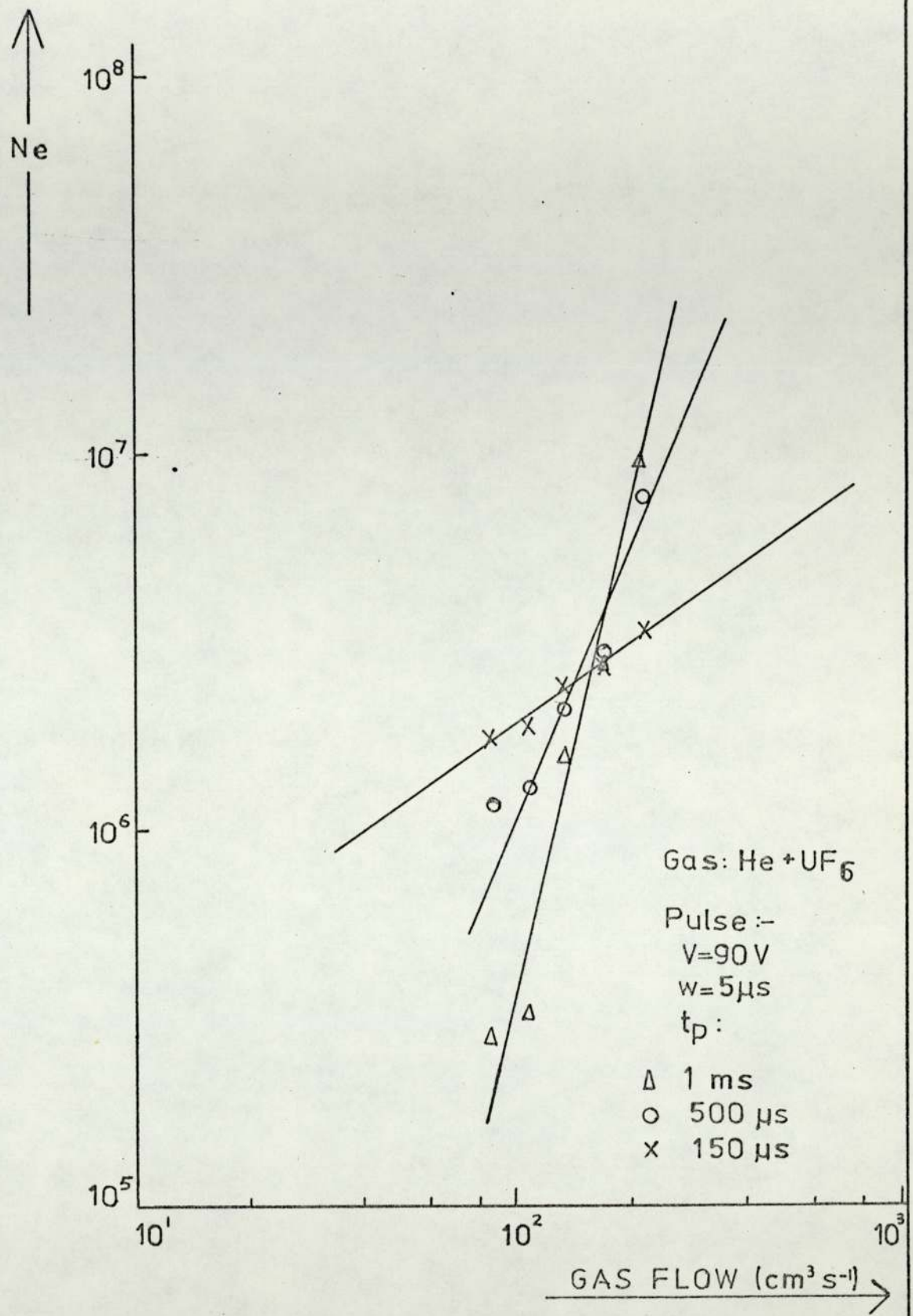

FIG. 46

VARIATION OF Ne WITH GAS FLOW RATE THROUGH SATURATOR CONTAING UF_6

TABLE 7

CAPTURE RATE CONSTANT FOR UF_6 AT DIFFERENT SAMPLE CONCENTRATION

FLOW RATE	CONCENTRATION	PSEUDO RECOMBINATION COEFFICIENT	CAPTURE RATE CONST.
2.9 cm^3 s^{-1}	5.8 x 10^{16} cm^{-3}	2.86 x 10^3 s^{-1}	4.9x10^{-14} $cm^3 s^{-1}$
2.3 cm^3 s^{-1}	6.6 x 10^{16} cm^{-3}	3.47 x 10^3 s^{-1}	5.1x10^{-14} $cm^3 s^{-1}$

decrease the concentration further, a mixture of sodium sulphate (anhydrous + decahydrate) was used instead. Equilibrium established between the two states at different temperatures[64] gives varying H_2O vapour pressure and is expressed by

$$\log P = - \frac{2837.83}{T} + 10.7866$$

where P is the vapour pressure in mm. of Hg and T is the absolute temperature. Glasstone[65] points out that a salt-hydrate system requires the presence of two solid phases in addition to vapour; the vapour pressure for the system is then definite and independent of the relative amounts of the two hydrates. In $Na_2 SO_4$ the dehydration proceeds gradually to completion without the appearance of intermediary hydrates.

To saturate the carrier gas with water vapour, it was allowed to filter through the salt mixture. Also for conditions to normalise in the detector, the gas was passed through the cell for about 3 hours before taking the first readings. $Al_2 O_3$ traps at the end of the gas line confirmed the presence of water vapour in the carrier gas stream.

Fig. (47) shows the variation of Ne with the pulse interval. It is clear from the graph that G.C. operators working at a pulse interval of about 500 μs would observe a negligible change in the standing current at very low water vapour concentrations. The effect is more pronounced at long pulse periods. The observed variation is very similar to that reported by Wiel and Tommassen[59] for the presence of oxygen in the carrier gas stream. They also noted that water concentration in their investigation was 3 p.p.m. and that although electron attachment in water is negligible[66], reference has been made to electron capturing properties of water[67]. Karasek and Kane[68], using the technique of plasma chromatography have identified $(H_2O)n\ O_2^-$ and $(H_2O)n\ H^+$ as the predominant ions when trace amounts of air is present in the carrier gas. The formation of positive species in nitrogen containing small concentrations of water vapour have been studied by Good

FIG. 47

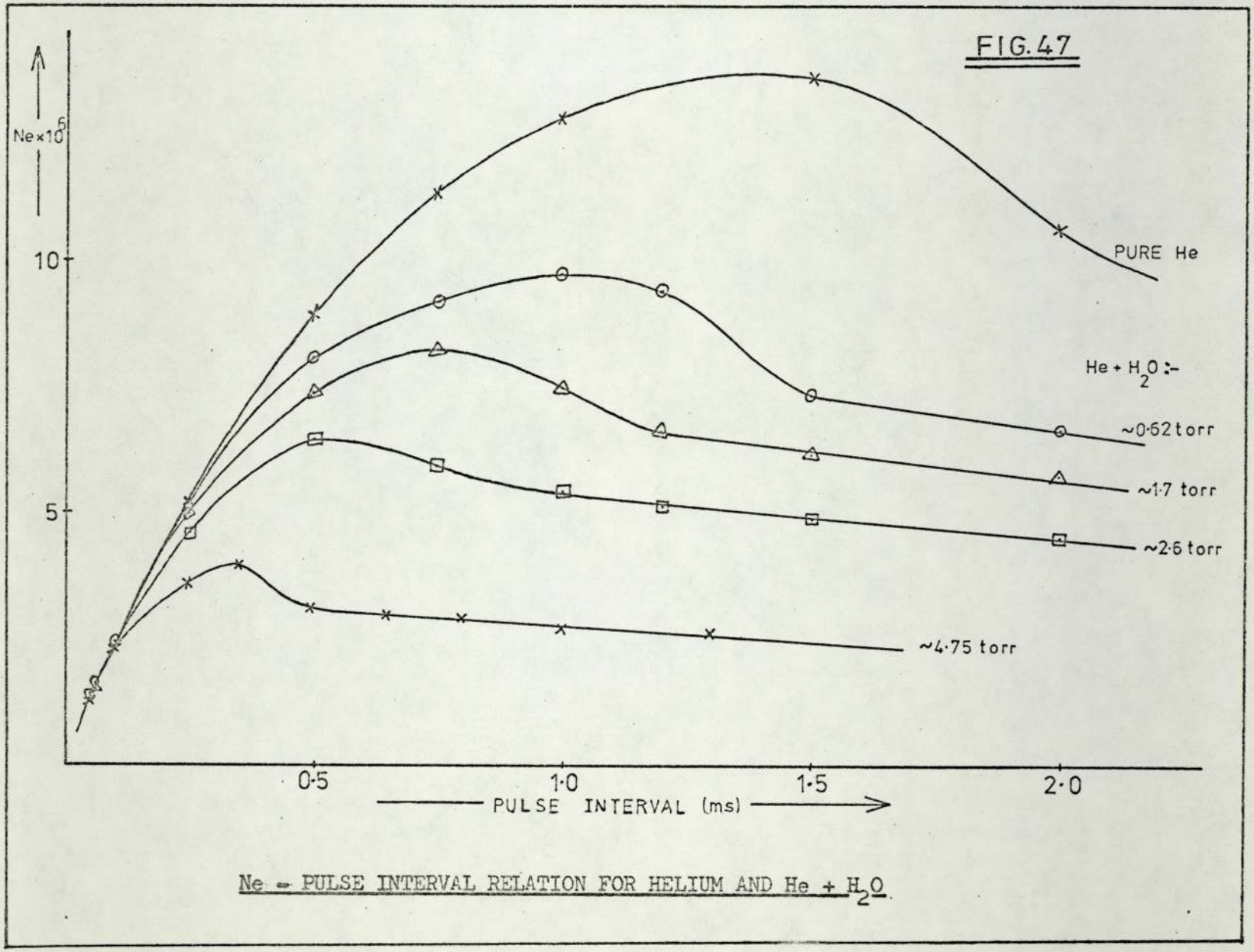

Ne - PULSE INTERVAL RELATION FOR HELIUM AND He + H_2O.

et al.[69] Based on their schematic outline of the reactions occurring, the following step reactions can be proposed for moist helium:

$$He_2^+ + H_2O \longrightarrow H_2O^+ + 2He$$

$$H_2O^+ + H_2O \longrightarrow H_3O^+ + OH$$

$$H_3O^+ + H_2O + He \longrightarrow H^+(H_2O)_2 + He$$

It appears that both in the present work and in Tommassen's the predominant negative ion is $(H_2O)n\ O_2^-$, thus explaining the similarity in the observations made.

The capture rate constant (k_1) for the water clustered oxygen ion is estimated to be about 1×10^{-13} cm^3 s^{-1}. As in the case of UF_6, the calculation is based on Lovelock's stirred reactor model[42] and properties of the holomorphic function; $k_d = 2 \times 10^3$ s^{-1} and $C = 2.15 \times 10^{16}$ molecules cm^{-3} (for $P_{H_2O} = 0.62$ torr), whereby $k_1 \simeq k_d / C$. The value obtained is of the right order of magnitude when compared with that given for oxygen by Hasted.[22]

A systematic series of investigations of the ionisation in pre-mixed $H_2 + O_2 + N_2$ flames has been made over a considerable period.[70, 71] In the presence of even a small hydrocarbon impurity, the main positive ion produced is H_3O^+. It is also a major ion (besides NO^+) in the lower levels of the ionosphere. At atmospheric pressure, the recombination coefficient for

$$H_3O^+ + e^- \longrightarrow H_2O + H$$

has been found to be $2.2 \pm 1.0 \times 10^{-7}$ cm^3 s^{-1}. This value was obtained by Green and Sugden[72] from measurements made in flames at temperatures around 2000 K. There is some controversy as to whether the recombination coefficient for H_3O^+ is temperature dependent or not. The proposed model for the ECD does allow the

rate constant to be evaluated from the response observed when small amounts of water vapour are introduced in the carrier gas at room temperature. Helium was chosen as the carrier gas because of its very low recombination coefficient.

The positive ion mobility can be assumed to be about 4 cm^2 V^{-1} s^{-1}. For the slightly heavier negative species, $(H_2O)O_2^-$, the mobility has been reported to be about 2.9 cm^2 V^{-1} s^{-1} (68). The mean value for the 'Gaines factor', R, is then 1.90×10^2. The value of Ne at s = 1.3 ms is 6.3×10^6 electrons per pulse for the case where the water vapour pressure is 1.7 torr. The recombination coefficient, k_2, for H_3O^+ (presumably) is $3.6 \pm 1.0 \times 10^{-6}$ cm^3 s^{-1}, calculated from Eq. [45].

Measurement of the rate constant at different flame temperatures(81) showed that it had little or no temperature dependence. However, as pointed out in section 3.2, Thomson's theory of three-body recombination(35) predicts a $T^{-3/2}$ dependence at gas pressures between 700 and 1000 torr. Jensen and Padley(82) have shown that the recombination coefficient for reactions involving alkali metal ions and electrons is temperature dependent in accordance with Thomson's theory. Hasted(22) too, points out that recombination processes involving inert gas ions (Ne_2^+ and Ar_2^+) and electrons show a $T^{-3/2}$ dependence but only at higher electron temperatures. The possibility of H_3O^+ behaving in a similar way was thus considered.

Using Green and Sugden's value of the recombination coefficient ar 2100 K(72) and assuming a power dependence of (-3/2) for the temperature, the recombination rate constant for H_3O^+ ion at 300 K would be,

$$k_{2(300)} = (2.2 \times 10^{-7})\ cm^3\ s^{-1} \cdot \left[\frac{300\ K}{2100K}\right]^{-3/2}$$

$$= 4.1 \times 10^{-6}\ cm^3\ s^{-1}$$

This value compares very well with that obtained in the present study. Hence, the rate constant for the reaction

$$H_3O^+ + e^- \longrightarrow H_2O + H$$

appears to be $T^{-3/2}$ power dependent as with other electron - ion reactions indicated above.

CHAPTER FIVE - EXPERIMENTAL VERIFICATION OF ASSUMPTIONS

Many of the assumptions made in theoretical models of the ECD (outlined in section 3.3) have been justified to some extent on the basis of information obtained from experiments where parameters of the applied voltage source were varied. Other experimental methods, to confirm these assumptions, were investigated.

5.1. OSCILLOGRAPHIC STUDIES

Electrons resulting from ionisation of gas molecules are assumed to be highly energetic initially but to lose energy rapidly upon collisions until their average energy is thermal. Calculations [18] of the time taken by electrons to reach thermal energy show that it is well within the normal applied pulse time. An oscilloscope trace of individual current pulses could provide further information.

The circuit (Fig. 48) used consisted of two cells of identical geometry connected in parallel. However, only one cell was equipped with a radiation source; the other cell, with two plane electrodes, acted as a dummy to offset any capacitance effect arising from the cell body. Rectangular pulses were applied to both and the resulting signals were fed into an oscilloscope with a high gain differential amplifier. The oscilloscope was Teleequipment's model 43 equipped with type B amplifier.

It was not possible to amplify sufficiently the output signal obtained under normal operating conditions, ie. $w = 5\ \mu s$ and $s = 1$ ms. Hence, traces were obtained under the following pulse conditions: $w = 8$ ms, $s = 98$ ms and $V = 30$ Volts. Photographs one to six show the observed current pulse when the cell separation is increased from 0.2 cm, 0.65 cm, 0.85 cm, 1.05 cm and

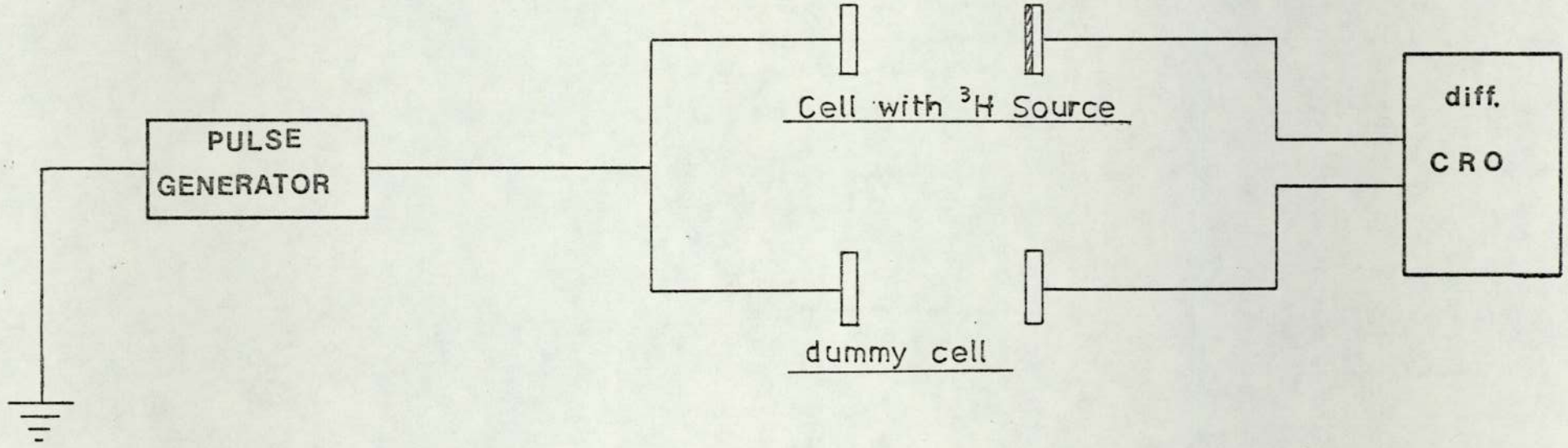

FIG.48

ELECTRICAL CIRCUIT FOR OSCILLOGRAPHIC STUDIES

OSCILLOSCOPE TRACES OF CURRENT PULSE

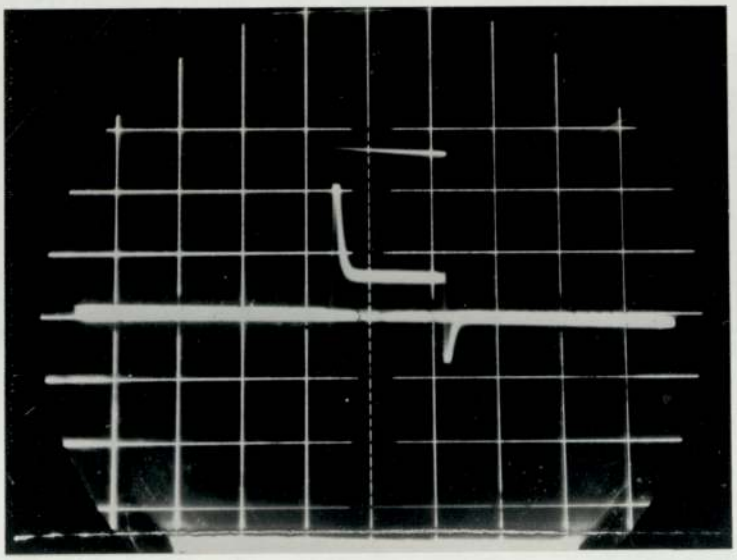

PHOTOGRAPH ONE: electrode separation = 0.2cm

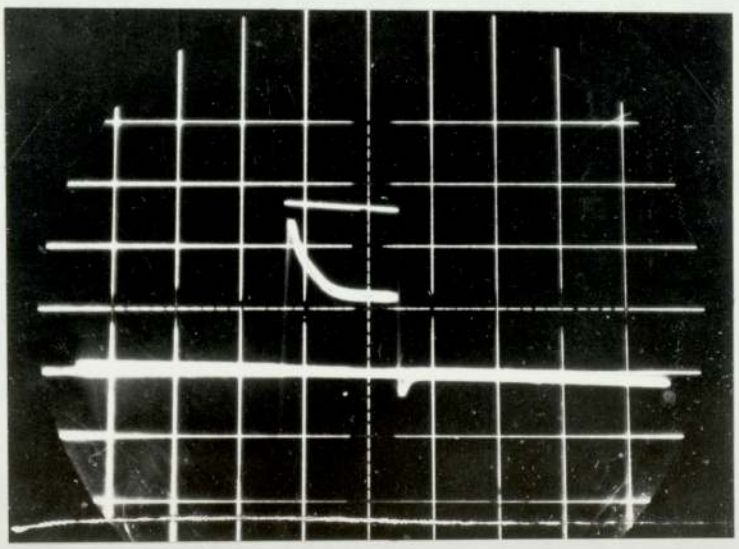

PHOTOGRAPH TWO: electrode separation = 0.45cm

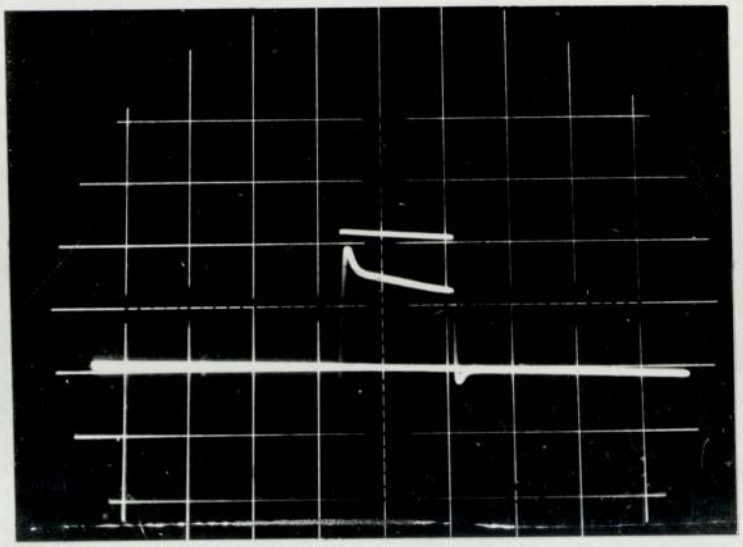

PHOTOGRAPH THREE: electrode separation= 0.65cm

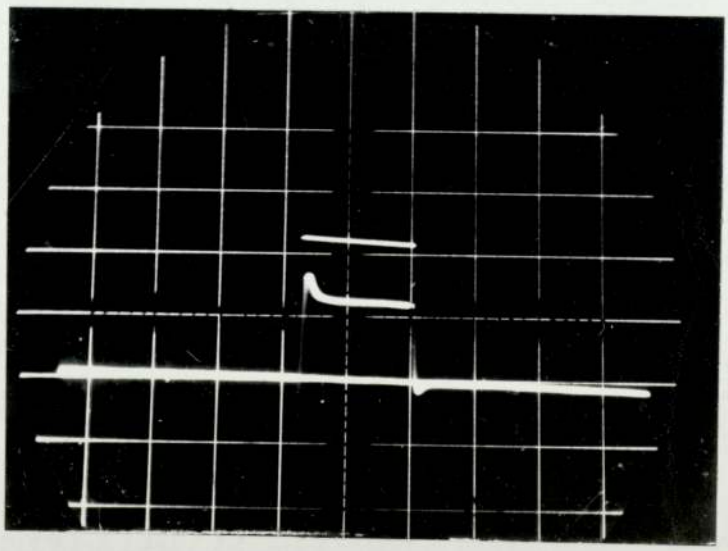

PHOTOGRAPH FOUR: electrode separation = 0.85cm

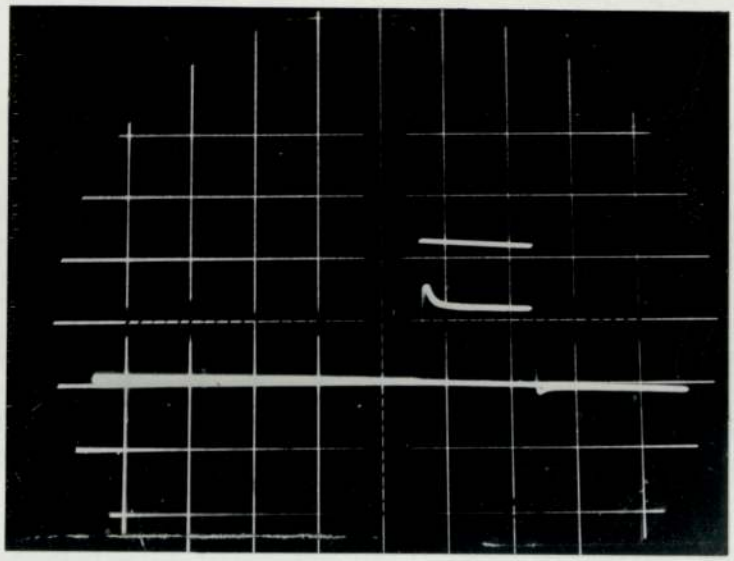

PHOTOGRAPH FIVE: electrode separation = I.05cm

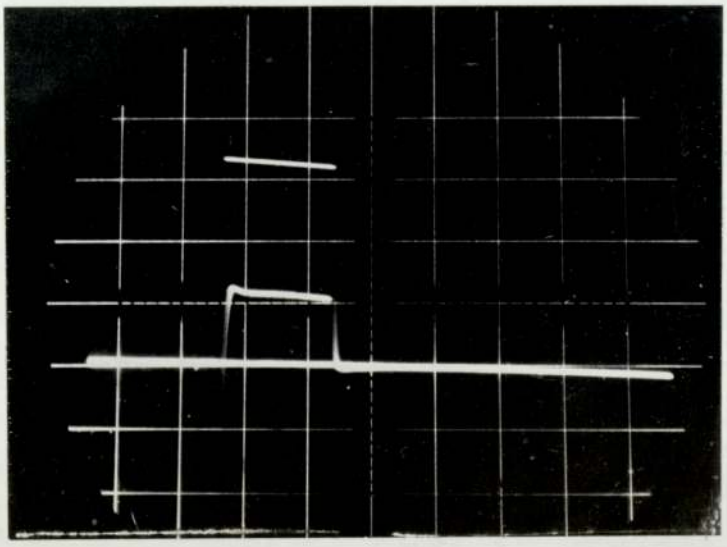

PHOTOGRAPH SIX: electrode separation = I.45cm

1.45 cm. The gas flowing through the cells was nitrogen at a flow rate of 3.6 cm^3 s^{-1}. The Y - base was set at 5 mV cm^{-1} and the time-base sweep was 5 ms cm^{-1} for all cell separations except l = 0.2 cm where the Y-base was 10 mV cm^{-1}.

The effect of decreasing the pulse width from 8 to 1.9 ms was to shorten the width of the output pulse. The initial peak was not affected. The height of the observed pulse began to decrease when the pulse amplitude was lower than 20 Volts (at l = 0.85 cm).

The height of the pulse represents the current flowing through the circuit. Table 8 compares the measured current with that calculated from the pulse height at various inter-electrode separations. The input resistance of the oscilloscope was 10 MΩ. The height cannot be measured accurately when the top of the pulse is not horizontal and consequently there is a small difference in the magnitudes of the two currents.

The photographs indicate a very short delay time and a rise time of about 0.26 ms. This is quite small (3.2%) when compared with the applied pulse time. Hence, the current pulse can be said to be rectangular indicating that the electrons collected are of similar energy. The top of the pulse represents the time of arrival of the slowest electrons. A more rounded pulse would have indicated a broad energy spectrum for the electrons in the cell. The time constant of the circuit, calculated from photograph 2 is about 1.8 ms which is sufficiently long to allow collection of slow electrons. The oscilloscope traces show that the electrons have a reasonably narrow energy distribution; the average energy is likely to be about thermal.

As stated earlier, the width of the current pulse decreased as the applied pulse time was made shorter. Only at very small pulse

TABLE 8

COMPARISION OF THE MEASURED CURRENT WITH THAT CALCULATED FROM THE PULSE HEIGHT IN PHOTOGRAPHS 1 – 6

PHOTOGRAPH NUMBER	PULSE HEIGHT	CURRENT ($X10^{-10}$ A)	
		CALCULATED	MEASURED
1	0.55 cm	1.40	1.40
2	1.05 cm	5.25	5.20
3	1.23 cm	6.15	5.85
4	1.10 cm	5.50	5.60
5	1.05 cm	5.25	5.40
6	0.95 cm	4.75	4.95

width (< 1ms), did the height of the current pulse decrease. This would seem to indicate that all electrons present in the cell are collected as they only require a few microseconds to traverse the cell. As a first approximation, electrons farthest from the anode (10 mm. away) would only take about three times the time taken by electrons closest to the electrode to be collected. Hence, the collection of charged particles is completed in the initial upsurge of the observed current pulse.

Output pulses from a circuit consisting of a coupling capacitor and an input impedance (Fig. 49) have similar characteristics to the current pulses observed in the present study. The tail of the electron pulse represents the natural decay of the RC network at the amplifier input.[73] The coupling capacitor determines the tilt or droop of the horizontal section of the waveform, seen in the photographs. If the input voltage pulse is Vi and the output voltage Vo, then the two are related by,

$$\frac{dVi}{dt} - \frac{dVo}{dt} = \frac{Vo}{RC}$$

For a rectangular pulse input, the solution of the above equation is $Vo = V \cdot \exp - (W / RC)$ where V is the applied pulse amplitude and W it the pulse width.[74] The above equation predicts a larger output voltage with increasing values of RC. Consequently, the tilt of the decay curve becomes increasingly horizontal. Hence, photographs of the electron pulse taken at small cell separations (0.2 and 0.45 cm) exhibit steeper decay curves than those taken at longer electrode spacings (0.65, 0.85 and 1.05 cm) where the charge density is high.

The oscilloscope traces have provided further data on the state of the electrons in the detector and have also aided in the interpretation of the measured current.

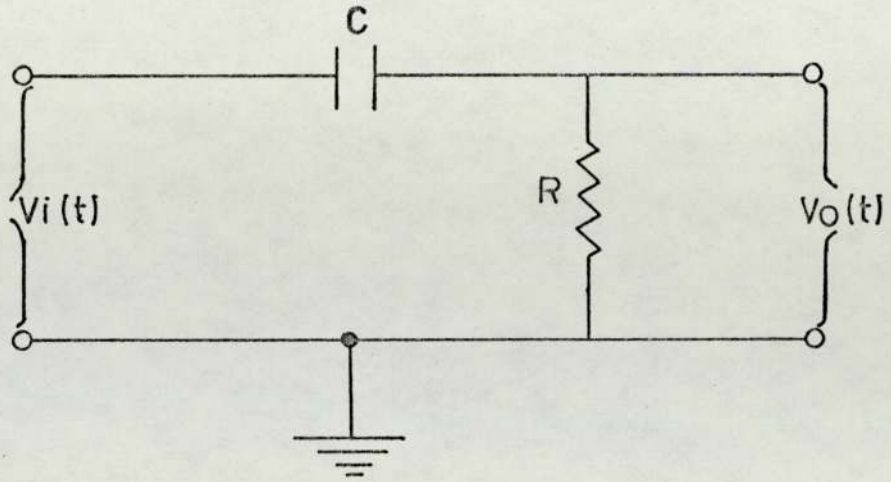

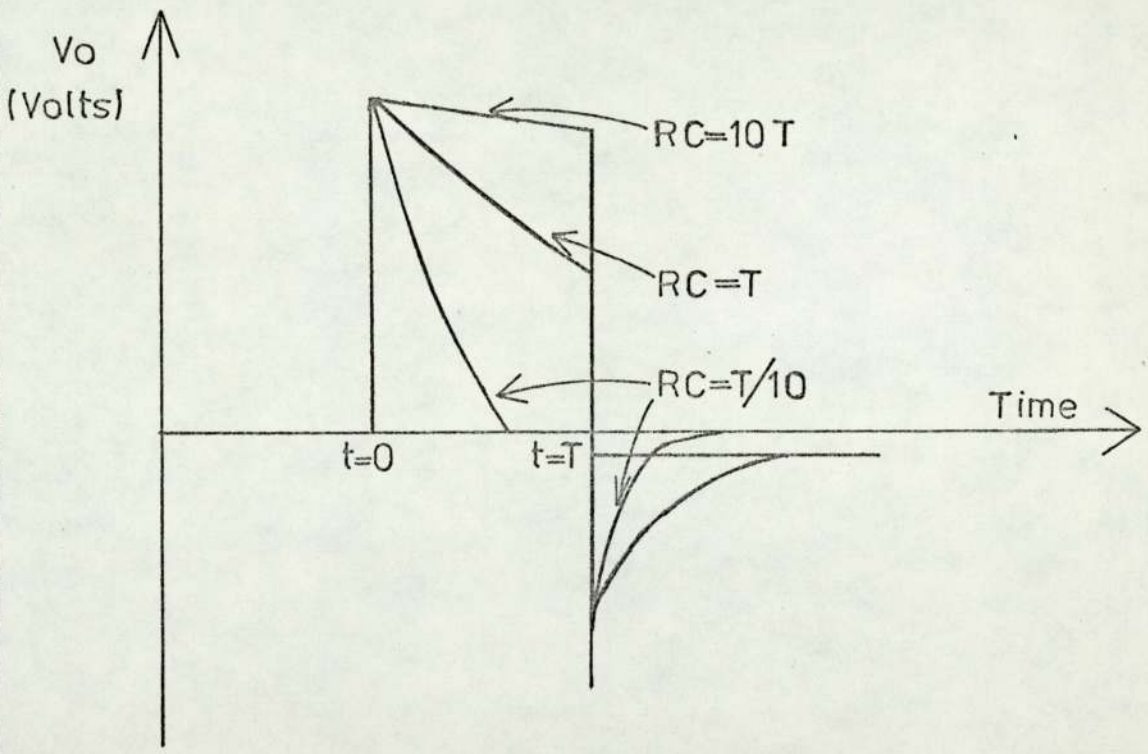

FIG. 49

DIFFERENTIATING CIRCUIT AND OUTPUT PULSE

5.2 PROBE STUDIES

The difference in electron and ion mobilities has been held responsible for the large excess of positive ions in the ECD. Kinetic analysis of the processes occurring in the cell becomes meaningful only when the concentration of positive species is considered to be about a thousand times greater than the free electron concentration. An attempt was thus made to determine the positive ion density in the cell using electrostatic probes.

Experimentally, electrostatic probes are simple devices consisting merely of an insulated wire (platinum) used with a d.c. power supply and an ammeter (Fig. 50). However, the theory of probes is extremely complicated. The difficulty stems from the fact that probes are boundaries to a plasma, and near the boundary the equations governing the motion of the ions in the plasma change their character.

The current drawn by a probe is a function of the charged species, the number density, the applied potential and local conditions around the probe surface. Fig. (51) shows the current-voltage graph obtained with a double-probe system. It has three distinct regions :

a) REGION AB

At large negative voltages, the current is relatively insensitive to the applied voltage and corresponds to positive ion saturation on probe 2. All electrons are repelled and an ion sheath surrounds the probe.

b) REGION BC

A transition region close to zero applied potential where the current changes rapidly with voltage due to the ability of electrons to approach both probes.[75] As the probe voltage is made less negative, some of the high energy electrons penetrate the ion sheath and reach the probe. The less negative the voltage relative to the

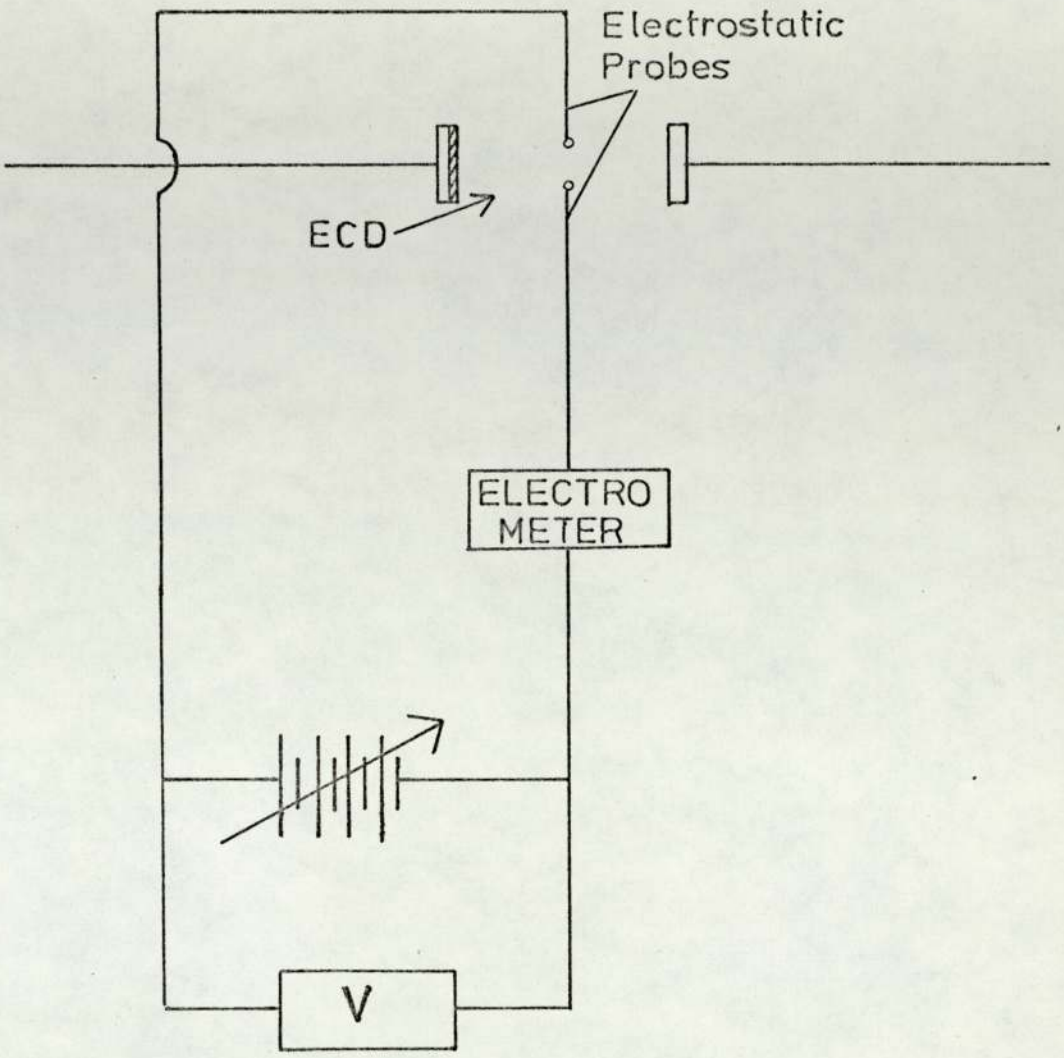

FIG.50

CIRCUIT DIAGRAM FOR A DOUBLE PROBE SYSTEM

plasma, the more electrons will have sufficient energy to overcome the retarding field. Thus, the current steadily increases.

c) REGION CD

A region at large positive voltages where the current is relatively independent of the applied voltage and corresponds to negative charge saturation on probe 1. If the probe voltage is made positive relative to the plasma, electrons are accelerated towards the probe. Near the probe surface there is therefore an excess of negative charge, which builds up until the total charge is equal to the positive charge on the probe.(76)

Johnson and Malter(77) developed the double probe technique. The operation of a double probe system is governed by two factors :

i. Kirchhoff's law that the total net current drawn by the probes is zero, ie. the electron current collected by the probes is always equal to the total positive ion current collected by them.

ii. The electron current to each probe is governed by the Boltzmann Law.

At high pressures ($>$ 1 mm Hg) a positive ion experiences many collisions with neutral molecules within the sheath surrounding the probe. Under these conditions the mean free path for the charged species is very much smaller than either the Debye length or the probe diameter. The effect istwo fold : first, the motion of the ions within the sheath becomes mobility controlled and secondly, a fraction of the ions entering the sheath is lost from the sheath due to the scattering.

The theoretical treatment of Su and Lam(78) has probably had the widest application to probe theory in high pressure, collision dominated plasmas. They determined the charge distribution

about a spherical probe using the continuity equations together with Poisson's equation making no assumptions regarding the presence of a boundary layer sheath.

A quantitative analysis of the results obtained has been made, using three different theories developed by workers[79] using electrostatic probes to measure positive ion concentrations in flames. Conclusions reached have to be treated with caution as it is assumed that the theories are generally applicable.

The circuit for the double probe system used is shown in Fig. (50). Current was measured on an AVO 1388 B d.c. amplifier. The ECD was not part of the probe circuit. Each probe consisted of a platinum wire enclosed in a glass tube (0.128 in. in diameter). The end of the wire was turned into a sphere of radius 2.9×10^{-4} m. Care had to be taken to ensure that the two probes had very similar areas. Studies were made with a slow flow of nitrogen through the cell and a fixed inter-electrode separation of 0.5 cm. Fig. (51) shows the current-voltage plot obtained. Analysis of results is as follows :

1) TRAVERS AND WILLIAMS APPROACH[75]

One assumption needs to be made; at high pressures, the positive ion current density reaching the edge of the sheath layer surrounding the probe is equal to the positive ion random current density in the plasma.

Within the sheath, the positive ion current, ip, at a radius r is given by,

$$ip = -4\pi r^2 N_+ e \mu_+ X$$

where, N+ is the positive ion density (m^{-3}) and μ_+ is the mobility of the positive ion. Substitution of Poisson's equation for charge density gives,

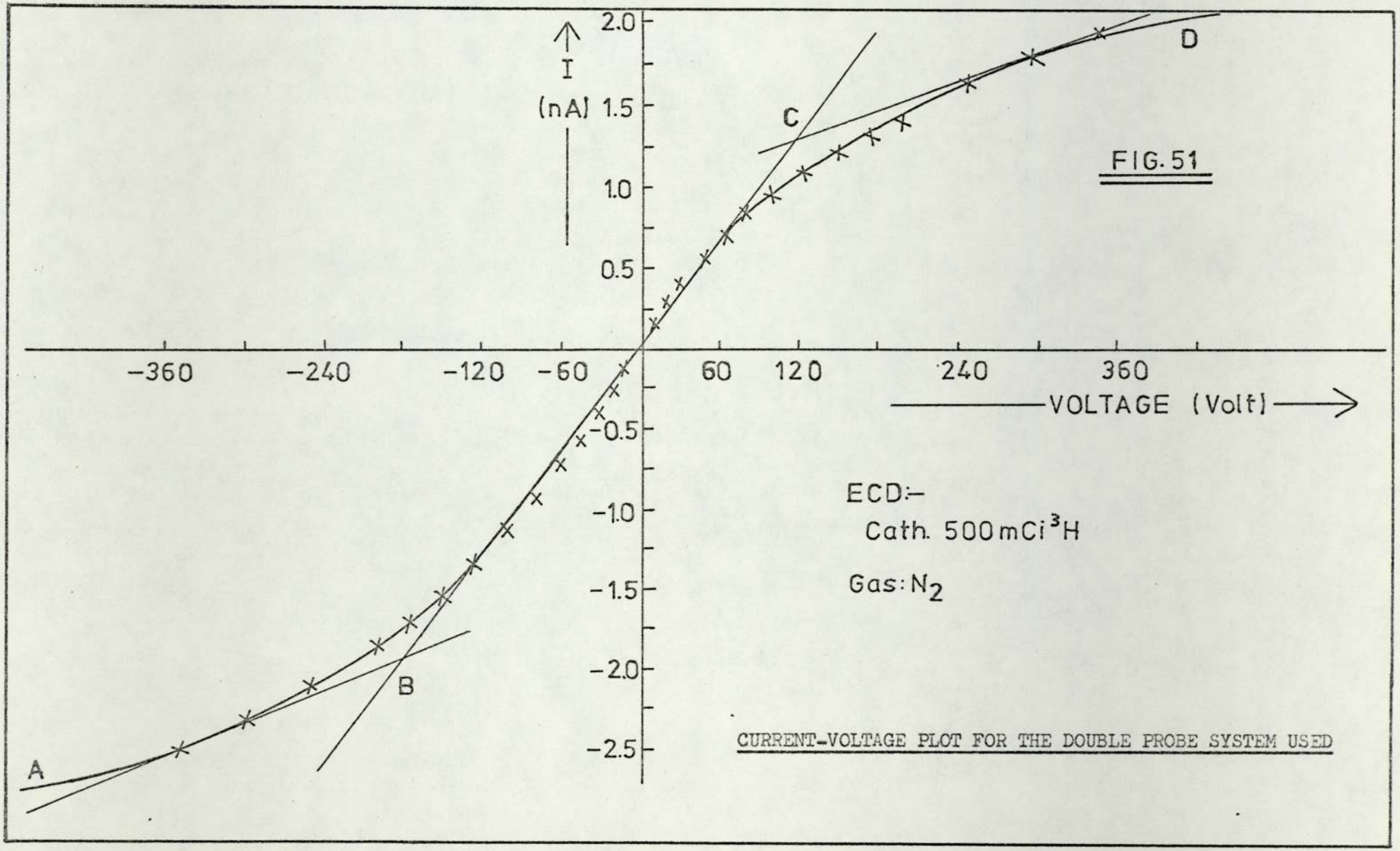

FIG. 51

CURRENT-VOLTAGE PLOT FOR THE DOUBLE PROBE SYSTEM USED

$$\frac{d^2V}{dr^2} + \frac{2}{r}\frac{dV}{dr} = \frac{-ip}{4\pi\mu_+ \varepsilon_o r^2 (dV/dr)}$$

Integrating once and applying boundary conditions that $dV/dr = 0$ at $r = \bar{a}$ (the sheath radius) leads to,

$$V = \left[\frac{ip}{6\pi\mu_+ \varepsilon_o}\right]^{1/2} \int \frac{(\bar{a}^3 - r^3)^{1/2}}{r^2}\, dr \qquad [47]$$

As no analytical solution of the above integral has been found, a numerical integration was performed between the limits $r = \bar{a}$ and $r = r_p$ for a range of values of the ratio $\bar{a} / r_p$ where r_p is the probe radius. To facilitate this, the integral was made non-dimensional by means of the substitution $x = r/\bar{a}$. Making this substitution the above integral becomes,

$$\bar{a}^{1/2} \int_{1/n}^{1} \frac{(1 - x^3)^{1/2}}{x^3}\, dx$$

where $n = \bar{a} / r_p$. Equation [47] can now be written as,

$$Vp = \left(\frac{ip}{6\pi\mu_+ \varepsilon_o}\right)^{1/2} (\bar{a}^{1/2} I) \qquad [48]$$

where Vp is onset potential for saturation currents and

$$I = \int_{1/n}^{1} \frac{(1 - x^3)^{1/2}}{x^3}\, dx$$

At Vp = 130 Volts, the positive ion current, ip, is the sum of the currents to probe 1 and 2, ie.

$$ip = ip_1 + ip_2 = (1.10 + 1.38)\ nA$$

$$= 2.48\ nA$$

Hence $(I\, \bar{a}^{1/2}) = 0.54$, calculated from Eq. [48]. The value of

$\bar{a}$ can be obtained from a graph of $(\bar{a}^{1/2} I)$ versus $\bar{a}$. Table 9 gives the values of I and $\bar{a}$, calculated from the probe radius. The value of $\bar{a}$ when $(I\bar{a}^{1/2}) = 0.54$ is 3.18×10^{-3} m. The time for an unscattered positive ion to cross the sheath is given by,

$$t_+ = \frac{1}{\mu_+} \left[\frac{2}{3} (\bar{a}^3 - r_p^3) \right]^{1/2} \frac{(\bar{a}^{1/2} I)}{V_p}$$

$$= 2.38 \times 10^{-3} \text{ s.}$$

The positive ion current, ip, can be expressed by,

$$ip = \frac{6\pi \bar{a}^2}{2\alpha} \frac{Jr}{P} \qquad [49]$$

where Jr is the positive ion random current density; α is the scattering coefficient ($torr^{-1}$) and P is the gas pressure. The value of α calculated from the collision frequency, ν_c and t_+ is,

$$\alpha = \frac{\nu_c t_+}{P} = 2.29 \times 10^{-4} \text{ torr}^{-1}$$

at atmospheric pressure. The random ion current density, Jr, calculated from Eq.[49] is 2.27×10^2 Am^{-2}. Jr can alternatively be expressed by

$$Jr = e N_+ \left(\frac{K T_+}{2\pi M_+} \right)^{1/2}$$

where T_+ is ion temperature (equal to the gas temperature) and M_+ is the mass of positive ion (N_4^+). Hence,

$$N_+ = \left(\frac{2\pi M_+}{K T_+} \right)^{1/2} \frac{Jr}{e}$$

$$N_+ = 1.70 \times 10^{13} \text{ cm}^{-3}$$

2) SU AND LAM APPROACH

The theory allows the determination of positive ion concent-

TABLE 9

NUMERICAL VALUES OF THE INTEGRAL I FOR VARIOUS VALUES OF $\bar{a}/r_p$

n	I	$\bar{a} = nr_p$	$I\ \bar{a}^{-1/2}$
1	0	2.90×10^{-4} m	0
2	0.770	5.80×10^{-4} m	1.86×10^{-2}
3	1.734	8.70×10^{-4} m	5.12×10^{-2}
4	2.722	11.60×10^{-4} m	9.28×10^{-2}
5	3.716	14.50×10^{-4} m	1.42×10^{-1}
6	4.713	17.40×10^{-4} m	1.97×10^{-1}
8	6.715	23.20×10^{-4} m	3.24×10^{-1}
10	8.716	29.0×10^{-4} m	4.70×10^{-1}

ration from the measurement of positive ion current drawn by a spherical probe operated at plasma potential. This is the potential where no sheath exists and hence the probe is at the same potential as the plasma. In the absence of any electric field at this point, charged particles migrate to the probe purely because of their thermal velocities. The plasma potential corresponds to that point on the graph (Fig. 51) where the regions BC and CD meet. The relation that expresses the positive ion concentration is,

$$N^+ = I^+ / (4 \pi r_p D^+ e) \qquad [50]$$

where D^+ is the positive ion diffusion coefficient and I^+ is the positive ion current at plasma potential. The values are :

$D^+ = 6.2 \times 10^{-6}$ m^2 s^{-1} (for N_2^+)(11) and $I^+ = 1.65$ nA at $V = -162$ Volts. Hence, the ion density is 4.56×10^{11} cm^{-3}.

3) BOHM, BURHOP AND MASSEY'S APPROACH(76,80)

In the case of spherical probes and in the limit $\lambda \ll r_p$.

$$I^+ = \frac{n+ \bar{v} Ap}{4} \quad \frac{3 \lambda e}{4 r_p} \qquad [51]$$

The mean free path, λ, ($\simeq 10^{-6}$ cm) is very much smaller than the probe radius, $r_p \simeq 10^{-2}$ cm. $\bar{v}$ is the average magnitude of the thermal velocity and is calculated from the kinetic theory. The probe area, $Ap = 4 \pi r_p^2$. I^+ is as defined previously. The positive ion concentration is given by,

$$N+ = \frac{4 I^+}{3 \bar{v} \pi r_p \lambda e}$$

$$N+ = 4.9 \times 10^{11} \text{ cm}^{-3}$$

The Travers and Williams approach has been found to give a value of N+ one or two orders of magnitude higher than that obtain-

ed with other theories.[79] There is very good agreement between the other two values obtained and hence the positive ion concentration in the detector (for nitrogen) can be said to be about 4.7 x 10^{11} cm^{-3}. A typical current density of about 10^{-10} A gives an electron concentration of 1.6 x 10^{9} cm^{-3}. Hence, the Gaines factor, as the ratio of positive ions to electrons is 3 x 10^{2}; this is comparable to the mean value of R (3.4 x 10^{2}) calculated from the values given in Table (6).

5.3 FLOW OUTLET CURRENT

Carrier gas flow has been considered to be a plausible mode of loss for positive ions in the cell. It would lead to an increase in free electron concentration as losses through volume recombination diminish. The time constant for removal of ions through flow is comparable to that of other processes responsible for the loss of positive ions from the cell (as shown in section 4.6). Wentworth et al.,[18] assumed that there was slow removal of material from the detector by flow of the carrier gas. They attributed the observed peak in the graph of (Ne versus s) to a change in the mechanism by which positive ions were removed from the detector. Lyons et al.,[39] suggested that the concentration of positive ions was inversely proportional to the gas flow rate. However, no experimental evidence was presented in either of these studies and so an attempt was made to verify experimentally whether carrier gas flow was a possible mode of loss for positive ions in the cell.

An electrometer was connected to the gas outlet which as described in section 4.1, was a brass tubing threaded half way through the cell body. The electrical contact was insulated by a PTFE sleeve. An external source of potential was not included as this would have introduced additional difficulties in interpretat-

ing the current. The electrometer was thus floating, ie. it could assume a potential positive or negative with respect to the cell potential. The ECD was operated in the normal way and its response was not affected by the current measured on the gas outlet.

Figures (52) and (53) show the variation in this current with d.c voltage as applied to the detector. The cell length was also varied. It is to be noted that a high gas flow rate (4.7 cm^3 s^{-1}) was used in these experiments. The current measured on the gas outlet is a function of the applied potential as an electric field exists between one of the cell electrodes and the gas outflow tube. Hence, at low potentials, the current increases and when at high potentials the current flowing in the ECD circuit reaches its plateau value (indicating the collection of all charged species in the cell), the current measured on the gas outlet decreases. The decrease in the field intensity between one of the cell electrodes and the gas outflow tube is also responsible for the observed decrease in current (at a given voltage) with increasing inter-electrode spacing. At cell separations greater than 1 cm, the polarity of the electrodes seems to be reversed and consequently the sign of the current changes.

The current measured on the gas outlet also varied with the carrier gas flow rate (Fig. 54). The graph shows that at low flow rates (20 cm^3 min^{-1}) the current measured is very small but it increases ten fold when the gas flow is 180 cm^3 min^{-1}. In the pulsed mode, at short pulse periods, the current increases steeply to a maximum; thereafter it declines gradually to a steady level at long pulse interval.

The current measured on the outflow tube could either be due to electrons or positive ions being removed from the cell by carrier gas flow. It cannot be the former because, as Lovelock[42] has

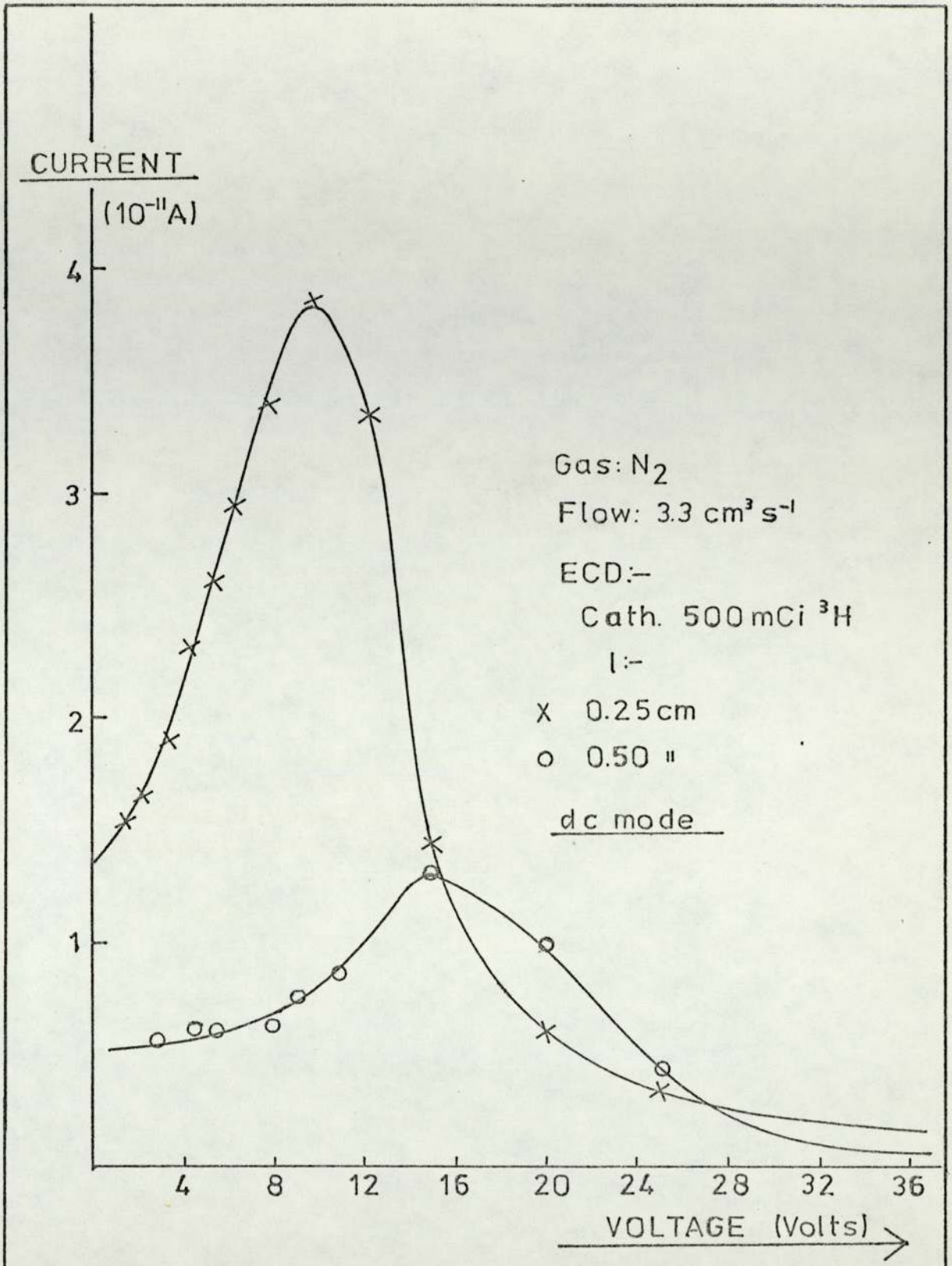

FIG. 52

VARIATION OF CURRENT (MEASURED ON GAS OUTLET) WITH DETECTOR VOLTAGE

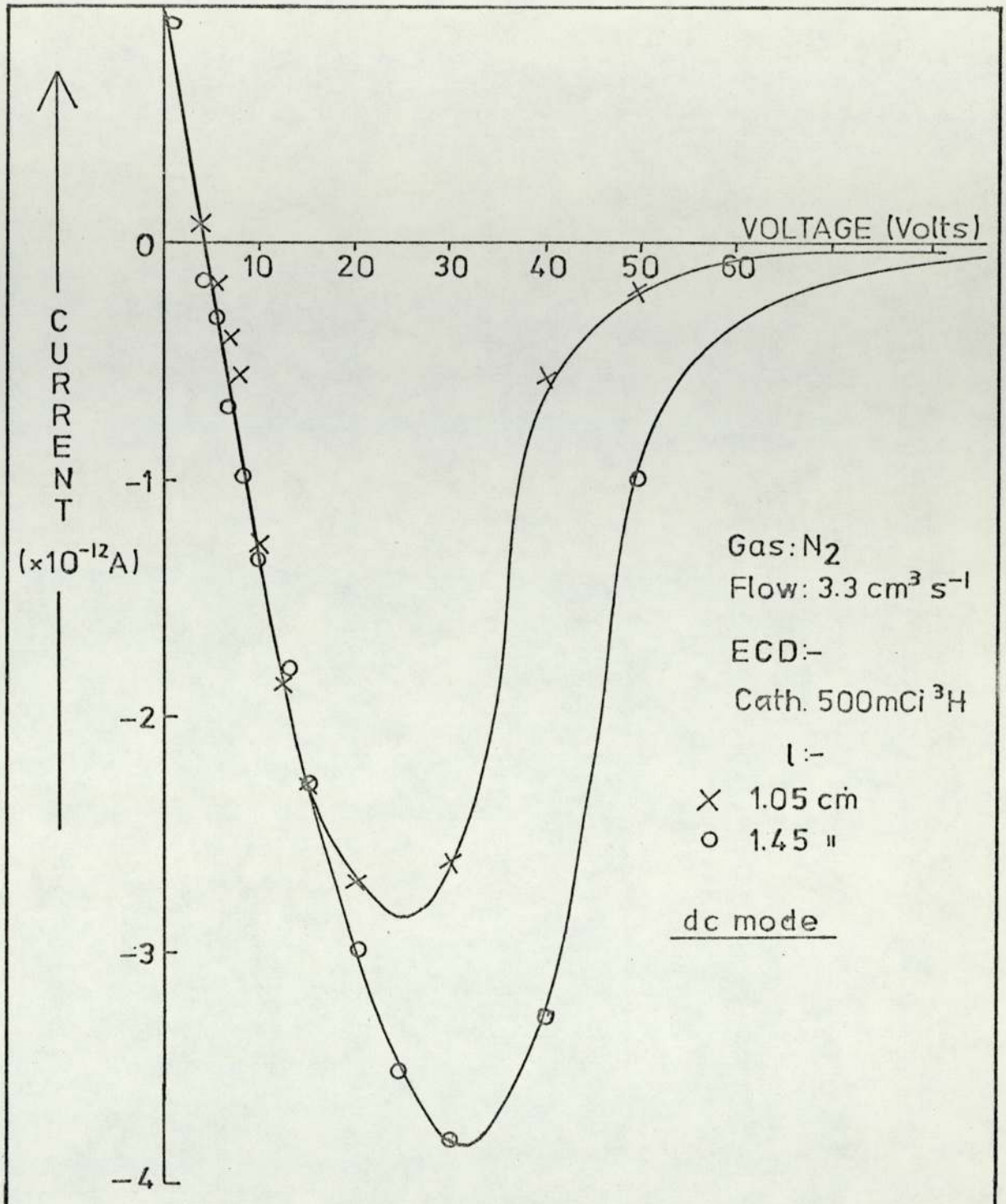

FIG. 53

VARIATION OF CURRENT (MEASURED ON GAS OUTLET) WITH DETECTOR VOLTAGE

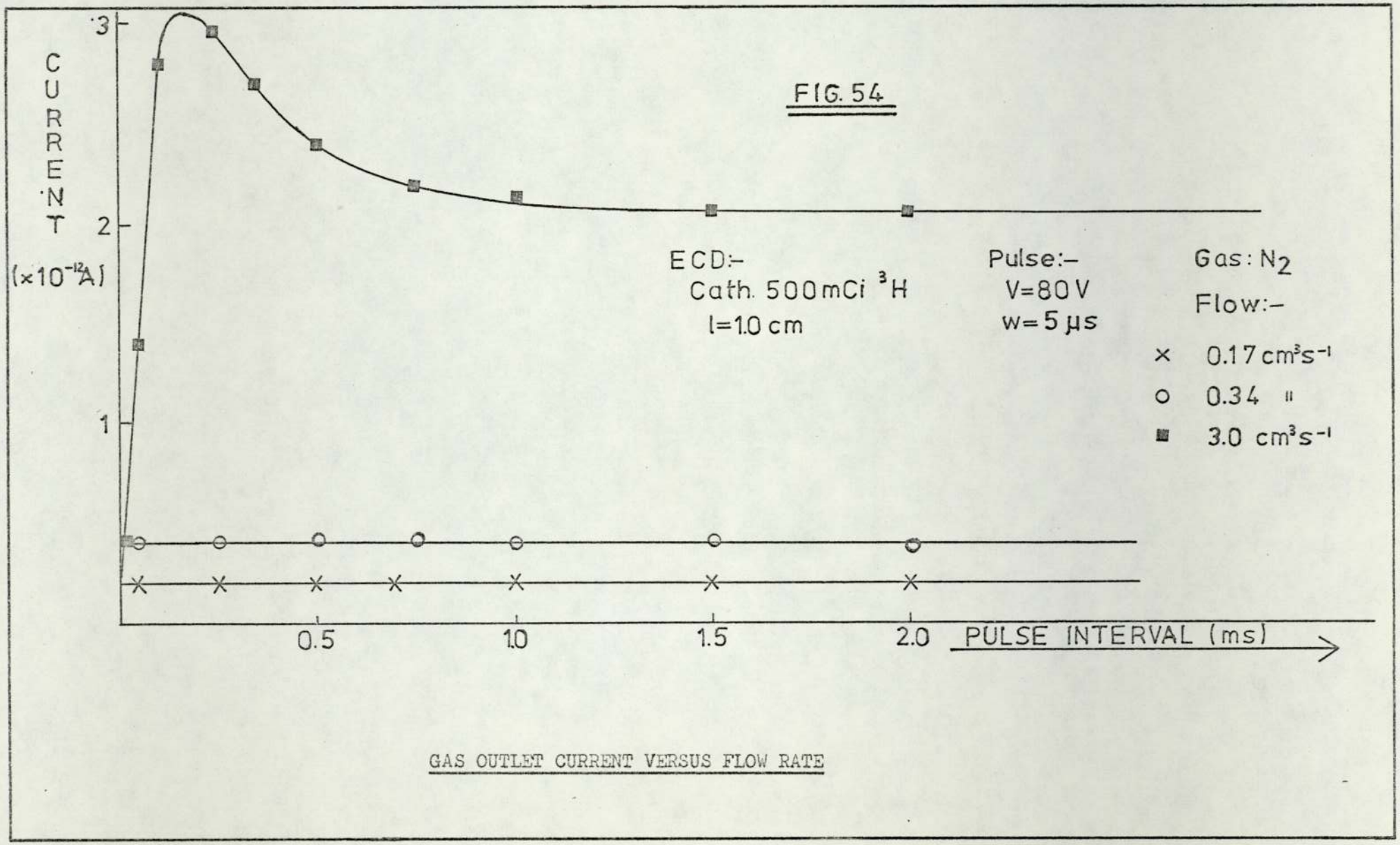

GAS OUTLET CURRENT VERSUS FLOW RATE

pointed out, the residence time of electrons within the detector is too short for a sensible proportion of them to leave the cell in the carrier gas stream. The magnitude of the measured current (10^{-12} to 10^{-11} A) is also rather large for it to be an 'electron current.

The directional drift imposed on the positive ions by the applied field does not significantly alter the residence time of the ions. Their velocity will be comparable to that of gas molecules and hence, the observed current is probably due to the removal of positive species from the cell by gas flow. It can also be concluded from Fig. (54) that at short pulse periods and in the d.c. mode both negative and positive species contribute to the ECD current and at long pulse periods there seems to be a steady removal of positive ions from the cell when the gas flow rate is high.

CHAPTER SIX - CONCLUSION

During the past fifteen years, a fundamental understanding of electron capture detection has been gradually developing. This study has been a further attempt to relate the detector's response to operating parameters and also to detector characteristics. The instrument's potential use as a means of investigating electron-ion processes at normal temperature and pressure has also been put to test. A theory of the detector has been developed to assist in this account and to generally predict the observed signal.

A detector of cylindrical geometry with variable electrode spacing enabled the depth of the reaction zone to be determined. Results obtained with a ^{63}Ni source supported the normally accepted value of about 9 mm. for the range of β^- particles. With ^{3}H sources, the reaction zone seems to extend to about 6.5 mm. from the source and hence does not support the value of 2mm. quoted by Wentworth et. al.,[18] The range-energy relationship showed that the range of average energy β^- particles is about 2 mm. However, in the ECD, it appears that high energy Beta particles are responsible for ionisation, thereby extending the reaction zone to about 6.5 mm. with the normal carrier gases flowing through the cell.

The gas pressure is expected to alter the range of β^- particles and consequently the plasma volume and the degree of ionisation. Results obtained confirmed theoretical predictions that the current should vary linearly with gas pressure when the range of β^- particles is greater than the cell length (at very low pressures) and be independent of pressure when the electrode spacing exceeds the path length.

Studies carried out with two sources of different activities (500 mCi and 150 mCi ^{3}H) showed that the ratio of the observed currents for the two foils depended very much on the characteristics

of the applied potential. In the pulsed mode of operation, at long pulse interval, the ratio was nearly the same as that of the two activities but at short pulse period and in the d.c. mode, the current ratio was about one half the theoretical ratio of the activities. Strong space charge effects, under the latter conditions, could probably be responsible for reducing the current from the 500 mCi source.

The carrier gas flow has been shown to have two effects on the processes occurring in the cell. Firstly, a high gas flow rate tends to diffuse the plasma and hence effect better mixing; secondly, it seems to remove positive ions from the cell at a steady rate. The current variation with electrode spacing in a cell of assymmetric configuration showed that even at large electrode separations ($>$ 1 cm), the current remained very close to its maximum value. This would seem to indicate that the vortices in the flow pattern have dispersed the charged species over a much larger volume than the space in the vicinity of the cathode and consequently more charges were collected during the applied pulse time (w).

The residence time for gas molecules, at high gas flow rates, has been shown to be comparable to the time constants for processes removing positive ions from the cell, ie. volume recombination and surface recombination at the cathode. Experimental evidence included the measurement of a current on the gas outlet. This current was inferred to be due to positive ions since electrons could not be removed from the cell as their residence time is too short for a sufficient number to leave the detector and thus account for the measured current. At long pulse interval the current on the outflow tube reached a steady level, possibly indicating a constant removal of material in the high flow region, where the ECD standing current is independent of carrier gas flow.

Analysis of the current variation with flow of carrier gas is complicated by the presence of a capturing impurity in the gas line. Besides enhancing the diffusion of the plasma and removal of positive species from the cell, a higher gas flow also decreases the concentration of the contaminant, leading to an increase in current. Large changes in standing current with gas flow seem to indicate a predominant effect of the latter as a gas line suspected of leakage showed.

The ECD was used in both the d.c. and pulsed modes of operation. In the former mode, the standing current has been shown to be proportional to V^2 and inversely proportional to l^3 at reasonably high gas flow rates ($> 1\ cm^3\ s^{-1}$).

Kinetic analysis of the detector's response in the d.c. mode, based on the proposed model, has been attempted; however, the agreement was not very good. It is difficult to make reasonable assumptions concerning the various processes occurring in the cell under this mode as it has inherent sources of error: the electron energy distribution is likely to be higher than thermal; a relatively dense space charge may oppose applied potential and absorption of material on electrodes gives rise to contact potentials. The detector could also respond to other parameters of the sample besides electron attachment. The use of the detector in the d.c. mode, at least for routine chemical analysis, is to be avoided.

The pulsed mode of operation was suggested by Lovelock[12] to avoid many of the problems faced in the d.c. mode. In literature reviews,[7,61] the interpretation of the detector response and the physical state in the cell under the pulsed mode, are often not clearly stated or even on occasions erroneous.

The observed current is attributed to the collection of free electrons only and the contribution of positive ions is said

to be negligible. Results obtained in the present study show that the current at small pulse periods does approach the d.c. saturation current. Hence, both electrons and positive ions are removed from the cell by the applied potential. If the pulse width is sufficiently long (1 to 5 μs, depending on detector geometry and size), all the free electrons in the cell are collected and an equal number of positive ions are neutralised by surface recombination at the cathode. Under these conditions, the observed current is a measure of the electron concentration in the cell. The current variation with pulse width and also with the applied voltage, exhibit a plateau after an initial increase. This would seem to indicate that all free electrons are being collected. Oscillographic traces of the current pulse tend to support this conclusion as well. They also show that the electrons have a narrow energy distribution. It seems likely that the average energy is about thermal, ie. $\simeq$ 0.03 eV.

With the use of electrostatic probes, the positive ion density has been shown to be very much greater than that of the electrons. In the pulsed mode, space charge effects are said to be minimised since charge separation occurs only during the short time the pulse is applied for. Studies of the pulse amplitude required for saturation current at various cell separations showed a potential trough similar to that observed under the d.c. mode. It seems that a space charge of positive ions is evident even under the pulsed mode.

Measurement of current at various pulse widths allowed the electron deift velocity to be determined. Wentworth et. al.,[18] also found this to be the case. Velocities obtained in various gases have been tabulated. Agreement with literature values is good and hence it can be concluded that the ECD has a potential use as a means of determining electron drift velocities in various polyatomic gases at low values of X/P.

A theoretical model for the ECD is presented. The analysis is based on treating the detector as a system of rate processes. The significance and the necessary inclusion of a parameter for the build up of positive ions in the cell has been pointed out. The model also makes use of known values of electron-ion recombination coefficients and positive ion mobilities to predict the observed response. The theory developed so far shows an improvement on simpler approaches but still does not conform completely to experiment, notably in not predicting the maximum observed when Ne is plotted against the pulse interval.

In the presence of small molecules, electron attachment leads to a decrease in free electron concentration in the cell. Studies investigating the stability of negative ions have shown that electron detachment is not a very likely process to occur at ordinary temperatures. Small concentrations of UF_6 were introduced in helium as carrier gas in an attempt to study this phenomenon. The detector response, however, was difficult to interpret as dissociative attachment seem to have occurred.

To study the effect of water vapour on the ECD response, small amounts of H_2O were introduced in the carrier gas stream with the help of anhydrous and hydrated $Na_2 SO_4$. The current decreases with increasing concentrations of H_2O and the effect is more pronounced at long pulse periods. The electron attachment coefficient has been evaluated, basing the calculation on Lovelock's stirred reactor model.[42] Also, the electron-ion recombination coefficient for the most likely positive ion (H_3O^+) has been calculated from the proposed model. The rate constant's temperature dependency has also been discussed.

Electron capture detection is a continuously growing field. Recently the ECD has undergone structural changes designed to make

the detector response absolute and independent of the ambient variables of temperature and pressure for strongly electron capturing compounds. The coulometric ECD[42,84] consists of a metal tube about 5 cm. in length and a fine wire running down the centre of the tube, forming the anode. The radio-active source is ^{3}H giving a saturation current of between 30 and 50 nA. An extremely high ionisation efficiency (about 93%) is achieved under the following experimental conditions :

i) high electron concentration in the cell, well in excess of sample concentration.

ii) operation of the cell under the pulsed mode with s $>$ 150μs.

iii) low gas flow rate and a cell with a large volume.

The limit of detection has been found to be 1×10^{-13} g of SF_6 injected.[85] Atmospheric halocarbons, CCl_3F, CCl_4 and $CCl_2 = CCl_2$ have been determined by this technique.[86]

Other developments have been the drift tube detector by Karasek and Kane,[68] the photo-electron capture detector[87] (using an external photon source instead of the traditional radio-active source) and Horning et. al.,[88] have coupled the ECD to a mass-spectometer. These developments emphasise the need to identify the species involved in various reactions taking place in the cell.

This study has attempted to solve some of the pressing problems faced in the normal use of the ECD. Assumptions made in previous theoretical models concerning the physical state inside the detector have been further justified on the basis of experimental evidence obtained. The detector's behaviour is not yet fully understood but because it is an indispensible instrument in today's trace analysis, further attempts have to be made to domesticate the detector completely.

REFERENCES

1. Lovelock J. E. and Lipsky S.R. J.Am.Chem. Soc., 82, (1960), 431.

2. Lovelock J. E. "Physical Processes in Radiation Biology", Academic Press, Inc., N.Y. (1964).

3. Lovelock J. E., Zlatkis A. and Becker R.S., Nature 193, (1962) 540.

4. Lovelock J. E., Fenimore D.C. and Zlatkis A. J. Gas Chromatogr., (1967), 392.

5. Wentworth W. E., Becker R. S. and Tung R., J. Phys. Chem., 71, (1967), 1652.

6. Smith R. V. Amer. Lab., 3, Nov. (1971), 58.

7. Aue W. A. and Kapila S. J. Chromat. Sci. 2, (1973), 255.

8. Halász I. Anal. Chem., 36, (1964), 1428.

9. Scolnick M. J. Chromat. Sci. 7, (1969), 300.

10. Morrison M. E. and Corcoran W. H. Anal. Chem., 39, (1967), 255.

11. Von Engel A. "Ionised Gases" Oxford University Press (1965)

12. Lovelock J. E. Anal. Chem., 35, (1963), 474.

13. Seymour J. "Physical Electronics", Pitman Press, (1972).

14. Sharpe J. "Nuclear Radiation Detectors", p. 130-4, Methuens, London (1955).

15. Friedlander G, Kennedy J. W. and Miller J. M. "Nuclear and Radiochemistry", John Wiley, (1964).

16. Wang C. H. and Willis D. L. (Editors) "Radiotracer Methodology in Biological Science" Prentice Hall, Englecliffs, N. J., (1965) p.68.

17. Warman J. M. and Sauer M. C. J. Chem. Phys., 52, (1970), 6428.

18. Wentworth W. E., Chen. E. and Lovelock J. E. J. Phys. Chem., 70, (1966), 455.

19. J. E. Lovelock and N. L. Gregory, "3rd Int. Symp. Gas Chromatogr.," Academic Press, N.Y. (1962), p. 219.

20. Landowne R. A. Anal. Chem., 42, (1970) 1468.

21. Maggs R. J., Joynes P. L. Davis A. J. and Lovelock J. E. Anal. Chem. 43, (1971), 1966.

22. Hasted J. B. "Physics of Atomic Collisions", Butterworths, London (1972).

23. Farragher A. L., Page F. M. and Wheeler R. C. Disc. Faraday Soc., 37, (1964), 203.

24. Wentworth W. E., Becker R. S., and Tung R. J. Phys. Chem. 71, (1967) 1652.

25. Lyons L. E., Morris G. C., and Warren L. J. J. Phys. Chem., 72, (1968) 3677.

26. Page F. M. and Goode G. C. "Negative Ions and the Magnetron", John Wiley & Sons, London (1968).

27. Stanton H. E. J.Chem. Phys. 32, (1960) 1348.

28. Ferguson E. E., Fehsenfeld F. C., and Schmeltekopf A. L., J.Chem. Phys. 47, (1967) 3085.

29. Massey H. S. W. "Electronic and Ionic Impact Phenomena" Vol.II. Clarendon Press, Oxford (1969).

30. Massey H. S. W. "Electronic and Ionic Impact Phenomena" Vol.III. Clarendon Press, Oxford (1971).

31. Blaunstein R. P. and Christoporou L. G. Radiat. Res. Rev., 3, (1971) 69.

32. Burdett M. Ph.D. Thesis, University of Aston in Birmingham, (1968).

33. Zlatkis A. and Lovelock J. E. Clin. Chem., 11, (1965), 259.

34. Zielinski W. L., Fishbein L. and Thomas R. O. J. Chromatogr., 30, (1967), 77.

35. Thomson J. J. Phil. Mag. 47, (1924), 337.

36. Loeb L. B. "Basic Processes of Gaseous Electronics" p. 205, University of California Press, (1955).

37. Lovelock J. E. Anal. Chem. 33, (1961) 162.

38. Healy R. H. and Reed J. W. "The Behaviour of Slow Electrons in Gases", Amalgated Wireless Limited, Sydney, (1941).

39. Lyons L. E., Morris G. C. and Warren L. J. Aust. J. Chem., 21, (1968), 853.

40. Meisels G. G. J. Am. Chem. Soc., 87, (1965), 950.

41. Sullivan J. J. and Burgett C. A. Cromatographia 8, (1975) 176.

42. Lovelock J. E. J. Chromatogr. 99, (1974), 3.

43. Ramey R. L. "Physical Electronics", Prentice-Hall, London (1961).

44. Page F. M. Unpublished work, University of Aston.

45. Frank-Kamenetskii D. A. "Plasma - The Fourth State of Matter", Macmillan Press, N.Y. (1972).

46. Scolnick M. E. M.Sc. Thesis, University of Aston in Birmingham (1969).

47. Vlcek A. A. Nature, 180, (1957), 753.

48. Lovelock J. E. Seventh International Symposium on Gas Chromatography, Copenhagen, (1968).

49. Wang Y. (Editor) "Handbook of Radioactive Nuclides", Chemical Rubber Co. (1969).

50. Radiochemical Centre Limited, Amersham, England. Private communication.

51. Hucks E. B.Sc. project, University of Aston in Birmingham (1966).

52. Lubkowitz J. A. and Parker W. C. J. Chromatogr., 62, (1971), 53.

53. Shoemake G. R., Fenimore D. C. and Zlatkis A. J. Gas Chromatogr., August, (1965), 285.

54. Kahn L and Goldberg M. C. J. Gas Chromatogr., Ibid, August (1965), 287.

55. Taylor, M.P. J. Chromatog. 9, (1962), 28.

56. Chamberlain A. T. Pye Unicam Limited, Cambridge. Private communication.

57. Devaux P. and Guiochon G. J. Chromatogr. Sci. 7, (1969) 561.

58. Lovelock J. E. Bowerchalke, Salisbury. Private communication.

59. Van de Wiel H. J. and Tommassen P. J. Chromat. 71, (1972) 1 - 7.

60. Brown S. C. "Basic Data of Plasma Physics", Technology Press, N.Y. (1961).

61. Pellizzari E. D. J. Chromatogr., 98, (1974), 323.

62. Oskam M. and Middlestadt V. Phys. Rev., 132, (1963), 1445.

63. Stockdale J., Compton R. N and Schweinler H. C. J.Chem. Phys. 53, (1970), 1502.

64. Mellor J. W. 'Comprehensive Treatise on Inorganic and Theoretical Chemistry' Vol. II. Longmans, London (1961).

65. Glasstone S. 'Textbook of Physical Chemistry', Macmillan and Co. Limited, London (1960) p. 783.

66. Moruzzi J. L. and Phelps A. V. J.Chem. Phys. 45, (1966), 4617.

67. Devaux P. and Guiochon G. Bull. Soc. Chim. Fr., (1966) 1404.

68. Karasek F. W. and Kane D. M. Anal. Chem. 45, (1973), 576.

69. Good D., Durden D. A. and Kebarle P. J.Chem.Phys. 52, (1970) 212.

70. King I. R. J. Chem. Phys. 24, (1957), 817.

71. Calcote H. F. 8th International Symposium on Combustion, Baltimore. Williams and Wilkins Co. (1962), p. 184.

72. Green J. A. and Sugden T. M. 9th International Symposium on Combustion, New York, Academic Press Inc. (1963) p. 607.

73. Lovelock J. E. Private communication to F. M. Page, University of Aston in Birmingham.

74. Nicholson P. W. "Nuclear Electronics", Wiley - Interscience, London (1974).

75. Travers B. L. and Williams H. Report: The use of electrical probes in low pressure flames", Rocket Propulsion Establishment, Wescott, (1963).

76. Huddlestone R. H. and Leonard S. L. "Plasma Diagnostic Techniques", Academic Press, New York (1965).

77. Johnson E. O. and Malter L. Phys. Rev., 80, (1950) 58.

78. Su C. H. and Lam S. H. Phys. Fluids 6, (1963), 1479.

79. Carabetta R. and Porter R. P. "Twelfth International Symposium on Combustion" Combustion Institute, Pittsburgh, Pennsylvania. (1969).

80. Bohm D., Burhop E. H. S. and Massey H. S. W. "The Characteristics of Electrical Discharges in Magnetic Fields", McGraw-Hill (1949).

81. Page F. M. "Physical Chemistry of Fast Reactions", edited by Levitt B. Plenum Press, London (1973), p. 214.

82. Jensen D. E. and Padley P. J. Trans. Faraday Soc., 62, (1966) 2140.

83. Langevin P. Annals. Chim. Phys. 28, (1903), 289, 433.

84. Lovelock J. E., Maggs R. J. and Adlard E. R. Anal. Chem., 43, (1971), 1962.

85. Bros. E., Chamberlain A.T., Page F. M. and Patel S. P. Int. Sym. on Development of Nuclear - Based Techniques for Measurement, Detection and Control of Environmental Pollutants, I. A. E. A., Vienna (1976).

86. Lillian D. and Singh H. B. Anal. Chem. 46, (1974), 1060.

87. Wentworth W., Tishbee A, Batten C. and Zlatkis A. J. Chromatogr., 112, (1975), 229.

88. Horning et. al., Anal. Chem., 45, (1973), 936.

THE ELECTRON CAPTURE DETECTOR

A thesis submitted for the degree of

DOCTOR OF PHILOSOPHY

by

SURENDRA PUNAMBHAI PATEL

in

THE UNIVERSITY OF ASTON IN BIRMINGHAM

JULY 1976

SUMMARY

Practical problems encountered in the use of the electron capture detector have been investigated. A theoretical model is also proposed for the instrument.

Detector characteristics and operating parameters are discussed and an experimental study investigated their influence on the detector response. The two principal processes occurring within the cell, electron attachment and recombination are also discussed and partly based on the consideration of these processes, a kinetic model is proposed for the ECD. An attempt has been made to verify experimentally some of the assumptions made in the present theory and in other previous models (which have been discussed as well). The experiments included the use of electrostatic probes to determine the positive ion density in the cell, oscilloscope traces of the current pulse and current measurements on the gas outlet to observe the effect of carrier gas flow.

The proposed model has shown an improvement in the prediction of the detector response observed when only pure carrier gas is flowing through the cell. It is further used to determine the electron-ion recombination coefficient for the most likely positive ion (H_3O^+) present when moist helium is used as carrier gas.

PREFACE

This thesis, which is being submitted for the Degree of Doctor of Philosophy in the University of Aston in Birmingham, is an account of the work done under the supervision of Professor F. M. Page, B.A., Ph.D, Sc.D., in the Department of Chemistry of the University of Aston in Birmingham from October 1972 to May 1976. Except where references have been given in the text, the work described herein is original and has not been submitted for any other award.

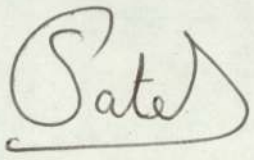

"To climb steep hills
requires a slow pace at first."

Shakespeare, Henry VIII Act I, Sc.I

ACKNOWLEDGEMENTS

I wish to express my gratitude to Professor F. M. Page for his continued guidance and encouragement throughout the course of this work.

Thanks are due to other members of the University of Aston in Birmingham for their helpful discussions and suggestions on particular aspects of the work. I also wish to thank two great friends, Mehmet Konuray and Fikret Ateş, with whom three most enjoyable and rewarding years were shared.

Finally, I am grateful to the University of Zambia, Lusaka, for financial support and to Mrs L. Perkins for typing this thesis.

To my mother
and father

CONTENTS

LIST OF FIGURES

FIG.16

CURRENT AT VARIOUS ELECTRODE SPACINGS (SOURCE ^{63}Ni)

FIG.17

CURRENT-ELECTRODE SEPARATION RELATION FOR d.c. MODE

FIG.18

THE INVERSE OF CURRENT VERSUS ELECTRON TRANSIT TIME

FIG.19

CURRENT-SEPARATION PLOTS FOR He AND Ar + CH_4

FIG.20

CURRENT VARIATION IN AN ASSYMMETRICAL CELL - ANODE FIXED

FIG.21

CURRENT VARIATION IN AN ASSYMMETRICAL CELL - CATHODE FIXED

FIG.22

THE EFFECT OF REVERSAL OF CELL POLARITY - SOURCE ON ANODE

FIG.23

CURRENT VARIATION WITH INTER-ELECTRODE SEPARATION - SOURCE ON ANODE

FIG.24

CURRENT VARIATION WITH GAS PRESSURE (BELOW ATMOSPHERIC)

FIG.25

CURRENT VARIATION WITH GAS PRESSURE (ABOVE ATMOSPHERIC)

FIG.26

CURRENT - CELL LENGTH RELATION AT VARIOUS PRESSURES

FIG.27

PULSE INTERVAL VERSUS PRESSURE CORRESPONDING TO MAXIMUM CURRENT

FIG.28

THE EFFECT OF CARRIER GAS (N_2) FLOW ON CURRENT IN d.c. MODE

FIG.29

CURRENT VARIATION WITH GAS FLOW IN THE PULSED MODE

FIG.30

CURRENT VARIATION WITH GAS (Ar + CH_4)

FIG.31

CURRENT VARIATION WITH GAS FLOW IN A SYSTEM SUSPECTED OF LEAKAGE

FIG.32

THE EFFECT OF CONTAMINANTS ON OBSERVED CURRENT

FIG.33

CURRENT-VOLTAGE PLOTS FOR DIFFERENT/FLOW RATES AT SMALL ELECTRODE SEPARATION

FIG.34

CURRENT-VOLTAGE RELATIONSHIP IN d.c MODE AT HIGH GAS FLOW RATE

FIG.35

VARIATION OF CURRENT WITH VOLTAGE IN d.c. MODE

FIG.36

CURRENT-VOLTAGE RELATIONSHIP AT LOW GAS FLOW RATE

FIG.37

ONSET VOLTAGE FOR SATURATION CURRENT AT DIFFERENT ELECTRODE SPACINGS (d.c. MODE)

FIG.38

ONSET VOLTAGE FOR SATURATION CURRENT UNDER THE PULSED MODE ($Ar + CH_4$)

FIG.39

CURRENT VARIATION WITH PULSE AMPLITUDE AT VARIOUS ELECTRODE SEPARATION

FIG.40

CURRENT-PULSE INTERVAL RELATION FOR VARIOUS GASES

FIG.41

COMPARISION OF RESULTS BETWEEN THEORY AND EXPERIMENT

FIG.42

PREDICTION OF THE PROPOSED MODEL COMPARED WITH EXPERIMENTAL DATA FOR ARGON

FIG.43

SATURATOR USED FOR INTRODUCING SAMPLE IN CARRIER GAS

FIG.44

CURRENT VARIATION WITH PULSE INTERVAL FOR HELIUM AND HELIUM + UF_6

FIG.45

Ne - PULSE INTERVAL RELATION FOR HELIUM AND He + UF_6

FIG.46

VARIATION OF Ne WITH GAS FLOW RATE THROUGH SATURATOR CONTAINING UF_6

FIG.47

Ne - PULSE INTERVAL RELATION FOR HELIUM AND He + H_2O

LIST OF TABLES

LIST OF FIGURES

Symbol	Representation
$\bar{a}$	Radius of sheath around an electrostatic probe.
A	Area.
C_o	Concentration of contaminant.
d	Distance.
D_a	Ambipolar diffusion coefficient.
e	Electron concentration; electronic charge.
E_a	Electron Affinity
F	Gas flow rate
G	Ion-pairs formed by a β^- particle.
I	Current.
k, K	Boltzmann constant.
k_1 A	Rate of production of electrons.
k_2	Electron-ion recombination rate coefficient.
k_3	Electron capture rate coefficient.
k_4	Ion-ion recombination rate coefficient.
ℓ	Length of cell.
m	Concentration of sample molecules.
n	Negative ion concentration.
N_e	Number of electrons per pulse.
p	Positive ion concentration
P	Gas pressure
r_p	Probe radius
R	'Gaines' factor.
s	Field free interval between pulses.
t	Time
t_p	Pulse interval
T	Temperature

V	Applied potential; Volume.
V_a	Ambipolar speed.
w	Pulse width.
X	Electric field strength.
λ	Debye length
ν_x	Drift velocity of species x.

The conductivity of gases in an ionisation chamber is exquisitely sensitive to small changes in gas composition. Several detectors, based on this observation, have been constructed for use in gas chromatographic systems. The recent emphasis on analysis of environmental pollutants present in trace amounts has brought one of these detectors, namely, the electron capture detector (ECD), to the forefront.

The ECD, since its inception in 1960 by Lovelock and Lipsky[1] has been extensively used in investigations of biological, physical and chemical importance. Its contribution to topics of scientific interest can be chiefly attributed to its extreme sensitivity, and the ease with which it can be operated. Its design is also relatively simple and has only been slightly modified since it was originally devised. The ECD still is a two-electrode ion chamber with an internal radiation source.

Physiochemical aspects of free electron reactions have been studied with the aid of the ECD. The toxicity or biological activity of compounds such as dinitrophenol and thyroid hormones has been suggested[2] to be due to their ability to function as irreversible electron traps. Carcinogenic activity of compounds such as polycyclic aromatic hydrocarbons, halogenated aliphatic hydrocarbons, azo dyes and quinolinol N- oxides has been loosely linked[3] to the ability of these compounds to extract electrons from their normal path in a living cell.

Characteristic 'spectra' based on the measurement of cross-section for electron attachment at different electron energies have been obtained[4] by applying radio-frequency potentials to the ECD.

Dissociative electron capture or attachment has also been the subject of many investigations in which the ECD has played a

paramount role. Studies[5] have attempted to distinguish between two mechanisms by which attachment of thermal electrons to aliphatic and aromatic halogen compounds proceeds :

a) electron attachment to a thermally excited molecule followed by direct dissociation into a halide ion and a radical

$$AB^{*} + e^{-} \longrightarrow A^{-} + B^{\bullet}$$

b) electron attachment to form a stable negative ion of the molecule which in turn becomes thermally activated to undergo dissociation into the halide ion and a radical

$$AB + e^{-} \longrightarrow (AB^{-})^{*} \longrightarrow A^{-} + B^{\bullet}$$

The electron capture detector has been most widely used however, for analytical purposes. It has provided reliable results in analysis of pesticide traces in materials of biological origin. This is but one example of its use in this field; others are its use in the determination of a vast array of suitably derivatised biochemicals and drugs, chelated metals, meteorological tracers, air pollutants and lead alkyls. The literature, consequently is voluminous. An extensively comprehensive review on the application of the ECD to various fields, but primarily concerned with its function under various analytical circumstances, has been published by R. V. Smith[6].

It is the detector's use as an analytical tool that has attracted attention and aroused controversy. Aue and Kapila[7] point out that entirely due to the ECD, terms such as polychlorinated biphenyls' have ascended to household prominence and it is partly responsible for the discontinued use of DDT in countries around the world.

The instrument's controversial nature arises largely from a lack of understanding of its mode of action. This becomes

apparent from the difficulties and problems faced by GC operators : the ECD is or is not disturbed by water; its standing current is or is not dependent on either gas flow rate or temperature; it is or it is not a mass-sensing device. Negative excursions below the baseline after the emergence of a peak and shifting baseline are phenomena experienced regularly.

Besides these practical problems there exists theoretical deficiencies. Models, explaining numerically the signals it generates, are often inadequate for various reasons outlined later in this work when they are more fully discussed. The ECD's response is a complicated function arising from the interaction of several physiochemical parameters. This has made the task of predicting the signals it generates difficult.

A programme of fundamental study has therefore been undertaken to resolve some of the practical problems faced and a theoretical model is proposed for the ECD. The model makes use of carrier gas parameters, such as positive ion mobilities and electron-ion recombination coefficients (which have been well established by other techniques) to calculate empirical factors introduced in the theory.

CHAPTER TWO - DETECTOR AND OPERATION CHARACTERISTICS

2.1 DETECTOR CLASSIFICATION

A gas chromatographic detector senses the variation in the amount of sample passing through it. The response can be classified as concentration dependent, mass flow-rate dependent, or as a mixed function. The concentration detector produces a signal that is proportional to the amount of solute per unit volume of carrier gas passing through the cell. A mass flow-rate detector gives a signal that is proportional to the amount of solute passing through it in unit time, but is independent of the volume of carrier gas required for elution. The flame ionisation detector is an example of this latter class while the electron capture detector has been classified as a concentration detector for certain classes of compounds.

Qualitative gas chromatographic analysis involves separation of the sample into its constituents. Quantitative evaluation of the resulting chromatogram consists of determining the absolute or relative quantities of individual components. This necessitates the determination of peak areas, ie. integration of the detector signal with time. With detectors of the first category, the signal is proportional to the sample concentration, C, in the carrier gas. The peak area, A is expressed as

$$A = q \int C \, dt = q \int \frac{f_1}{f_1 + f_2} \, dt \qquad [1]$$

where q is a constant of proportionality and f_1 and f_2 are the flow-rates (moles per second) of the sample and the carrier gas respectively. A proportionality between peak area, A, and the quantity of the sample holds true only for constant flow-rate $(f_1 + f_2)$, as can be seen from Equn. [2].

$$A = \frac{q}{f_1 + f_2} \int f_1 \, dt \qquad [2]$$

at a given temperature and pressure.

The signal produced by detectors of category two is proportional to the mass flow-rate of the sample. In this case, the peak area is proportional to the size of the component, even if the flow-rate of the gas mixture, $(f_1 + f_2)$, changes during the measurement.

Fluctuations in the carrier gas flow-rate give erroneous results for the concentration-sensitive detectors. Halász[8] has pointed out that this adverse effect can be minimised by the addition of a scavenger gas though at the expense of some loss in sensitivity.

2.2 CELL CONFIGURATIONS

The ECD is basically a two-electrode chamber through which gas can flow and which contains a source of ionising radiation. There are three principal forms in use today and these are illustrated in Fig.(1) Early ECD's were generally converted argon ionisation detectors operated at low applied potentials. Such detectors have coaxial geometry with the anode located along the axis of the cell and surrounded by a cylindrical cathode to which is attached the radioactive source. In the plane parallel configuration, the anode and the cathode are arranged parallel to one another at the end of an electrically insulated chamber. In the concentric cylinder ECD[9], the cathode houses the radioactive foil but the anode is removed and isolated by a Kovar glass union. The third version is really only useful when a continuous d.c. voltage is applied across the electrodes.

These detectors function satisfactorily if due attention is paid to the peculiarities of each, and care is taken to optimise

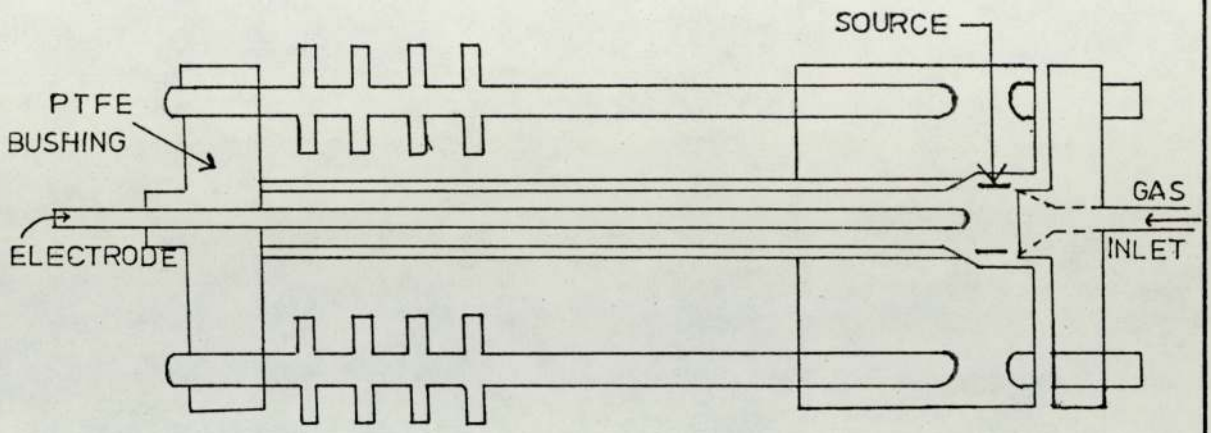

COAXIAL ECD

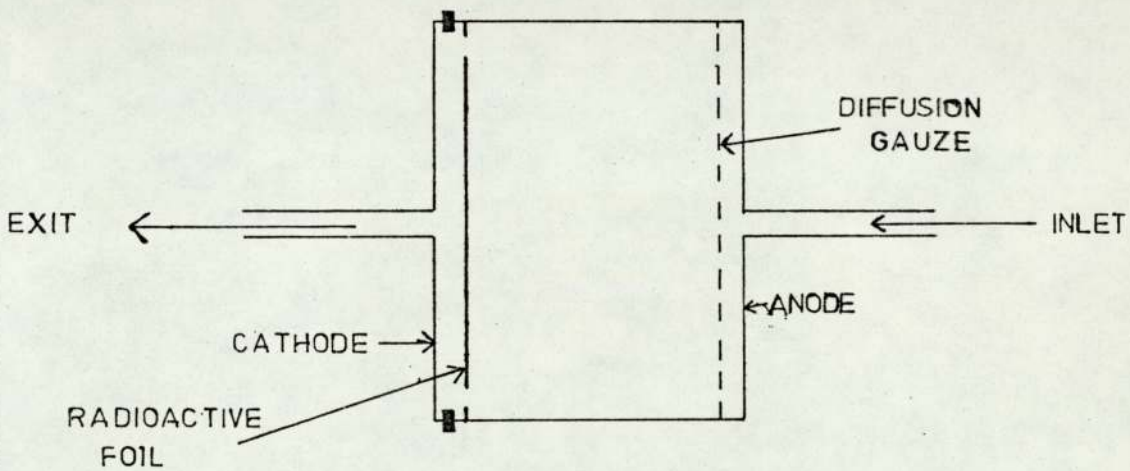

PLANE PARALLEL ECD

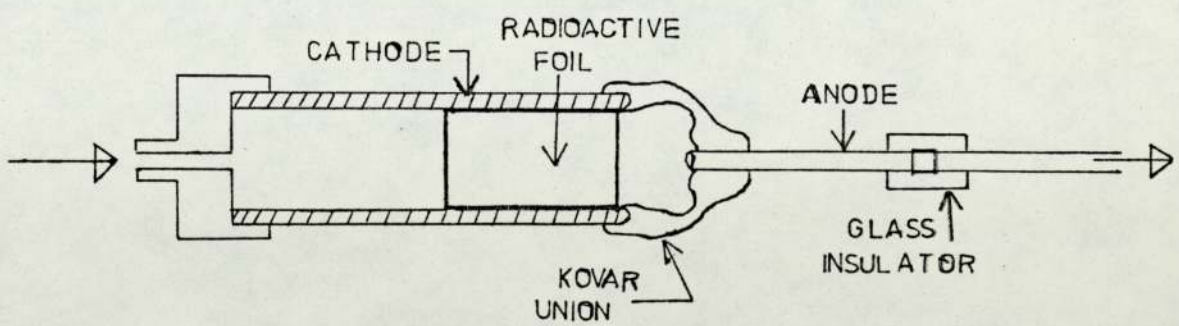

CONCENTRIC CYLINDER ECD

FIG. 1

ELECTRON CAPTURE CELL CONFIGURATIONS

the operating parameters. A comparison between these geometrical types has been reported[10] but they are difficult to evaluate because a large number of experimental variables affect their overall performance. In the design of a practical detector, the dimensions are certainly more important and these are considered in the experimental section where a plane parallel cell used in the present studies is fully described.

2.3 BASIC PRINCIPLES OF OPERATION

At normal temperatures and pressures a gas behaves as a perfect insulator; if however, electrically charged atoms, molecules or free electrons are present, their motion in the direction of an electrical field renders the gas conducting. The radio-active source emits energetic β^- particles which undergo ionising collisions with carrier gas molecules. The application of a voltage across the two electrodes creates a potential difference, allowing the collection of charged species present in the cell. The resulting current is measured on an electrometer connected in series with the ECD.

At atmospheric pressure, the principal process causing the loss of ions at low field strengths is the recombination of negative and positive ions to regenerate neutral molecules. The probability of recombination between a free electron and a positive molecular ion is between 10^5 and 10^8 less than between oppositely charged molecular ions. The formation of negative ions through electron capture results in a rapid disappearance of charged species in the cell at low applied fields. Consequently, the presence of an electron capturing gas or vapour reduces the observed signal of the ECD corresponding to a decrease in the standing current (ie. current when only

pure carrier gas is flowing).

2.4 SPACE CHARGE DEVELOPMENT

The current-voltage relationship of a gas filled insulated vessel containing two plane parallel electrodes is well established[11]; as the voltage increases the current tends towards a constant level, the saturation current, corresponding to the collection of all ions and electrons generated within the chamber (Fig. 2). At higher voltages the current increases again and tends to infinity at some finite applied potential. This is because the electrons originally formed by irradiation (or by any other ionising source) in the gas, gain energy from the field and reach velocities which enable them to ionise gas molecules. The length of the saturation current plateau depends upon the nature of the gas and on the density of ionisation. Practical ionisation detectors need to be operated at some voltage in the plateau region so as to provide a current directly related to the concentration of the sample present.

J. E. Lovelock[12] has pointed out that in an ion chamber where the applied potential is low and ion density is high, the current flow is strongly affected by the development of space charges. The situation is similar to one that exists in gas filled electronic diodes[13]. So many electrons are emitted from the thermionic cathode that only a fraction of them are collected by the anode at the working potential. The remainder form a 'cloud' of negative charges, known as a 'space charge', near the cathode. In the ECD, the positive ion concentration may be several thousand times greater than the free electron concentration. This is simply due to the fact that the free electrons are collected very soon after their formation whereas the positive ions with their lower drift velocity

FIG. 2

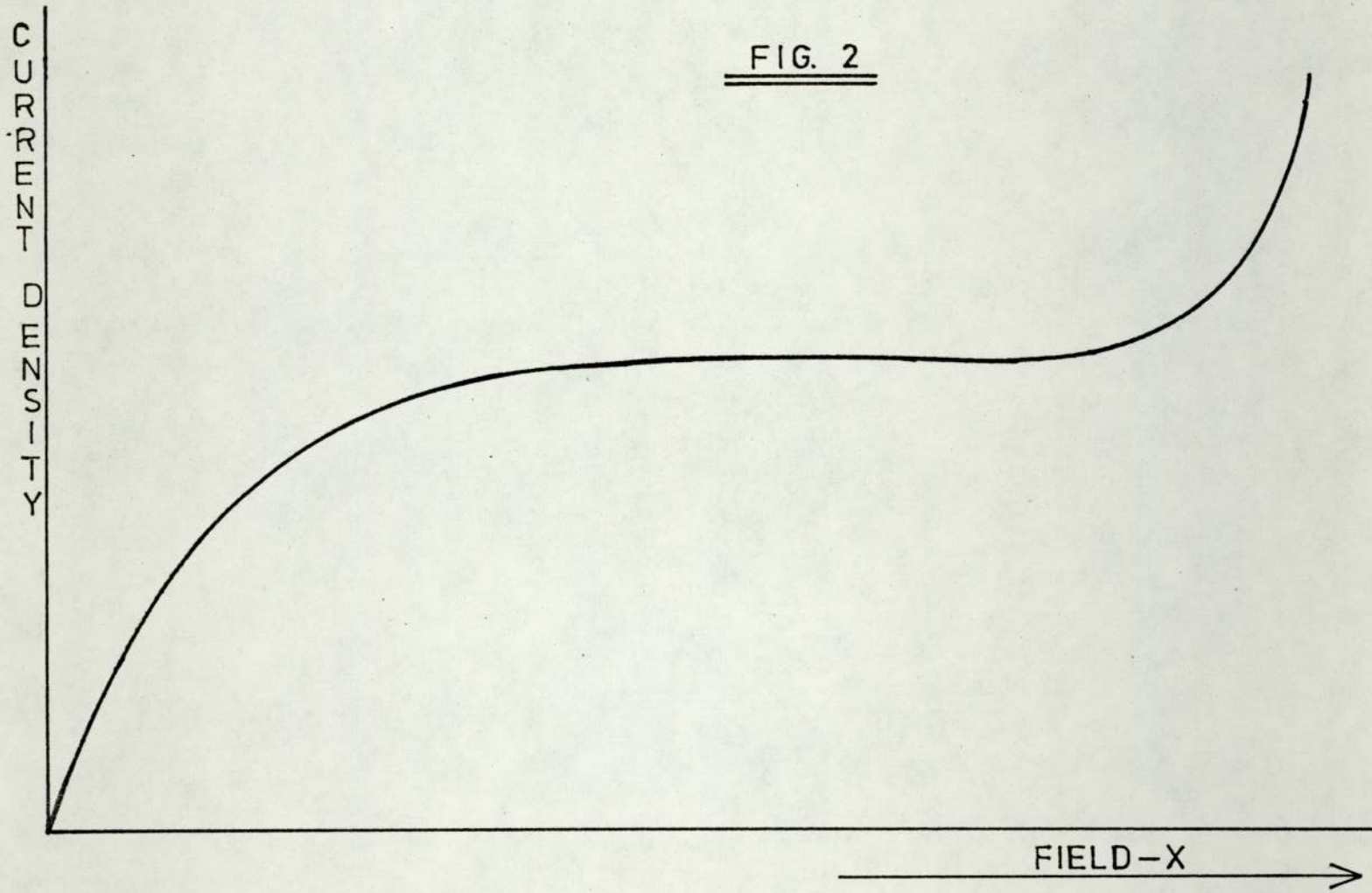

RELATION BETWEEN CURRENT DENSITY, j, AND FIELD X IN A GAP WITH PLANE ELECTRODES

move only slowly to the cathode and accumulate there as a space-charge cloud. In general, electrons have a mobility a thousand times greater than the positive ions in their own gas. For a plane parallel geometry chamber, Sharpe's[14] equation derived for space charge limitation is

$$N = \frac{k^- V^2}{\pi d^4} \qquad [3]$$

where N is the rate of ion production; k^-, is the electron mobility; V, is the applied potential and d is the electrode separation. N is that at which the space charge reduces the field at the anode to zero. The equation suggests that the extent of space charge limitation is reduced by using small chamber dimensions and a high potential.

2.5 PRODUCTION OF THERMAL ELECTRONS

Secondary electron production in the cell occurs through inelastic and elastic collisions between the primary electrons, ie. the β^- particles and molecules of the carrier gas. Beta-particles released from a ^3H source have a maximum energy of 17.6 - 18.9 keV, while those from ^{63}Ni are about 67 keV[15]. However, these particles rapidly lose their energy in ionising collisions until their energy is less than that necessary for formation of an ion pair. Approximately 36 eV are expended in forming a nitrogen ion pair, while 28 eV are necessary in argon-methane[15]. The electrons produced by the β's will initially have an energy in excess of thermal energies but they rapidly lose energy in collisions until their average energy is thermal (about 0.03 eV). With nitrogen as carrier gas, the reactions are as follows :

$$\beta^- + N_2 \longrightarrow N_2^+ + e^- + e^*$$

$$N_2^+ + N_2 \longrightarrow N_4^+$$

In pure argon, only elastic collisions can take place once the energy is below the excitation level of argon. However, if argon containing a quench gas (eg. methane) is employed, then the energetic electrons produced are thermalised during collision with the quench gas. The decay of argon metastables via the quench gas is also facilitated. The reactions can be stated as follows:

$$\beta^- + Ar^o \longrightarrow Ar^{\pm} + e^- + e^*$$

$$Ar^{\circ}_{\pm} + e^- \xrightarrow[\text{potential}]{\text{Applied}} (Ar^-)^* \quad (11.6\ eV)$$

$$(Ar^-)^* + CH_4 \longrightarrow Ar^o + e^- + CH_4 \pm \text{energy}.$$

Possible modes for the loss of energy in the presence of methane are through excitation of low-level vibrational and rotational states of the gas. Thus, a reduction in temperature and deceleration of the fast electrons results.

An estimation of thermalisation times has been made by Warman and Sauer[17]. They demonstrated that thermalisation of electrons occurred in fractions of a microsecond when n-hexane is used with monatomic or diatomic gases; in the absence of a quench gas, the electrons were not completely thermalised even after 50 ms. Wentworth et al.,[18] estimated that an electron with an energy of 10 keV is cooled to 10% above thermal energies in 0.076 μs. As the energy of activation or electron affinity for a solute molecule may be 0 - 4 eV, it is apparent that the thermalisation of electrons occurring from highly energetic β^- particles is necessary in order to allow or enhance the capturing process while minimising solute ionisation.

2.6 MODES OF OPERATION

The ECD has basically three modes of operation :

a) d.c. continuous mode

b) pulsed mode

c) constant current mode.

In the first mode, a constant potential is applied and this produces a migration of charged species towards electrodes of opposite polarity[19]. As a result, a composite current of electrons and ions results, rather than a pure electron current. Detector configuration and the species to be measured determine the choice of the d.c. potential as well as carrier gas composition and detector contamination[20]. This requires an initial determination of the detector output current versus voltage for a set of analytical conditions.

There are some inherent errors in this mode of operation. Application of a direct potential prevents the electrons from reaching thermal equilibrium with the carrier gas molecules and therefore decreases the probability for capture. The problem is acute in the noble gases and to a lesser extent in nitrogen, since the energy gained by the electrons from the applied field is not easily lost during their elastic collisions with the gas molecules[12]. Besides the electron energy, the probability of electron absorption depends also on the half-life of the electron in the cell. Changes in this quantity leads to a non-linear response to varying sample concentration[12].

The space charge of positive ions in the vicinity of the cathode sets up a potential in opposition to that applied to the ECD and it may hinder the collection of free electrons. The presence of a polyatomic vapour in the cell changes the electron mobility and as a result, the extent of the space charge cloud and the observed current.

The temporary absorption of a trace of an eluted component upon one of the electrode surfaces can give rise to a contact potential which may either enhance or oppose the applied potential.

Lovelock[12] has pointed out that where the contact potential opposes the applied potential, the chromatogram peak has an erroneously large area and frequently shows severe tailing; where the potential enhances that applied to the detector, there is a diminished response and the peak may show a drift below the base line at the tailing edge. There is also the additional effect of reducing the number of Beta particles emitted if the absorption has occurred on the electrode with the radiation source.

In the d.c. mode, the ECD could respond to other parameters of the sample introduced in the carrier gas stream besides electron attachment[12]: ionisation cross-section, electron mobility and metastable atom ionisation processes ("argon" detection). The extent to which these other detection processes predominate in the d.c. mode, depends upon the gas composition in the cell, the intensity of the radiation source, the geometry of the detector and the magnitude of the applied potential.

When the ECD is responding as an argon or as a cross-section detector, in addition to its function by electron absorption, peaks below the base-line have appeared together with a reduction in peak height.

It is difficult to avoid these and other possible sources of error inherent in the d.c. mode. There are however, alternative methods in which electron absorption takes precedence over the other detection methods outlined and anomalous effects of space charge limitation, contact potentials and changes in electron energy can be avoided.

In the pulse mode of operation, square wave voltage pulses (Fig. 3) are applied across the electrodes for a very short time - 1 to 5 μ s depending on the carrier gas and the geometry of the cell. The pulse amplitude (V) and width (W) is sufficient to

FIG. 3

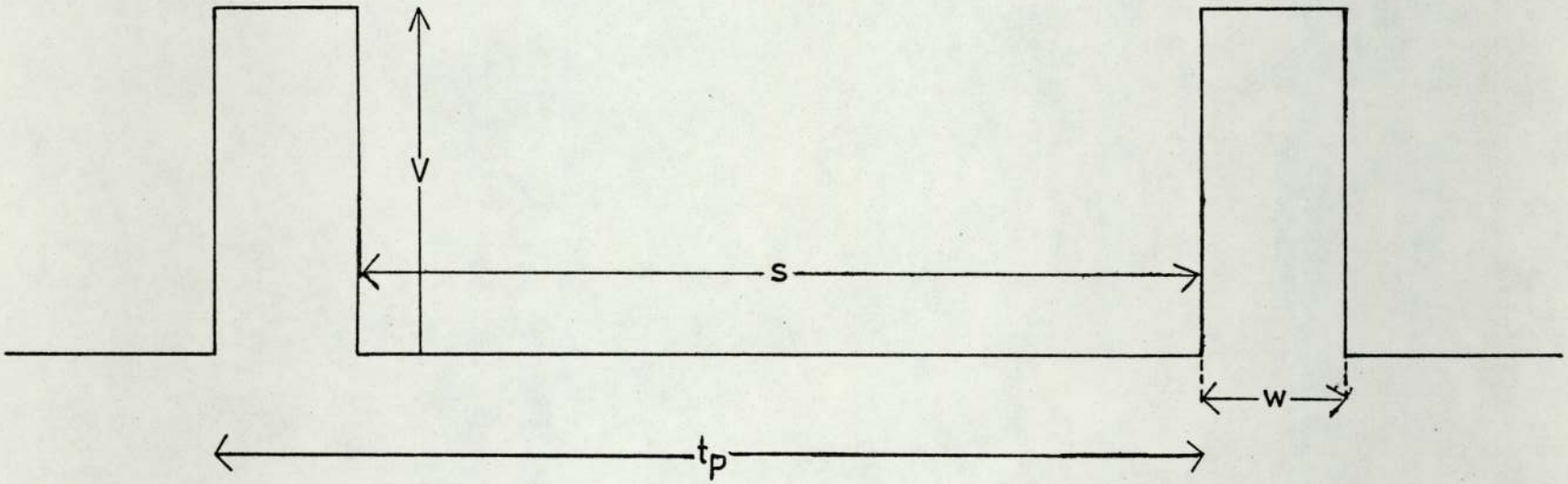

APPLIED PULSE CHARACTERISTICS

collect all electrons and it is generally stated that the contribution of ions to the current is negligible. When the applied potential is zero, ie. during the pulse interval (s), the electrons in the cell are in thermal equilibrium and there is no drift of charged species in either direction; consequently, space charge effects are minimised. It is also generally[12] believed that with the pulse sampling technique, contact potential effects are rarely encountered as the pulse amplitude (about 50 Volts) is sufficiently large to counteract the contact potential and yet collect all electrons present in the cell. With argon + methane as carrier gas and the cell operated in the pulse mode, the detector cannot function either as an argon detector or an electron mobility detector, as the electron energy is maintained at a constant thermal level. Hence, many anomalous responses are avoided and the highest sensitivity and stability is usually obtained by operating in this mode.

The third mode of operation is where the detector current is held constant while the frequency of the applied pulses is varied.[21] Briefly, a reference current, I_r, is compared with the average current, I_D, and the applied pulsed frequency, maintains via feedback the relationship $(I_D - I_r) = 0$

As I_D begins to decrease due to an electron capturing species entering the detector a ΔI is produced. The magnitude of ΔI is amplified and the amplifier output voltage proportionally changes the applied pulse frequency so as to maintain the above relationship.

Thus, the magnitude of change in pulse frequency becomes a measure of the concentration of the electron capturing vapour. The linear dynamic range has been reported[21] to be 5×10^4 for a 10 mCi ^{63}Ni detector operated in this mode.

Some of the notions generally accepted regarding the ECD's operation are illfounded; these will be discussed in the experimental

section. It is to be noted here that they relate to the possible effects of the space charge and the interpretation of the observed current in various modes of operation.

CHAPTER THREE - THEORY

3.1 ELECTRON ATTACHMENT

When an "electron capturing" solute enters the detector, a large number of low-energy free electrons are available, providing an ideal environment for electron attachment. The solute molecule may attach an electron to form either a negative molecular ion,

$$e^- + AB \longrightarrow AB^- + \text{energy}$$

or a neutral radical and a negative ion

$$e^- + AB \longrightarrow A^{\cdot} + B^- \pm \text{energy}$$

The collisions in which electrons attach to atoms to form stable negative ions involve a release of energy, since a stable negative ion has an energy somewhat below that of its parent atom and free electron. The binding energy of the extra electron is known as the electron affinity, EA. In the case of a molecular negative ion its 'adiabatic electron affinity' is defined as the difference between the electronic energies of the molecule and the negative ion state and thus different from the vertical attachment energy[22].

Only for a few organic compounds has the electron affinity been measured. Thermodynamic techniques are more suited to investigations of molecular electron affinities than other techniques such as photodetachment and electron impact thresholds. In the magnetron device[23], a very pure metal filament is surrounded by two grids and a cylindrical anode. A magnetic field is applied parallel to the filament. The first grid is held several hundred volts positive to the filament to minimise space charge current limitation. The second grid suppresses secondary emission from the anode. The total electron-plus-negative ion current is measured in the absence of the

magnetic field and the negative ion current is measured on its own when the field is applied. From a measurement of the temperature dependence of the relative abundances of electrons and negative ions, the electron affinity is calculated using Boltzmann statistics.

Electron affinities, measured with the aid of the ECD, have been reported for several aromatic compounds[18, 24, 25]. They are presented in Table One; their derivation is based on the kinetic theory developed by Wentworth and his co-workers[18]. The theory is discussed in section (3.3). The electron affinities need to be used with caution as most of them have not been confirmed by other techniques; in cases where they have been measured by other methods, a serious discrepancy exists. For example, Page and Goode[26] measured EA for azulene by the magnetron technique and found it to be 2.66 eV.

It has been shown[27] that the problem of negative ion stability can only be approached by using the nuclear kinetic operator. For stability of a negative ion, the wave function must contain at least as many molecular spin orbitals of given spin symmetry as does that of the neutral molecule.

TABLE ONE

ELECTRON AFFINITIES FOR SELECTED AROMATIC COMPOUNDS

COMPOUND	ELECTRON AFFINITY (eV)
Naphthalene	0.152
Triphenylene	0.284
Phenanthrene	0.308
Anthracene	0.552
Pyrene	0.579
Azulene	0.587
Nitrobenzene	0.850
Chlorobenzene	0.860
O-Chlorotoluene	1.100
m-Dinitrobenzene	1.430

There is also an additional factor affecting the existence of stable molecular negative ions. The lowest stable state of a given system of nuclei and electrons must always posses a certain geometrical configuration. Should the addition of a single electron to a system imply a change in the geometrical configuration, then it is difficult, if not impossible, to form the negative ion by collisions of the molecule with electrons[28]. When the formation of a negative ion requires deformation, a significant 'activation energy' of attachment may arise, even though the adiabatic electron affinity is positive (ie. stable negative ion).

The molecular attachment process, yielding the negative ion of the parent molecule, can only proceed via an excited state, since it is a resonance process and the molecule has a real electron affinity. The excited state, which may be purely vibrational, may either be deactivated collisionally (three-body attachment) or pass radiatively to the ground state. A third possibility is that the negative ion exists for periods of the order of a few microseconds, detaching spontaneously after this time.

The rate of formation of stable AB^- by electron capture followed by collision stabilization is proportional to the pressure at low pressures but, owing to saturation, becomes independent of it at higher pressures. Massey[29] showed that the total probability, ρ', of the ion being stabilised by collision before it breaks up is

$$\rho = \int_0^\infty \exp\left\{-t\left(\frac{1}{\tau} + \frac{1}{\theta}\right)\right\} dt/\tau$$

$$= \theta / (\theta + \tau)$$

$$\rho = P/(P + P')$$

where P is the gas pressure and P' a critical pressure for which $\theta = \tau$. The average time taken for a vibrationally excited ion

$(AB^-)^*$ to lose its excess energy through collision with a gas molecule is τ ; the time before spontaneous dissociation occurs is θ. The above equation suggests that if P is large enough then ρ becomes independent of it.

Dissociative attachment proceeds by resonance capture of an electron by the molecule AB, into an antibonding quasi-stationary state AB^-. There is then competition between dissociation and the autodetachment process $AB^- \longrightarrow AB + e$. Fig. (4) illustrates the potential energy curves for both the dissociative and non-dissociative capture processes. In all three cases (a), (b) and (c) curve I is the potential energy curve of the initial state of the neutral molecule AB while the second curve in each case represents that for the state of the negative molecular ion into which the electron is captured. Briefly, the three possibilities are:

Case (a)

Electrons with energies between E_1 and E_2 are captured and molecular dissociation results, giving atoms A and ions B^- with kinetic energies lying between E_3 and E_4.

Case (b)

Electrons with energies between E_1 and E_3 are captured and lead to molecular dissociation while electrons with energies between E_2 and E_3 give rise to a vibrationally excited molecular ion $(AB^-)^*$.

Case (c)

Electrons with energies of about E_6 are captured giving rise to an excited molecular ion which at higher pressures is stabilised.

Negative ions formed by the capture of very slow electrons (with thermal energy) will normally be molecular ions AB^- formed as described above. The reverse process, ie. detachment proceeds through collisions with gas molecules

$$AB^- + X \longrightarrow AB + X + e^-$$

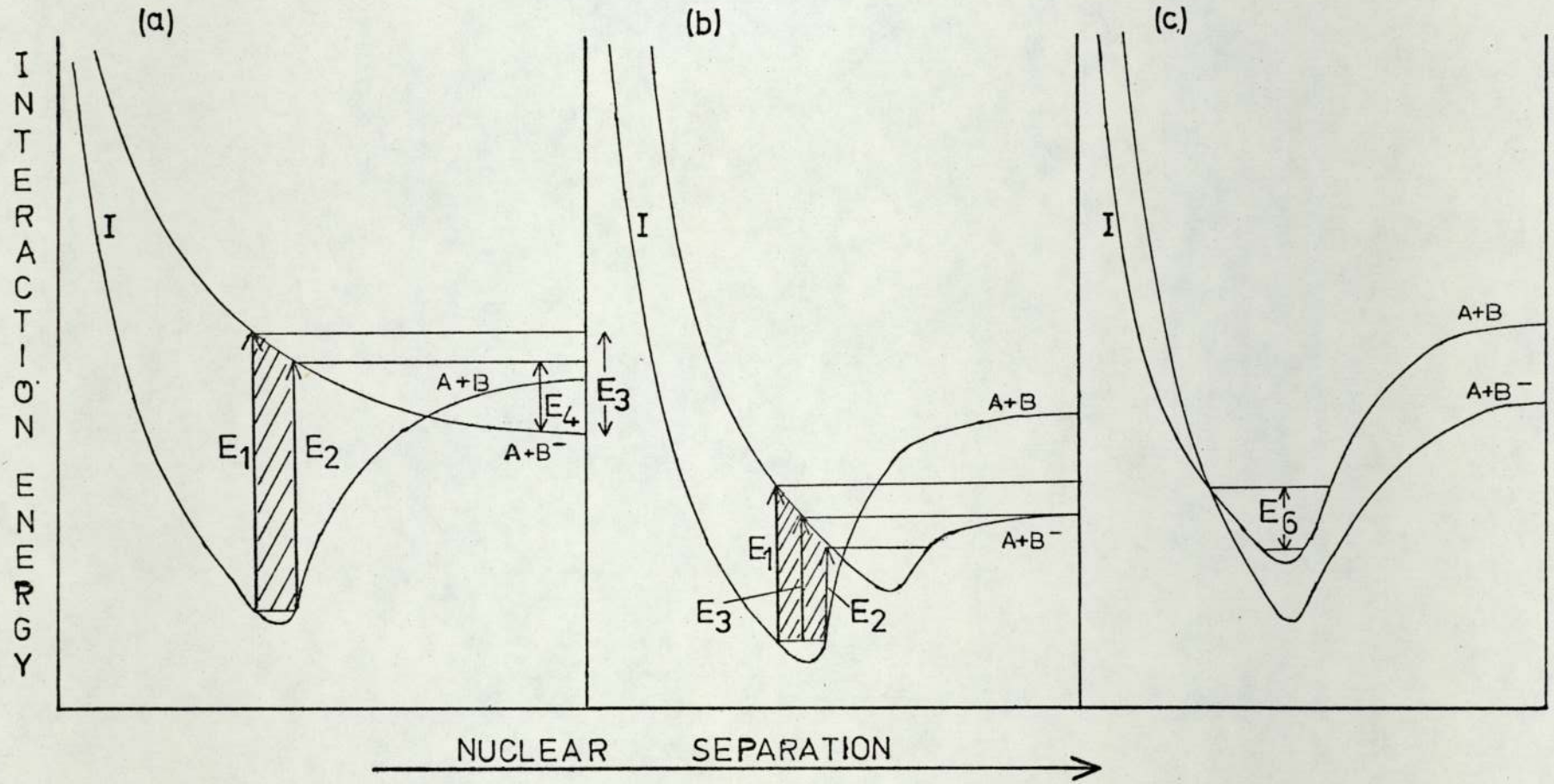

FIG. 4

POTENTIAL ENERGY CURVES ILLUSTRATING 3 POSSIBLE WAYS IN WHICH NEGATIVE IONS MAY BE FORMED BY ELECTRON CAPTURE

and the energy required to detach the electron is obtained by transfer from kinetic energy of relative motion[30]. At ordinary temperatures, T, the fraction of gas molecules possessing sufficient translational energy will be small, unless the electron affinity of X is comparable with 3/2 kT or the electric field accelerating the ions is large enough for them to acquire that energy.

The electron affinity for a parent molecule which forms a stable negative ion will determine the overall parent ion stability but not necessarily its "electron attachment capacity". The probability of electron attachment can be interpreted in terms of the capture cross-section. For dissociative capturing molecules, the process may occur with a high capture cross-section and with almost zero energy electrons if the molecules contain electrophores whose electron affinity exceeds the bond dissociation energy[31]. This suggests that an absolute measurement of the electron attachment capacity of a sample molecule is its capture cross-section and not its electron affinity. Hence, the probability of electron attachment is related to electron affinity, energy of activation, cross-section for collision and consideration of bond stability versus dissociation into stable ions. The electron capture coefficient, K, is the net result of all these processes.

Burdett[32] concluded that the response of the ECD does not vary directly with the electron affinity of the molecules which are introduced in the gas stream but rather with their electron capture cross-section. As indicated above, this depends on the nature of the molecules besides the energy of the attaching electrons. Hence, it is necessary to investigate the relationship of molecular structure to sensitivity in electron capture detection.

It is generally recognised by investigators who employ electron attachment techniques that only relatively few organic compounds

readily accommodate thermal electrons. The probability of electron attachment for different solute species, as shown in Table 2, cover a wide range of at least a million fold.[19,33] The relative attachment coefficient, K', for thermal electrons by compounds is generally made with respect to chlorobenzene, which is assigned a value of one.

For halogen-containing compounds, the magnitude of K' is inversely related to electronegativity and bonding energy. A decrease in K' is observed for the series I > Br > Cl > F.

Studies have been made on the relative contribution of chloro, nitro and amino substituents and their influence through aromatic ring substitution on overall sensitivity[34]. Observations can be rationalised on the basis of increased or diminished electron density in the aromatic ring via resonance and the electron-withdrawing and releasing character of the function groups.

Examples of good electron capturing compounds are alkyl di- and trisulphides and organometallics. In alkyl-lead compounds, some correlation exists between increasing alkyl chain length (possibly electron-releasing effect of ethyl) and overall sensitivity.

Predicting coefficients for attachment becomes more complicated as the complexity of the molecule increases. In general, knowledge of the structure of negative ions formed is seriously lacking, making it difficult to predict the effect of functional groups when present in large molecules.

3.2. RECOMBINATION PROCESSES

In the d.c. mode, at low applied potentials, the major process causing the loss of ions and electrons is recombination. It also occurs in the pulsed mode at long pulse interval. Hence, an understanding of the recombination phenomenon is necessary if a kinetic study of the processes taking place in the ECD is to be

TABLE TWO

RELATIVE ATTACHMENT COEFFICIENTS FOR VARIOUS COMPOUNDS

CHEMICAL CLASSES	K^1	SELECTED EXAMPLES
Alkanes, alkenes, alkynes, aliphatic ethers, esters.	0.01	Hexane Benzene Cholesterol Naphthalene
Aliphatic alcohols, ketones, aldehydes, amines, nitriles	0.10	Vinyl chloride Chlorobenzene
Barbiturates, thalidomide, alkyl-leads	1.0	
Pesticides, dibromo and trichloro compounds	300	
Polychloro, quinones, dinitro compounds	1000	
	10,000	

undertaken.

When an electron and a positive ion recombine, energy must be released in some form. The different mechanisms for carrying off this surplus energy give rise to the possible processes of recombination. They may be summarised as follows:

a) Radiative recombination

$$A^+ + e^- \longrightarrow A + h\nu$$

b) Dielectronic recombination

$$A^+ + e^- \longrightarrow A''$$

$$A'' \longrightarrow A' + h\nu$$

or $$A'' + B \longrightarrow A' + B + \text{kinetic energy.}$$

Here, the surplus energy is given to a second electron in the positive ion so that a doubly excited atom or molecule is formed. It may then be stabilised by emission of radiation or by collision.

c) Dissociative recombination

$$AB^+ + e^- \longrightarrow A' + B'$$

d) Three-body recombination

$$A^+ + e^- + B \longrightarrow A' + B + \text{kinetic energy.}$$

At high neutral gas pressures, the latter process is certainly the most important for removing surplus energy. The process is amenable to classical treatment; in the original analysis by Thomson[35], recombination took place if a collision with a third body is suffered by either ion or electron when its distance, d, from the third body is $d \leqslant \frac{2e^2}{3kT}$

where e is the electronic charge; k, the Boltzmann constant, and T is the temperature.

This assumption leads to the following expression for the recombination coefficient, α_T, in terms of the electron momentum

transfer cross-section σ_d :

$$\alpha_T = \frac{64\,(3\pi^2)^{1/2}}{81} \quad \frac{e^2\,Me\,\sigma_d\,No}{Mo(kT)^{5/2}}$$

where the subscript zero refers to the neutral species and No is Loschmidt's number.

Besides 'volume' electron-ion recombination, there is the possibility of losing charged particles through recombination at the walls of the cell. The electrons, which travel the fastest, tend to diffuse outwards and stick to the cell walls, where they remain until neutralised by an incident positive ion. In the steady state, the number of electrons crossing unit area in unit time at any point is equal to the number of ions and the 'ambipolar speed', V_a , is given by

$$Va = - Da \frac{1}{N} \frac{dN}{dx}$$

where N is the charge density and Da is the ambipolar diffusion coefficient. It is normally expressed in terms of the diffusion and mobility coefficients (D and k respectively) of the charged particles:

$$Da = \frac{D+\,k-\, + D-\, k+}{(k+\, + \, k-)}$$

Operation of the ECD in the pulse mode minimises wall recombination as a result of ambipolar diffusion, since the applied field lasts a very short time only. Loeb[36] has pointed out that in a time of 10^{-5} second, the amount of diffusion is negligible.

Collisions between a positive ion A^+ and a negative ion B^-, which can lead to neutralisation of charge may be summarised as follows:

a) two body process,

$A^+ + B^- \longrightarrow A + B$ in which the excess energy is distributed as kinetic energy among the collision products.

b) three body process,

$A^+ + B^- + C \longrightarrow A + B + C$ where excess internal energy is removed by another atom or molecule.

Thomson's[35] three body recombination theory has proved very successful for gas pressures less than 10^3 torr. The recombination coefficient, α_T, in terms of the masses of the two ions, M1 and M2 is expressed by

$$\alpha_T = \frac{8\,(3\pi^2)^{1/2}}{9} \frac{e^4}{(kT)^{3/2}} \left(\frac{M1 + M2}{M1 \cdot M2}\right)^{1/2}$$

for pressures in air between 700 and 1000 torr.

Langevin[83] based his calculation of the recombination coefficient, α_E, at pressures greater than two atmospheres on the mobilities of the ions :

$$\alpha_E = 4\pi e^2 (k_+ + k_-)$$

In the presence of sample molecules, the recombination of negative ions (formed by electron attachment) with positive ions resulting from ionisation of carrier gas molecules, will dominate that involving electrons as the negative species. At long pulse periods, it may be possible to calculate recombination coefficients for certain species (eg. H_3O^+) from the response of the ECD as recombination is certainly the principal process occurring under these conditions.

3.3. PRESENT KINETIC MODELS

The earliest attempt to describe quantitatively the ECD's response is the Beer's Law interpretation due to Lovelock[37]. This model is based on electron attachment phenomena, as discussed in the text by Healey and Reed[38]. The detector response, S, is related to the concentration of electron capturing species according to the following equation :

$$S/Io = 1 - \exp(-KxC) \qquad [4]$$

where Io is the detector current in the absence of electron acceptors

and S is the loss in current due to the presence of the capturing species whose concentration is C. x is a characteristic dimension of the detector. The constant K is related to the electric field strength and the electron capture cross-section of the sample. As a first approximation, the above equation serves well to predict the observed current but is not meant to represent all the processes occurring in the cell. Moreover, it is only applicable when the ECD is operated in the d.c. mode.

A kinetic model for the mechanism leading to stable negative ion formation has been developed by Wentworth, Chen and Lovelock[18]. Differential equations describing the processes occurring in the ECD when operated in the pulse-sampling mode are solved using the steady state approximation.

Several assumptions are made in the model:

a) The rate of production of thermal electrons is constant and not affected by the presence of the added capturing species.

b) The reaction zone is localised in the region about 1 to 2 mm. from the tritium foil.

c) The reaction zone includes a cloud of ions, electrons and radicals in addition to the argon-methane mixture and the electron capturing species.

d) The 'cloud' is not neutral but has an excess of positive ions and radicals.

e) The reaction zone is homogeneous and can be treated as a static system with respect to the electron concentration.

f) There is slow removal of material from the cell by flow of the carrier gas.

g) Recombination is the principal process by which electrons are lost in the presence of the carrier gas alone. Diffusion losses are minor.

h) If the negative ions are stable, then detachment of the

electrons can occur or they can recombine with positive ions. A host of subsequent reactions are possible when the negative ions dissociate.

i) The amount of material which undergoes electron capture is small in comparison to the total amount of material present. The process taking place in the cloud and their respective rate constants are described as :

$$\beta^- + Ar + CH_4 \xrightarrow{k_{pR}} \oplus + e^- + \beta^{-*}$$

$$\oplus + e^- \xrightarrow{kN'} \text{neutrals}$$

$$R^\bullet + e^- \xrightarrow{kR'} R^-$$

$$AB + e^- \underset{k_{-1}}{\overset{k_1}{\rightleftharpoons}} AB^-$$

$$AB^- + \oplus \xrightarrow{kN1} \begin{cases} A^\bullet + B^\bullet + R^\bullet \\ AB + R^\bullet \end{cases}$$

$$AB^- + R^\bullet \xrightarrow{kR1} \begin{cases} ABR^- \\ AB + R^- \\ AR + B^- \end{cases} + \oplus \longrightarrow \text{neutrals}$$

where

$\oplus$ = concentration of positive ions

k_{pR} = rate for thermal electron production

a = concentration of capturing species, AB

b = electron conc . in the absence of a capturing species.

In the absence of an electron capturing species,

$$\frac{d[e^-]}{dt} = kpR - kN' [\oplus][e^-] - kR' [R^\bullet][e^-] \quad [5]$$

which when solved gives

$$b = \frac{kpR}{k_D} \left[1 - \exp(-k_D t) \right] \quad [6]$$

where $k_D = kN' [\oplus] + kR' [R^\bullet]$

In the presence of a capturing species, the electron concent-

ration is given by

$$[e^-] = \frac{k_p R}{k_D \left(\frac{k_L k_1 a}{k_D (k_L + k_{-1})} + 1 \right)} \qquad [7]$$

where $k_L = \left(k_{N1} [\oplus] + k_{R1} [R^\cdot] \right)$

At time infinity,

$$b^\infty = \frac{k_p R}{k_D}$$

so that,

$$\frac{b^\infty - [e^-]}{[e^-]} = \frac{k_L k_1 a}{k_D (k_L + k_{-1})} \qquad [8]$$

$$= k a$$

where k is the capture coefficient.

Since the capture coefficient contains the term $(k_L + k_{-1})$, it is convenient to consider the case where $k_L \gg k_{-1}$ and $k_{-1} \gg k_L$ in order to examine the type of temperature dependence. If the temperature variation for the forward reaction is small, corresponding to no energy of activation for the addition of an electron, and if the electron affinity of the molecule is appreciable then the backward rate constant k_{-1} must have a significant temperature variation.

For $k_{-1} \gg k_L$ Eq.[8] becomes,

$$\frac{b - [e^-]}{[e^-]} = \frac{k_L}{k_D} k_{eq} a \qquad [9]$$

and since

$$k = \frac{k_L}{k_D} k_{eq.} = \frac{k_L}{k_D} A T^{-3/2} \exp (E_a/kT)$$

$$\text{Ln. } k T^{3/2} = \text{ln. } \frac{k_L}{k_D} + \text{ln } A + E_a/kT \qquad [10]$$

By plotting ln. $k T^{3/2}$ against 1/T, Wentworth et al.[18] calculated the electron affinities of several aromatic hydrocarbons from the slope of the graphs.

For $k_{-1} \gg kL$, Eq.[8] becomes,

$$\frac{b - [e^-]}{[e^-]} = ka = \frac{k_1}{k_D} a \qquad [11]$$

If there is no energy barrier to the addition of an electron, k should be insensitive to temperature.

The capture coefficient, k, is obtained by integration with respect to the volume of gas passing through the detector during the residence time of a peak.

$$\int_0^v \frac{Ib - Ie}{Ie} dv = k \int_0^v a \, dv \qquad [12]$$

where Ib is the maximum standing current in the absence of the capturing species and Ie is the current in its presence.

$$v = \frac{Fr}{Cs} \cdot W$$

where W is the peak width; Fr, the gas flow rate and Cs is the chart speed.

Therefore,

$$\frac{Fr}{Cs} \int_0^W \frac{Ib - Ie}{Ie} dW = \frac{Fr}{Cs} \cdot A = k n$$

and $$k = \frac{Ib - Ie}{Ie} \cdot W\,1/2 \cdot \frac{Fr}{sM} \qquad [13]$$

where W 1/2 is the peak width at half height; s is sample size (μl); M is the molar concentration; A is the peak area and n is the number of moles.

The Wentworth model allowed for the first time the study of

electron attachment phenomena under conditions of atmospheric pressure, low fields and with low energy electrons in the presence of complex organic molecules. Most of the assumptions made in the model are justifiable though for some experimental evidence is lacking, eg. the dimensions of the reaction zone, the excess of positive ions and the removal of material by carrier gas flow.

Some of the arguments in the model become obscure when unknown and probably unknowable reaction steps are considered. There is as yet little experimental evidence of any of the species assumed to be present in the cell. Also, the system of rate equations is solved using the steady state approximation, ie. on the basis that the reduction in detector current is due to an equilibrium between electrons, capturing molecules, ions and molecules. The rate constant for the processes by which electrons are lost, k_D, is calculated from the initial slope of the graph of the number of electrons per pulse versus the pulse interval (gives kpR) and the saturation current ($bt \longrightarrow \infty$). Equation [6] is then used to predict the above described graph, having obtained the initial increase and also the plateau value from it. A satisfactory fit is to be expected, since a circular argument is presented for an equation describing an exponential increase to a constant level.

A few other models of the ECD based on the steady state approximation are to be found in literature. Lyons et al[39] proposed reaction steps, similar to Wentworth's for ethylene as the carrier gas, based on the observation of positive ions and radicals by Meisels[40] when ethylene undergoes primary irradiation. Equilibrium electron concentrations are calculated from kinetic schemes for three situations : before any pulses are applied, during the application of a voltage pulse and after a large number of pulses. Diffusion of charges to the cell walls is considered together with loss of

positive ions by flow. An error is made in the calculation of the rate of production of electrons; the Y-axis intercept of the straight line obtained when log $\left[Ne - (Ne)_b \right]$ is plotted against log tw, is regarded as the number of electrons produced at zero pulse width (tw).

Burdett[32] attempted to measure electron affinities using Wentworth's model; however, the values calculated were not in agreement with those obtained by other methods. A possible mechanism for electron capture proportional to the cross-sectional area of the molecules has been suggested as an alternative. The approach assumes a steady state situation for the electrons in the cell.

Scolnick[9] obtained empirical equations relating the observed current to the applied voltage and to functions of gas pressure and temperature. A concentric cylinder ECD with an isolated anode was used for the purpose and as such the equations are likely to be applicable only to detectors having that configuration.

Recently, Sullivan and Burgett[41] presented a theoretical model for the detector when used in the d.c. mode. The processes removing electrons, ie. ambipolar diffusion, mass transport out of cell, recombination and capture by bleed and impurities are collectively expressed by one rate constant which is assumed to be first order. This simplification leads to an erroneous conclusion: linearity of response is predicted to be better if the separation column has high bleed.

Lovelock[42] has also recently described the performance characteristics of the ECD. The stirred reactor model describes the processes causing the removal of electrons and molecules from the cell as follows :

$$e^- + AB \xrightarrow{k_1} \left.\begin{matrix} \\ \\ \end{matrix}\right\} \text{Inert products} \qquad [14]$$

$$e^- + \oplus \xrightarrow{k_d} \qquad [15]$$

$$AB + X \xrightarrow{k_x} \qquad [16]$$

$$AB \xrightarrow{U/V} \text{Ventilation} \qquad [17]$$

Reaction 14 is an irreversible second-order reaction with rate constant k_1. Reactions 16 and 17 concern the removal of sample molecules by processes other than in reaction in the gas phase with electrons. The detector volume is V and the gas flow rate U, the rate of injection of electrons A and of sample molecules B. The steady state electron concentration in the absence of sample molecules is

$$e^- = \frac{A\left\{1 - \exp(-kdt)\right\}}{k_d} \qquad [18]$$

which is the same as that derived by Wentworth et al.(Eq. 6). The theory is based on similar assumptions; excess of positive ions in the cell, uniform mixing and the removal of all electrons by a sampling pulse. However, the sample molecule is assumed to have a high capture rate constant unlike in the Wentworth model. After simplification, the sample concentration, C is expressed by

$$C = B/\ (k_1 e^- + kx + U/V) \qquad [19]$$

Conditions under which sample molecules are removed by processes other than by reaction with charged species have not been fully explained. The removal of sample molecules (with high capture rate constant) by ventilation during the flow of the carrier gas is considered to be the most important process yet the sample molecules remain for a sufficiently long time in the cell under conditions whereby the electron capture process is enhanced. It is uncertain which of these processes is dominant.

The presence of the positive ions and the effects of the

space charge need further consideration. The density of the ions continues to increase as electrons are collected but a limit must exist maximising their concentration. The assumption that the gas molecules and the electrons are uniformly mixed would imply that the space charge is no longer confined to the neighbourhood of the cathode. Also, the possible loss of electrons as they traverse the cell is not estimated.

An approach based on treating the ECD as a chamber containing two plane parallel electrodes and an internal ionisation source, with diffusion and recombination responsible for loss of charged particles, has been attempted. Ramey[43] has treated the case where volume recombination in a gas can be neglected, but in the ECD it has to be taken into consideration.

The current density at any point in space in the reaction volume is equal to the net production or loss of ion-pairs at that point.

$$\frac{dJ}{dx} = eNo - eknp$$

where:

J - current density

N_o - rate of production of ion-pairs

n - electron concentration

p - positive ion concentration

k - recombination coefficient

$$J = \int_0^x eNo\, dx - \int_0^x eKnp\, dx$$

$$= eNox - eknpx \qquad \text{where } No \neq f(x)$$

The current due to electrons only can also be expressed as:

$$J = -en\, \nu_d - eD^- \, dn/dx$$

ν_d is the electron drift velocity and D^- is the electron diffusion coefficient.

$$eNox - e\,knpx = -en\,\mathcal{V}d - e\,D^{-}\,dn/dx$$

$$\frac{dn}{dx} + \left(\frac{\mathcal{V}d}{D} - \frac{kpx}{D}\right) \cdot n = \frac{-No}{D}\,x$$

This is of the form,

$$\frac{dy}{dx} + p(x) \cdot y = Q\,(x)$$

Let $A = \mathcal{V}d/D$, $B = kp/D$ and $C = -No/D$

The integrating factor, I is

$$I = \exp \int (A - Bx)\,dx = \exp\,(Ax - 0.5Bx^2)$$

$$\frac{d}{dx}\left[\exp\,(Ax - 0.5\,Bx^2) \cdot n\right] = C\,x\,\exp\,(Ax - 0.5\,Bx^2)$$

$$\exp\,(Ax - 0.5\,Bx^2) \cdot n = C \int^{x} \exp\,(Ax - 0.5\,dx^2)\,dx$$

The solution of the integral on the R.H.S is

$$-\frac{1}{B}\,\exp\,(Ax - 0.5\,Bx^2) + \frac{A}{B}\int \exp\,(Ax - 0.5\,Bx^2)\,dx$$

The resulting integral has to be solved numerically and using both the Trapezium and Simpson's Rules, the values obtained were 4.12 and 4.20 for the low and high applied voltage cases respectively. The electron diffusion coefficient for nitrogen is calculated from the mean free path and the average velocity ($De = \bar{C}\ \lambda e/3$).

The electron concentration is then given by,

$$n = \frac{No}{kp}\left[\frac{4.2\,\mathcal{V}d}{D}\ \exp - (Ax - {}^{1}/_{2}\ Bx^2) - 1\right]$$

The measured current, I, is

$$I = \left(eNo\ V - es^{-} \cdot \mathcal{V}d^{-} \cdot n - es^{+} \cdot \mathcal{V}d^{+} \cdot p\right)$$

where V is cell volume and s is the electrode surface area.

The first term on the R.H.S. represents the saturation current. The second and third terms should reduce the current with decreasing applied voltage. With nitrogen as the carrier gas, the saturation

current term is 4.9 nA. Considering the average electron and positive ion concentrations ($\simeq 10^6$ cm^{-3} and 10^{10} respectively), the contribution of both the second and third terms (5.8×10^{-8}A and 4.6×10^{-7}A) is greater than the saturation current. Analysis of the ECD response on the basis of this approach is obviously not possible. The theory would probably be applicable in cases where the electron and positive ion concentrations are similar (ie. negligible space charge effects) and losses by recombination are very small.

In the section following, a theory for the ECD is proposed to overcome some of the deficiencies outlined in the discussion of various kinetic models. The theory is partly based on experimental observations made and these are fully described in chapters four and five.

3.4. PROPOSED MODEL FOR THE ECD

The basic approach to the problem is kinetic, ie. the detector is described by a system of rate processes[44]. A 'plasma' is created by energetic β^- particles emitted by the radio-active source. It contains Ve electrons Vp positive ions and Vn negative ions in a volume V. A given species, x, is removed from this 'plasma' by diffusion and volume flow rate F and has a mobility of μx under the appropriate conditions during a pulse. The cell has a cross-sectional area A and length l and the rate at which β^- particles leave the foil is $k_1 A$, each particle yielding G ion-pairs. The formation of one secondary electron and a positive ion by ionisation of a carrier gas molecule is referred to as an ion-pair.

A given species x may undergo a charge transfer process to yield a new species x j,

$$x + \text{neutral 1} \longrightarrow x\,j + \text{neutral 2}$$

or it may undergo attachment to yield xk,

$$x + \text{neutral} \longrightarrow xk.$$

Recombination processes involving positive ions and electrons or negative ions can be regarded as being of the first type together with reactions such as,

$$x^+ + Y \longrightarrow x + Y^+ + \Delta E \quad \text{and}$$

$$x^+ + x \longrightarrow x + x^+$$

It is a truly formidable task to list all X_i while the rates of none of these processes are known. Even if they were, the only actual measurement is that of total charge so that no detailed analysis would be possible. The discussion, therefore, is confined to the total species x while noting the fact that the rate constants used are weighted average rate constants, eg. for the recombination of electrons and positive ions,

$$\text{Total rate} = \sum_{P_i} k_i e p_i = ep \left[\frac{\sum k_i P_i}{\sum P_i}\right] = kep$$

where

$$p = \sum P_i \quad \text{and} \quad k = \frac{\sum k_i P_i}{\sum P_i}$$

As ki is not strongly dependent on the species P_i, little inaccuracy is introduced. Recombination coefficients for common molecular ions (except He_2^+) are in the range 10^{-7} to 10^{-6} $cm^3 s^{-1}$ [22].

The rates of removal of various species can be expressed as follows:

(Rate of formation) - (Rate of attachment) - (Rate of recombination) - (Rate of mass transport) - (Rate of migration)

Between pulses, the rates are :

$$V\frac{de}{dt} = k_1 AG - k_2 Vep - k_3 Vem - Fe \cdot e \qquad [20]$$

$$V\frac{dp}{dt} = k_1 AG - k_2 Vep - k_4 Vnp - Fp \cdot P \qquad [21]$$

$$V\frac{dn}{dt} = k_3 em - k_4 Vnp - Fn \cdot n \qquad [22]$$

where

e = electron concentration

p = positive ion concentration

n = negative ion concentration

m = concentration of sample molecules

Fe, Fp and Fn correspond to diffusion and volume flow rate for electrons, positive and negative ions respectively. The concentrations have units of particles cm^{-3}

During application of a pulsed voltage, a term ($- V x.A.x$) has to be added to each equation; $V x$ is the drift velocity of the species x. The charged particles are said to be contained within a 'plasma' occupying a volume V, which may be different from that of the detector. A plasma is defined[45] as a system of charged particles with a nett charge equal to zero and in which the space scale for charge separation is much smaller than the dimensions of the plasma. The space scale for charge separation, called the Debye length, λ refers to the radius of the sphere of oppositely charged particles around a charge necessary to screen the electrostatic force of the central charge.

The Debye length is expressed by:

$$\lambda = \left(\frac{kT}{4\pi e^2 Ne} \right)^{1/2} \qquad [23]$$

where k is the Boltzmann constant; T is the electron temperature (298K); e is the electron charge and Ne is the average electron density.

In the ECD, a typical average electron density is about 5×10^6 cm^{-3} and the value of λ is then 0.05 cm. The charge density in the cell is sufficiently large and consequently the Debye length is much smaller than the dimensions of the plasma volume (the reaction zone is said to be confined within a distance of 0.25 cm. from the cathode).

The removal of electrons from the plasma by the applied field, creates a space charge of positive ions as explained in section 2.4. This space charge clearly cannot continue to build up and some mechanism must exist to limit its growth.

It is helpful to consider the situation under the pulse mode of operation. A β^- particle forms p' and e' positive ions and electrons respectively. If it is assumed that a constant fraction, r, of positive ions is removed during each cycle, then the number of ions remaining in the cell at the end of the first pulse is $p_{+1} = p' (1-r)$. During the following pulse interval, p' positive ions again form and after losing the fraction r, the number remaining after the application of the second pulse is $p_{+2} = (1 - r) (p_{+1} + p')$. This process continues as more pulses are applied :

$$p_{+1} = (1 - r)\, p'$$

$$p_{+2} = (1 - r)\ (p_{+1} + p')$$

$$p_{+n} = (1 - r)\ (p_{+(n-1)} + p')$$

Subsitution gives,

$$p_{+2} = (1 - r) \left[(1 - r) \cdot p' + p'\right]$$

$$= p' (1 - r)^2 + p' (1 - r)$$

and at the end of n pulses,

$$p_{+n} = p' \sum_{n=1}^{n} (1 - r)^n$$

After a large number of pulses, the density of the positive ions converges to a limiting value,

$$p = \lim_{n \to \infty} \frac{p' \left[1 - (1 - r)^n\right]}{\left[1 - (1 - r)\right]}$$

$$= p' / r = e' / r \quad \text{(ion-pair formation)} \qquad [24]$$

As pointed out by A. F. Gaines, the term $R = r^{-1}$ expresses the ratio of positive ion to electron density at the beginning of

the applied pulse. The magnitude of the 'Gaines factor' approaches close to infinity after collection of electrons during the pulse. As the electron concentration in the cell builds up again during the following pulse interval, the 'Gaines factor' approaches its limiting value, R. The pulse interval would have to be sufficiently long for this to occur and factors governing the electron concentration would determine its magnitude. The continuous variation in the 'Gaines factor' during the pulse interval leads to an integration over the pulse period to obtain its average value.

The first point in the development of the model is to evaluate R from the rate equations already stated.

Once the space charge of positive ions has formed, no accumulation of charge occurs over a complete cycle, so that

$$\sum \int_0^s \frac{dX}{dt} + \sum \int_0^w \frac{dX}{dt} = 0 \qquad [25]$$

where s denotes the field free interval and w is the pulse width. Assuming that,

$$\frac{de}{dt} + \frac{dn}{dt} = \frac{dp}{dt}$$

and substituting equations [20] [21] and [22] in the above equation gives,

$$\left(Fe.e + Fn.n - Fp.p\right) = 0 \qquad [26]$$

During application of the pulse, the addition of the drift velocity term results in,

$$e\,(Fe + \nabla e.A) + n\,(Fn + \nabla n.A) - p\,(Fp + \nabla p.A) = 0 \qquad [27]$$

Substitution of equations [26] and [27] in [25] gives,

$$\int_0^s (Fe\cdot e + Fn\cdot n - Fp\cdot P)dt + \int_0^w \left[e\,(Fe + \nabla e.A) + n(Fn + \nabla nA) - p(Fp + \nabla p\cdot A)\right]dt = 0 \qquad [28]$$

Solution of equation [28] involves solving integrals for e, p and n over the field free interval and the pulse width.

The positive ion concentration can also be expressed as the sum of the ions remaining in the cell after a pulse has been applied and those generated as ion-pairs during the preceeding pulse interval, ie. $p = (p_o + e)$. If p and e are thus linked and negative ions are neglected, equation [20] becomes,

$$V \frac{de}{dt} = K_1 AG - K_2 Ve (p_o + e) - Fe \cdot e$$

$$= K_1 AG - e (K_2 VP_o + Fe) - K_2 Ve^2$$

$$V \frac{de}{dt} = a + be + Ce^2$$

where, $a = K_1 AG$, $b = -(K_2 VP_o + Fe)$ and $C = -K_2 V$.

Integrating the above equation with the boundary conditions $e = 0$ at $t = 0$ (beginning of the field free interval) gives :

$$\frac{1}{V} \int_0^t dt = \int_0^e \frac{de}{(a + be + Ce^2)}$$

$$\frac{t}{V} = \left[\frac{1}{\lambda} \ln. \frac{2Ce + b - \lambda}{2Ce + b + \lambda} \right] \Bigg/ \Bigg|_0^e \qquad [29]$$

where $\lambda = (b^2 - 4aC)^{1/2}$

$$\frac{1}{\lambda} \left[\ln \frac{2Ce + b - \lambda}{2Ce + b + \lambda} - \ln \frac{b - \lambda}{b + \lambda} \right] = \frac{t}{V}$$

$$\frac{2Ce + b - \lambda}{2Ce + b + \lambda} \cdot \frac{(b + \lambda)}{(b - \lambda)} = \exp (\lambda t/V)$$

$$\frac{\left[\frac{2Ce + b - \lambda}{b - \lambda} \right]}{\left[\frac{2Ce + b + \lambda}{b - \lambda} \right]} \cdot \frac{(b + \lambda)}{(b - \lambda)} = \exp (\lambda t/V)$$

Let $X = \frac{2Ce}{b - \lambda}$ and $Y = \frac{b + \lambda}{b - \lambda}$

$$X - \frac{X}{Y} \cdot \exp(\lambda t/V) = \exp(\lambda t/V) - 1$$

$$X = \frac{\exp(\lambda t/V) - 1}{1 - \exp(\lambda t/V)/Y}$$

$$\frac{2Ce}{b-\lambda} = \frac{[\exp(\lambda t/V) - 1]\ (b+\lambda)}{(b+\lambda) - (b-\lambda)\cdot\exp(\lambda t/V)}$$

$$2Ce = \frac{[\exp(\lambda t/V) - 1]\ (b^2 - \lambda^2)}{(b+\lambda) - \{(b-\lambda)\cdot\exp(\lambda t/V)\}}$$

$$e = \frac{1}{2C} \frac{(b^2 - \lambda^2)\ [\exp(\lambda t/V) - 1]}{\lambda[\exp(\lambda t/V) + 1] - b[\exp(\lambda t/V) - 1]}$$

$$e = \frac{2a[\exp(\lambda t/V) - 1]}{\lambda[\exp(\lambda t/V) + 1] - b[\exp(\lambda t/V) - 1]} \qquad [30]$$

The above equation describes the build up of electron concentration during the field free interval. However, its use is limited; further integration over the pulse width leads to an overwhelmingly complicated solution. Consider the case where p is constant.

$$V\frac{de}{dt} = K_1\ AG - K_2 \cdot Vep - Fe.e$$

$$= K_1\ AG - e\ (K_2 \cdot Vp + Fe.e)$$

Let $a = K_1\ AG$ and $b = (K_2 \cdot Vp + Fe.e)$

Integration over the field free interval leads to,

$$\int_0^e \frac{de}{(a - be)} = \frac{1}{V} \int_0^t dt$$

$$\frac{t}{V} = -\frac{1}{b}\left[\ln.(a - be) - \log a\right]$$

$$1 - \frac{be}{a} = \exp(-bt/V)$$

$$e = \frac{a}{b}\left[1 - \exp(-bt/V)\right] \qquad [31]$$

Equation [31] can be used to determine the decrease in electron concentration during the pulse width (w). The boundary conditions now are $e = e_t$ at $t = o$ and $e = e$ at $t = w$. Considering the drift velocity term and in the absence of sample molecules, Equation [20] becomes :

$$V \frac{de}{dt} = K_1 AG - K_2 Vep - Fe.e - \mathcal{V}e .Ae$$

$$= K_1 AG - e (K_2 Vp + Fe.e + \mathcal{V}e.A)$$

Let $a = K_1 AG$ and $b' = (K_2 Vp + Fe.e + \mathcal{V}e.A)$

$$\int_{e_t}^{e} \frac{de}{(a - b' e)} = \frac{1}{V} \int_{o}^{t} dt$$

The integral is of the same form as the previous one and its solution is,

$$- \frac{b't}{V} = \ln \left(\frac{a - b'e}{a - b'e_t}\right)$$

$$(a - b'e) = (a - b' e_t) \exp (-b't/V)$$

$$e = \frac{a}{b'} \left[1 - \exp (-b't/V)\right] + e_T \exp (-b't/V) \qquad [32]$$

It is now necessary to evaluate the total charge in the cell during the field free interval. This is done for the case where p is constant, since where $p = p_o + e$, the integrals are again very unwieldy. Using equation [31] ,

$$\int_{o}^{t} e \, dt = \int_{o}^{t} \frac{a}{b} \left[1 - \exp (-bt/V)\right] dt$$

$$= \frac{a}{b} \left[t + \frac{V}{b} \exp (-bt/V) - \frac{V}{b}\right]$$

$$= \frac{a}{b}\left[t - \frac{V}{b}\left(1 - \exp(-bt/V)\right)\right] \qquad [33]$$

Similarly, the total charge lost during the application of the pulse is obtained by integrating equation [32].

$$\int_0^t e\,dt = \frac{a}{b'}\int_0^t \left[1 - \exp(-b't/V)\right] dt + \int_0^t e_T \exp(-b't/V)dt$$

$$= \frac{a}{b'}\left[t - \frac{V}{b'}\left(1 - \exp(b't/V)\right)\right] + \frac{e_t V}{b'}\left[1 - \exp(-b't/V)\right] \qquad [34]$$

Graphical representation of the equations derived is shown in Figure(5). Having obtained integrals for the electron concentration equation [28] can now be considered. Without the negative ion terms it is :

$$\int_0^s (Fe.e - Fp.p)\,dt + \int_0^w \left[e(Fe + \mathcal{V}eA) - p\,(Fp + \mathcal{V}pA)\right] dt = 0$$

Making the substitution $p = (p_o + e)$ gives,

$$\int_0^s (Fe - Fp)\,e\,dt + \int_0^w (Fe + \mathcal{V}eA)\,e\,dt = Fp\,p_o\,s + \int_0^w (Fp + \mathcal{V}pA)pdt$$

Inserting the various integrals involved, the left-hand-side (L.H.S) of the above equation becomes,

$$(Fe - Fp)\,\frac{a}{b}\left[s - \frac{V}{b}\left(1 - E^{-bs/V}\right)\right] + (Fe + \mathcal{V}eA)\left\{\frac{a}{b'}\left[w - \frac{V}{b'}\left(1 - E^{-b'w/V}\right)\right] + \frac{e_t V}{b'}\left(1 - E^{-b'w/V}\right)\right\}$$

and the R.H.S. is,

$$Fp\,p_o s + (Fp + \mathcal{V}pA)\left\{\frac{a}{b''}\left[w - \frac{V}{b''}\left(1 - E^{-b''w/V}\right)\right] + \frac{(Po + e_t)V}{b''}\cdot\left(1 - E^{-b''w/V}\right)\right.$$

[35]

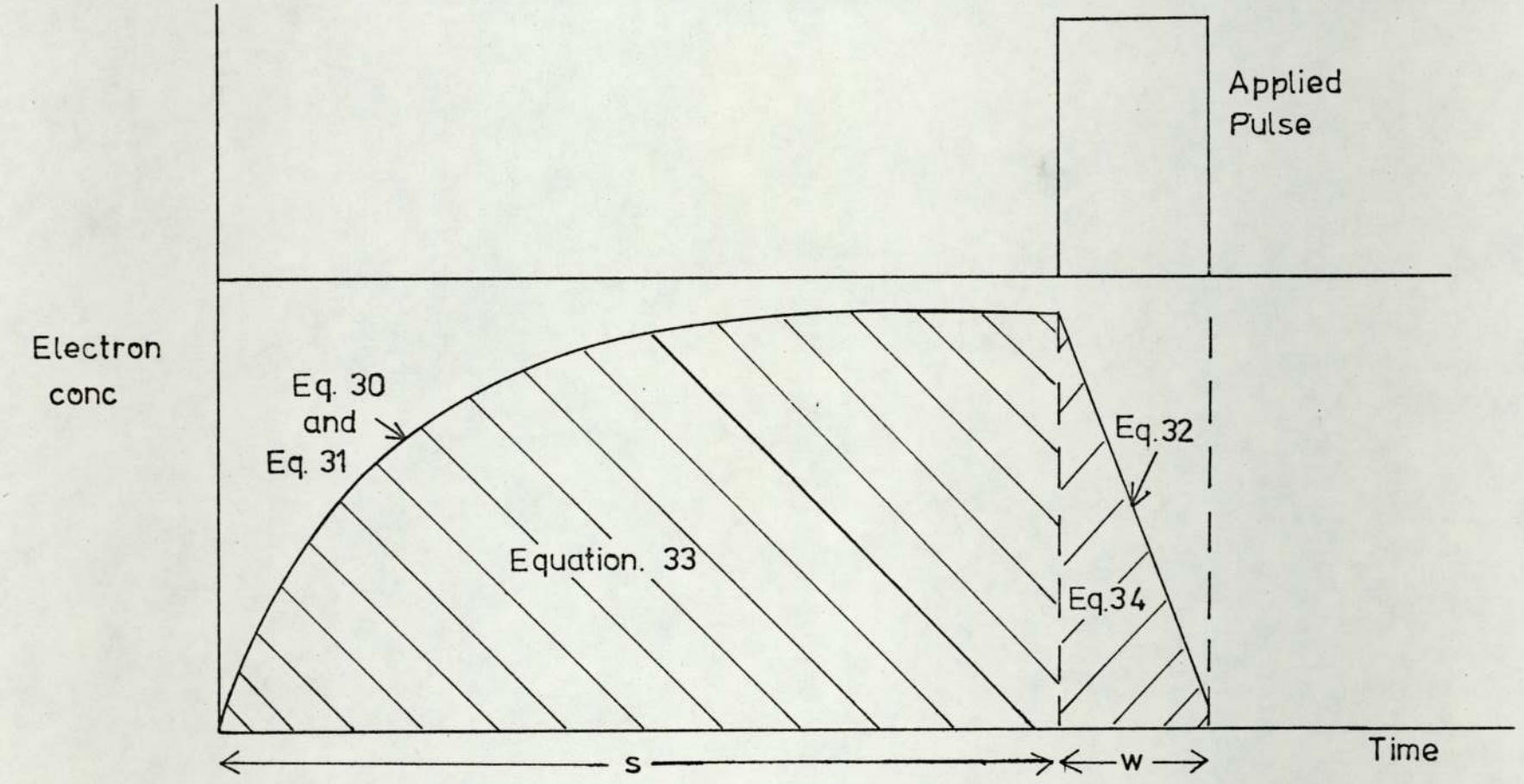

FIG. 5

GRAPHICAL REPRESENTATION OF EQUATIONS DERIVED IN THE PROPOSED MODEL

The integral expressing the positive ion concentration is of the same form as that for the electron density and the constant $b'' = (K_2 Ve + Fp + \nu pA)$.

The term $(Fe + \nu e.A)$ can be replaced by $(b' - K_2 Vp)$ and similarly for $(Fp + \nu pA) = (b'' - K_2 Ve)$. As the number of electrons removed, through collection at the anode, is small in comparision to the positive ion density, $p = p_o + e \simeq po$. Further simplification of equation [35] is achieved by making approximations under real conditions. An order of magnitude analysis of various terms is given below :

$$b' = (K_2 Vpo + Fe + \nu eA) \simeq (10^3 + 3 + 10^5) \simeq 10^5 \quad cm^3 \; s^{-1}$$

$$b'' = (K_2 Ve + Fp + \nu pA) \simeq (10^{-1} + 3 + 10^3) \simeq 10^3 \quad cm^3 \; s^{-1}$$

$$\frac{V}{b}\left[1 - \exp\,(-bs/V)\right] \simeq 10^{-4} \quad s^{-1}$$

$$\frac{V}{b'}\left[1 - \exp\,(-b'\, w/V)\right] \simeq 10^{-6} \quad s^{-1}$$

$$\frac{e_t V}{b'}\left[1 - \exp\,(-b'\, w/V)\right] \simeq 1 \; scm^{-3}$$

$$Fp\, P_o s \simeq 10^6$$

$$\frac{V}{b''}\left[1 - \exp\,(-b''\, w/V)\right] \simeq 10^{-4} \; s^{-1}$$

$$\frac{(Po + et)\, V}{b''} \simeq 10^7 \; scm^{-3}$$

The L.H.S. of equation [35] simplifies to,

$$\frac{(b' - K_2\, Vpo)\, e_t}{b'}$$

while the R.H.S. becomes,

$$Fp\, pos + (b'' - K_2\, Ve)\left[w\,(po + e_t)\right]$$

Substituting $a = be_t$ and $p_o = (R-1)e_t \simeq Re_t$ gives,

$$\frac{(b' - K_2 V p_o)\, e_t}{b'} = Fps\,(R-1)e_t + (b'' - K_2 Ve)\,(Re_t w)$$

$$= R\left[Fps + w\,(b'' - K_2 Ve)\right] - Fps$$

Hence,

$$R = \frac{1 - \frac{K_2 V p_o}{b'} + Fps}{(b'' - K_2 Ve)\,w + Fps}$$

Since, $b' \gg K_2 V p_o$, the 'Gaines factor' is expressed by,

$$R = \frac{1 + Fps}{(Fp + \mathcal{V}pA)\,w + Fps}$$

$$R = \frac{1 + Fps}{\mathcal{V}p \cdot Aw + Fp\,(w + s)} \qquad [36]$$

It is to be noted that the above expression is merely an approximation for R; its value is dependent on gas parameters and also on pulse characteristics, ie. a function of time. The average value of R is obtained by integrating over the pulse interval and dividing by the period.

$$\int_o^t R\,dt = \frac{1}{s} \int_o^t \frac{1 + Fpt}{(Fp + \mathcal{V}p.A)\,w + Fpt}\,dt$$

Let $(Fp + \mathcal{V}pA)w = Q$

$$\int_o^t R\,dt = \frac{1}{T}\left[\int_o^t \frac{dt}{(Q + Fpt)} + \int_o^t \frac{Fpt}{Q + Fpt}\right] dt$$

$$\int_0^t \frac{dt}{(Q + Fpt)} = \frac{1}{Fp} \ln (Q + Fpt) \Big/_0^t$$

$$= \frac{1}{Fp} \left[\ln \left(1 + \frac{Fpt}{Q}\right) \right]$$

$$\int_0^t \frac{Fpt}{Q + Fpt} dt = t - \frac{Q}{Fp} \left[\ln Q (Q + Fpt) \right]$$

In real terms, the magnitude of the latter integral is very much smaller than that of the former and hence,

$$\int_0^s Rds = \frac{1}{Fps} \ln \left[1 + \frac{Fps}{(Fp + VpA)W} \right] \qquad [37]$$

Having obtained the 'Gaines factor', it can now be used to determine the positive ion density in the cell. As a first approximation, the rate of production of ion-pairs can be equated to the product of the electron concentration and the rates of loss by recombination and volume flow.

$$a = be = e (K_2 Vpo + Fe)$$

If Fe is small,

$$Po = eR = \frac{R\,a}{(K_2 Vp_o)}$$

The positive ion concentration is therefore given by

$$P_o = \left(\frac{Ra}{K_2 V} \right)^{1/2} \qquad [38]$$

It is axiomatic in the present work that mixing within the plasma is sufficiently rapid for the concentration to be uniform. A single criterion may be used to test the degree of mixing - if the electron drift velocity is much less than the gas kinetic velocity, mixing can be held to be complete but if the converse is

then there is very little.

The drift velocity for electrons is about 7×10^6 cms^{-1} at 100 Volts cm^{-1} in argon + methane, while the gas kinetic velocity at STP is $(RT/M)^{1/2} = 1.2 \times 10^7$ cms^{-1}. The criterion is indecisive and mixing cannot be held complete but is certainly significant. This point is further discussed in the experimental section where the effect of carrier gas flow is considered.

Experimental verification of the model is now possible for the case where only the pure carrier gas response is observed under the pulse mode of operation.

CHAPTER FOUR - AN EXPERIMENTAL STUDY OF THE ECD

4.1 DETECTOR DESIGN AND CONSTRUCTION

For the purpose of the present study, a cell had to be constructed since the commercially available detectors do not offer the necessary flexibility needed to investigate the various characteristics of the instrument. The design was kept as simple as possible to avoid any complexities arising from the detector's geometry yet was comparable to that of commercial detectors.

Scolnick[46] showed that if the ECD were to function as a concentration detector, the volume of the chamber has to be about 0.5 cm^3. The ratio of the detector time constant to the chromatogram peak width at 60.6% of the maximum sample concentration, has to be small to minimise loss in peak resolution. Another point which requires consideration is the choice of the inter-electrode insulator. At high temperature Scolnick found that the conductivity of glass insulators used in many concentric ECDs, is not small in comparision to the conductivity of the ionised gas.

Figure (6) illustrates the ECD constructed. It is of the normal parallel plane configuration except for the gas flow arrangement - the inlet and exit were perpendicular rather than parallel to the electrodes. This allowed the electrode separation to be varied and the vortices in such a flow system would probably provide better mixing. The main cell body was of PTFE; the wall thickness being 1.27 cm. The gas inlet and outlet were 0.635 cm. brass tubing threaded half way through the cell body. The electrodes consisted of a brass disc (1.27 cm. in diameter) and a stainless steel rod (0.3175 cm. in thickness). They were locked into the desired position by PTFE nuts pressing onto an 'O' ring. The cell was

FIG. 6

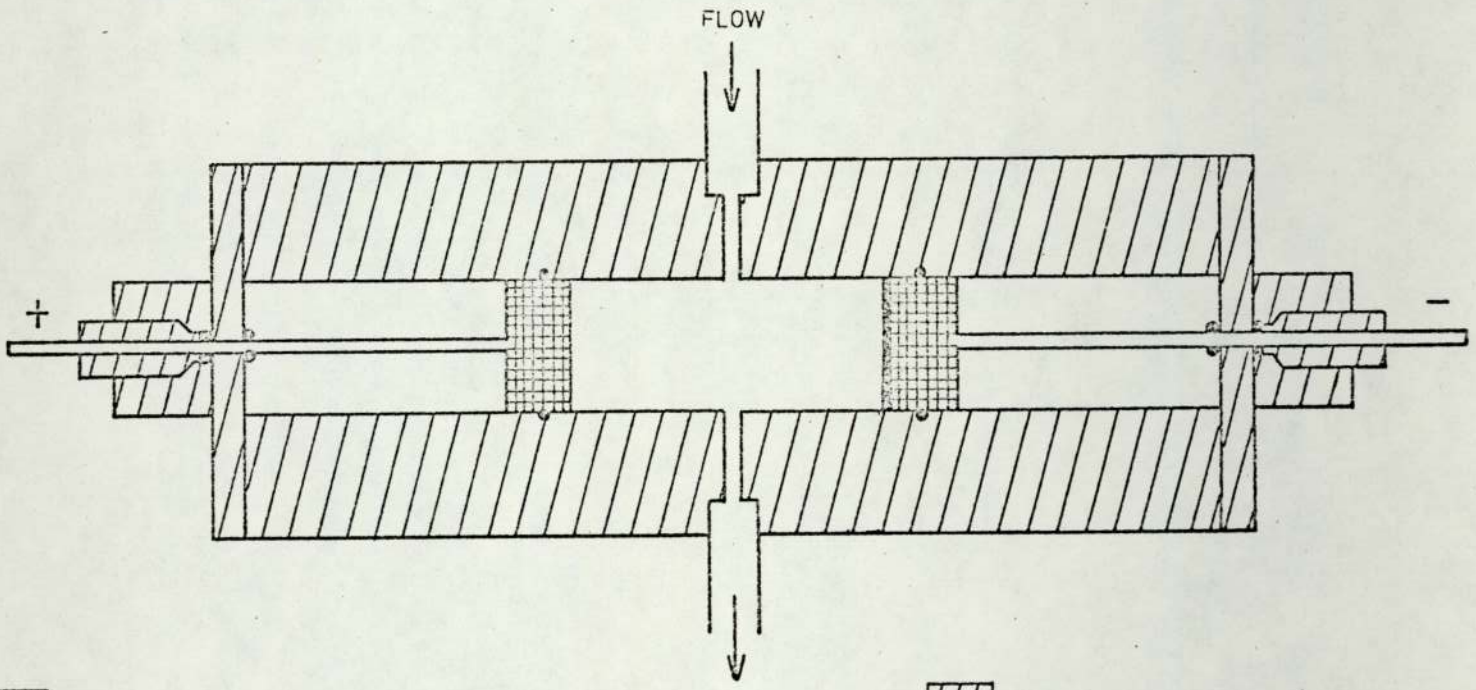

CATHODE WITH RADIOACTIVE SOURCE

ANODE : BRASS CYLINDER (DIAMETER = 1·7 cms)

THE ELECTRON CAPTURE DETECTOR.

made leak proof by having rubber 'O' rings both on the electrodes and at either ends of the cylindrical body. The radioactive foil consisted of ^{3}H occluded on a titanium surface with a copper backing. The foil was soldered on to the brass disc to form the cathode of the cell. This was done using a low melting solder (85°C) so as to avoid any loss of radioactivity.

The ECD was housed in an aluminium box with its own separate gas supply to prevent back diffusion of atmospheric oxygen(46). A loose fitting lid provided access to the detector while permitting the vented gas finally to escape into the atmosphere. The metal container also prevented possible interference from stray capacitance and other outside electrical disturbances.

4.2 ELECTRICAL CIRCUIT

Figure (7) shows the electrical circuit used for normal operation of the cell. The voltage source was a Hewlett Packard model 214A pulse generator providing a maximum pulse amplitude of 100 volts and had continuously variable pulse width and interval. The applied pulses were monitored on an oscilloscope. The current flowing through the cell was measured as a voltage drop across the high input resistance of a vibrating reed electrometer. The instrument used was an E.I.L model 33C Vibron with two additional resistances of 10^{7} and 10^{8} ohms fitted in the convertor unit. The full scale deflection of the meter was 1000 mV and the input resistance was variable from 10^{7} to 10^{12} ohms in powers of 10. At 10^{12} ohms, the time constant is stated to be about 30 seconds and is much less with lower resistances. Since the currents measured were in the nano- to pico A region, it was necessary to eliminate local leakage current loops set up as a result of slight potential differences existing between various earth points. Care had to be taken to

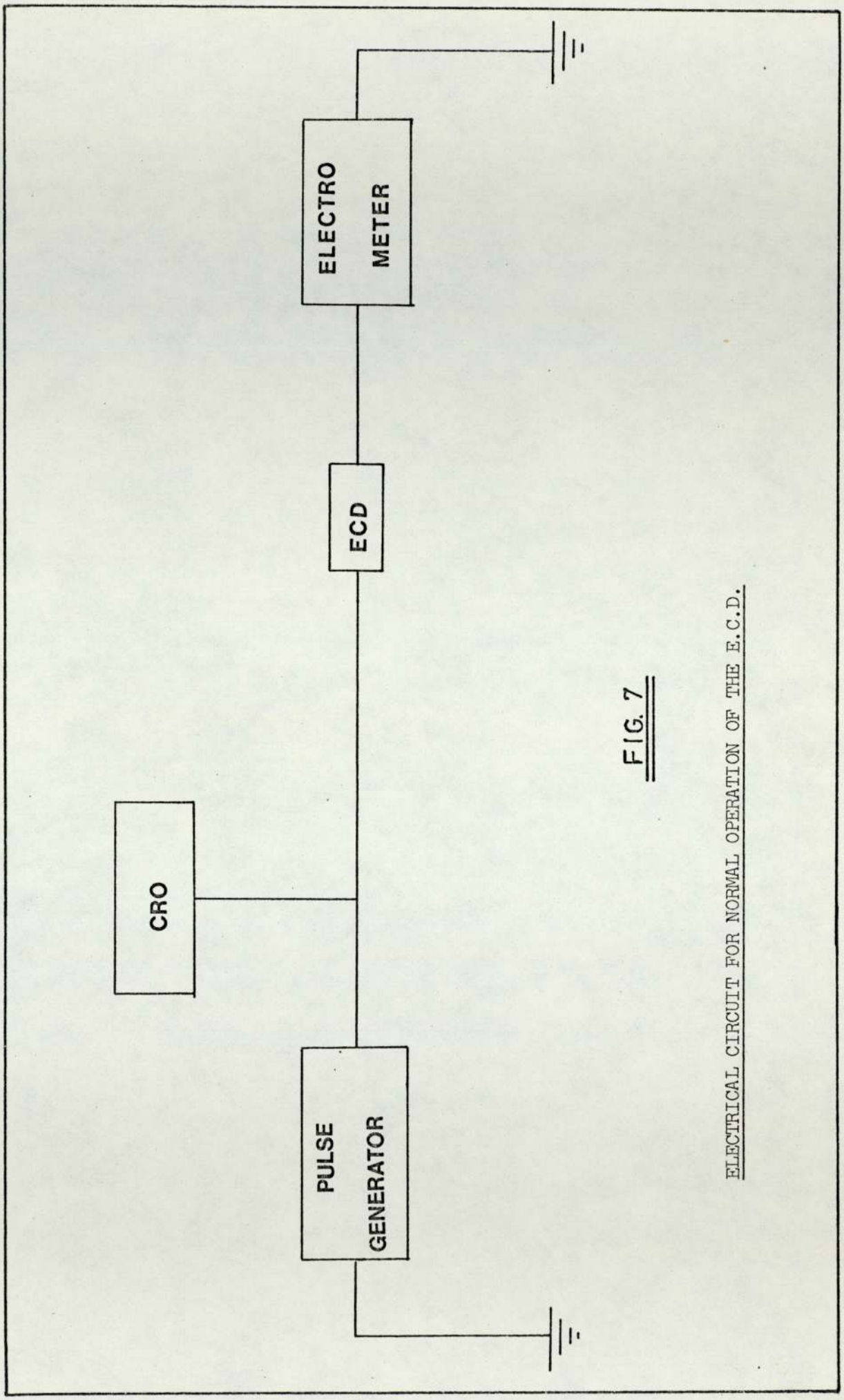

FIG. 7

ELECTRICAL CIRCUIT FOR NORMAL OPERATION OF THE E.C.D.

avoid inefficient shielding of cables and also of the ECD.

4.3 GAS PURIFICATION

To study various parameters of the detector, nitrogen was mainly used as the carrier gas. The 'white spot' nitrogen supplied by the British Oxygen Company was exclusively used. The flow rate was regulated by rubber diaphragm type of valves and was measured on flowmeters supplied by the Rotameter Manufacturing Company. These were calibrated by means of a bubble flow meter. 0.25 in. O.D. copper tubing and thick-walled nylon tubing were used for gas transport. Diffusion through the walls of the latter did not seem to occur as the current was not affected when the length of tubing was changed. All connections were made with 'Enot' fittings. The gas after monitoring passed through a molecular sieve, supplied by Kenmore Incorporated, for the removal of moisture. Before entering the cell, the gas also passed through an 'Oxy Trap' which was supplied by Allteck Associates. All joints were thoroughly tested for leaks with soap solution and the line was evacuated to about 10^{-2} torr. Precautions for good performance, as laid down by Lovelock[42], were taken as far as it was practically possible. These included the use of metal diaphragm pressure regulators, clean short tubing for all gas connections and the avoidance of flow regulators at the head of the gas line.

To check on the presence of oxygen in the carrier gas, a chemical test was carried out. A solution of Co $(dipy)_3$ $(ClO_4)\cdot 3H_2O$ in dimethyl sulphoxide (DMSO) was reduced by an aqueous solution of sodium borohydride. Nitrogen from the ECD was bubbled through the solution. The product of the reduction remains deep blue in the absence of any oxygen and turns colourless to yellowish in the presence of the smallest amount[47]. The carrier gas was found to

be oxygen free. The whole apparatus had to be removed because the solvents were back-diffusing through the gas line to the detector.

Another simple check of the cleanliness of the carrier gas is to determine the electron half-life within the chamber[48]. This is done by finding the pulse period at which the detector standing current falls to half of that measured at the shortest pulse interval. Under ideal conditions with really clean gas, it may be as much as 1 ms and has to be greater than 300 μs. With nitrogen as carrier gas, the electron half-life was about 750 μs.

4.4 CHARACTERISATION OF THE DETECTOR

Under the pulsed mode of operation, the detector current depends partly upon the pulse amplitude, width and interval. Preliminary experiments were carried out to determine the optimum operating conditions necessary for the detector regarding pulse characteristics.

Figure (8) shows the current variation with applied voltage. The current rises steeply and reaches a steady level at about 20 volts. At low applied voltages, electrons and ions are lost through recombination as the field strength is not sufficiently high to allow their collection at the respective electrodes. At constant pulse amplitude and width and temperature and pressure, the number of electrons per pulse, N_e, is expressed by,

$$N_e = \frac{I \times s}{1.6 \times 10^{-19}}$$

where I is the observed current and s is the pulse interval. The voltage corresponding to the onset of theplateau in Fig. (8) is independent of the pulse interval but depends on the pulse width.

It is desirable to have the pulse width (w) as short as possible so that the number of ion-pairs formed during the pulse is

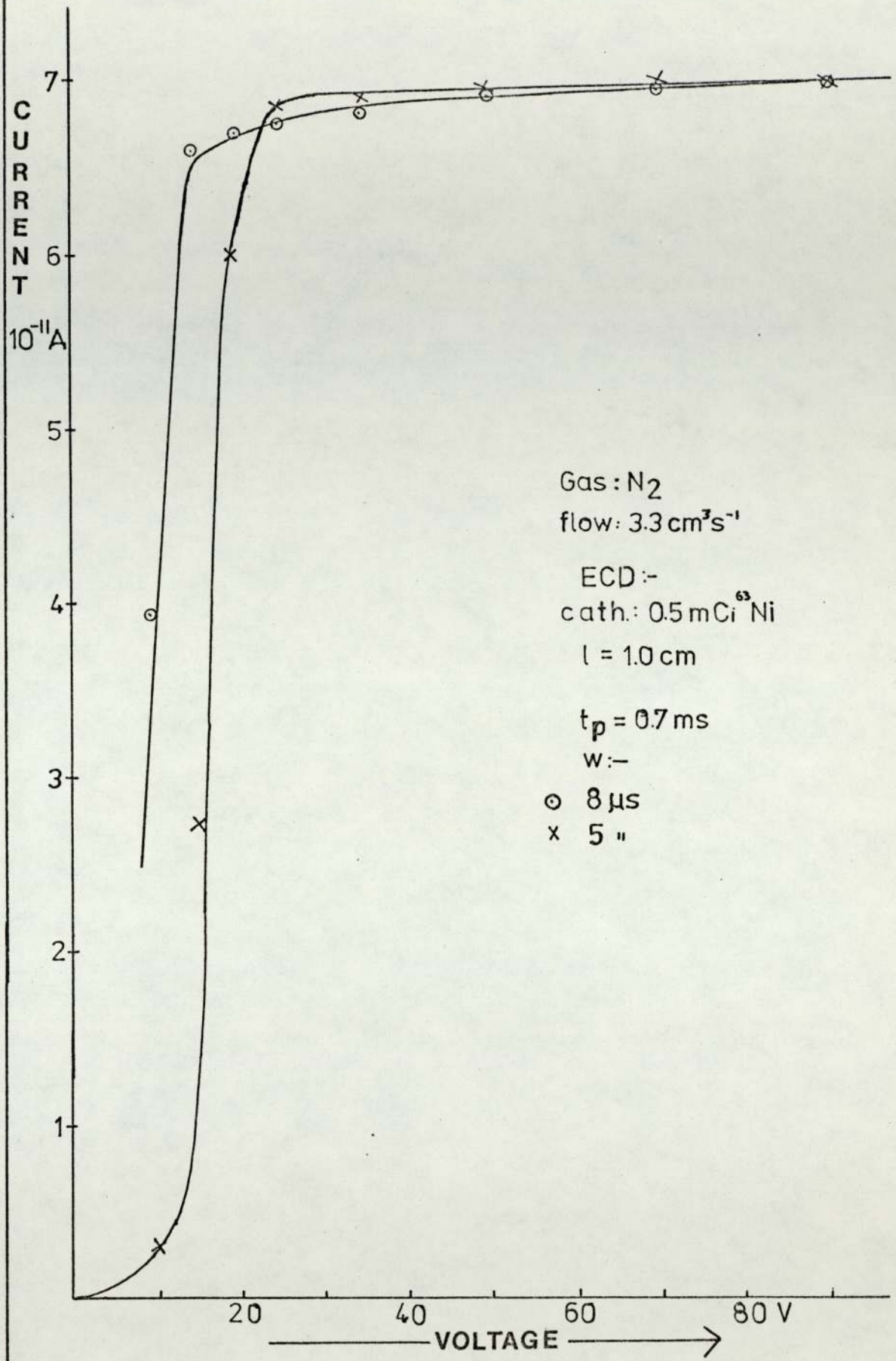

FIG. 8

CURRENT (I) VARIATION WITH PULSE AMPLITUDE (V)

not appreciable and the electrons have the maximum possible time to reach thermal equilibrium. If the duration is too short however, there is not sufficient time to collect all electrons and hence the saturation current is not reached. From Fig. (9) it can be seen that a pulse width of about 3.5μs is sufficient to remove all electrons. Normally pulses of 5 μ s duration were employed. The critical pulse width at which the curve effectively flattens off is said to correspond to the electron transit time between the two electrodes. Electron drift velocities have been calculated from this data[18,39].

Besides the amplitude of the voltage and the length of time for which it is applied, the interval between pulses also affects the current flowing through the cell. The current is proportional to the number of pulses per second, that is, inversely proportional to the period (Fig. 10). This relation does not work at small pulse interval as an 'equilibrium' has not been established between the process of production of ion-pairs and those processes responsible for their loss. The relationship between the number of electrons per pulse (Ne) and the pulse interval is more difficult to explain as often a maximum is observed (Figs. 11 and 12). A good test for the kinetic models outlined in the previous chapter is to predict the above relationship. This point is discussed more fully in section 4.7 this chapter.

4.5 RADIATION SOURCES AND INTER-ELECTRODE SPACING

The nature of the ionisation source has been found to be of primary importance. The dimensions of the ionisation zone are determined by the cross-sectional area of the radiation source and the range of the emitted β^- particles. The two most commonly used sources are ^{3}H and ^{63}Ni. As stated earlier, β^- particles released from a ^{3}H source have a maximum energy distribution between 17.6 and 18.9 KeV, while those from ^{63}Ni are about 67 KeV[15]. The

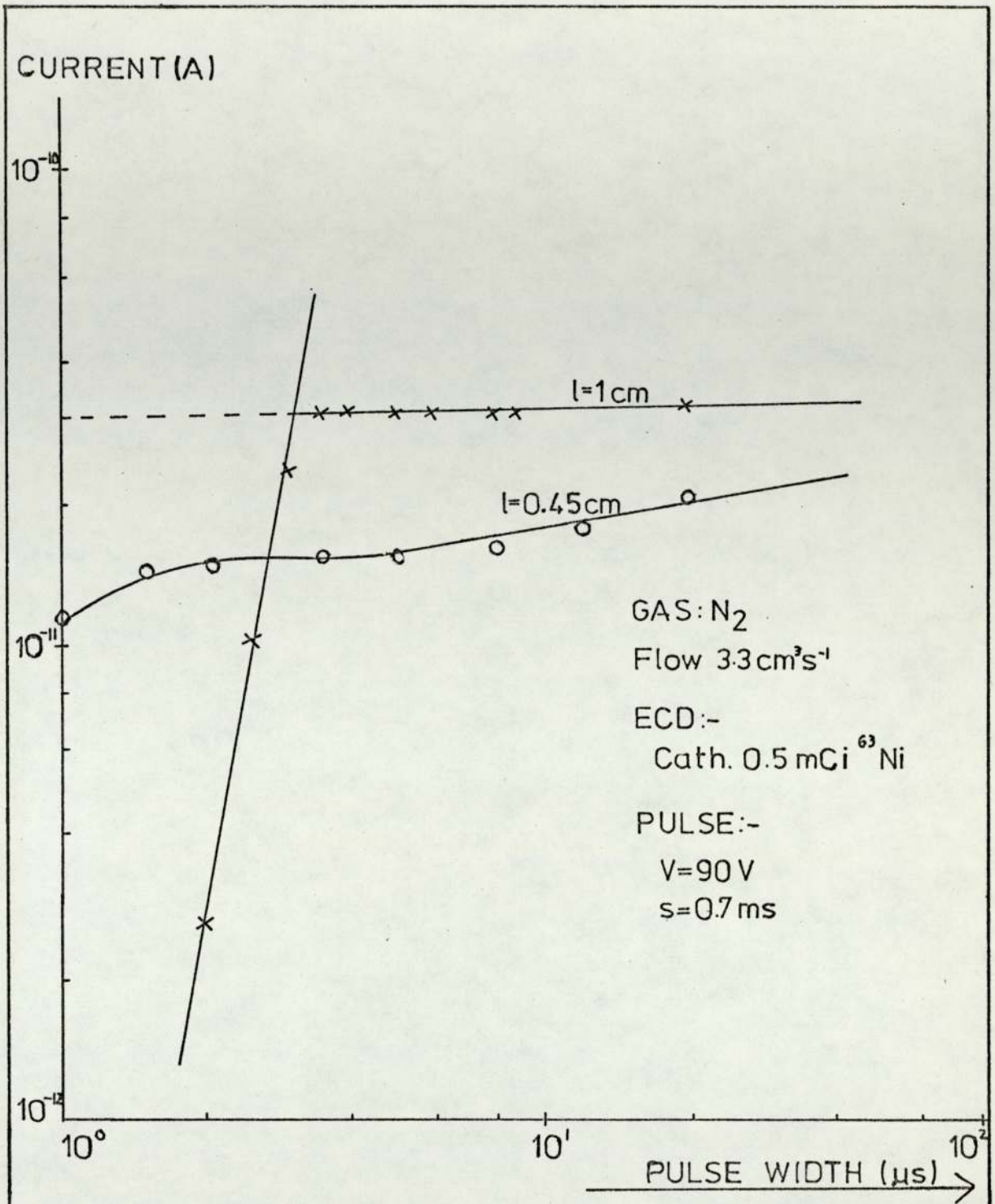

FIG. 9

CURRENT VARIATION WITH PULSE WIDTH (W)

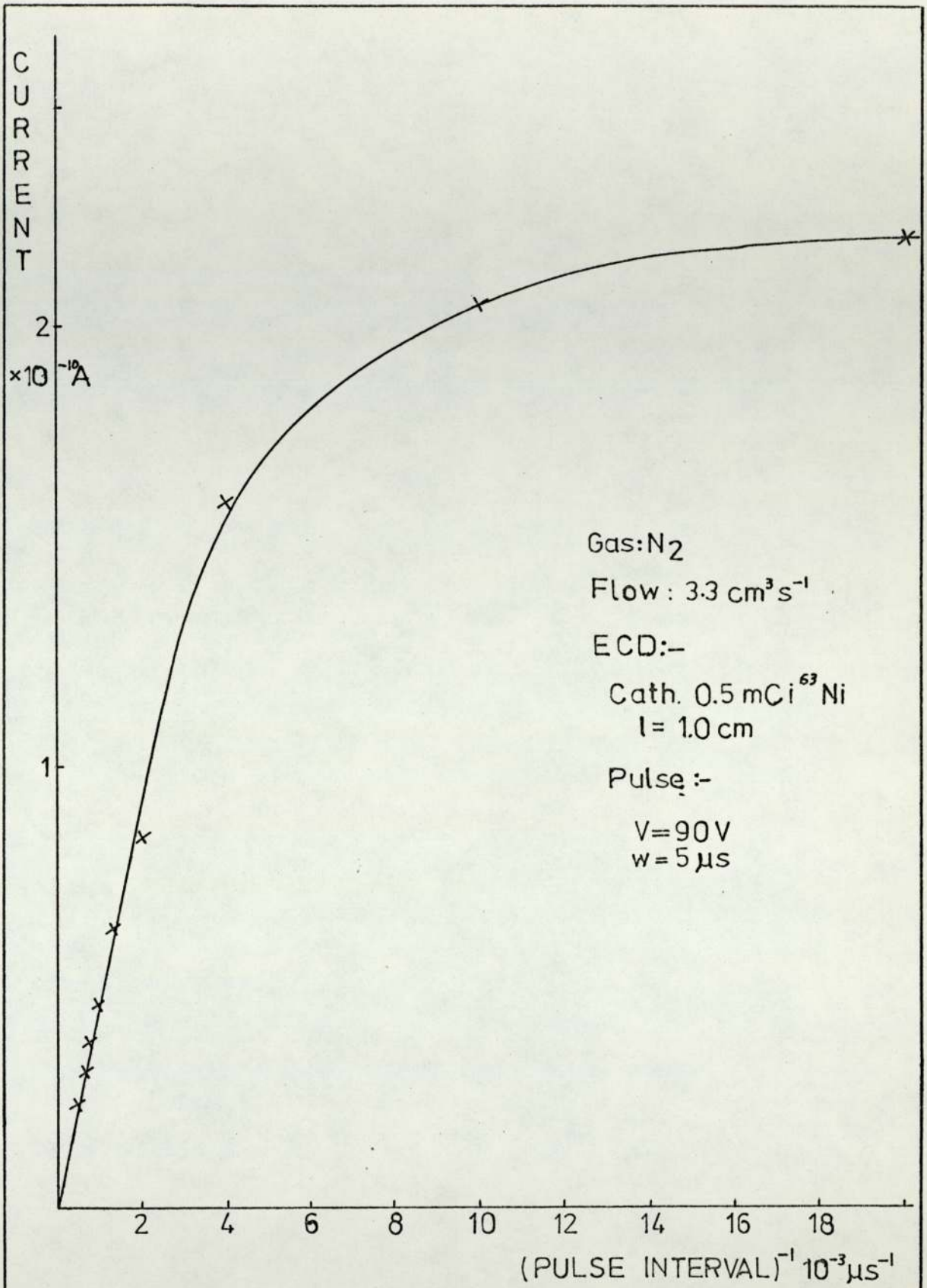

FIG. 10

CURRENT VARIATION WITH PULSE INTERVAL $(s)^{-1}$

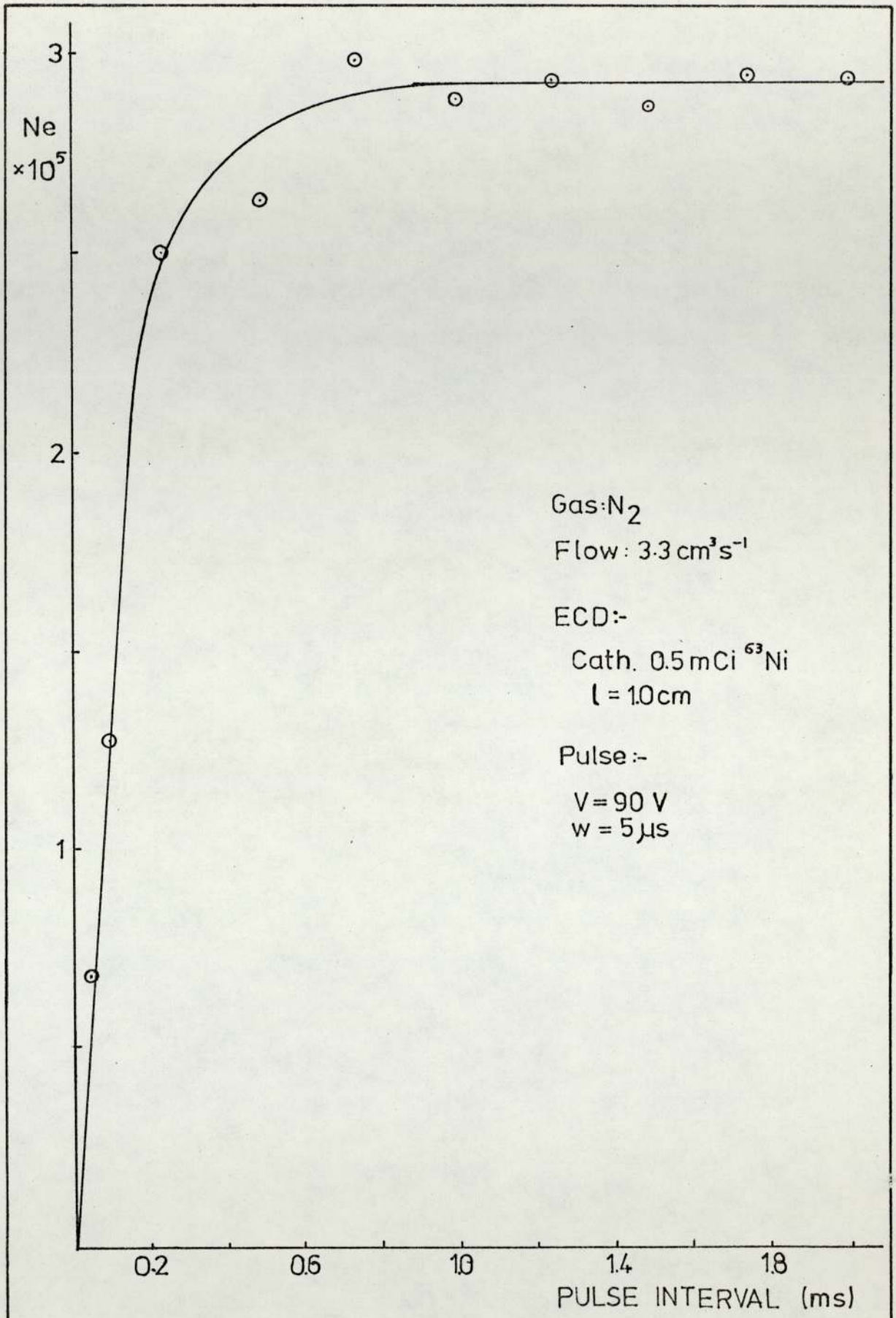

FIG. 11

Ne VERSUS s PLOT FOR ^{63}Ni SOURCE

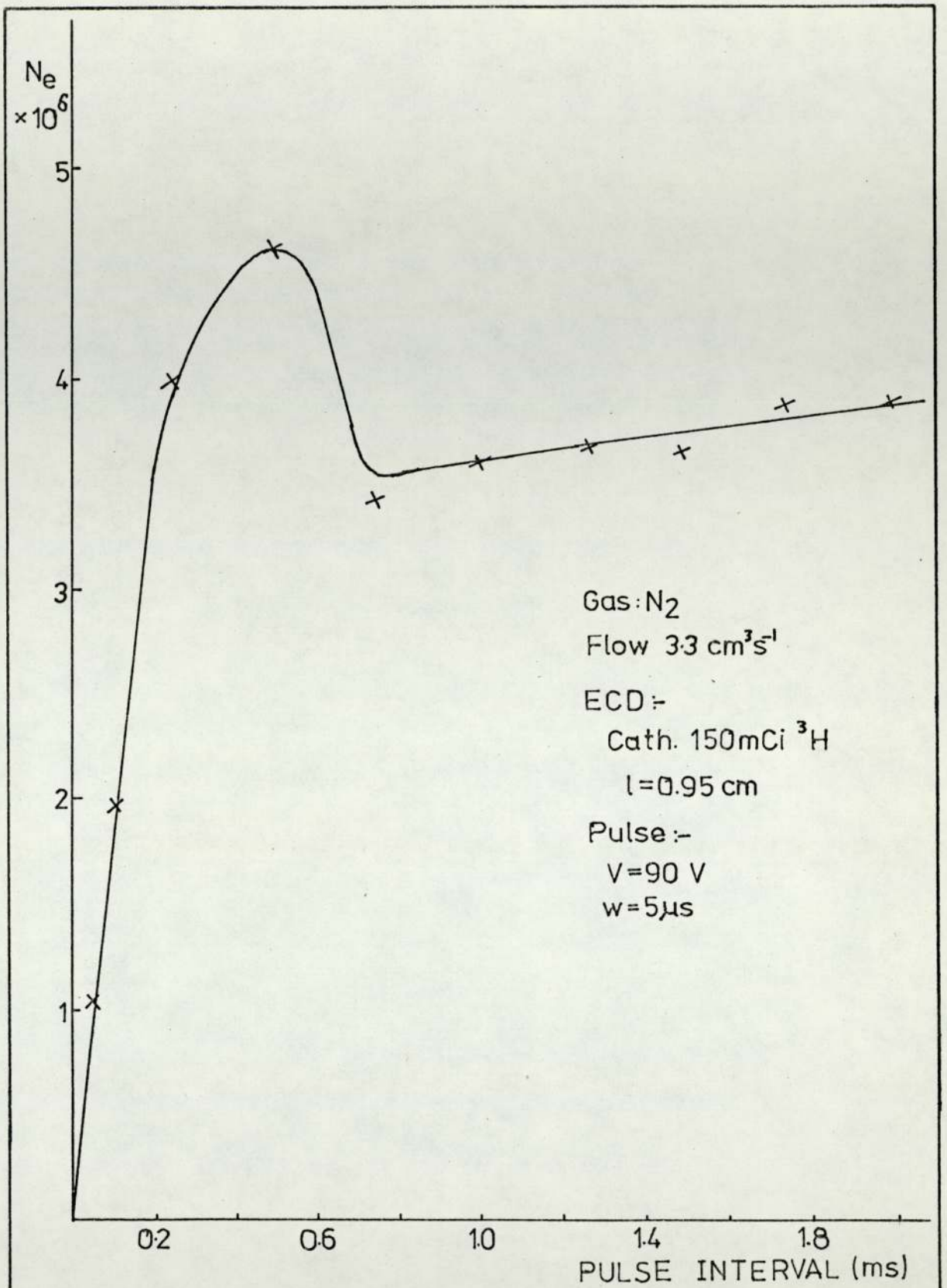

FIG. 12

Ne VERSUS s PLOT FOR 150 mCi SOURCE

average energy is about one third the maximum energy. The number of ion-pairs formed decreases with increasing energy of β^- particles (Fig.13), since the time in which energy can be transferred from the particle to the gas molecule upon collision decreases with increasing velocity. When low energy β^- particles are being considered, the range has been found to be almost independent of absorber material. The graph of specific ionisation, ie. the rate at which β^- particles lose energy in passing through air, versus range (Fig. 14) shows a very steep increase in the number of ion-pairs formed at a distance of about 2 mm. from the ^3H source[49]. There is then an exponential decrease in the number of pairs formed with increasing distance.

The range of the β^- particles, R, can be calculated from an empirical relationship,

$$\text{Ln. } E = 6.63 - 3.2376\ (10.2146 - \ln R)^{1/2}$$

where E is the maximum energy in MeV. The equation is valid for $0.01 \leqslant E \leqslant 2.5$ M eV. Weakly energetic β^- particles from a ^3H source travel about 2 mm. in air. Wentworth et al.[18] and the Radiochemical Centre[50] quote similar values. β^- particles of maximum energy travel about 6 mm. while those from the ^{63}Ni source have a range of about 9 mm. The combined effects of continuum spectra and scattering lead to an approximately exponential absorption law for β^- particles of a given maximum energy. The nearly exponential decrease applies both to numbers and specific ionisation of β^- particles. Hence, the energy and number distribution lead to the conclusion that there are many more β^- particles close to the source and because of their low energy, a large number of ion-pairs could be formed in this region.

Loss through self-absorption and scattering is much more pronounced with electrons than with heavy particles. Self absorp-

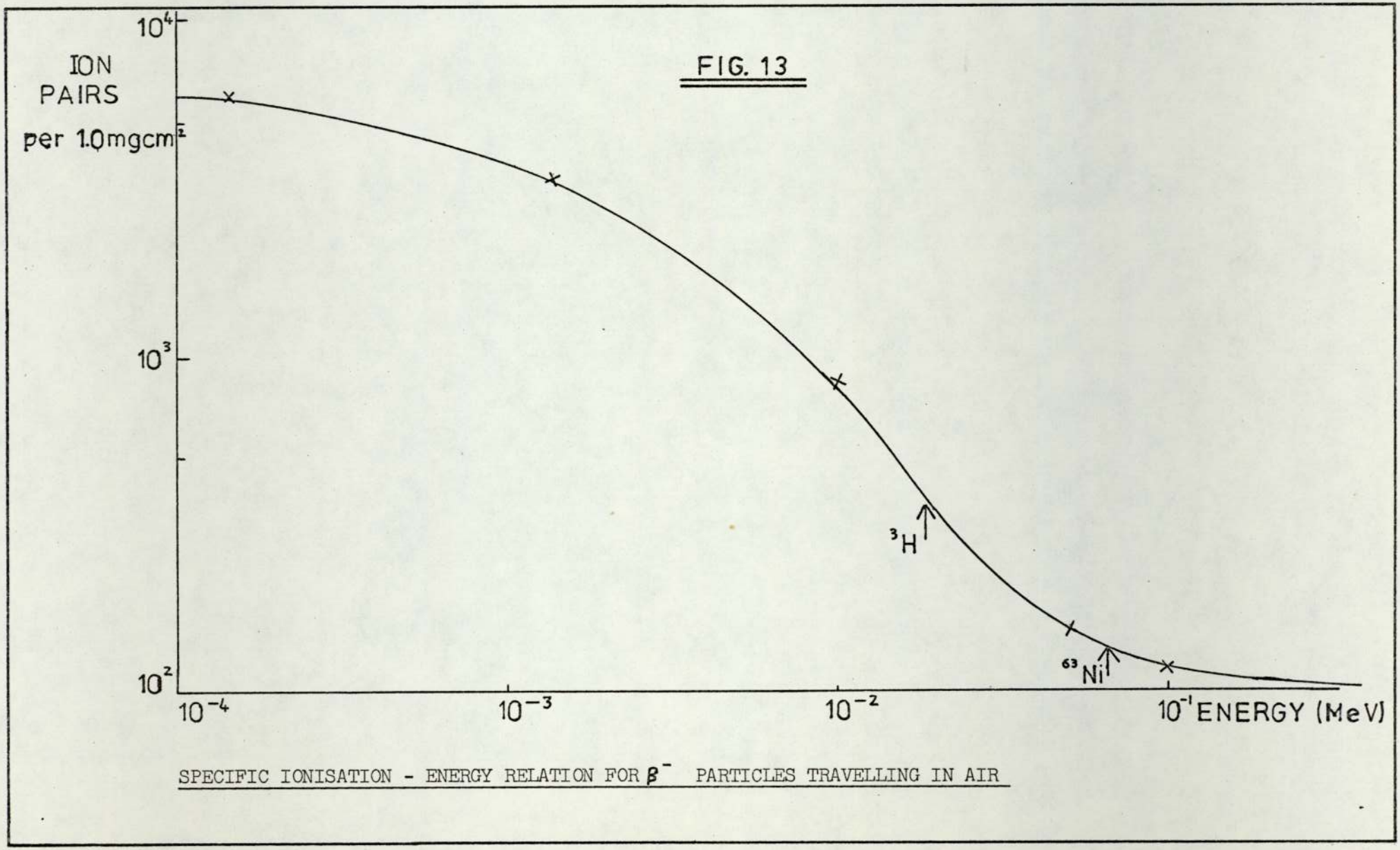

SPECIFIC IONISATION - ENERGY RELATION FOR β^- PARTICLES TRAVELLING IN AIR

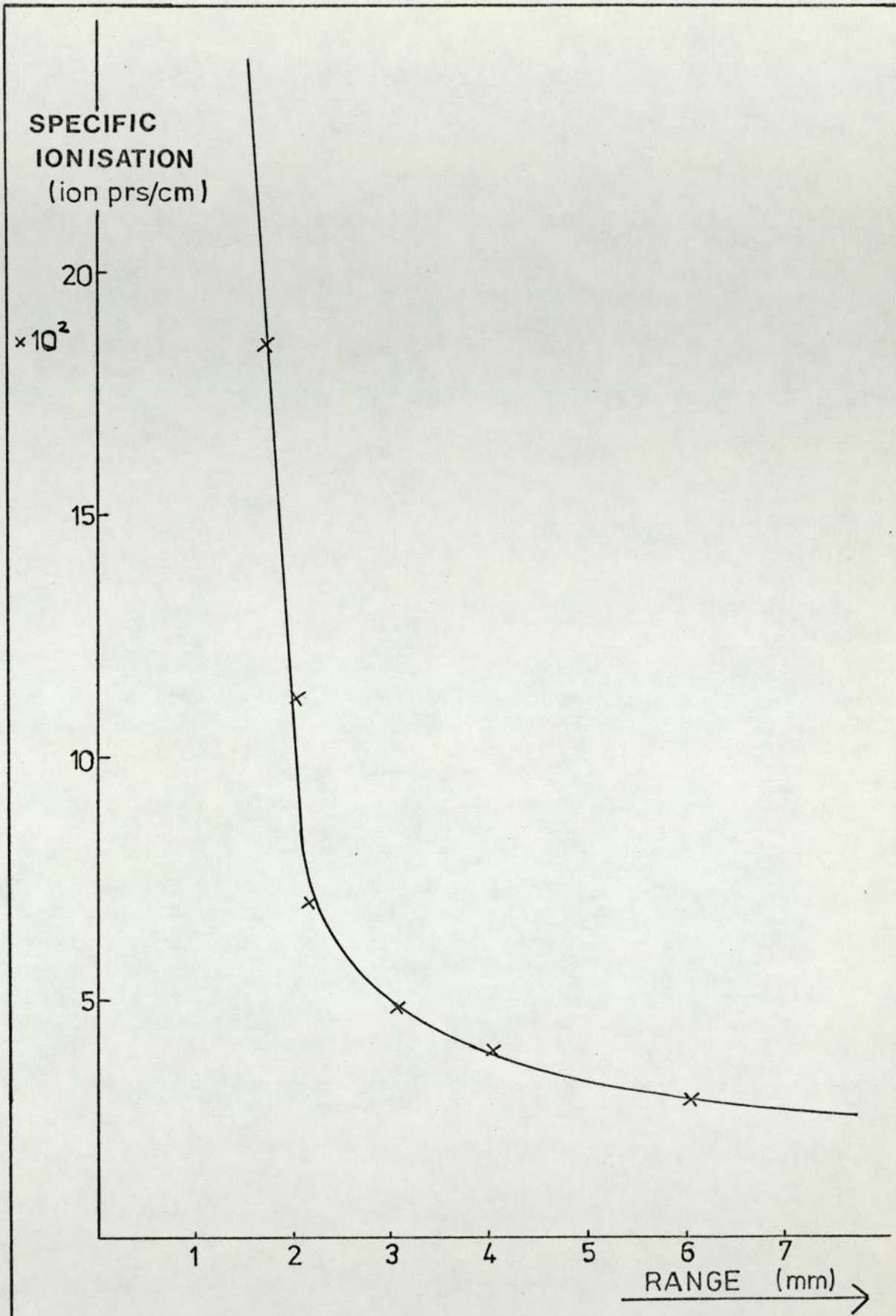

FIG. 14

SPECIFIC IONISATION - RANGE RELATION FOR β^- PARTICLES

tion can be calculated from the foil thickness (x) and the absorption coefficient (m),

$$\frac{R_o}{R} = \frac{1}{mx} \left[\exp (- mx) \right]$$

where R_o and R are the measured and true counting rate respectively. The foil thickness can be estimated as follows :

$$\beta^-\text{s emitted by foil} : (0.15\text{Ci cm}^{-2} \times 3.7 \times 10^{10}\ \text{s}^{-1}$$

$$= 5.55 \times 10^9\ \text{cm}^{-2}\ \text{s}^{-1}$$

The decay rate constant is $(0.6933/3.87 \times 10^8\ \text{s}) = 1.792 \times 10^{-9}$ s^{-1} and hence there are 3.097×10^{18} $\beta^-\ \text{cm}^{-2}$. Assuming one atom of tritium per atom of titanium, the foil thickness is,

$$\frac{3.097 \times 10^{18}}{6.02 \times 10^{23}} \times 50.92\text{g} = 0.26\ \text{mg cm}^{-2}$$

With a typical absorption coefficient of approximately 3.0 $\text{cm}^2\ \text{mg}^{-1}$, this gives a self absorption of 59%. Loss in emitted radiation through self-scattering is likely to be of the same magnitude.

An estimation of the current arising from ionisation of carrier gas molecules can now be made. Assuming that β^- particles emitted from the top 0.13 mg/cm^2 manage to escape, and considering losses through self absorption and scattering, a 150 mCi source is effectively about $0.15 \times 3\ (1/2) = 0.02\ \text{Ci cm}^{-2}$ which corresponds to 7×10^8 β^- particles $\text{cm}^{-2}\ \text{s}^{-1}$. Considering energetic electrons from a tritium source, the number of ion-pairs formed by each β^- particle is about 2.9×10^2. Hence, the number of electrons produced may be calculated to be 2.0×10^{11} electrons per second which corresponds to a current of 3.3×10^{-8} A. The measured current (3.4×10^{-9}) compares well with this, considering the assumptions made.

A radiochemical examination of the tritium foil[51] revealed the presence of two other radioactive species of 0.33 and 0.7 MeV. They were present in neglible amounts and considering their high energy, they could not contribute significantly to the ionisation of carrier gas molecules.

Figures (15) and (16) show the variation in current as a function of electrode spacing. At short separations the β^- particles emitted from the source (on the cathode) hit the anode and are lost through surface recombination. As the spacing is increased, more of them undergo ionising collisions with carrier gas molecules and hence the observed increase in current. However, when the electrode spacing exceeds the maximum range of the β^- particles, electrons formed in the plasma are lost through recombination as they traverse the cell. In the pulse mode of operation at large electrode spacings, the time the pulse is normally applied for (5 μs) is also too short for most of the electrons to be collected. In nitrogen the electron drift velocity is estimated to be 3.0×10^5 cms^{-1} (60). Hence, to travel a distance of 2.50 cm would require 8.33 μs — much longer than the applied pulse duration.

It is generally accepted that the range of β^- particles emitted by a ^{63}Ni source is about 8 - 9 mm. at NTP and this is borne out by Fig. (16). However, the results obtained with the ^{3}H source do not support the normally assumed value of about 2.5 mm. The maximumappears at about 6.5 mm. which is in agreement with the calculated maximum range of β^- particles from a tritium source. The result points towards a much larger reaction zone in ECD's equipped with this source.

Varying electrode separation while operating the cell in the d.c. mode (Fig. 17) also supports the above conclusion. The current reaches its peak value at about 6.0 mm. The graph also shows that at high field strength (40 Volts cm^{-1}) and flow, the

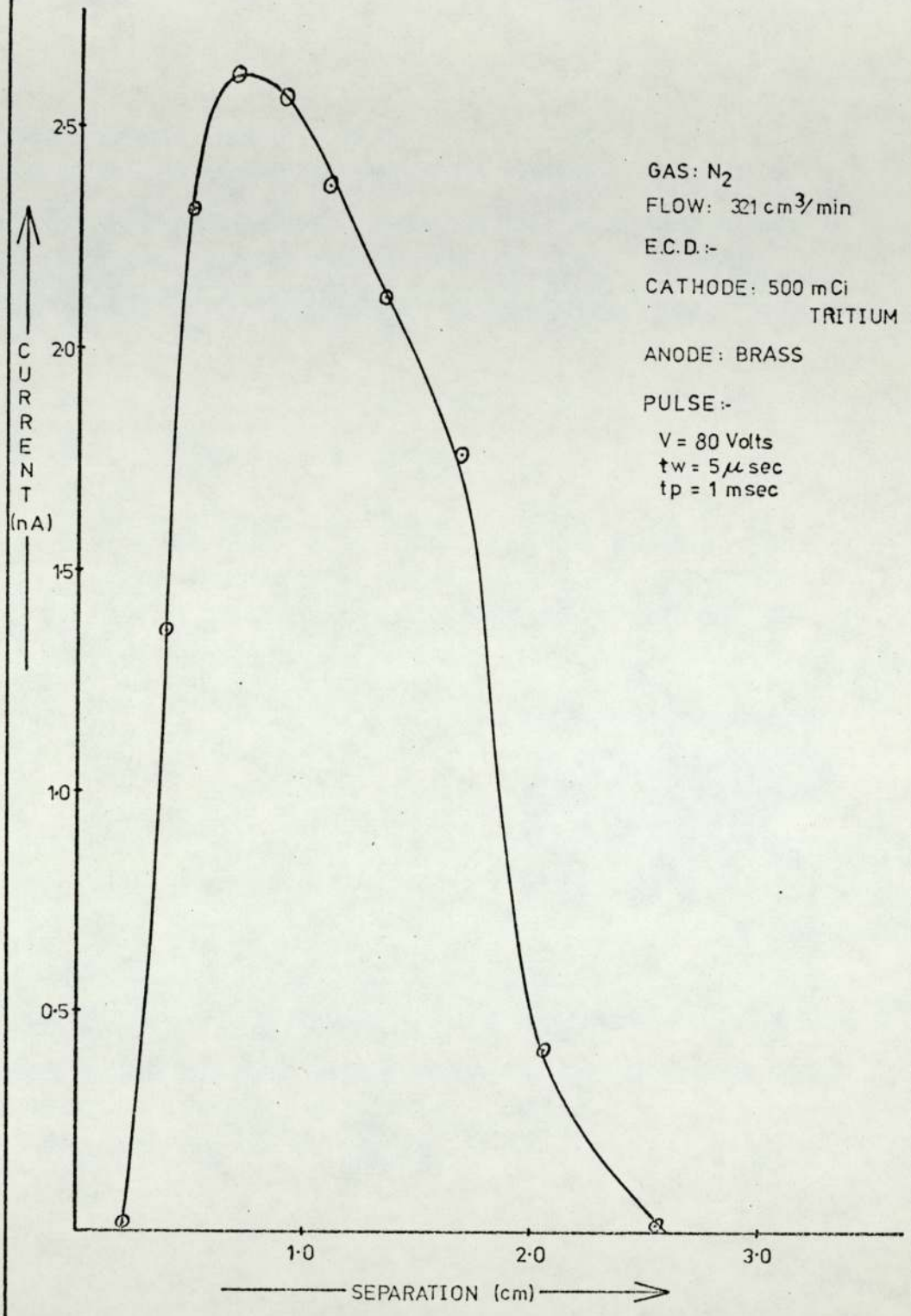

FIG. 15

CURRENT AT VARIOUS ELECTRODE SPACINGS
(SOURCE: ^3H)

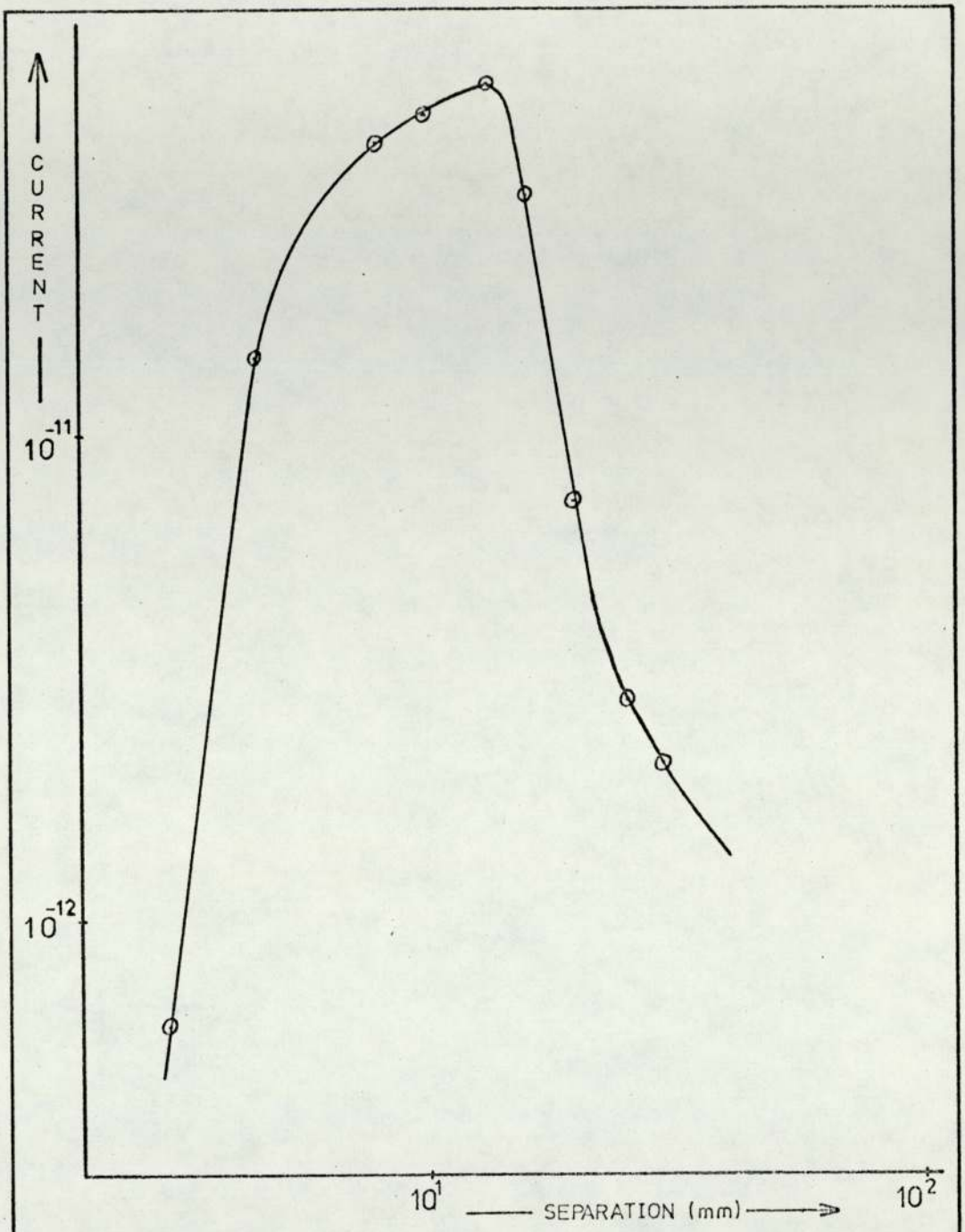

PULSE CONDITIONS:-

V = 90 Volts
tw = 5μsec
tp = 1 ms

GAS: N_2
FLOW: 135 (228 cm^3/min)
E.C.D. :-
CATHODE: 0.5mCi Ni^{63}
ANODE: BRASS

FIG. 16

CURRENT AT VARIOUS ELECTRODE SPACINGS (SOURCE: ^{63}Ni)

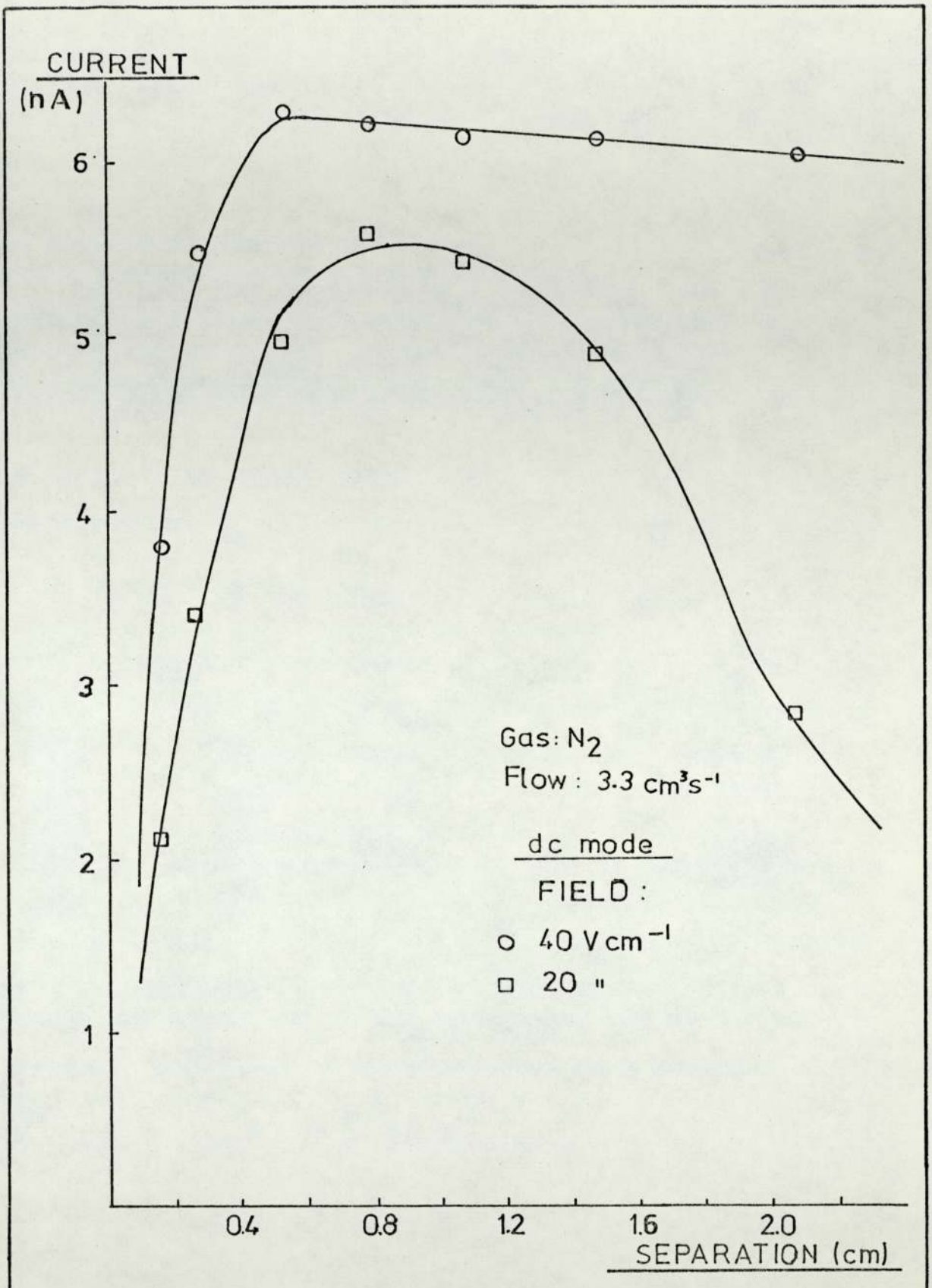

FIG. 17

CURRENT - ELECTRODE SEPARATION RELATION FOR d.c. MODE

current decreases very gradually with increasing separation indicating that almost all charged particles present in the cell are being collected at the electrodes. However, at low field strength (20 Volts cm^{-1}) the decrease in current is very steep, similar to that observed under the pulsed mode. As recombination seems to be the dominant process of loss under these conditions, an attempt was made to calculate the electron-ion recombination coefficient.

As a first approximation, the time rate of change of electron concentration is

$$\frac{de}{dt} = -ke^2$$

assuming that the electron and positive ion concentrations are equal. The solution of the above equation is

$$\frac{1}{e} = kt + \frac{1}{e_o}$$

where e_o is the initial concentration of ion-pairs. At a field strength of 20 Volts cm^{-1}, the electron drift velocity is 2.25×10^5 cms^{-1}. Hence, the time taken to cross the cell at various cell distances can be calculated. Fig. (18) shows the variation of the inverse of the current with time. The slope of the graph is 5.49×10^{13} A^{-1} s^{-1}, and the recombination coefficient for nitrogen is then 1.62×10^{-5} cm^3 s^{-1} which is about an order of magnitude too large. This is to be expected considering the simplifications and assumptions made.

Another approach explaining the decrease in current with increasing separation can be based on the consideration of Eq.(20) (without the negative ion term) at steady state.

$$V\frac{de}{dt} = k_1 AG - k_2 Vep - Fe.e = 0$$

The electron concentration is,

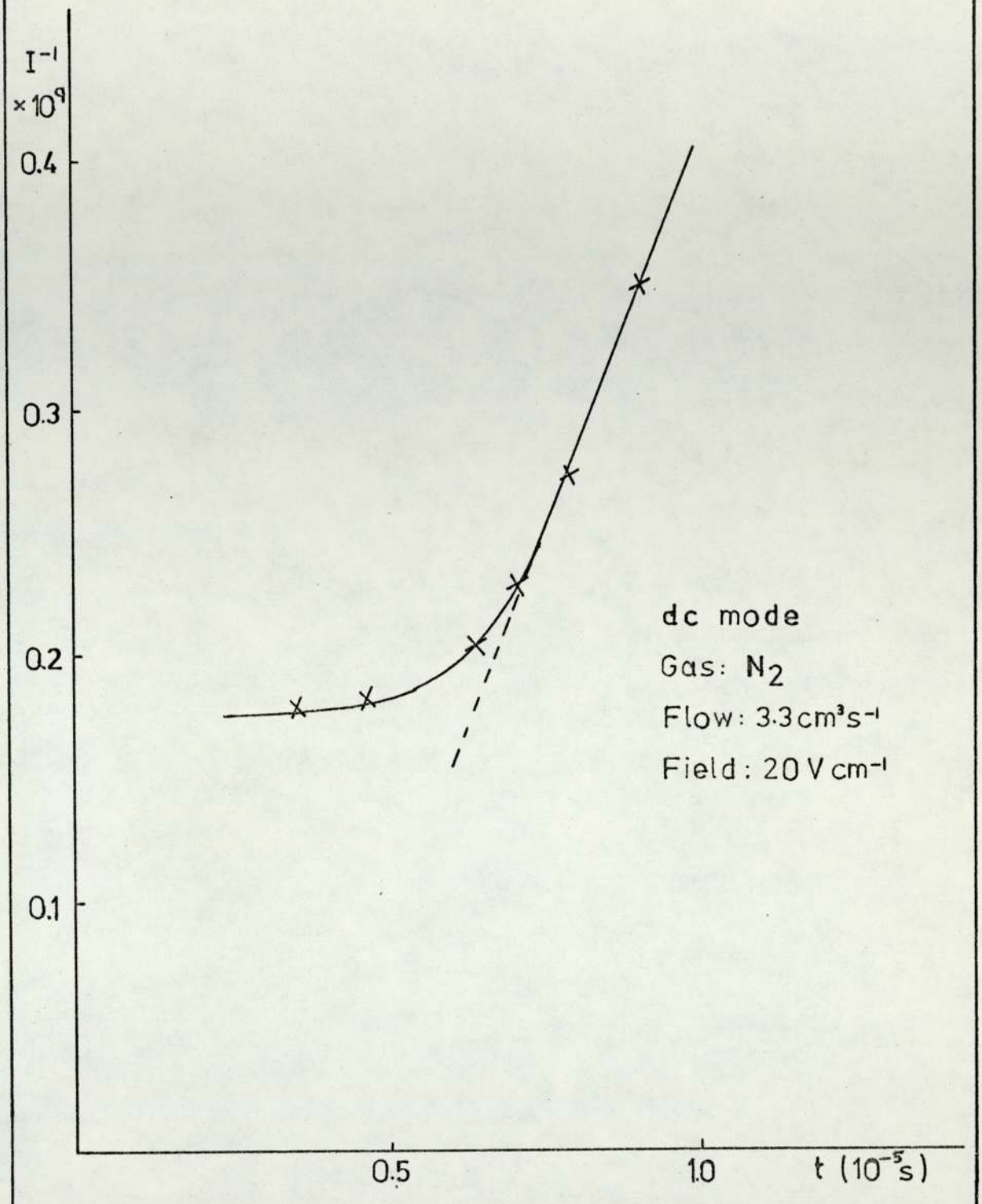

FIG. 18

THE INVERSE OF CURRENT VERSUS ELECTRON TRANSIT TIME

$$e = \frac{k_1 G}{(k_2 lp + Fe/A}$$

where l is the inter-electrode separation. Assuming an order of magnitude value for p ($\simeq 10^9$), the value of e at l = 1.8 cm. is 2.22×10^6 cm^{-3} which gives a current of 0.36 nA. This compares well with the experimental value of 0.72 nA, considering the approximate value of p.

Since the density of the medium has an effect on the range of the β^- particles, electrode spacing studies were carried out at constant pressure using various carrier gases. The density decreases in the following order :

$$Ar > Ar + CH_4 > C_2H_4 > N_2 > He$$

Fig. (19) compares the range of β^- particles in Ar + 5% CH_4 and He. The former has a density ($\simeq 0.1786$ gl^{-1}) which is about ten times greater than that of the latter. The graph shows that in helium the current reaches its peak value at about 1.25 cm. while in Ar + CH_4, the corresponding separation is about 0.6 cm. The behaviour is as expected and it appears that a ten fold increase in density of carrier gas corresponds to a reduction in range of β^- particles by one half.

As stated earlier, when the radiation source is considered on its own, a large number of ion-pairs form in close vicinity of the source. However, as part of the detector, it appears that most ion-pairs are formed some distance away from the source, indicating that high energy β^- particles are responsible for ionisation of carrier gas molecules. Scolnick[46] arrived at a similar conclusion.

Emission of bremsstrahlung radiation by the β^- particles has been suggested to be partly responsible for ionisation. The radiation in question arises from the acceleration of an electron

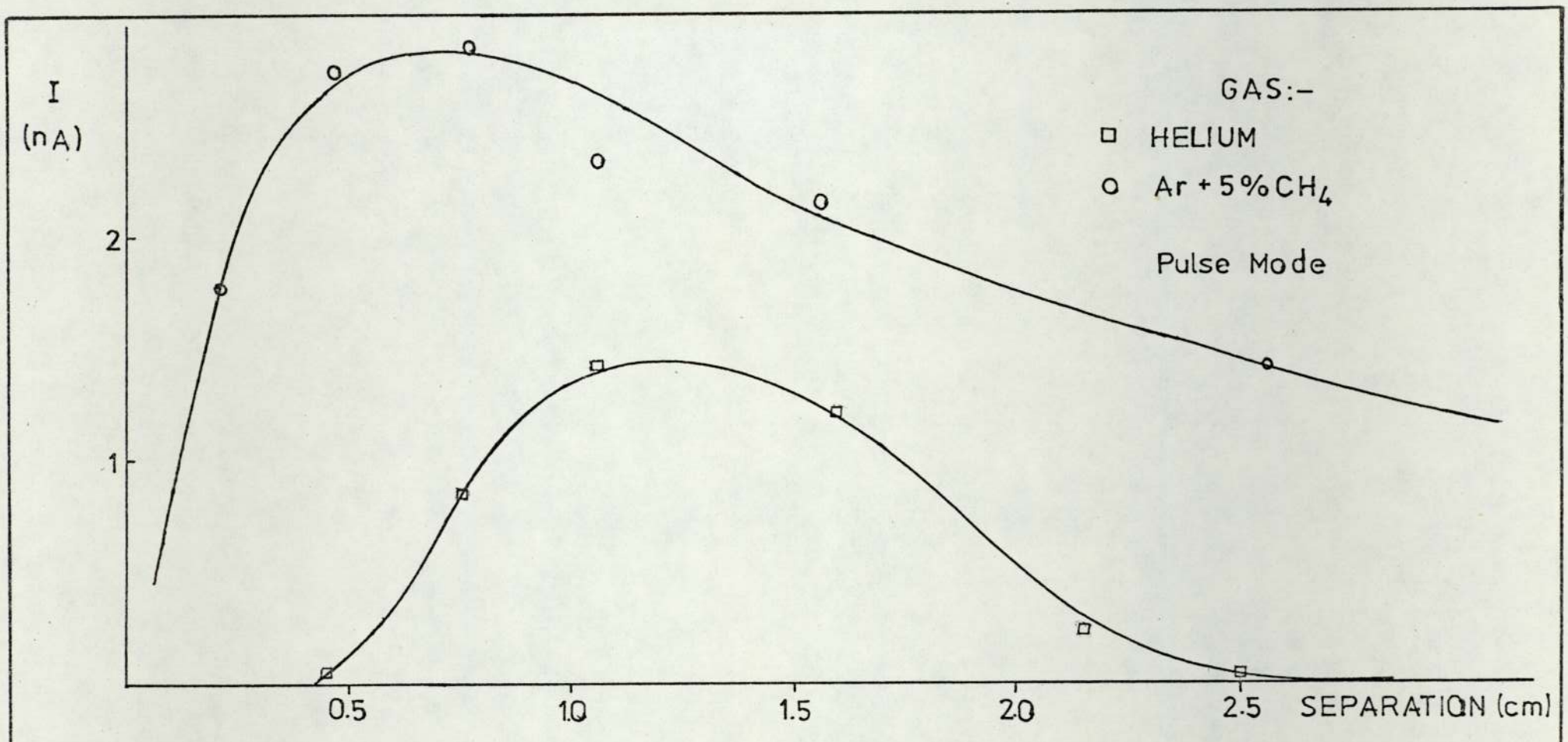

FIG. 19

CURRENT - SEPARATION PLOTS FOR **He** AND **Ar** + CH_4

by an atomic or ionic field. The ratio of energy loss by bremsstrahlung radiation to energy loss by ionisation in an element of atomic number Z is approximately equal to EZ/800, where E is the electron energy in MeV.[15] In the case of nitrogen, this energy loss is 0.016% for β^- particles from ^3H source and 0.058% for ^{63}Ni source. Ionisation arising from bremsstrahlung radiation appears to be unimportant for the sources normally used.

The effect on current flow in an assymmetrical cell was investigated. One electrode in turn was fixed very close to the gas inlet and the separation was varied by changing the position of the other. There was no significant difference between the two (Figs. 20 and 21) except for a slightly higher current for the case where the cathode was fixed. The effect of flow on the plasma may be responsible for this observation.

In comparison to the symmetrical cell, the plasma seems to be more diffused in both cases of the assymmetrical cell. In the latter configuration the current is either increasing or at its plateau value until the separation is about 1.4 cm; this is unlike the former configuration where the current is on the decline only after about 0.7 cm. The vortices in the flow pattern could enhance diffusion of the plasma contained in the assymmetric chamber since the electrode fixed close to the gas inlet behaves as a reflecting surface.

Two ^3H sources of different activities and of almost the same area were investigated. The activities were approximately 150 and 500 mCi. Assuming that the two foils had similar characteristics, such as the presence of other radiation sources, the theoretical ratio of their activities is 3.33. Currents measured for the two sources, under both the d.c. and pulsed modes, are given in Table 3. At long pulse interval the mean ratio of currents measured under similar conditions for the two sources is 2.84 while

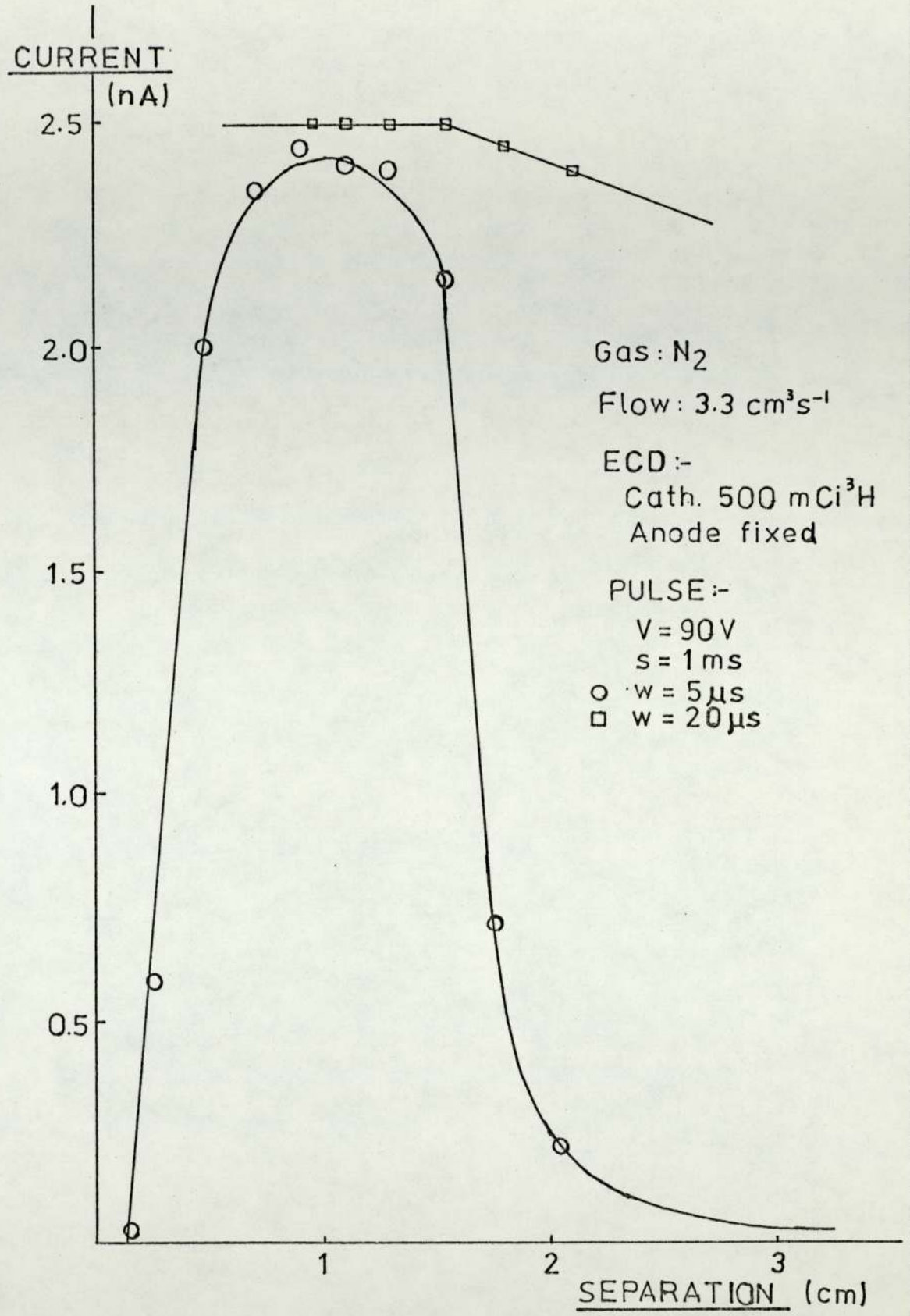

FIG. 20

CURRENT VARIATION IN AN ASSYMMETRICAL CELL - ANODE FIXED

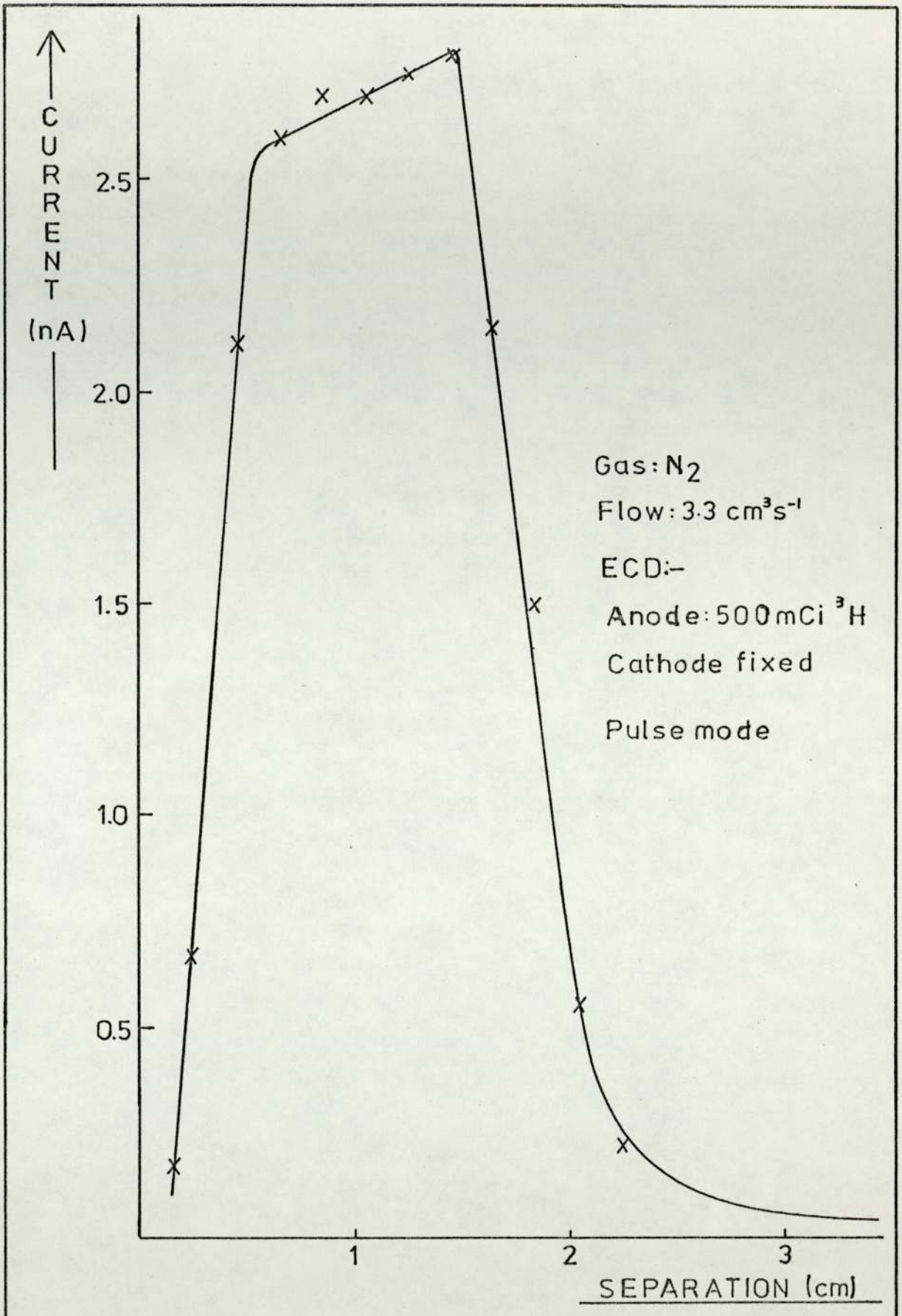

FIG. 21

CURRENT VARIATION IN AN ASSYMMETRICAL CELL - CATHODE FIXED

TABLE 3

COMPARISION OF CURRENTS FROM ^{3}H SOURCES OF DIFFERENT ACTIVITIES

gas : N_2 ECD :- Pulse:

Flow: 3.2 cm^3 s^{-1} Anode: Brass V = 90 Volts

Separation: 1.0cm. W = 5 μ s

SOURCE ^{3}H	d.c. SATURATION CURRENT I	PULSE INTERVAL, S					
		50μs	100 μ s	250 μ s	1 ms	1.5 ms	2.0 ms
500 mCi	6.50 nA	6.10nA	5.85nA	5.0 nA	2.40nA	1.65nA	0.87nA
150 mCi	3.40 nA	3.33nA	3.15nA	2.55nA	0.82nA	0.59nA	0.31nA
I0.5/0.15	1.91	1.85	1.86	1.96	2.93	2.80	2.81

short pulse interval and under the d.c. mode, the ratio is 1.90. Considering that the two activities are not precisely known (especially the lower one) it seems reasonable to conclude that the current at long pulse interval varies by the same ratio as that of the activities of the sources. However, at short pulse interval, the current ratio of the two foils is about one half of the theoretical ratio. Space charge effects may be responsible for the observed difference in the mean ratios. At short pulse periods, for the current ratio to be close to the theoretical, the 500 mCi currents need to be much higher. However, this in practice is not possible as relatively denser space charge exists since loss through recombination is minimal under these pulse conditions.

Comparison of detector currents arising from sources providing β^- particles of different energies is much more difficult as sources tend to have different activities as well. Considering a 500 mCi ^{3}H source and a 0.5 mCi ^{63}Ni source, the average current ratio was found to beabout ten times larger than the ratio of their energies, ie.

$$^{63}Ni\ /\ ^{3}H = 67\ KeV/18.6\ KeV = 3.60$$

Other sources which have recently come into use are ^{90}Sr, ^{147}Pm and ^{241}Am. Alternative sources are necessary mainly because of the need to work at higher detector temperatures. The generally acceptable temperature limit for the ^{3}H source is 225°C while that for the ^{63}Ni source is 350°C. Detectors equipped with ^{147}Pm can be heated to 400°C [52] and the maximum operating temperature for ^{241}Am is 500°C.[53] At elevated temperatures a considerable loss in activity results and this leads to large variations in day-to-day standing currents. The emanation of radio-active material into the atmosphere of the room however, is a more serious consequence. A low level contamination of the environment (constituting a health

hazard) occurs with ^{3}H sources when the detector temperature exceeds 230°C.[54] A comprehensive study of possible radiation hazards arising from radioactive sources in ECDs has been made by Taylor.[55]

In normal operation, the radiation source is placed on the cathode and hence the electrons present in the plasma are drawn across the cell to the anode. Their greater mobility ($\simeq 10^{3} cm^{2} V^{-1} s^{-1}$) ensures that a relatively small applied voltage (about 25 Volts) gives saturation current. However, when the polarity of the cell is reversed, a considerably larger voltage is necessary for current saturation (Fig. 22). This is to be expected as the heavier positive ions with their lower mobility ($\simeq 2.5 cm^{2} V^{-1} s^{-1}$) need to be drawn across the cell to the cathode. The β^{-} particles from the source on the anode recoil to the source forming few ion-pairs. Fig. (23) shows the current variation with inter-electrode separation. Maximum current is observed at very small spacing since β^{-} particles of average energy have been shown to have a range of about 2mm. The current gradually decreases until a separation of about 6 mm, corresponding to the distance travelled by particles of maximum energy. Thereafter, the current declines steeply as ion-pairs are no longer generated and also losses through recombination are considerable. The initial decrease in current substantiates the explanation given (that ionisation zone extends to about 6 mm. from the source) for the increase in current observed when the source is on the cathode (Fig. 17).

4.6 PRESSURE AND FLOW RATE OF CARRIER GAS

Since the range of β^{-} particles depends on the number of molecules in their path, a shorter range is to be expected at higher pressures. The plasma volume would consequently decline. Figs. (24) and (25) show the current variation at pressures below and above atmospheric. The term G, the ion pair yield, is potentially

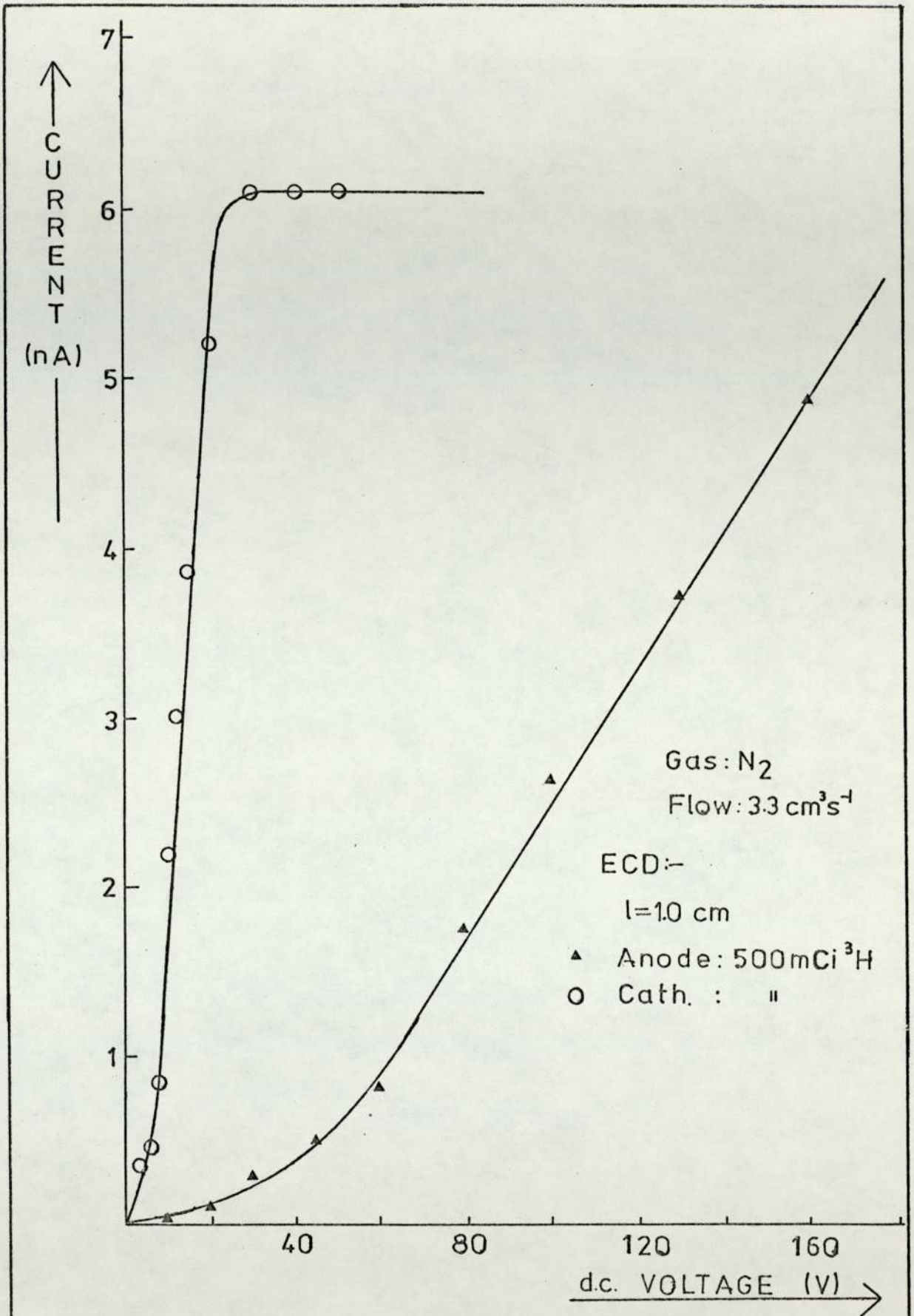

FIG. 22

THE EFFECT OF REVERSAL OF CELL POLARITY-SOURCE ON ANODE

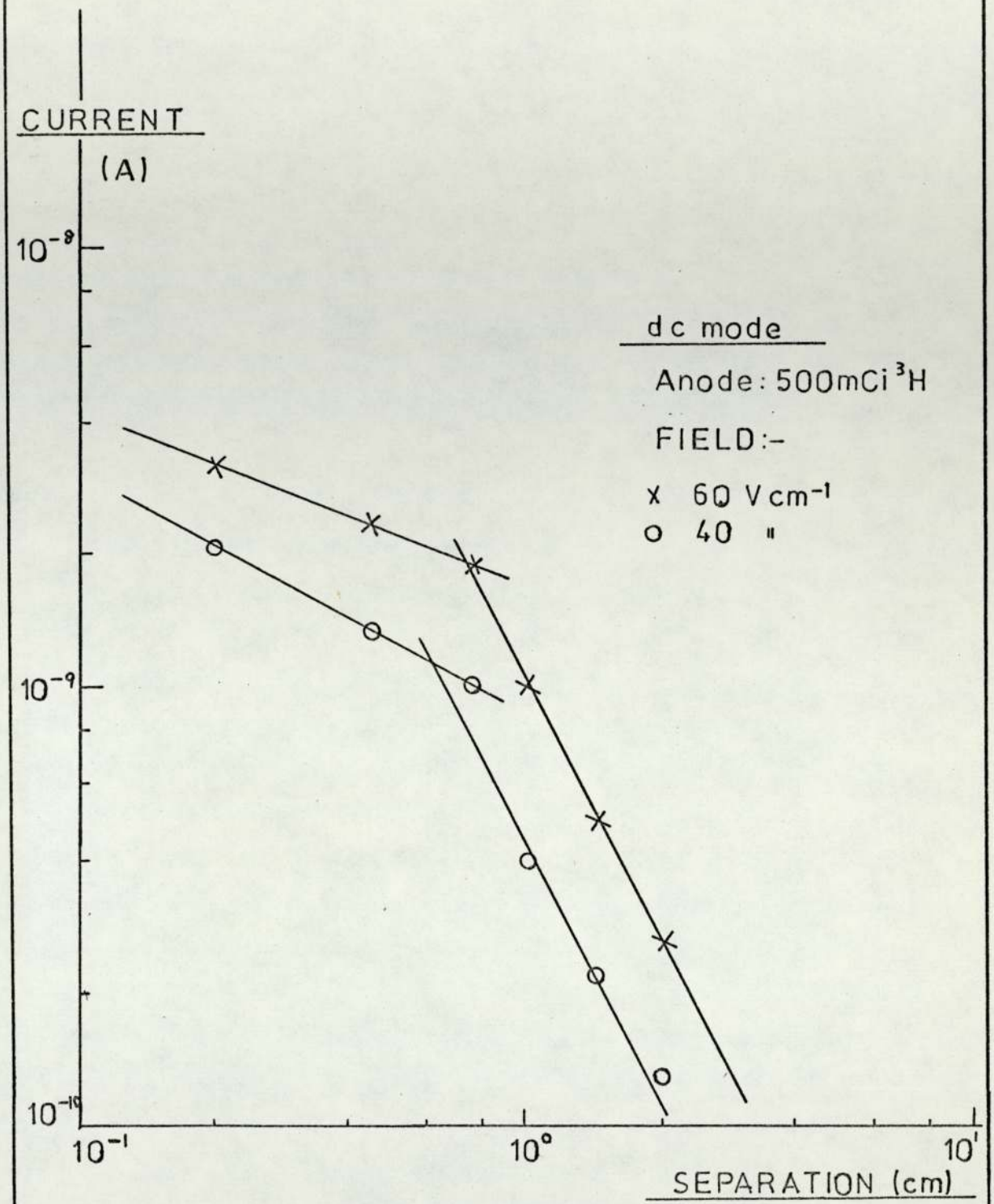

FIG. 23

CURRENT VARIATION WITH INTER-ELECTRODE SEPARATION - SOURCE ON ANODE

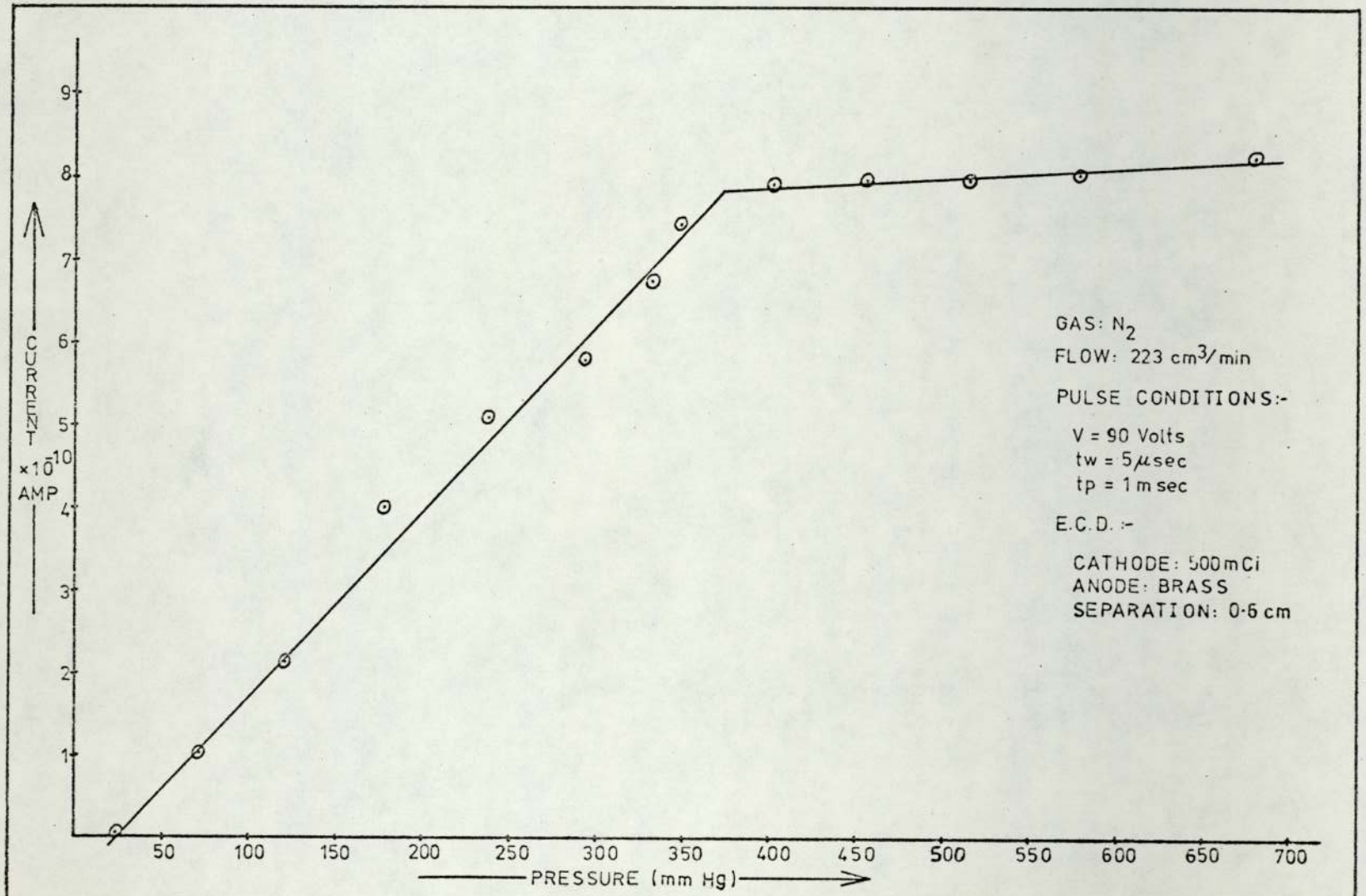

FIG. 24

CURRENT VARIATION WITH GAS PRESSURE (BELOW ATMOSPHERIC)

FIG. 25

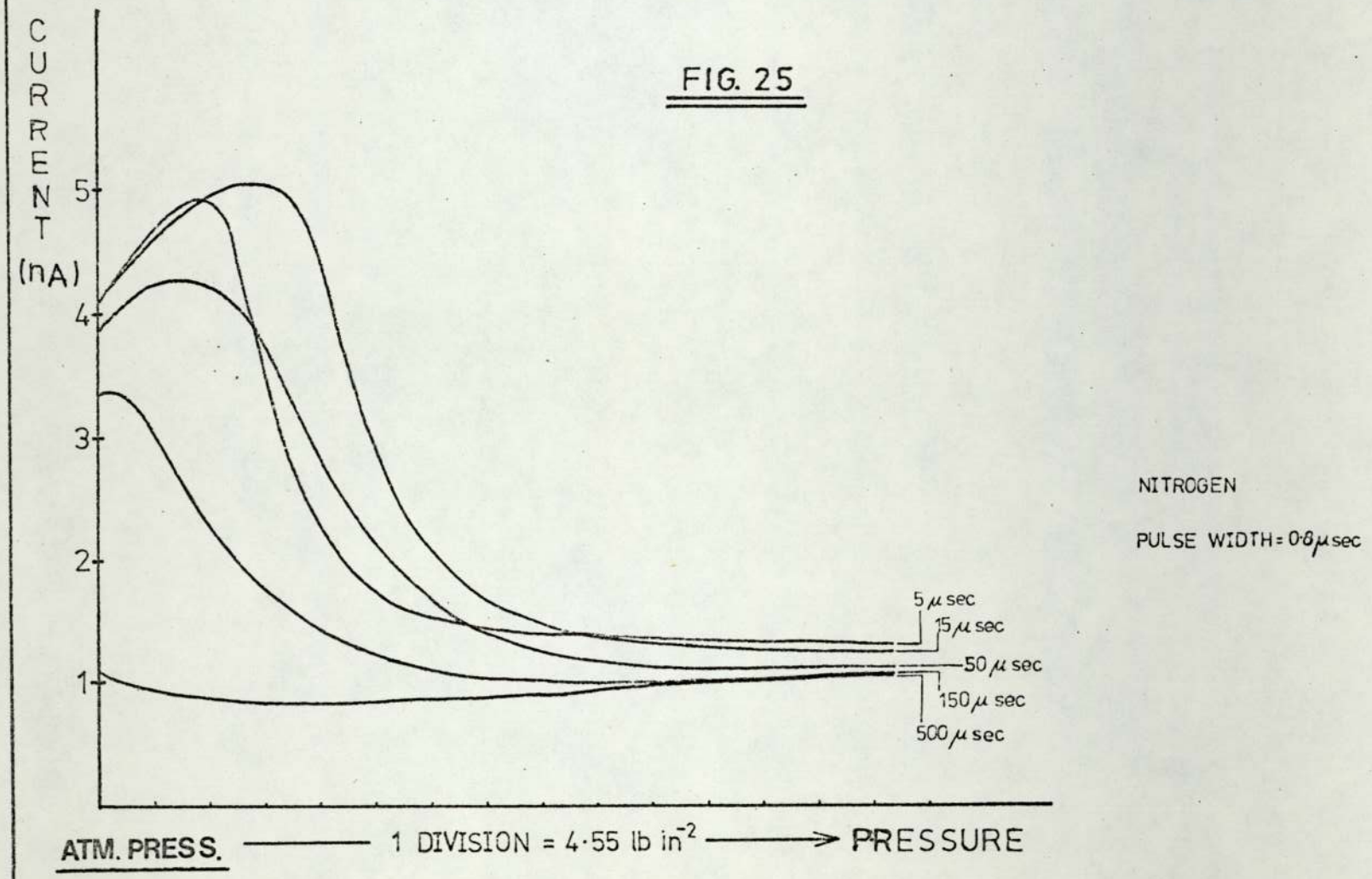

CURRENT VARIATION WITH GAS PRESSURE (ABOVE ATMOSPHERIC)

pressure dependent. The number of ion pairs formed, is equal to the product of the number of ion pairs per unit length and the path length. While the path (whose length is inversely proportional to the pressure) lies within the cell, this product is constant, but when the path length exceeds the inter-electrode spacing, the number of pairs will fall.

In terms of the proposed model,

$$a = be = e\,(k_2\, V p_o + Fe)$$

or $$\frac{a}{eV} = k_2\ p_o + \frac{Fe}{V}$$

If Fe/V is small and $p_o = eR$, then

$$e = \left(\frac{a}{k_2\, V\, R}\right)^{1/2}$$

The observed current, I, is to a close approximation, eV electrons per pulse. Hence,

$$I = V\left(\frac{a}{k_2\, V\, R}\right)^{1/2} = \left(\frac{k_1\, A\, G\, V}{k_2\, R}\right)^{1/2} \qquad [39]$$

The 'Gaines' factor, R depends partly on the relative drift velocities of electrons and positive ions and hence is a function of (X / P) where X is the applied field and P is the pressure. Since R is inversely proportional to the pressure and the volume of the plasma varies in a similar way, the current I, in accordance with Eq. [39], should be independent of the pressure as long as the path length is within the cell (ie. G is constant). This is the case at large pressures and the current is very nearly constant as shown in Fig. (24). At lower pressures, where G is proportional to the pressure, the current does exhibit a linear increase with pressure.

Changing electrode spacing at various pressures below atmospheric (Fig. 26) show that the range of β^- particles is considerably extended; for the tritium source, the range of particles

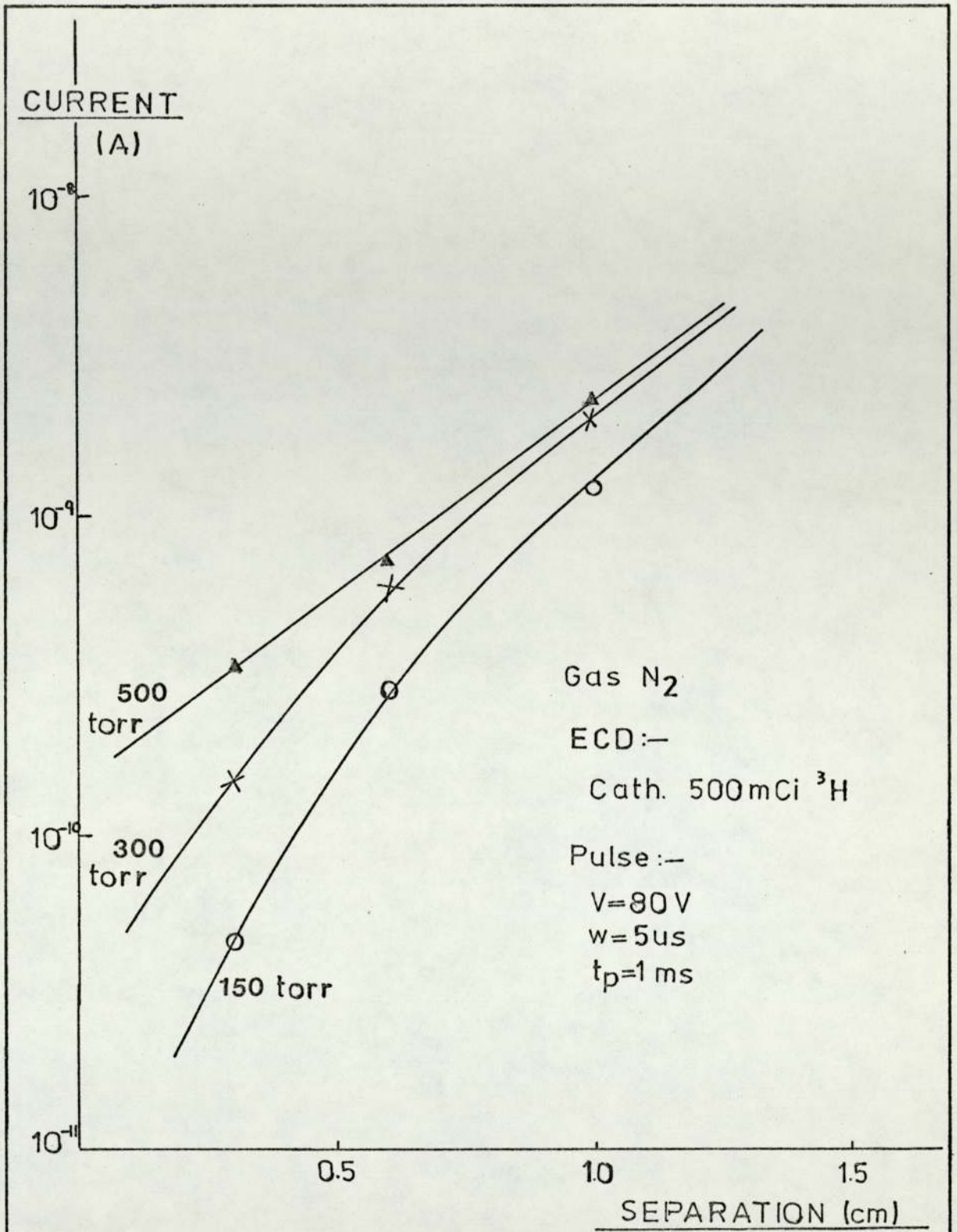

FIG. 26

CURRENT - CELL LENGTH RELATION AT VARIOUS PRESSURES

with high energy is greater than 1.0 cm even at pressures of about 500 mm Hg. Since studies were confined to a maximum cell length of 1.0 cm, it is not possible to determine exactly the dimension of the plasma at various pressures.

At pressures above atmospheric[56] the current declines steeply with increasing pressure. The high density of neutral molecules hinders collection of charges and also enhances volume recombination. Plotting the pulse interval against the magnitude of the pressure corresponding to the maximum current (Fig. 27) suggests that at atmospheric pressure, high electron concentrations (for coulometric response) are obtainable at long pulse periods (about 0.5 ms).

The effect of carrier gas flow rate on the response of the ECD has generated considerable controversy. As stated earlier, any detector whose response is concentration dependent would be affected by gas flow but only in the presence of sample molecules or varying pressure. However, in the ECD, the presence of a large excess of positive ions and the detector's extreme sensitivity has complicated the situation. Devaux and Guiochon[57] noted a decrease in standing current with decreasing flow rate. Burdett[32] concluded similarly. However, Lovelock[58] and Tommassen[59] have both found that the two parameters are not related in the pure carrier gas. Aue and Kapila[7] rightly pointed out there exists much confusion in the literature on this issue.

The present studies show that when the usual precautions are taken (as stated in 4.2) to obtain a 'clean' carrier gas in the normal ECD set up, there is a dependency on flow but only at very low flow rates. This was found to be the case in two different E.C. systems using metal and nylon tubing respectively. The variation in current was observed under both the d.c. (Fig. 28) and pulsed

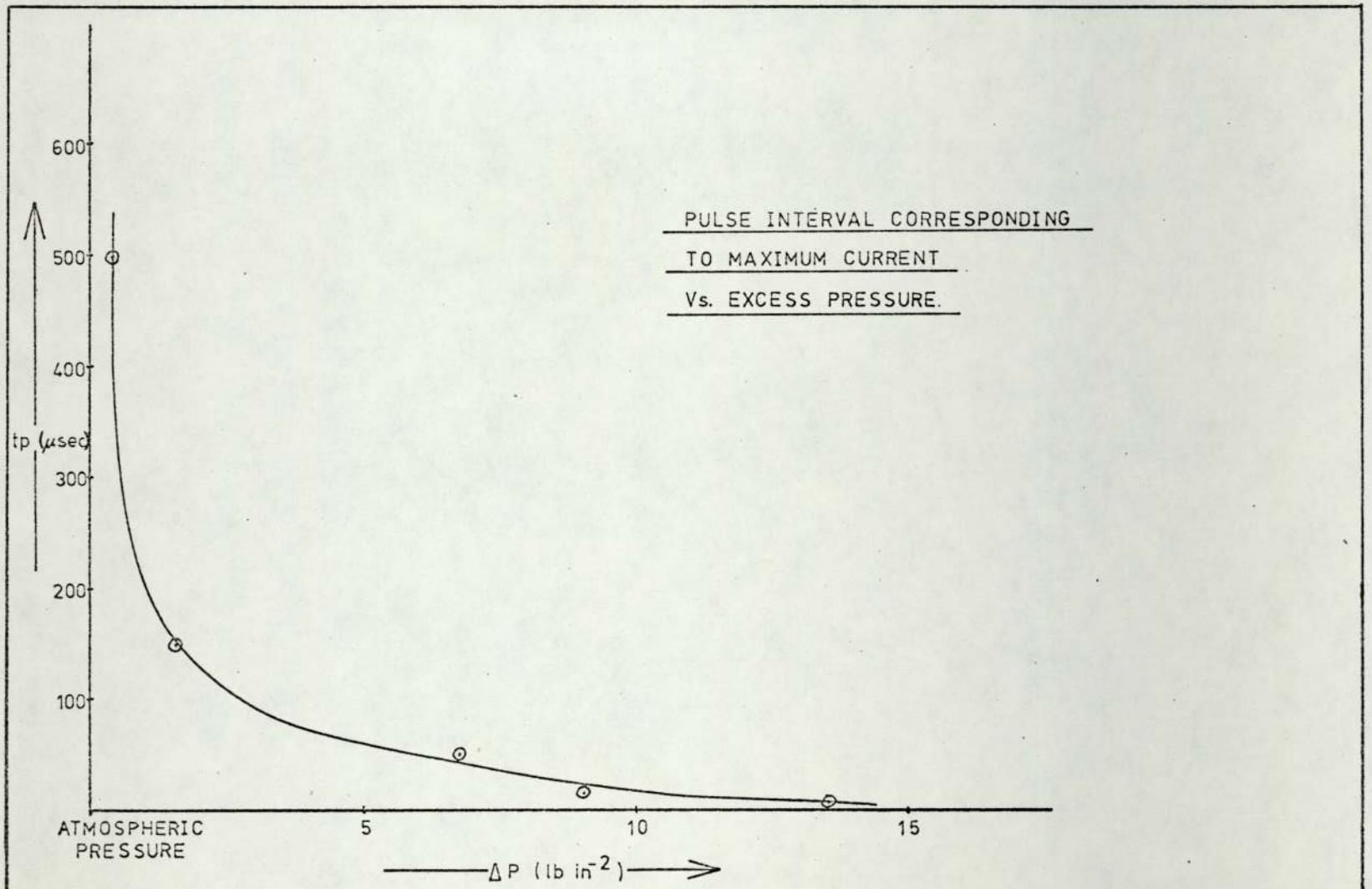
PULSE INTERVAL CORRESPONDING
TO MAXIMUM CURRENT
Vs. EXCESS PRESSURE.
600
500
400
300
200
100
tp (μsec)
ATMOSPHERIC
PRESSURE
5
10
15
ΔP (lb in⁻²)

FIG. 27

modes (Fig. 29) of operation. It is clear from these two graphs, that G.C. operators could have either observed a dependency on flow or not depending on the particular conditions under which results were obtained. In the continuous d.c. mode, the effect of flow is more apparent at lower voltages than at and above the critical voltage giving saturation current. In the pulsed mode, flow has a negligible effect on the standing current at shorter pulse interval and is magnified as the pulse period becomes longer. However, it seems that over a considerable range, above 20 cm^3 min^{-1}, there is almost no dependency, irrespective of the magnitude of the pulse interval. Similar results were obtained with 95% argon + 5% CH_4 as carrier gas (Fig. 30).

The presence of electron capturing contaminants in the carrier gas stream, whether originating from the gas itself or diffusing through the tubing and various joints, has been held responsible for the observed variation in standing current with gas flow rate.(59)

An analysis of the effects of a capturing impurity is briefly presented. Two possible situations could arise :

1) The concentration of the contaminant is constant, Co, and is entering the cell at the same flow rate as the carrier gas (U). This would be the case if it is present in the gas supply. At steady state,

Rate of entry of impurity = Co U/V

Rate of outflow = Co U/V

Rate of formation of negative ions = kC e

where k is the capture coefficient and e is the electron concentration in the cell.

Hence, $Co = C\,(1 + kVe / U)$

The rate of loss of electrons = $kCe = \frac{k\,Co\,e}{1 + (kVe/U)}$ [40]

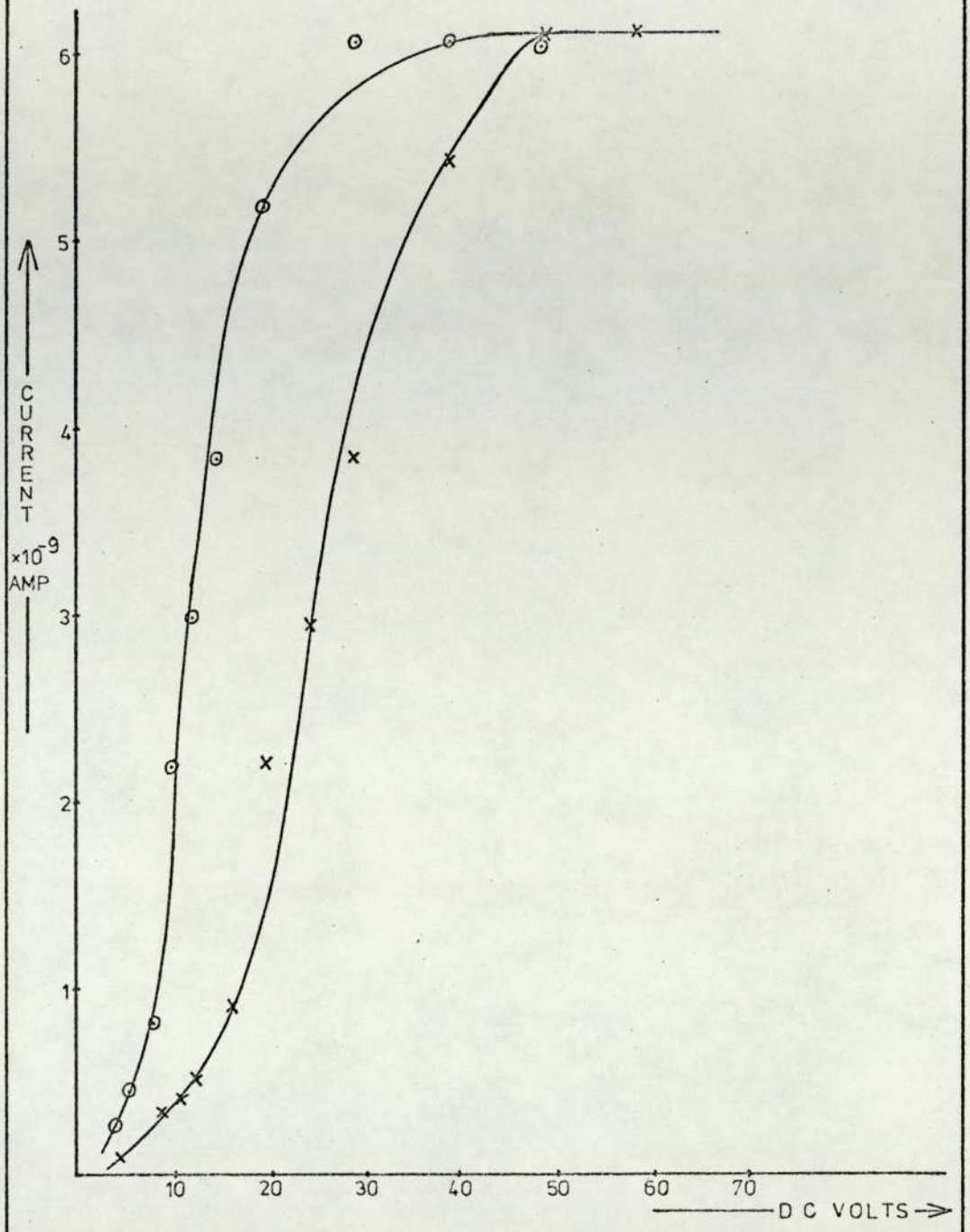

GAS: N_2

FLOW:-

× 6 cm^3/min

⊙ 230 cm^3/min

E.C.D. :-

CATHODE: 500 mCi TRITIUM

ANODE: BRASS

SEPARATION: 1·05 cm

FIG. 28

THE EFFECT OF CARRIER GAS (N_2) FLOW ON CURRENT IN d.c. MODE

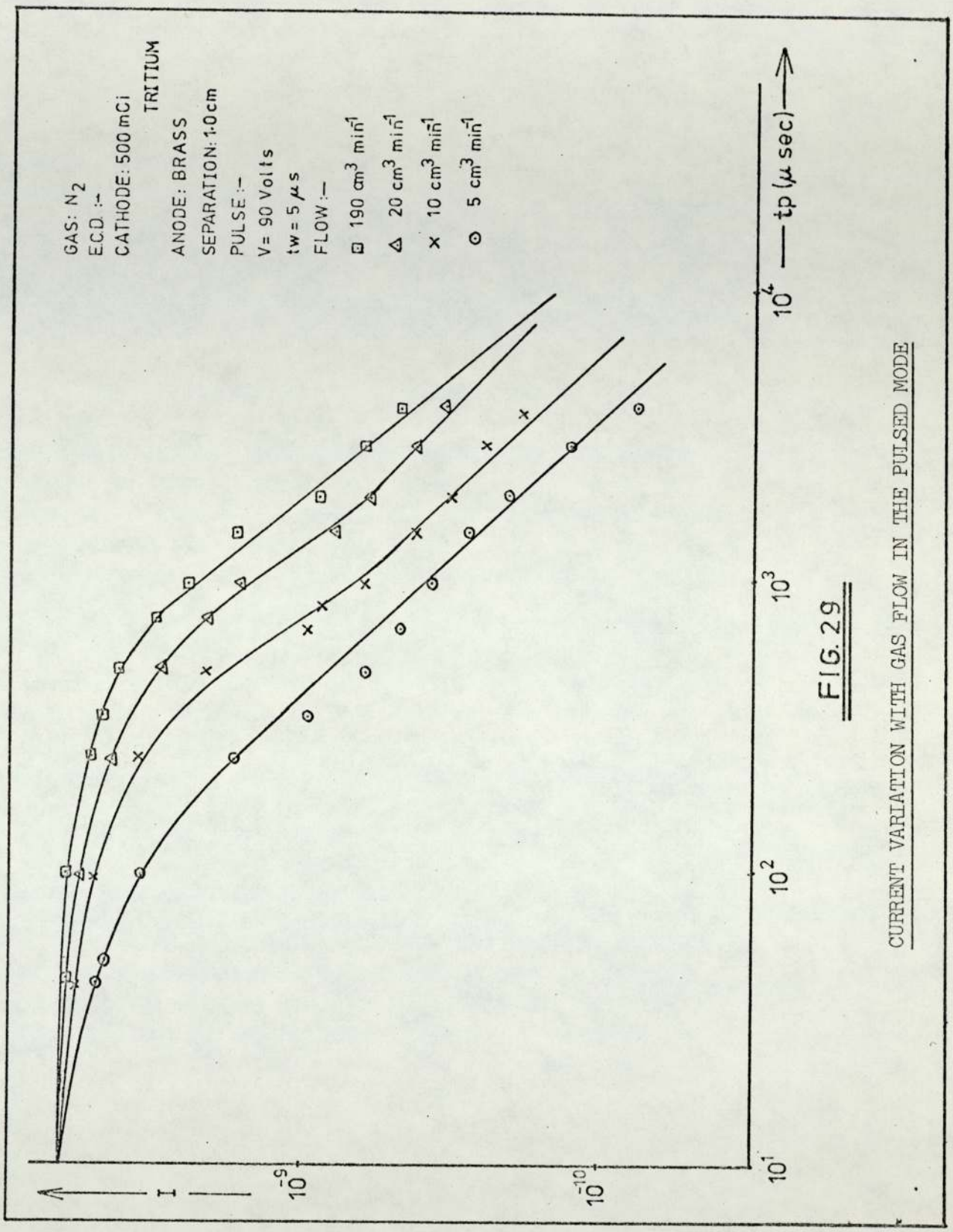

FIG. 29

CURRENT VARIATION WITH GAS FLOW IN THE PULSED MODE

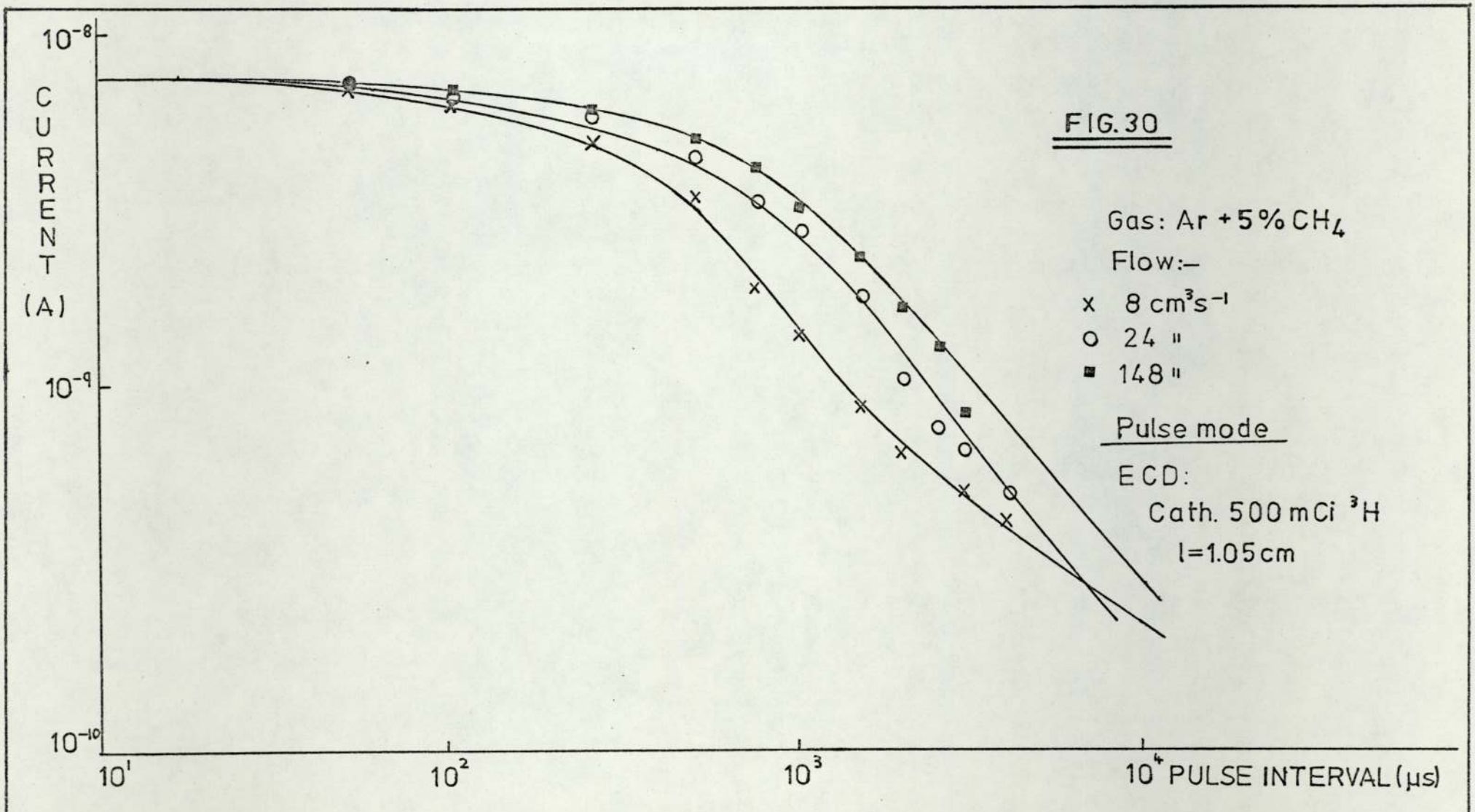

CURRENT VARIATION WITH GAS (Ar + CH_4) FLOW

which increases as U increases (as a first approximation) and consequently the standing current decreases. However, in practice the current is found to increase with carrier gas flow rate.

2. The contaminant is diffusing, bleeding or leaking into the carrier gas stream at some constant rate, Q, independent of the gas flow rate. Similar rate terms to those presented in case one can now be considered.

Rate of entry of impurity = Co Ux/V where Ux is the rate of flow of impurity.

Rate of outflow = C (Ux + U) /V

At steady state,

$Ux \cdot Co = k\,VCe + C\,(Ux + U)$

Hence,

$$C = \frac{Ux\ Co}{k\,Ve + (Ux + U)} \qquad [41]$$

Eq. [41] predicts that as the flow rate of carrier gas increases, the concentration of the impurity in the cell decreases and thus accounting for the observed increase in standing current.

Readings taken with a gas line suspected of leakage showed considerable dependency on flow as shown in Fig. (31). The difference between the asymptotic current value (Io) and that at a lower flow rate (I) is proportional to C in Eq. [41]. A linear relationship between $(Io - I)^{-1}$ and U is predicted by that equation. Fig. (32) shows that this is the case. As the gas line is made increasingly contaminant free, the slope becomes steeper and this parameter can be regarded as a measure of the concentration of impurity in the cell.

The earlier explanation for the variation of standing current with carrier gas flow was the dispersion and eventual removal of

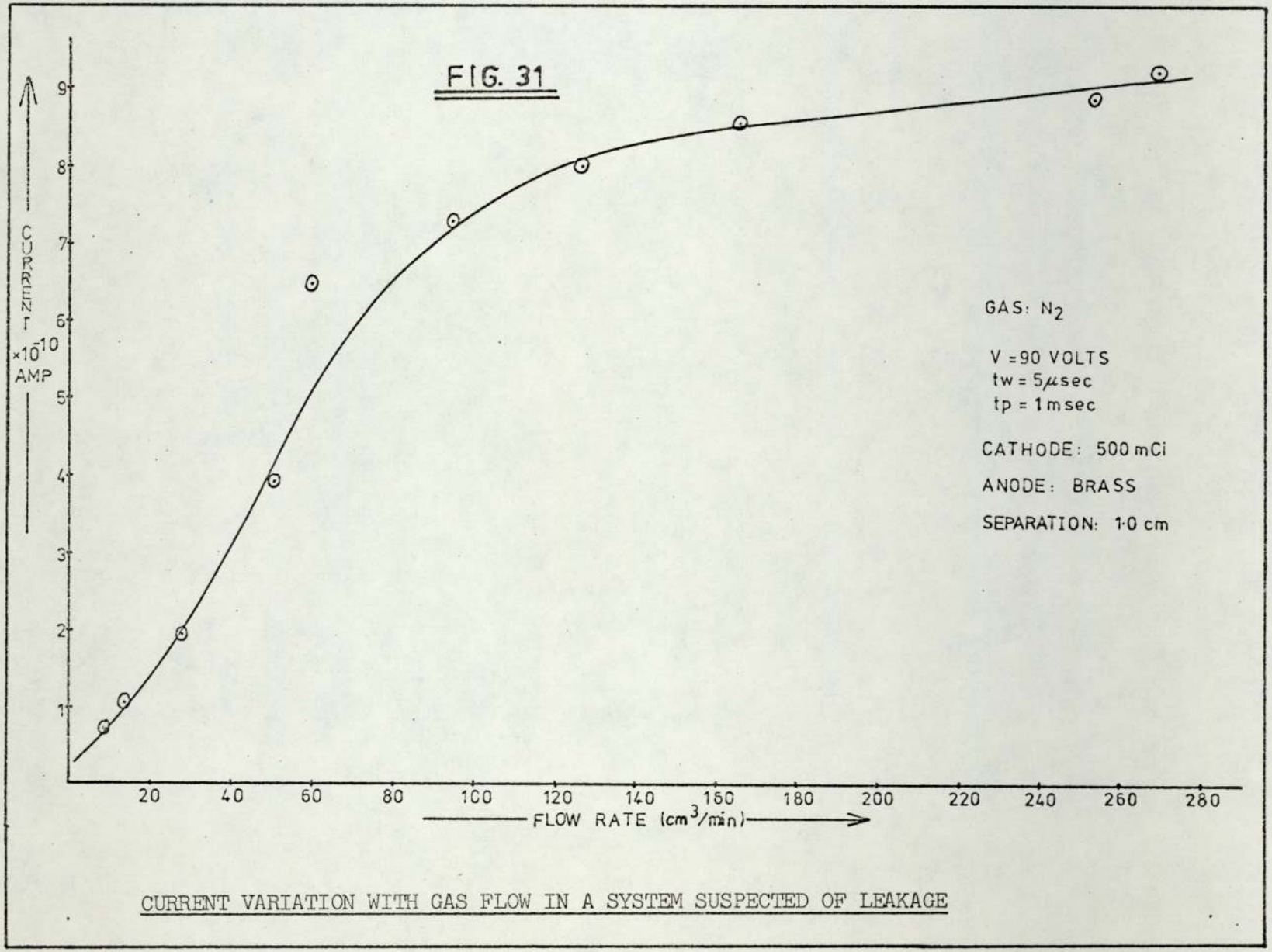

CURRENT VARIATION WITH GAS FLOW IN A SYSTEM SUSPECTED OF LEAKAGE

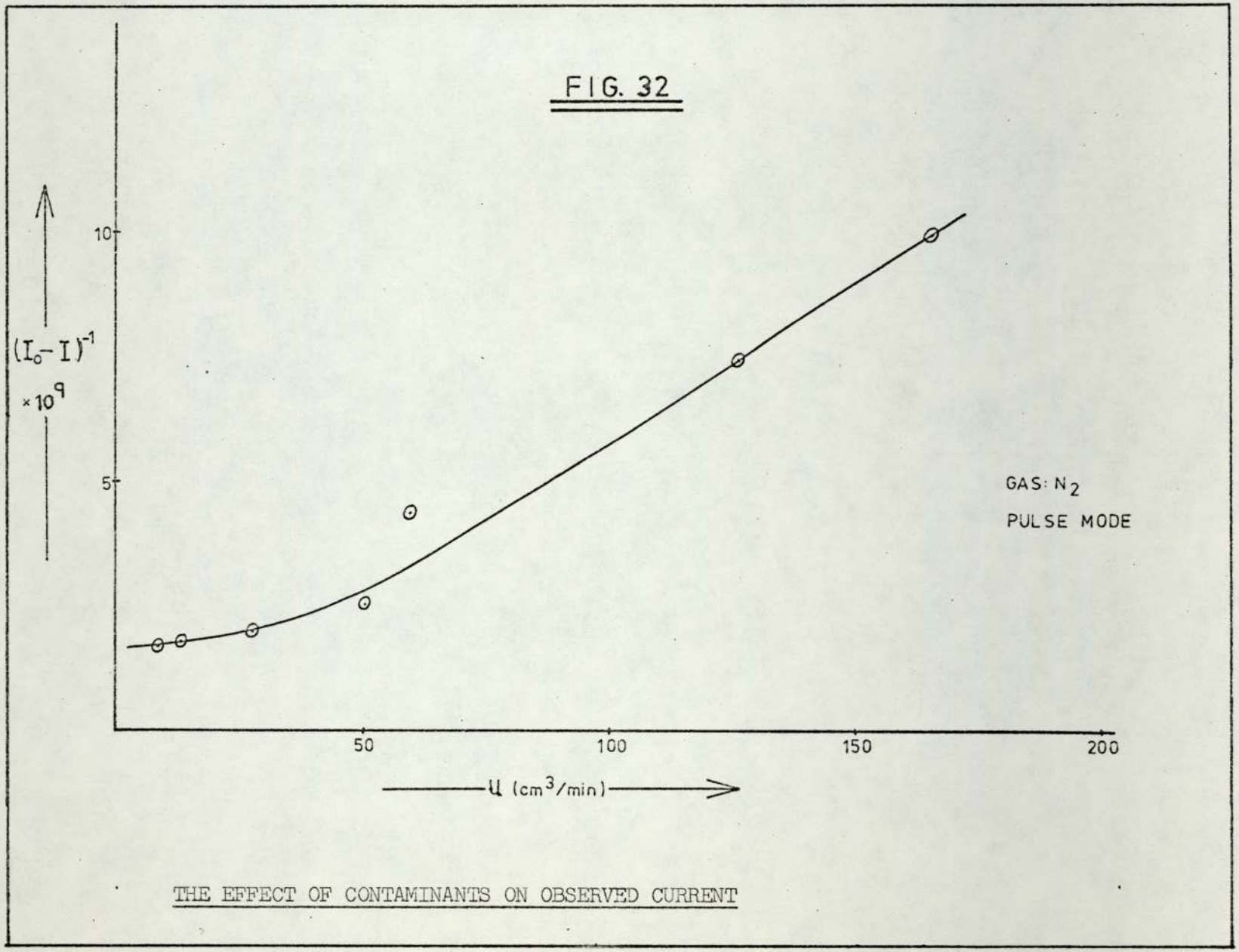

THE EFFECT OF CONTAMINANTS ON OBSERVED CURRENT

positive ions in the gas stream. Wentworth et al.,[18] noted that in the pulsed mode, loss of positive species may occur through flow out of the cell at longer pulse periods. Lyons et al.,[39] have suggested that two processes are involved. In the low flow region ($\simeq 100$ cm^3 min^{-1}) the positive space charge around the cathode is dispersed by increasing the gas flow. In the high flow region positive ions are removed in the gas stream so that the concentration of positive ions in the chamber is inversely proportional to the flow rate.

The rather large variation in current with carrier gas flow rate observed by Lyons et. al., is almost certainly due to the presence of a capturing impurity, as the results obtained from a system suspected of leakage have shown.

A possible effect of flow would be to influence the degree of mixing in the cell. As shown earlier, the electron drift velocity is comparable to the gas kinetic velocity, indicating that mixing is occurring in the cell but it is not sufficient to assume complete mixing. In the assymmetrical cell, the gas flow does seem to diffuse the space charge of positive ions as the current - electrode separation plots showed. Also, in the case where the cathode was fixed close to the gas outlet, the maximum current was higher than that measured when the position of anode remained fixed. This is possibly an indication of loss of positive species from the space charge in the vicinity of the cathode.

Lovelock[37] has pointed out that ionisation detectors are not usually sensitive to changes in gas flow rate. This is because the drift velocity of the ions is large compared with the linear velocity of the gas flowing through the detector. If, however, the drift velocity of either the positive or negative ions becomes comparable with the linear gas velocity, gas flow can affect the

detector current.

If flow out of the cell is to be a plausible mode of loss for positive ions, then the time constant for this process has to be comparable to that of recombination which is by far, the most important process by which the ions are lost. For a cell with an electrode spacing of 2.0 cm and assuming a high gas flow (3.67 cm^3 s^{-1}), the residence time for gas molecules is 3.45×10^{-1} s. Assuming an average positive ion density of 1×10^9 cm^{-3} and a recombination coefficient of about 1×10^{-7} cm^{-3} s^{-1}, the time constant is 1×10^{-2}s. The two values do not differ significantly.

Besides volume recombination, the positive ions can also be lost by surface recombination at the cathode. At low field strengths (10 Vcm^{-1}), the positive ion drift velocity in nitrogen is 2.55×10^1 cm s^{-1} and the time to cross the cell of spacing 2.0 cm. would be about 7.8×10^{-2} s. This value too, is comparable with the residence time for molecules at high gas flow. Hence, it seems that positive ions could be lost through flow out of the cell, when cell volumes are big and the flow rate is high.

At small electrode separations, flow was found to have no effect on the current (Fig. 33) but as the spacing was increased, a higher current was observed for a particular voltage when the gas flow rate was high (Fig. 28)

4.7 d.c. MODE OF OPERATION

Though this mode of operation has inherent sources of error, it is still quite widely used in analytical work. Hence, an attempt was made to analyse the typical response characteristic of the detector - a parabolic rise in current with applied voltage.

Several theories have been formulated for a discharge in a gas between two parallel plate electrodes. One approach based on calculating the current density at any point in space in the reaction volume, has already been outlined in section 3.3. Another

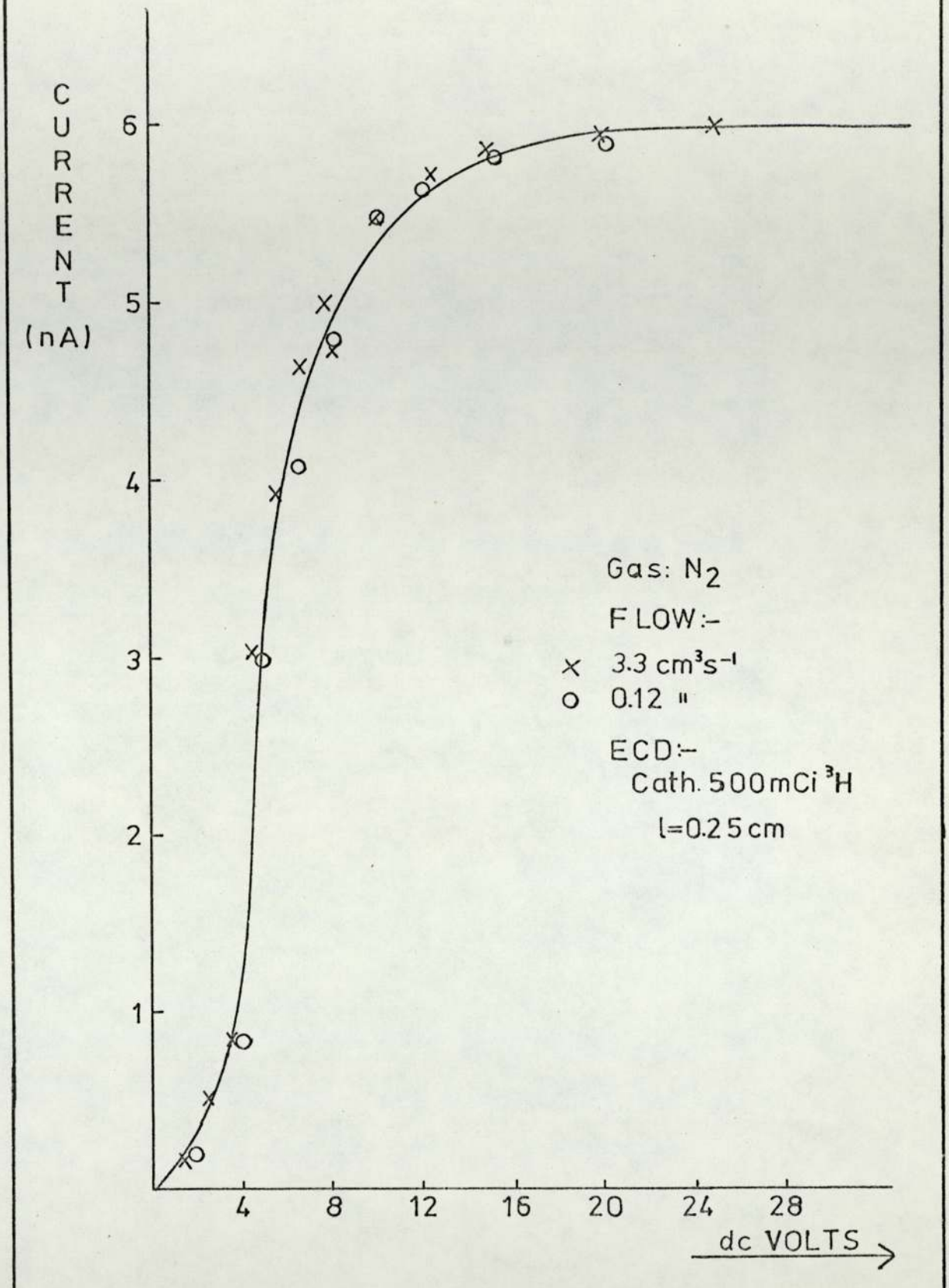

FIG. 33

CURRENT - VOLTAGE PLOTS FOR DIFFERENT FLOW RATES AT SMALL ELECTRODE SEPARATION

approach, based on Poisson's equation and applicable at high gas pressure and in the presence of a space-charge leads to the following relationship between the current density and voltage[13] :

$$j = \frac{2.95 \times 10^{-12} \mu V^2}{d^3} \qquad [42]$$

where μ is the mobility of the species responsible for the current and d is the electrode spacing. The electron current density calculated from the above equation for nitrogen is 5.8 nA m^{-2} while the measured current density (for the 500 mCi ^3H source) is 4.9×10^{-5} Am^{-2}. Several factors contribute towards the inadequacy of these theories in predicting the ECD current. It is assumed that ionisation is uniform throughout the cell; that the space charge is very dense and either electrons or positive ions are to be considered and not mixtures.

In terms of the proposed model, the electron density under the d.c. mode would be expressed by

$$e = (a / b')^{1/2}$$

$$= \left[\frac{k_1 AG}{(k_2 Vp + \sqrt{pA} + Fe)} \right]^{1/2}$$

The equation predicts an electron density several orders of magnitude smaller than that calculated from the observed current density. The inclusion of a diffusion term however improves the prediction. Since the latter process leads to surface recombination of the ion-pairs generated, the equation can be modified to :

$$e = \frac{k_1 AG (De + Dp) \; l}{(k_2 Vp + \sqrt{pA} + Fe)} \qquad [43]$$

Considering the case where the applied voltage is 20 volts, l = 1.0 cm and the source is500 mCi ^3H, the measured electron density in nitrogen is 2.58×10^{10} cm^{-3}. The density calculated from Eq. [43] is 6.2×10^{8} cm^{-3}.

As theoretical analysis has failed to explain satisfactorily the current-voltage behaviour, an empirical relationship was sought. The standing current is proportional to V^2 and inversely proportional to l^3 at high gas flow rates (Fig. 34 and 35) and in the low flow region, the relationships appear to be : $I \propto V^{3/2}$ and $I \propto d^{-2}$ (Fig. 36). Similar relationships are expressed by Child's law describing space-charge limited currents in vacuum and gas-filled electronic devices such as thermionic diodes.

The graph of the onset voltage for saturation current at different inter-electrode spacing (Fig. 37) shows the effect of space charge — a potential trough near the cathode. The intensity of the space charge is determined by the parabolic character of the curves; it appears that a denser space charge exists at very low gas flow rates. This would be the case if positive ions were being removed from the cell by flow. Similar results were obtained with 95% Ar + 5% CH_4 (Fig. 38).

4.8 PULSED MODE OF OPERATION

To overcome many of the problems faced when the detector is operated in the d.c. mode, Lovelock[12] suggested the use of square wave voltage pulses as the source of potential. Pulse variables - voltage, V, width, w and interval, s, were defined in section 2.6 and the detector used was characterised in terms of these parameters in section (4.4).

When the ECD operates in the pulsed mode, its response over a voltage range shows a plateau (Fig. 8); the particular voltage at which this plateau occurs depends upon the pulse width and the detector design. It is also indicative of cell and carrier gas purity. With nitrogen and 95% Ar + 5% CH_4 as carrier gases, the onset voltage for saturation current is about 20-30 volts under normal operating conditions. In the presence of electron

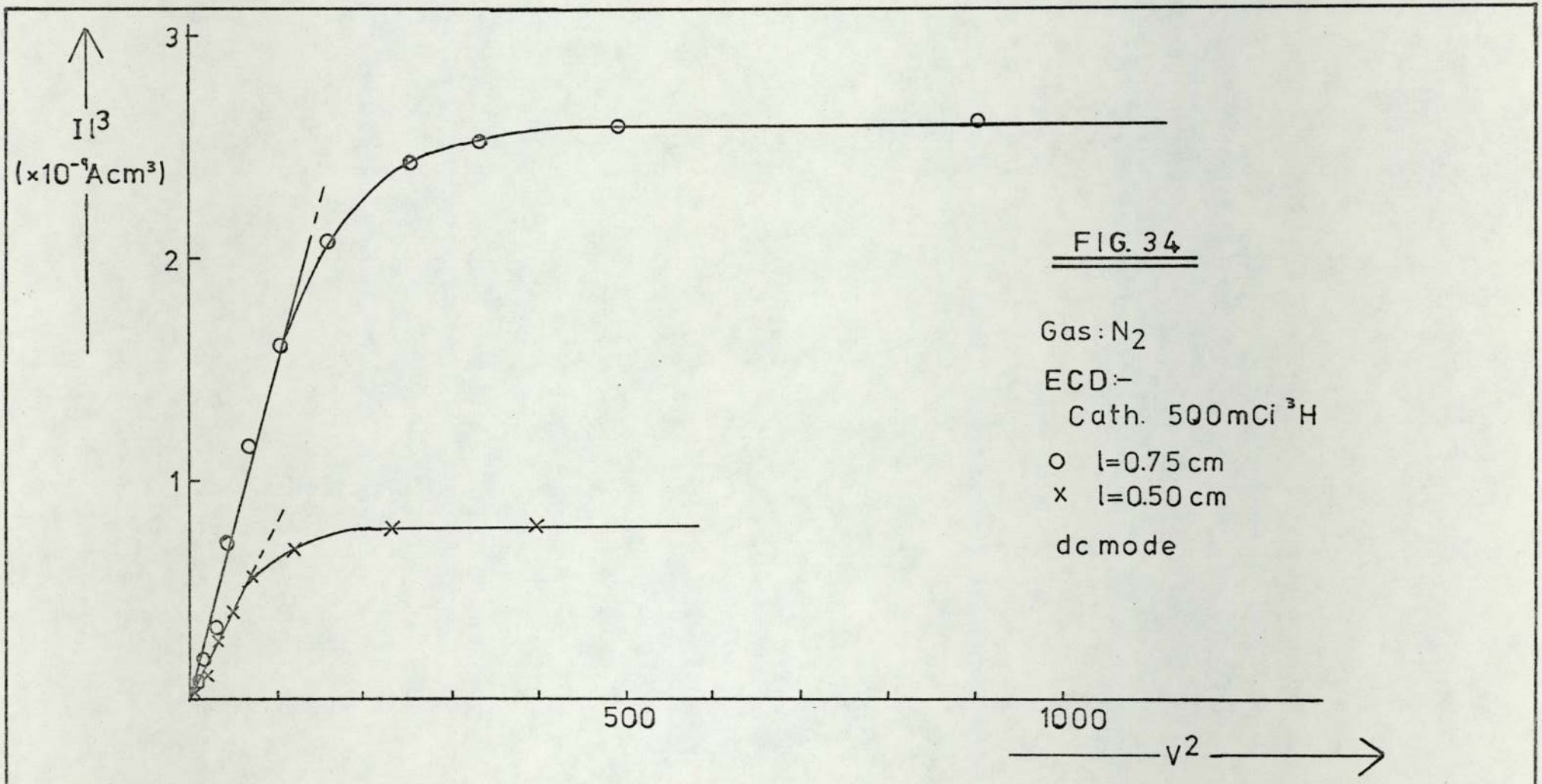

FIG. 34

CURRENT - VOLTAGE RELATIONSHIP IN d.c. MODE AT HIGH GAS FLOW RATE

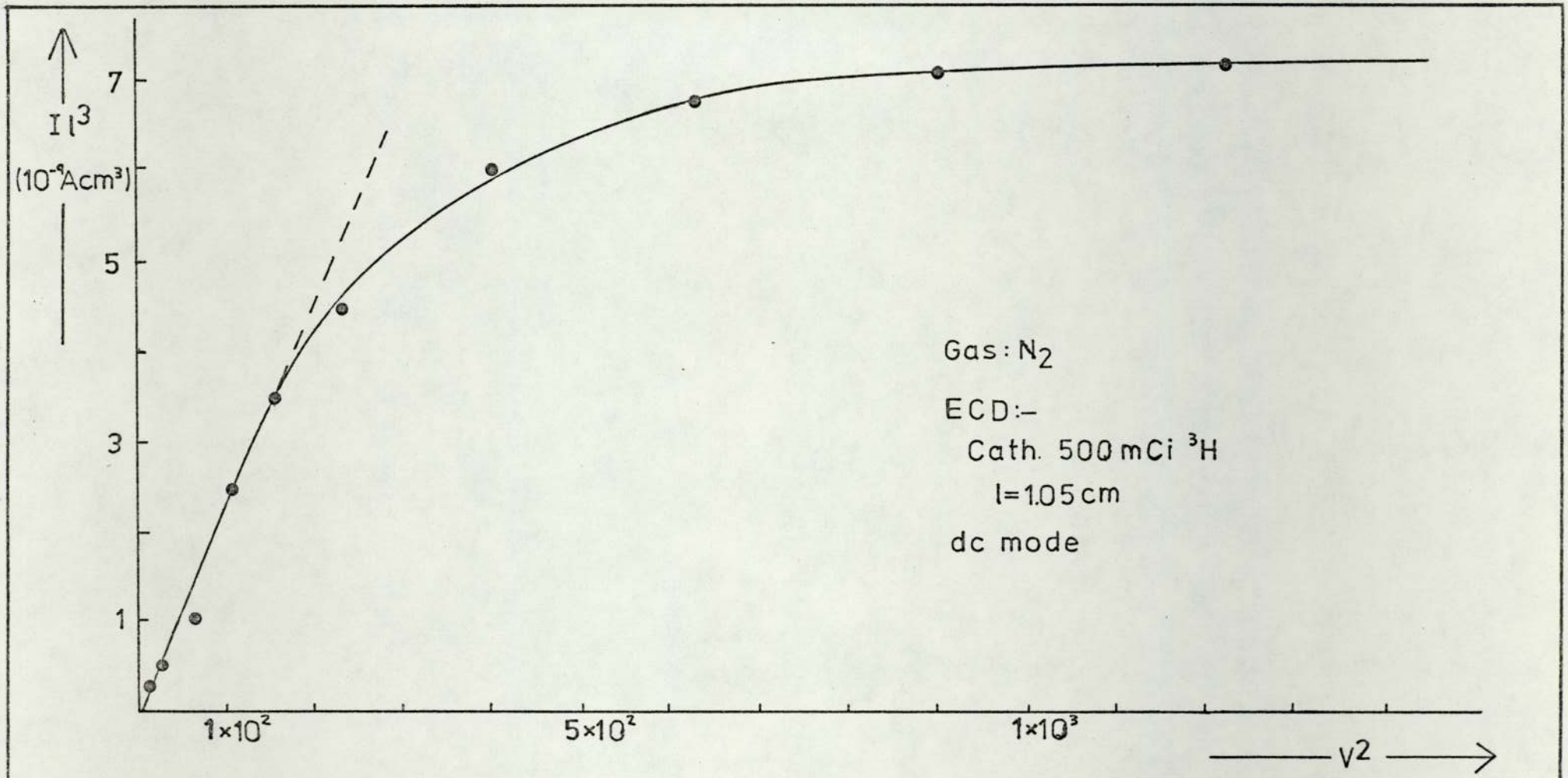

FIG. 35

VARIATION OF CURRENT WITH VOLTAGE IN d.c. MODE

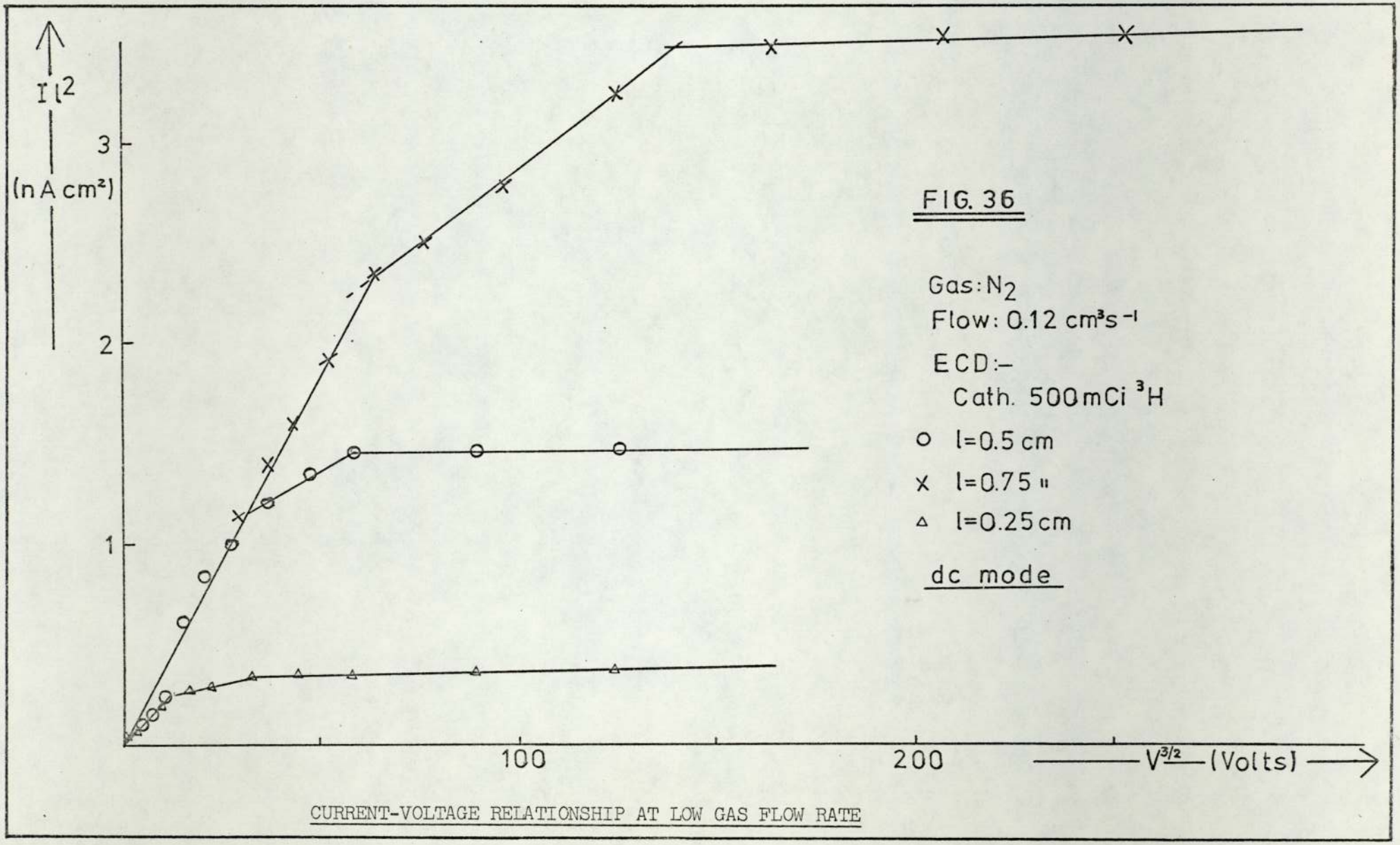

CURRENT-VOLTAGE RELATIONSHIP AT LOW GAS FLOW RATE

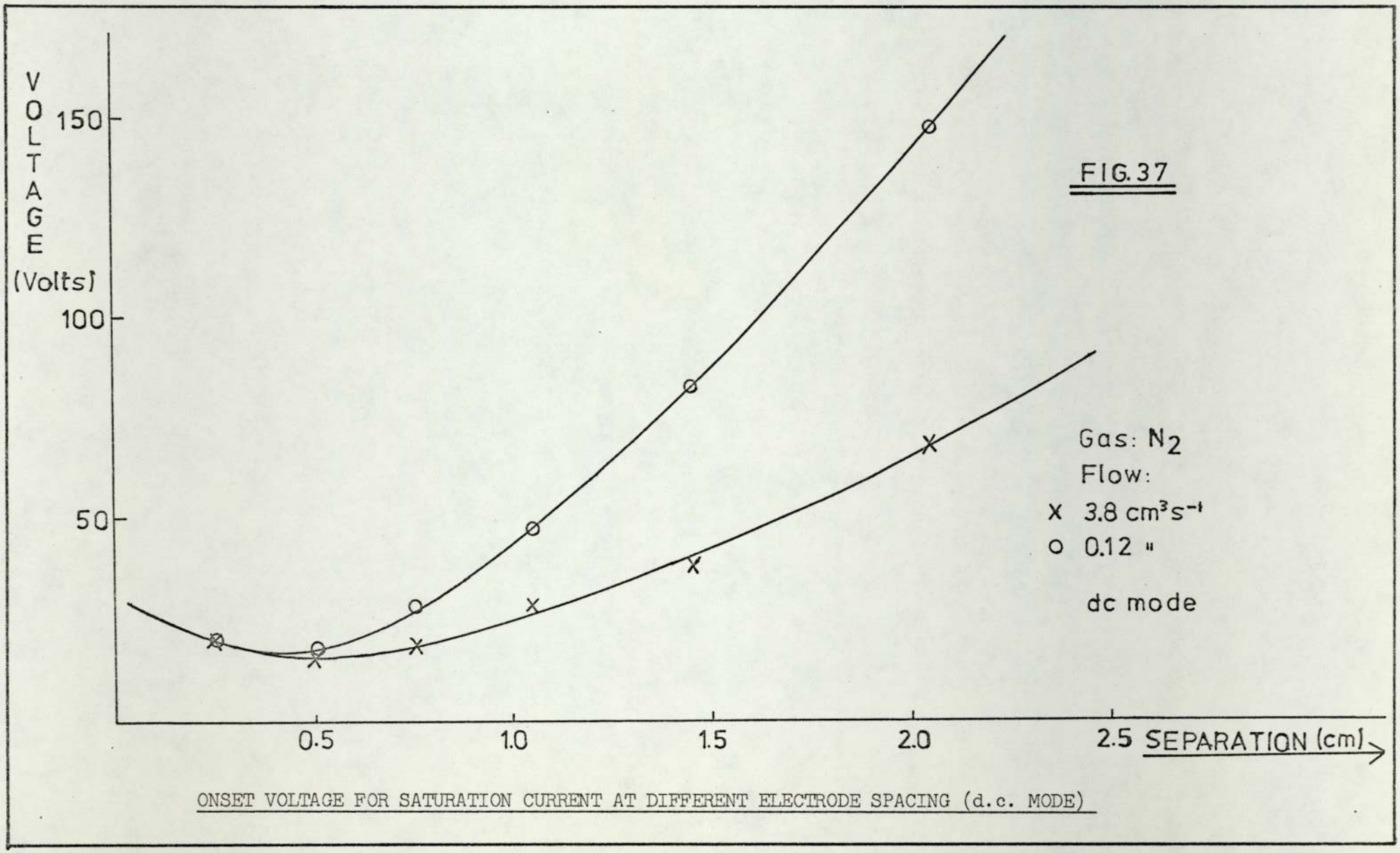

ONSET VOLTAGE FOR SATURATION CURRENT AT DIFFERENT ELECTRODE SPACING (d.c. MODE)

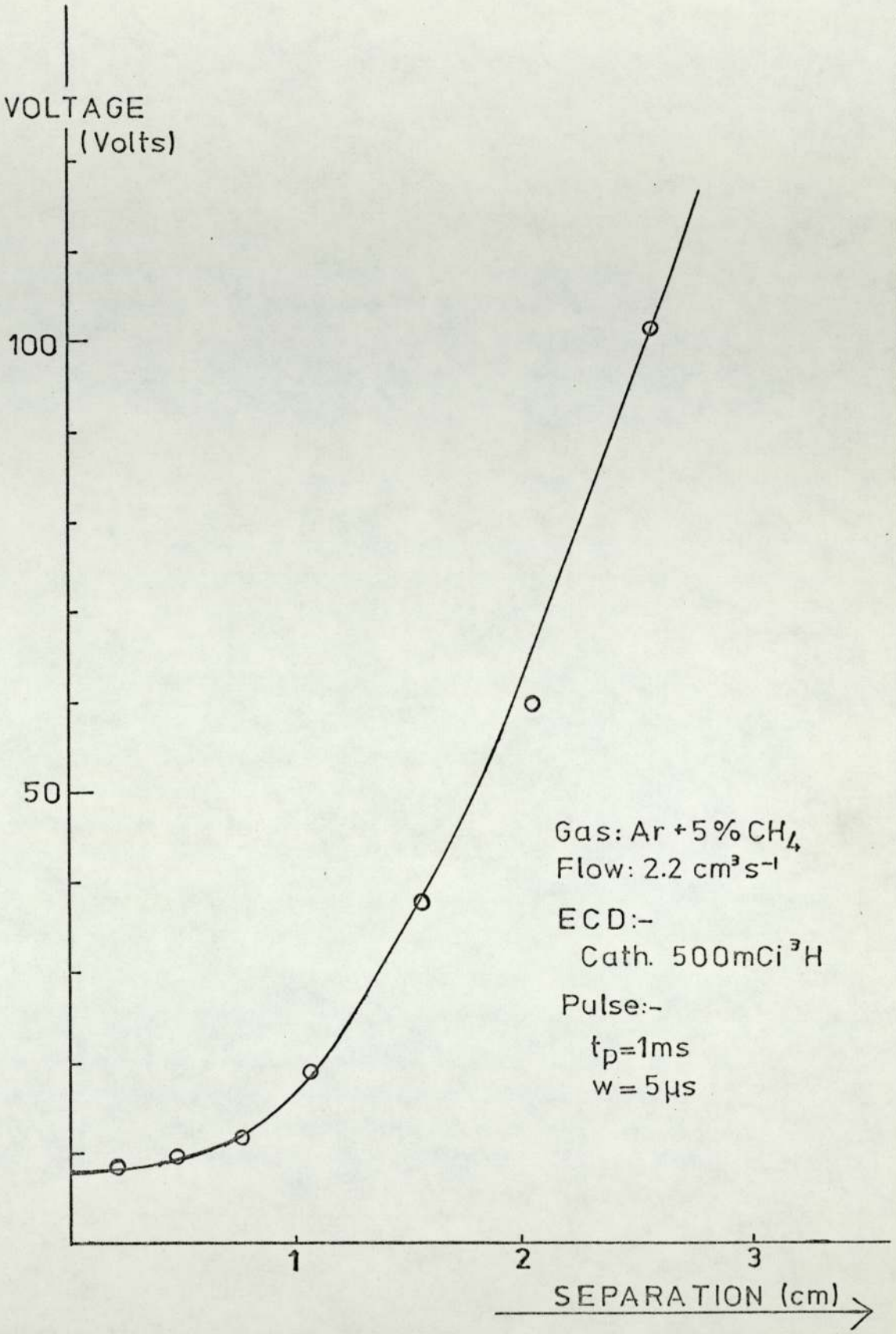

FIG. 38

ONSET VOLTAGE FOR SATURATION CURRENT UNDER THE PULSED MODE ($Ar+CH_4$)

capturing impurities, a larger voltage is necessary since the negative species formed upon capture are being collected as well.

In explaining the decrease in current at long inter-electrode spacings, it was shown that the normal pulse width of 5 μs is too short to allow collection of all electrons. This would imply that if the field intensity (which is proportional to V) were to be increased, the drift velocities of the charged species would increase as well and hence the saturation current be reached. Fig. (39) shows that this is the case.

As with the d.c. mode, if the onset voltages giving saturation current at various electrode separations were to be plotted against the separation (Fig. 38), a potential trough is observed. This would imply that a space charge of positive ions also exists under the pulsed mode of operation, contrary to what is normally stated.[18]

The current variation with pulse width is similar to that observed for the pulse amplitude — a steep increase initially, followed by saturation (Fig. 9). The slight increase in the saturation region is thought to be due to the collection of charges produced during the application of the pulse. As stated in section 4.4, the pulse width at which the current ceases to increase linearly denotes the electron transit time. If this is the case, then it should be possible to calculate the electron drift velocity from that time and the cell length. At $(X/P) = 0.07$ V cm^{-1} $torr^{-1}$, Brown[60] gives the electron drift velocity in nitrogen as 2.7×10^5 cm s^{-1}. Table 4 shows the drift velocities calculated with different ionisation sources and cell lengths. The electron transit time is denoted by Wc and the field strength (X) is assumed to be uniform in the cell. The average electron drift velocity in nitrogen calculated from the results given in Table 4 is 2.83×10^5

FIG. 39

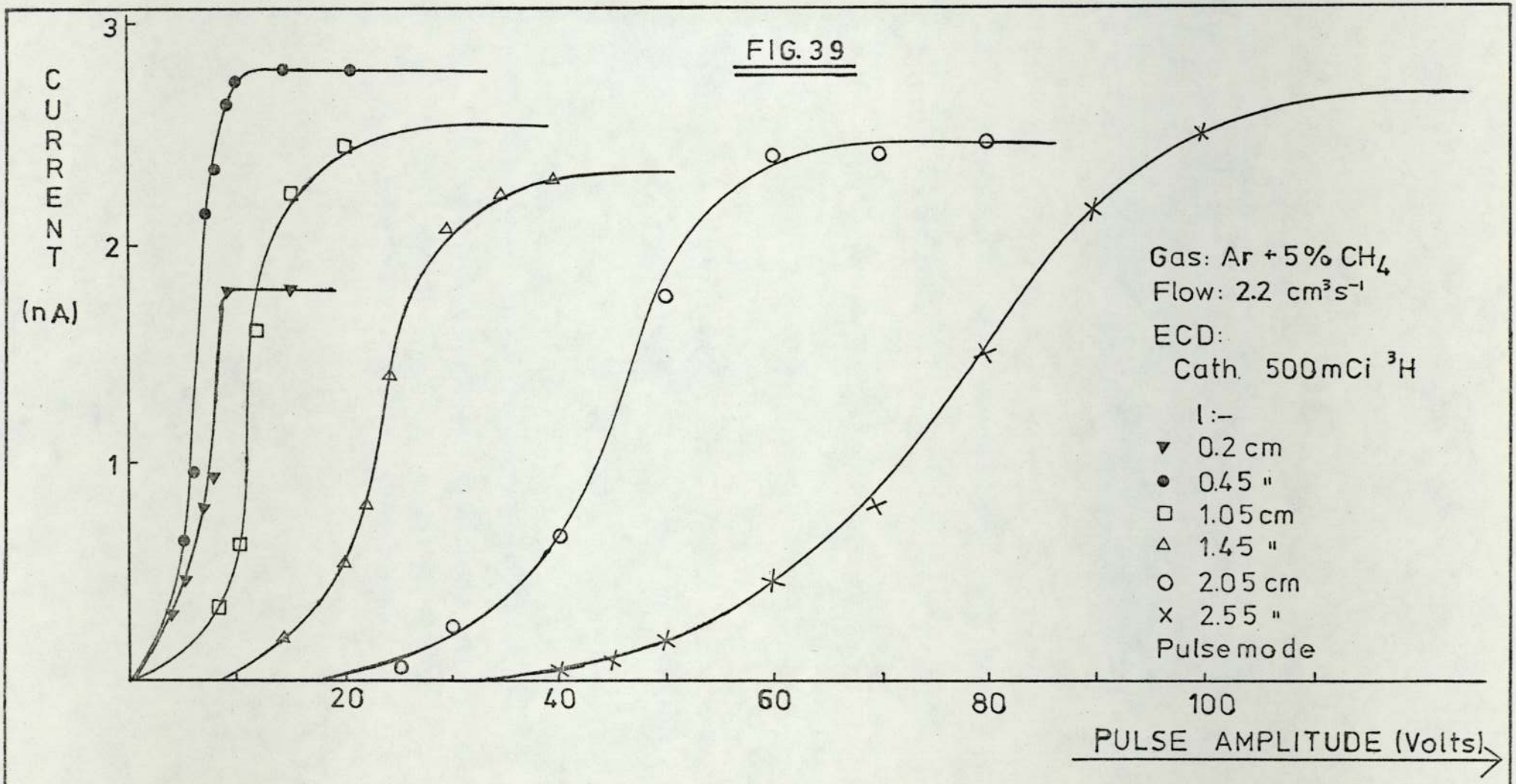

CURRENT VARIATION WITH PULSE AMPLITUDE AT VARIOUS ELECTRODE SEPARATIONS

TABLE 4

ELECTRON DRIFT VELOCITY (V_d) IN NITROGEN

SOURCE	CELL LENGTH	FIELD	Wc	V_d cms^{-1}
500 mCi ^{3}H	1.0 cm	50.0 Vcm^{-1}	3.50 μs	2.86 x 10^5
150 mCi ^{3}H	1.6 cm	56.25Vcm^{-1}	6.30 μs	2.54 x 10^5
150 mCi ^{3}H	0.95 cm	52.6 Vcm^{-1}	3.40 μs	2.79 x 10^5
0.5mCi ^{63}Ni	1.0 cm	50.0 Vcm^{-1}	3.20 μs	3.12 x 10^5
0.5mCi ^{63}Ni	1.55 cm	58.1 Vcm^{-1}	5.50 μs	2.82 x 10^5

TABLE 5

ELECTRON DRIFT VELOCITIES IN VARIOUS GASES AT LOW (X/P)

GAS	PRESENT STUDY V_d	LITERATURE VALUES V_d
Nitrogen	2.83 x 10^5 cms^{-1}	2.7 x 10^5 cms^{-1} (60)
Ar + 5% CH_4	2.65 x 10^6 cms^{-1}	3.5 x 10^6 cms^{-1} (18)
Argon	3.05 x 10^5 cms^{-1}	2.0 x 10^5 cms^{-1} (18)
Helium	3.22 x 10^5 cms^{-1}	3.5 x 10^5 cms^{-1} (60)
Ethylene	8.65 x 10^5 cms^{-1}	—

cm s^{-1}. The distance travelled by the electrons has been taken to be the entire cell length even though it appears that ionisation occurs some distance away from the source. This seems reasonable since most β^- particles are confined very close to the source as was pointed out in section 4.5.

Electron drift velocities in various gases have been calculated and are presented in Table 5 together with literature values (60) where available. Small changes in (X/P) in the range considered (at atmospheric pressure) have negligible effect on the drift velocity(29). The results obtained are in agreement with those acquired using other techniques for measuring electron mobility. The potential use of the ECD to measure electron mobilities at very low (X/P) values is amply demonstrated.

The experimental parameters expressing kinetic control of the reactions occurring in the detector are the number of electrons collected per pulse (Ne) and the pulse interval (s). Fig. (29) shows a typical current variation with pulse interval — gradual levelling off at short periods giving maximum current and a steep decrease with increasing s. The extrapolated current value at zero pulse period corresponds to the maximum current observed under the d.c. mode. In the case of nitrogen this is about 6.3 nA. However, with 95% Ar + 5% CH_4 the current at short pulse interval (50 μ s) was slightly higher (by 0.3 nA) than the d.c. saturation current (6.85 nA). With argon and ethylene, the latter was found to be slightly higher. These small fluctuations are within experimental error and it can generally be said that at short pulse periods, the current does approach the d.c. saturation current. This would imply the collection of positive ions under the pulsed mode, contrary to what is generally accepted (that only electrons are collected)(61).

Fig. (40) shows the current variation with pulse interval for different gases studied-argon, 95% Ar + 5% CH_4, ethylene, helium

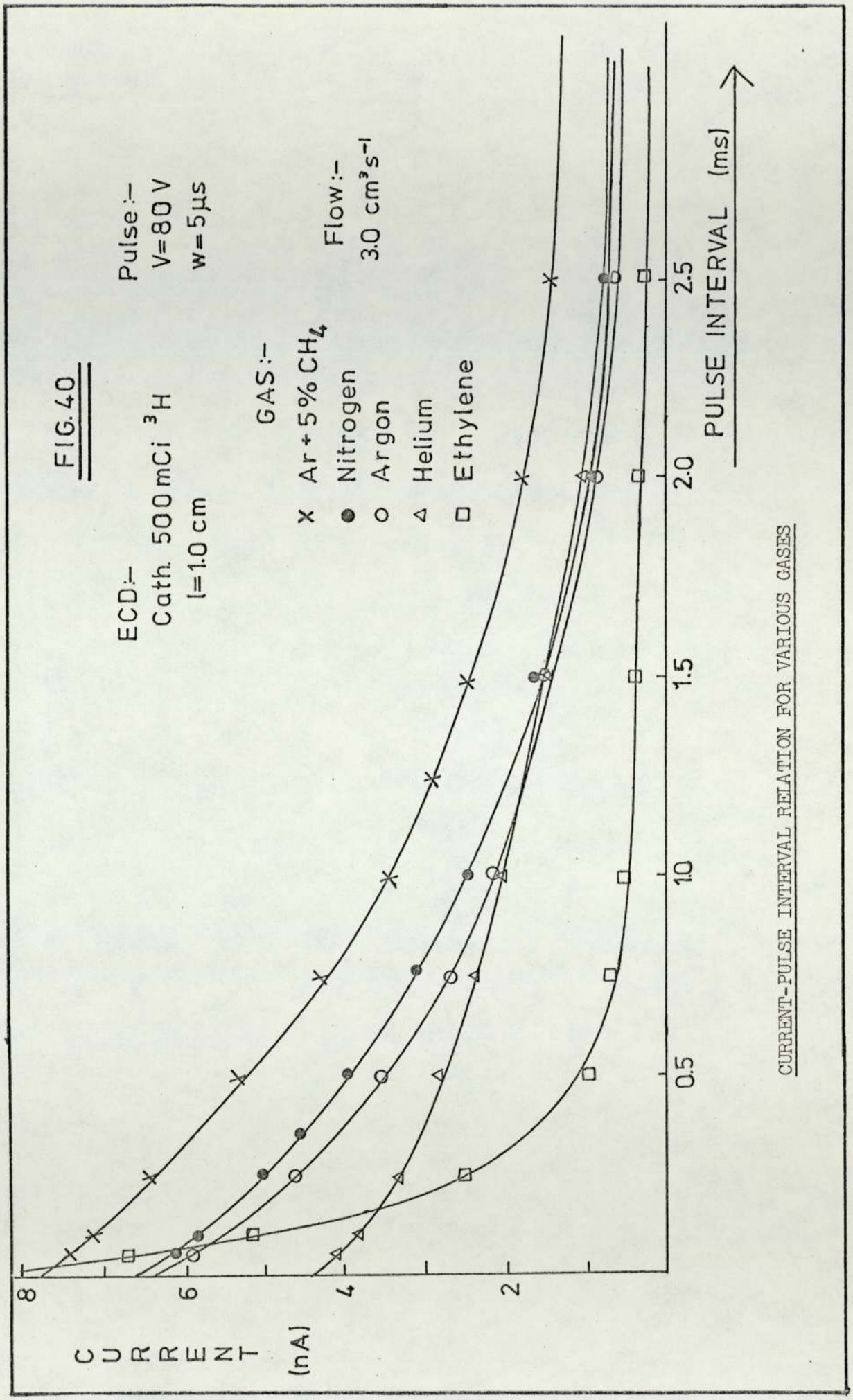

CURRENT-PULSE INTERVAL RELATION FOR VARIOUS GASES

and nitrogen. The addition of small amount of methane to argon maintains the electron energy at a constant thermal level and the quenching gas molecules also remove argon metastables in deactivating and ionising collisions. In pure argon, electrons are not completely thermalised during the applied pulse times and this probably accounts for the lower current observed in argon since the ionisation cross-section decreases with increasing electron energy. The metastable potential of helium is relatively high (20.7 eV)[11] and since ionisation of rare gas molecules occurs only via the excited state, the measured current is expected to be much smaller in comparison to that of argon. The reactions are :

$$He + e^- \longrightarrow He^* + e^-$$

$$He^* + He \longrightarrow He_2^+ + e^-$$

Fig. (40) also illustrates the loss of electrons and positive ions through recombination processes. Assuming that the rate of decrease in average current (as measured by the electrometer) with increasing pulse period is unaffected by the nature of the gas in the detector, the effect of different rates of recombination is clearly exhibited at long pulse interval. Helium, with its lower rate of recombination gave almost the same current as nitrogen and argon at long pulse periods. With ethylene as carrier gas, a very steep decline in current is observed. The formation of several positive species upon irradiation have been reported[40] : $C_2H_2^+$, $C_2H_3^+$, $C_2H_4^+$, and $C_4H_7^+$. Though an overall recombination coefficient is not known for the gas, it is expected to be large ($\simeq 10^{-6}$ cm^3 s^{-1}).

Equation [30] predicts the build up of electron concentration during the field free interval. The rate of production of ion-pairs, k_1 AG, is given by the initial slope of (Ne versus s) graph. For the 500 mCi ^{3}H source and nitrogen as carrier gas, k_1 AG = 2.41 x 10^{10} cm^{-3} s^{-1}. The mobility and electron ion recombination coefficient (for N_4^+) is 2.5 cm^2 V^{-1} s^{-1} and 1.50 x 10^{-6} cm^3

s^{-1} respectively.[22, 30] Fp is taken to be the flow rate of the gas. The 'Gaines factor', R, is calculated from Eq. [36] for several values of s and this allowed the positive ion concentration, Po, to be evaluated from Eq. [38]. Table 6 shows the values of these two parameters for nitrogen. All the factors involved in Eq. [30] are now known and hence the electron concentration can be calculated. Fig. (41) shows the prediction of the present theory together with that made by Lovelock's 'stirred reactor' model[42] and these are compared with the experimentally observed variation of Ne versus s. Eq. [33] giving the average electron concentration and the corresponding equation in Lovelock's model both fail to saturate at long pulse periods. This probably indicates that the current measured does not correspond to the electron concentration per pulse integrated over the pulse period but rather to the actual concentration of electrons at the end of thepulse period, as expressed by Eq. [30].

Expressing R as the ratio of positive ions to electrons in the cell simplifies Eq. [30] to :

$$e = \frac{a^{1/2}\,[\exp(q\,t) - 1]}{c^{1/2}\,[\exp(q\,t) + 1]} \qquad [44]$$

where $a = k_1\,AG$ $C = k_2 R$ and $q = 2\,(ac)^{1/2}$

The recombination coefficient, k_2, for Ar_2^+ is 6.7×10^{-7} $cm^3\,s^{-1}$ as calculated by Oskam and Middlestadt.[62] The drift velocity for the ion is 1.52×10^2 cms^{-1} at a field strength of 80 Vcm^{-1}. The mean value of R is 3.66×10^2. Fig. (42) shows the theoretical prediction according to Eq. [44] and also the experimental variation of Ne with the pulse interval.

An equation can easily be derived for the recombination coefficient from the proposed model,

$$k_2 = \frac{k_1 V^2}{n_e^2 R} - \frac{2V}{n_e R s} + \frac{1}{k_1 R s^2} \qquad [45]$$

TABLE 6

THE 'GAINES FACTOR' AND POSITIVE ION CONCENTRATION IN NITROGEN AT VARIOUS PULSE PERIODS

S ⟨μs⟩	R x 10^2	p_o x 10^9
43	6.33	3.97
100	5.68	3.76
250	4.46	3.33
500	3.29	2.86
750	2.63	2.56
1000	2.17	2.32
1500	1.62	2.01
2000	1.30	1.80

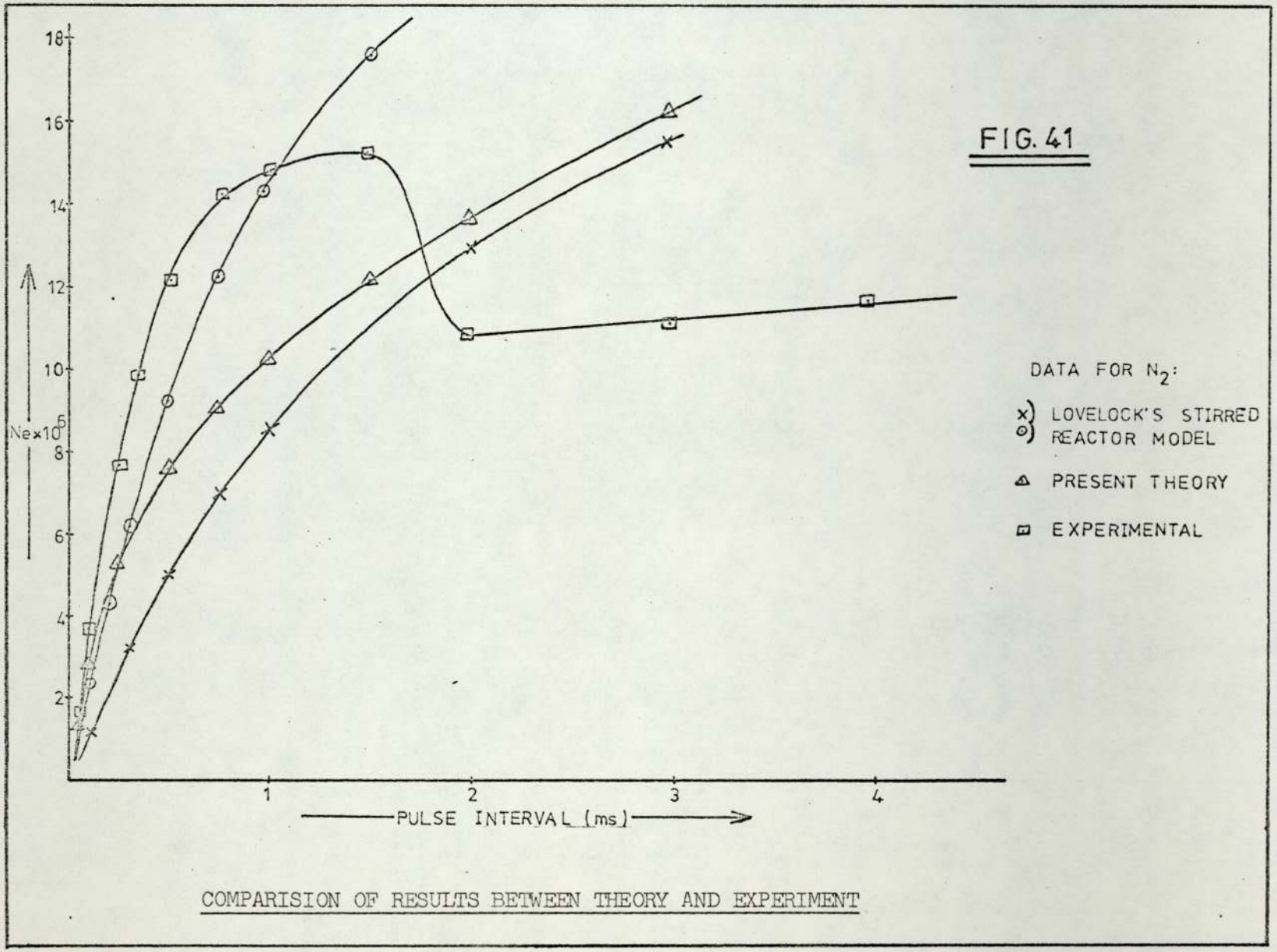

COMPARISION OF RESULTS BETWEEN THEORY AND EXPERIMENT

FIG. 42

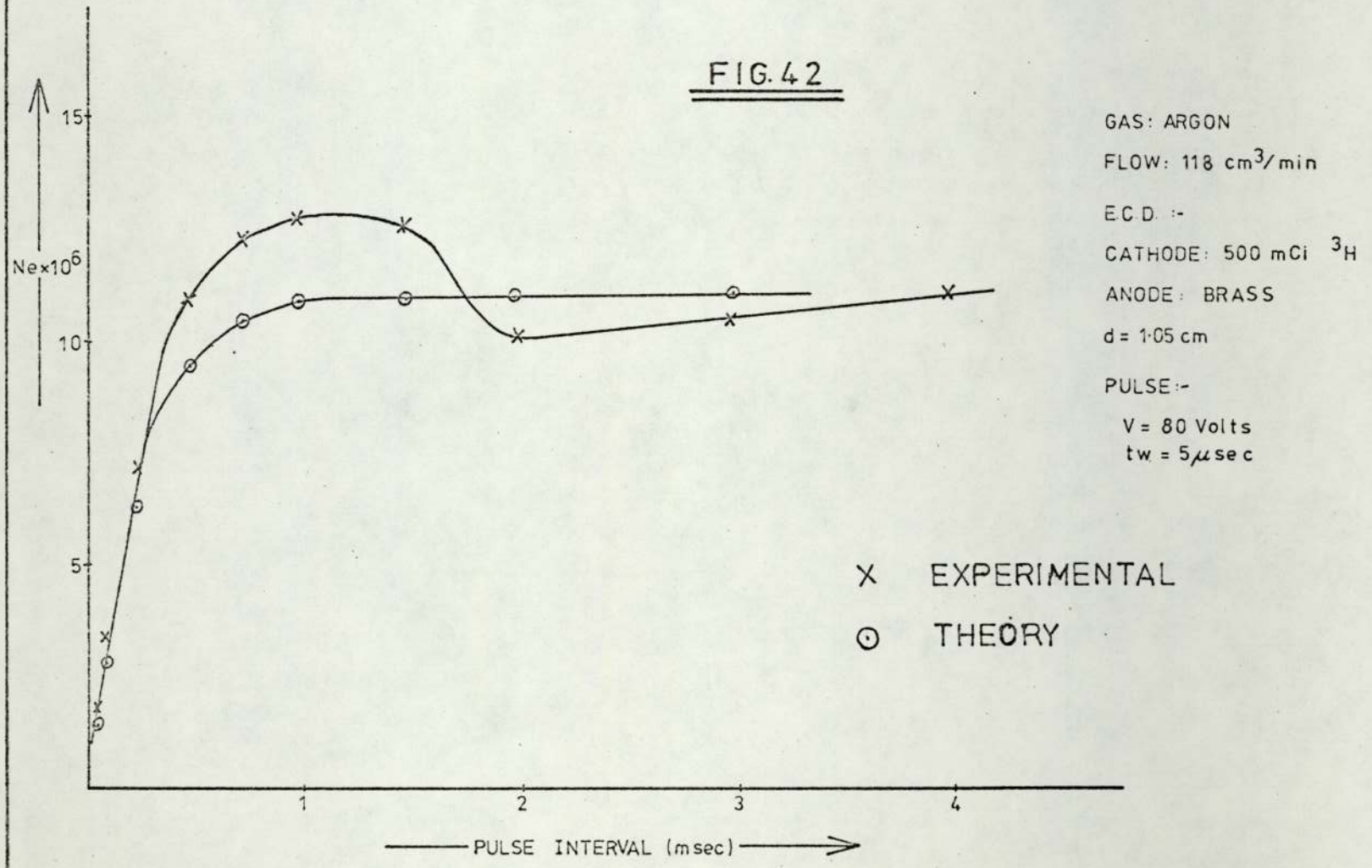

PREDICTION OF THE PROPOSED MODEL COMPARED WITH EXPERIMENTAL DATA FOR ARGON

The positive ion mobility in ethylene is approximately 2.5 $cm^2\ V^{-1}\ s^{-1}$ giving a drift velocity of 2.0×10^2 cm s^{-1} at a field strength of 80 V cm^{-1}.(39) The mean value of R is 4.66×10^2 and $k_1 = 2.84 \times 10^{10}\ cm^{-3}\ s^{-1}$ when the cell volume is 1.27 cm^3. As recombination is a dominant process at long pulse periods, the value of $Ne = 3.15 \times 10^6$ is taken at s = 1 ms. The electron-ion recombination coefficient for ethylene, calculated from Eq. [45], is then equal to $8.95 \times 10^{-6}\ cm^3\ s^{-1}$.

For helium, when the 'Gaines factor' is calculated from Eq. [36], the recombination coefficient, $k_2 = 1.35 \times 10^{-6}\ cm^3\ s^{-1}$ which is considerably larger than the reported values.(22) An alternative way of obtaining the 'Gaines factor' is to consider it as a function of the ratio of the mobilities of positive ions and electrons in the gas under study. Thus,

$$R = G \left(\frac{\mu p}{\mu e} + \frac{u s}{V}\right)^{-1} \qquad [46]$$

where G is the number ofion-pairs formed per number of β^- particles actually emitted; μp and μe refer to the mobility of positive ions and electrons respectively and u is the gas flow rate. R calculated in this way gives a value of 6.22×10^4 for helium. The rate of production of ion-pairs, $k_1 = 1.58 \times 10^{10}\ cm^{-3}\ s^{-1}$ and $Ne = 1.3 \times 10^7$ at s = 1 ms. Eq. [45] then gives the recombination coefficient for helium and is equal to $2.3 \times 10^{-9}\ cm^3\ s^{-1}$ which agrees very well with the values quoted by Hasted(22).

The use of known values of recombination coefficients and positive ion mobilities has made it possible to check the predictions of the proposed theory. Accounting for the positive ion space charge, through the 'Gaines factor', shows that the charge concentration in pure argon is about $4.0 \times 10^9\ cm^{-3}$ at s = 1 ms. Wentworth et al.,(18) estimated the value to be $1.1 \times 10^{11}\ cm^{-3}$.

Theory, however, failsto explain the observed maxima and

the subsequent sharp decline. The peak appeared in all the gases studied and it seems that a process with a reaction time of about 0.5 ms is responsible in almost all the cases. Wentworth et al.,[18] observed a similar peak in their studies and attributed it to a different process of loss for the positive ions in the cell. At short pulse periods the ions are collected at the cathode but at long pulse interval, they are lost through flow out of the cell. A different electron concentration would hence be reached at steady state and the curve would exhibit a distinct 'jump' from one level to another. The maxima has been observed mainly when less efficient ionisation sources have been used; Wiel and Tommassen[59] using a 10 mCi ^{63}Ni source did not observe such a peak. It seems that loss of ions through flow out of the cell becomes significant only with lesser electron input sources.

4.9 PRESENCE OF UF_6 AND H_2O IN CARRIER GAS

The ECD response to a capturing species depends upon the physico-chemical properties of the sample molecules. For a weakly electron capturing compound, the response is linear when the electron - molecule reaction takes place under conditions which ensure that the detector is operating in the pseudo-first order region[42]. This is the case when the sample concentration greatly exceeds that of the electrons, ie. with a less efficient ionisation source giving a low saturation current. For strongly electron capturing compounds a linear response is observed when the electron concentration within the detector exceeds that of the sample molecule concentration. Nearly all of the sample input is ionised; a high d.c. saturation current (10^{-8} A) is necessary for this to occur.

A considerable body of information on molecular electron affinities indicate that the negative ions formed are often far too stable for the reverse reaction to occur (ie. electron detach-

ment).[26] As stated in section 3.1, at ordinary temperatures, a very small fraction of gas molecules possess sufficient translational energy necessary to detach an electron from a negative ion. Thus the formation of negative ions can be considered to be proceeding only in one direction, ie. as a rate process. This point was further considered by Burdett[32] who showed that the detector does respond to the geometrical cross section of sample molecules when a group of organic compounds of the same type is considered. The electron detachment rate, depending on the electron affinity and activation energy has a much smaller effect in comparison.

In order to check these conclusions, the effect of small concentrations of UF_6 in helium was investigated. The sample was placed in a saturator - a U - shaped glass vessel (Fig. 43) with a sintered glass disc in the wider, gas outlet side to support the compound and effect better mixing of the carrier gas with the vapour of the compound. The saturator was placed in a flask containing dry ice. A known variable fraction of the carrier gas passed through the saturator and was pre-mixed with the main stream before entering the detector.

Fig. (44) shows the current variation with pulse interval for pure helium and helium containing different concentrations of UF_6. At short pulse periods, the current approaches the same d.c. saturation current in all cases - an indication that all charged species present in the cell are collected. The presence of different concentrations of sample in the carrier gas is consequently more apparent at long pulse periods, ie. between 0.5 and 1.5 ms. The graphs of Ne versus t_p (Fig. 45) exhibit an anomalous behaviour; the number of electrons collected per pulse decreases very steeply at long pulse interval instead of reaching a steady level as in the pure gas. Dissociative electron attachment ($UF_6 + e^- \longrightarrow UF_5^- + F$)

FIG. 43

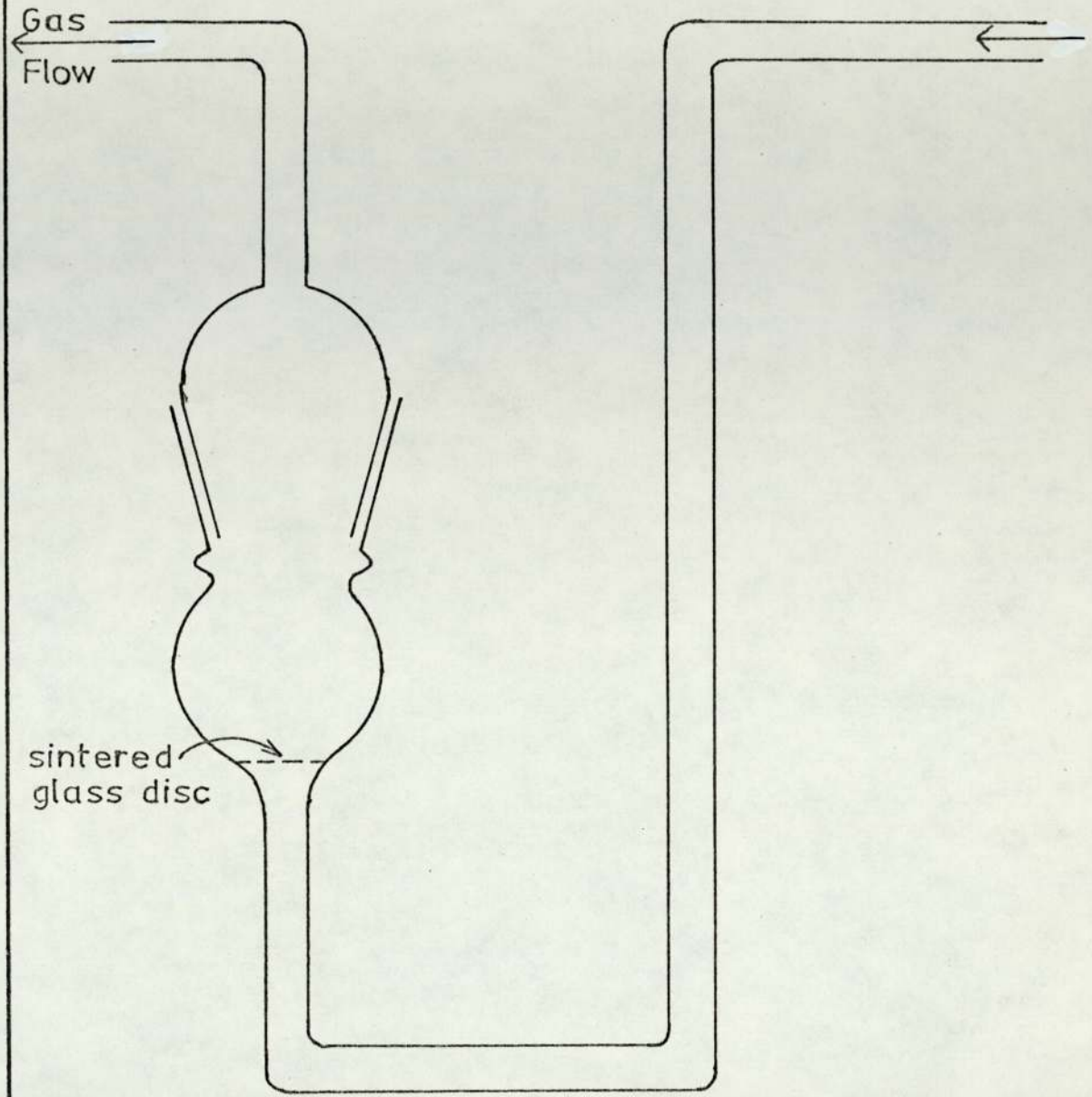

SATURATOR USED FOR INTRODUCING SAMPLE IN CARRIER GAS

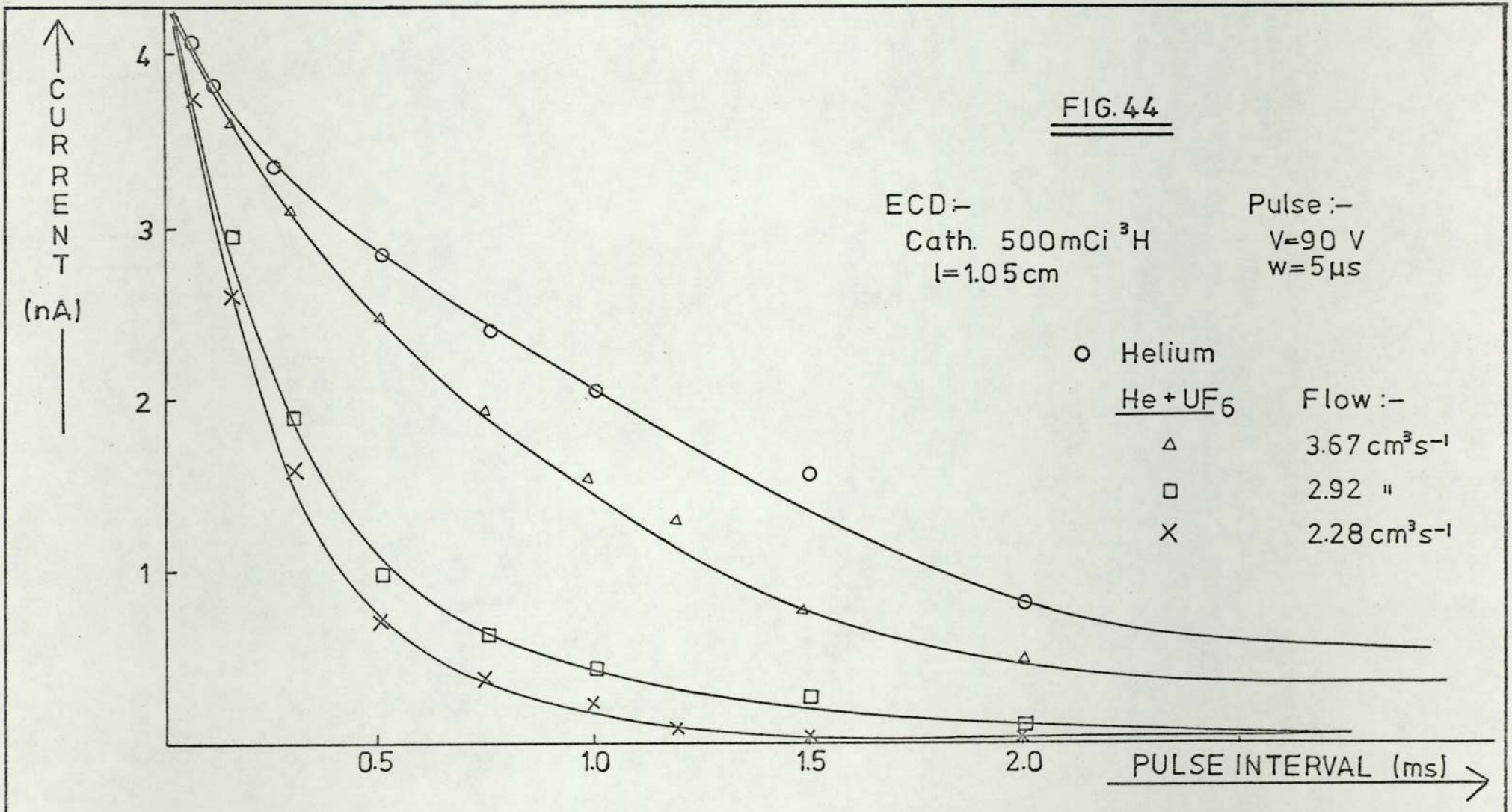

CURRENT VARIATION WITH PULSE INTERVAL FOR HELIUM AND HELIUM + UF_6

FIG. 45

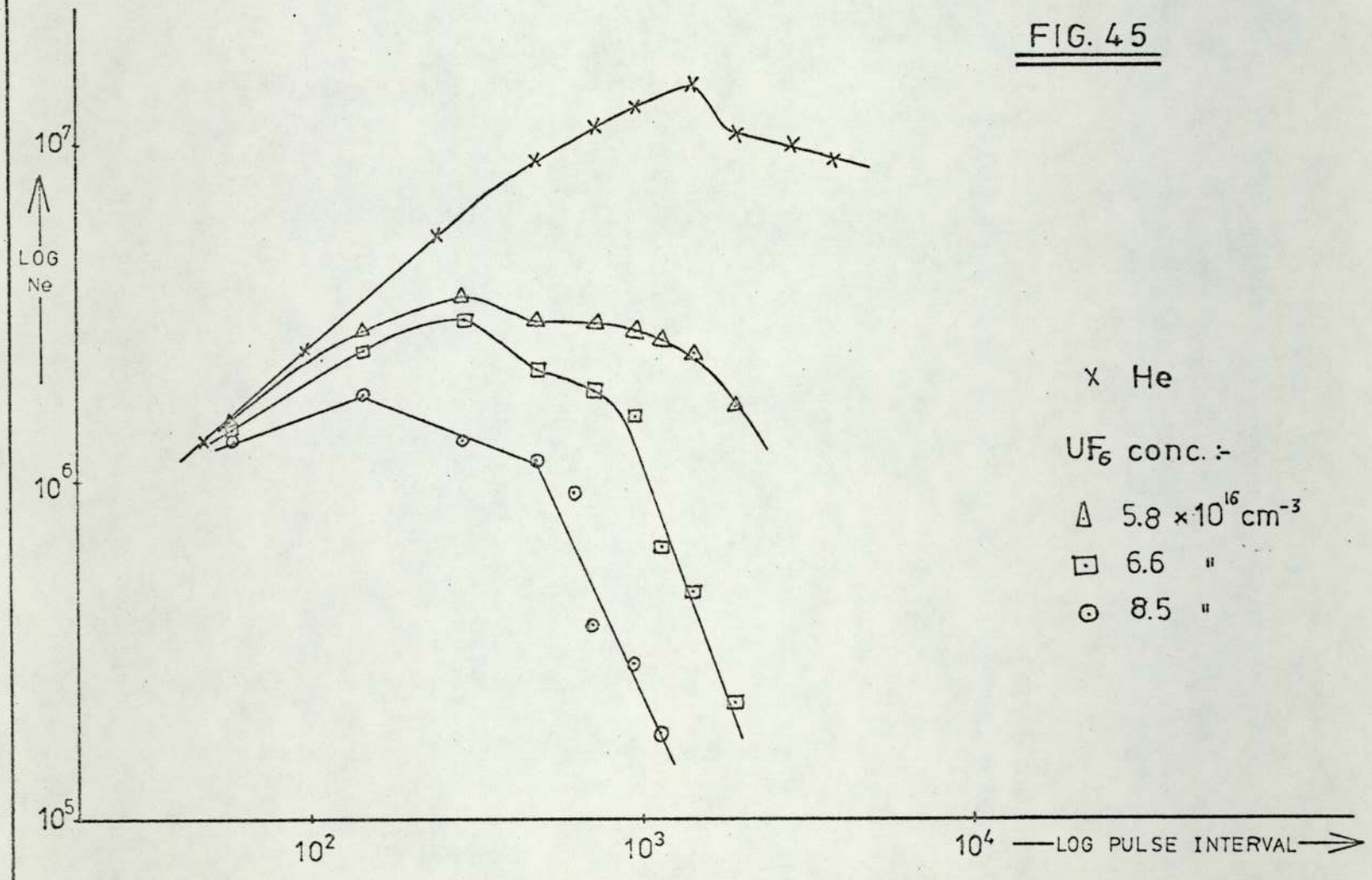

Ne - PULSE INTERVAL RELATION FOR HELIUM AND He + UF_6

leading to an highly capturing species as a product may well be responsible for this observation.

The flow rate which is inversely proportional to the concentration of UF_6 introduced, varies linearly with Ne (Fig. 46). Hence, a linear relationship exists between detector response and sample concentration. Basing the calculation on Lovelock's 'stirred reactor model', the capture rate constant for UF_6 is about 5.1×10^{-14} cm^3 $molecules^{-1}$ sec^{-1}. Table 7 shows the values obtained with two different sample concentrations. In comparision to the capture rate constant for SF_6 (approximately 2.5×10^{-7} cm^3 s^{-1}) the value obtained for UF_6 is very small. Stockdale and Compton[63] have shown that direct electron attachment in UF_6 is absent and this probably explains the low capture rate constant.

The need for a carrier gas free of electron capturing impurities has always been recognised. The presence of trace levels of oxygen in the carrier have been shown (59) to reduce the standing current to less than half its maximum value. However, the presence of water has been a controversial issue as both its effects and non-effects have been reported[7]. It is of practical importance to know its effect on the ECD response as many GLC samples are either prepared or present in an aqueous media. The presence of small quantities of water vapour in the detector may also facilitate the determination of the electron-ion recombination coefficient for H_3O^+ ion.

The apparatus used for the purpose was the same as that described for the introduction of UF_6 in the carrier gas stream. The saturator was filled with 10 cm^3 of boiled distilled water and a fraction of the gas stream was bubbled through it. With the saturator at a temperature of $0.5^{\circ}C$, the amount of water vapour present ($\simeq$ 4.75 mm. Hg. pressure) reduced the standing current by 25%. To

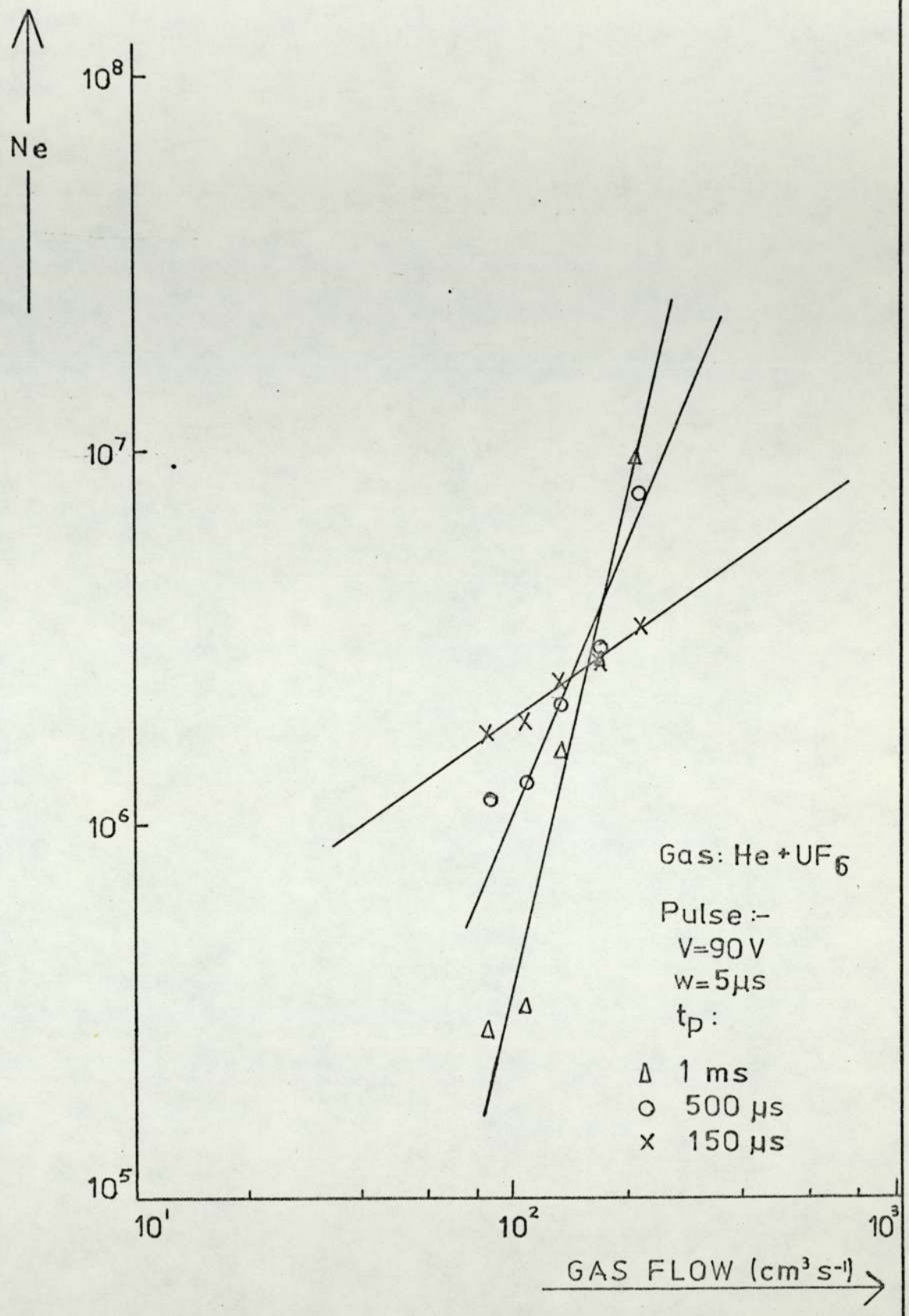

FIG. 46

VARIATION OF Ne WITH GAS FLOW RATE THROUGH SATURATOR CONTAING UF_6

TABLE 7

CAPTURE RATE CONSTANT FOR UF_6 AT DIFFERENT SAMPLE CONCENTRATION

FLOW RATE	CONCENTRATION	PSEUDO RECOMBINATION COEFFICIENT	CAPTURE RATE CONST.
2.9 cm^3 s^{-1}	5.8 x 10^{16} cm^{-3}	2.86 x 10^3 s^{-1}	4.9x10^{-14} $cm^3 s^{-1}$
2.3 cm^3 s^{-1}	6.6 x 10^{16} cm^{-3}	3.47 x 10^3 s^{-1}	5.1x10^{-14} $cm^3 s^{-1}$

decrease the concentration further, a mixture of sodium sulphate (anhydrous + decahydrate) was used instead. Equilibrium established between the two states at different temperatures[64] gives varying H_2O vapour pressure and is expressed by

$$\log P = - \frac{2837.83}{T} + 10.7866$$

where P is the vapour pressure in mm. of Hg and T is the absolute temperature. Glasstone[65] points out that a salt-hydrate system requires the presence of two solid phases in addition to vapour; the vapour pressure for the system is then definite and independent of the relative amounts of the two hydrates. In $Na_2 SO_4$ the dehydration proceeds gradually to completion without the appearance of intermediary hydrates.

To saturate the carrier gas with water vapour, it was allowed to filter through the salt mixture. Also for conditions to normalise in the detector, the gas was passed through the cell for about 3 hours before taking the first readings. $Al_2 O_3$ traps at the end of the gas line confirmed the presence of water vapour in the carrier gas stream.

Fig. (47) shows the variation of Ne with the pulse interval. It is clear from the graph that G.C. operators working at a pulse interval of about 500 μs would observe a negligible change in the standing current at very low water vapour concentrations. The effect is more pronounced at long pulse periods. The observed variation is very similar to that reported by Wiel and Tommassen[59] for the presence of oxygen in the carrier gas stream. They also noted that water concentration in their investigation was 3 p.p.m. and that although electron attachment in water is negligible[66], reference has been made to electron capturing properties of water[67]. Karasek and Kane[68], using the technique of plasma chromatography have identified $(H_2O)n\ O_2^-$ and $(H_2O)n\ H^+$ as the predominant ions when trace amounts of air is present in the carrier gas. The formation of positive species in nitrogen containing small concentrations of water vapour have been studied by Good

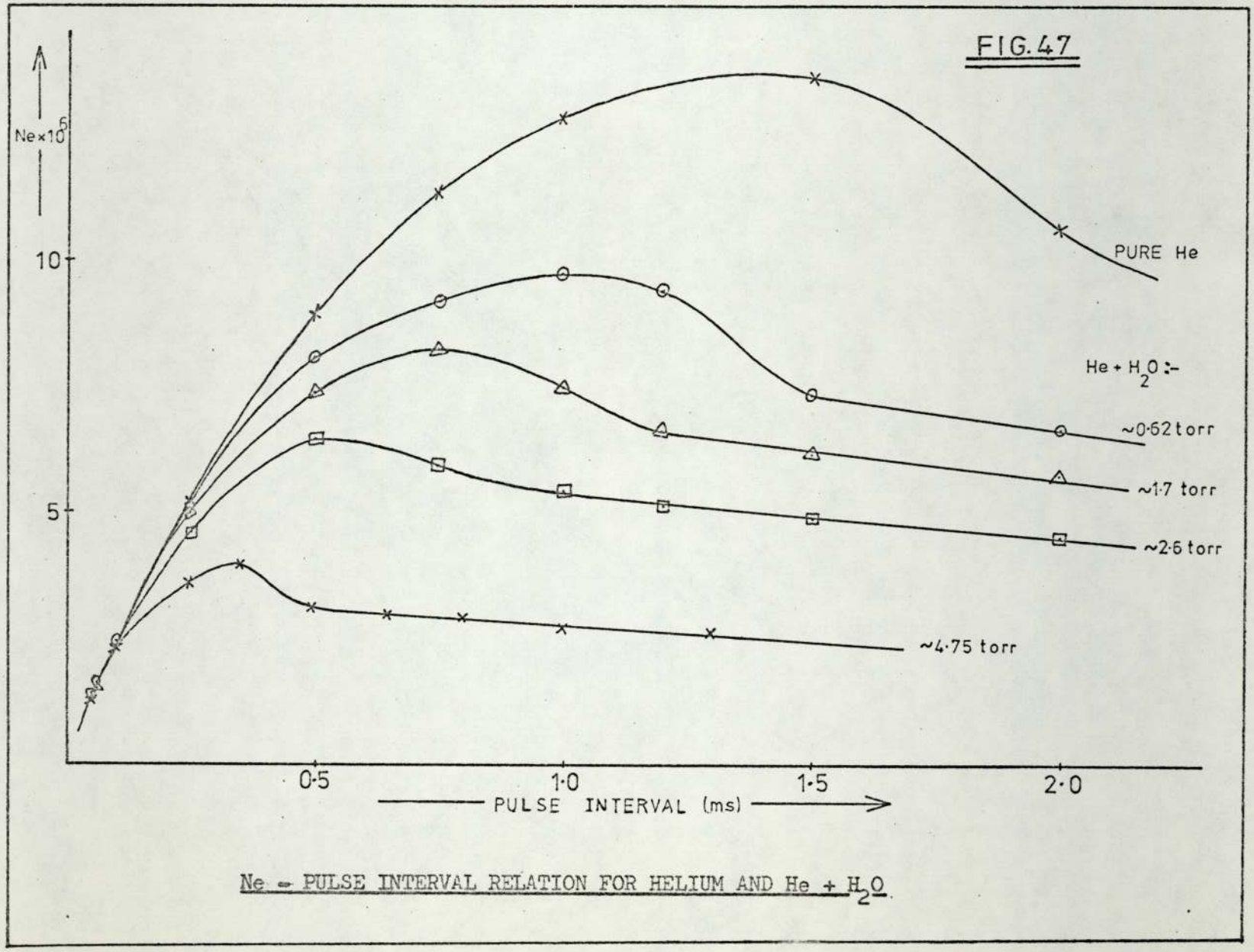

Ne - PULSE INTERVAL RELATION FOR HELIUM AND He + H_2O.

et al.[69] Based on their schematic outline of the reactions occurring, the following step reactions can be proposed for moist helium:

$$He_2^+ + H_2O \longrightarrow H_2O^+ + 2He$$

$$H_2O^+ + H_2O \longrightarrow H_3O^+ + OH$$

$$H_3O^+ + H_2O + He \longrightarrow H^+(H_2O)_2 + He$$

It appears that both in the present work and in Tommassen's the predominant negative ion is $(H_2O)n\ O_2^-$, thus explaining the similarity in the observations made.

The capture rate constant (k_1) for the water clustered oxygen ion is estimated to be about 1×10^{-13} cm^3 s^{-1}. As in the case of UF_6, the calculation is based on Lovelock's stirred reactor model[42] and properties of the holomorphic function; $k_d = 2 \times 10^3$ s^{-1} and $C = 2.15 \times 10^{16}$ molecules cm^{-3} (for $P_{H_2O} = 0.62$ torr), whereby $k_1 \simeq k_d / C$. The value obtained is of the right order of magnitude when compared with that given for oxygen by Hasted.[22]

A systematic series of investigations of the ionisation in pre-mixed $H_2 + O_2 + N_2$ flames has been made over a considerable period.[70, 71] In the presence of even a small hydrocarbon impurity, the main positive ion produced is H_3O^+. It is also a major ion (besides NO^+) in the lower levels of the ionosphere. At atmospheric pressure, the recombination coefficient for

$$H_3O^+ + e^- \longrightarrow H_2O + H$$

has been found to be $2.2 \pm 1.0 \times 10^{-7}$ cm^3 s^{-1}. This value was obtained by Green and Sugden[72] from measurements made in flames at temperatures around 2000 K. There is some controversy as to whether the recombination coefficient for H_3O^+ is temperature dependent or not. The proposed model for the ECD does allow the

rate constant to be evaluated from the response observed when small amounts of water vapour are introduced in the carrier gas at room temperature. Helium was chosen as the carrier gas because of its very low recombination coefficient.

The positive ion mobility can be assumed to be about 4 cm^2 V^{-1} s^{-1}. For the slightly heavier negative species, $(H_2O)O_2^-$, the mobility has been reported to be about 2.9 cm^2 V^{-1} s^{-1} (68). The mean value for the 'Gaines factor', R, is then 1.90×10^2. The value of Ne at s = 1.3 ms is 6.3×10^6 electrons per pulse for the case where the water vapour pressure is 1.7 torr. The recombination coefficient, k_2, for H_3O^+ (presumably) is $3.6 \pm 1.0 \times 10^{-6}$ cm^3 s^{-1}, calculated from Eq. [45].

Measurement of the rate constant at different flame temperatures(81) showed that it had little or no temperature dependence. However, as pointed out in section 3.2, Thomson's theory of three-body recombination(35) predicts a $T^{-3/2}$ dependence at gas pressures between 700 and 1000 torr. Jensen and Padley(82) have shown that the recombination coefficient for reactions involving alkali metal ions and electrons is temperature dependent in accordance with Thomson's theory. Hasted(22) too, points out that recombination processes involving inert gas ions (Ne_2^+ and Ar_2^+) and electrons show a $T^{-3/2}$ dependence but only at higher electron temperatures. The possibility of H_3O^+ behaving in a similar way was thus considered.

Using Green and Sugden's value of the recombination coefficient ar 2100 K(72) and assuming a power dependence of (-3/2) for the temperature, the recombination rate constant for H_3O^+ ion at 300 K would be,

$$k_{2(300)} = (2.2 \times 10^{-7})\ cm^3\ s^{-1} \cdot \left[\frac{300\ K}{2100K}\right]^{-3/2}$$

$$= 4.1 \times 10^{-6}\ cm^3\ s^{-1}$$

This value compares very well with that obtained in the present study. Hence, the rate constant for the reaction

$$H_3O^+ + e^- \longrightarrow H_2O + H$$

appears to be $T^{-3/2}$ power dependent as with other electron - ion reactions indicated above.

CHAPTER FIVE - EXPERIMENTAL VERIFICATION OF ASSUMPTIONS

Many of the assumptions made in theoretical models of the ECD (outlined in section 3.3) have been justified to some extent on the basis of information obtained from experiments where parameters of the applied voltage source were varied. Other experimental methods, to confirm these assumptions, were investigated.

5.1. OSCILLOGRAPHIC STUDIES

Electrons resulting from ionisation of gas molecules are assumed to be highly energetic initially but to lose energy rapidly upon collisions until their average energy is thermal. Calculations [18] of the time taken by electrons to reach thermal energy show that it is well within the normal applied pulse time. An oscilloscope trace of individual current pulses could provide further information.

The circuit (Fig. 48) used consisted of two cells of identical geometry connected in parallel. However, only one cell was equipped with a radiation source; the other cell, with two plane electrodes, acted as a dummy to offset any capacitance effect arising from the cell body. Rectangular pulses were applied to both and the resulting signals were fed into an oscilloscope with a high gain differential amplifier. The oscilloscope was Teleequipment's model 43 equipped with type B amplifier.

It was not possible to amplify sufficiently the output signal obtained under normal operating conditions, ie. $w = 5\ \mu s$ and $s = 1$ ms. Hence, traces were obtained under the following pulse conditions: $w = 8$ ms, $s = 98$ ms and $V = 30$ Volts. Photographs one to six show the observed current pulse when the cell separation is increased from 0.2 cm, 0.65 cm, 0.85 cm, 1.05 cm and

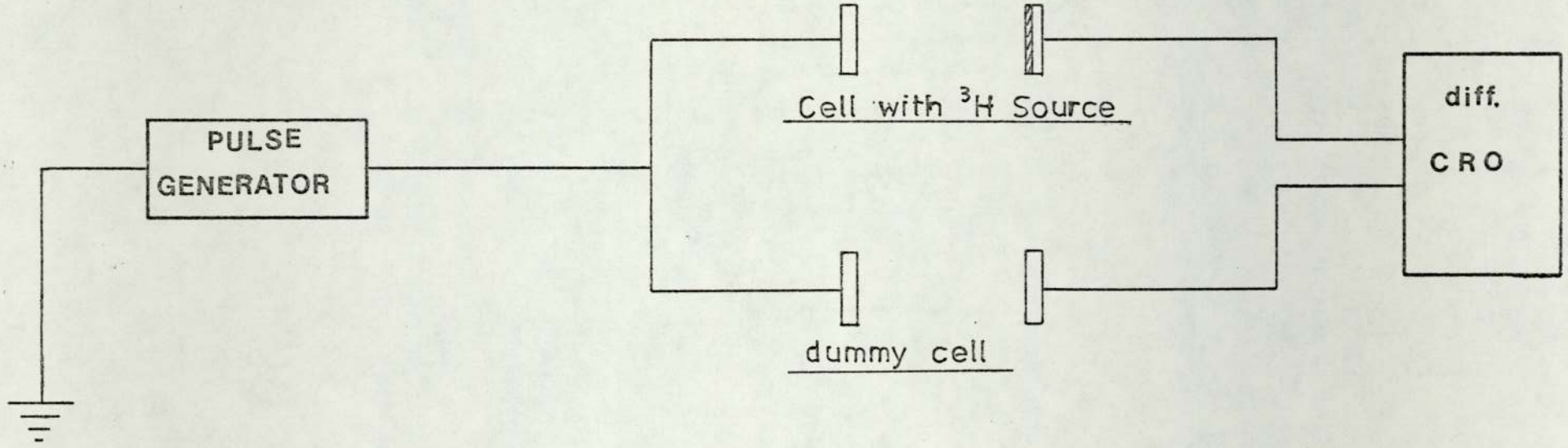

FIG.48

ELECTRICAL CIRCUIT FOR OSCILLOGRAPHIC STUDIES

OSCILLOSCOPE TRACES OF CURRENT PULSE

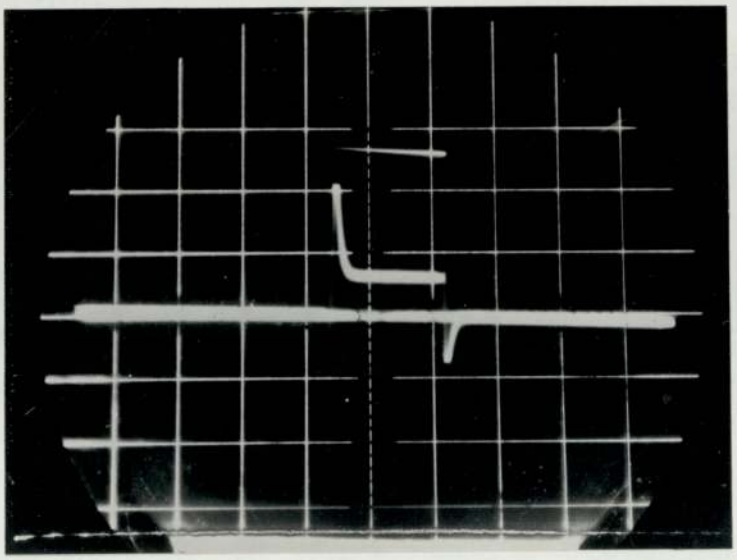

PHOTOGRAPH ONE: electrode separation = 0.2cm

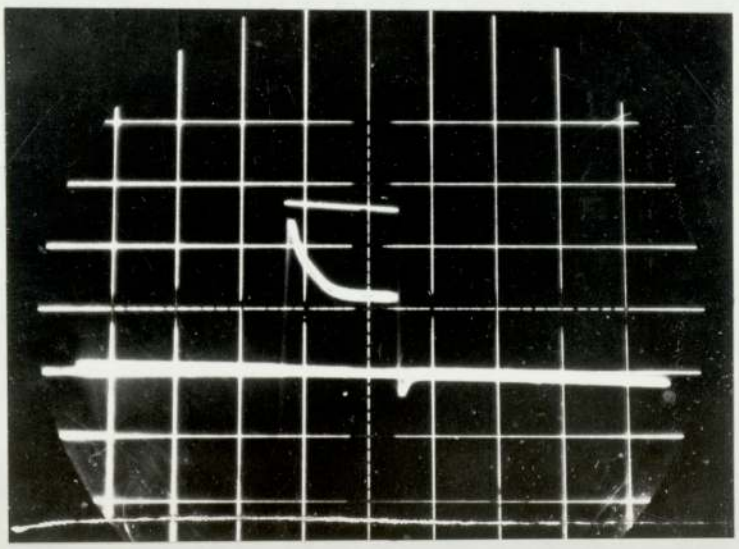

PHOTOGRAPH TWO: electrode separation = 0.45cm

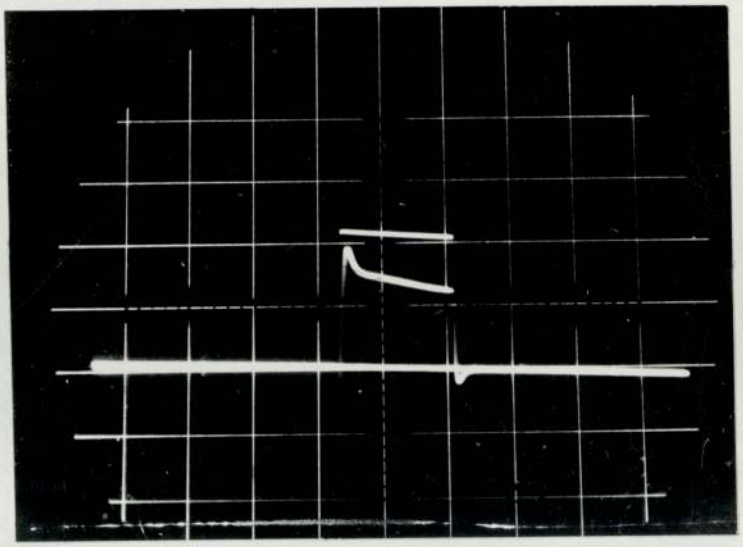

PHOTOGRAPH THREE: electrode separation= 0.65cm

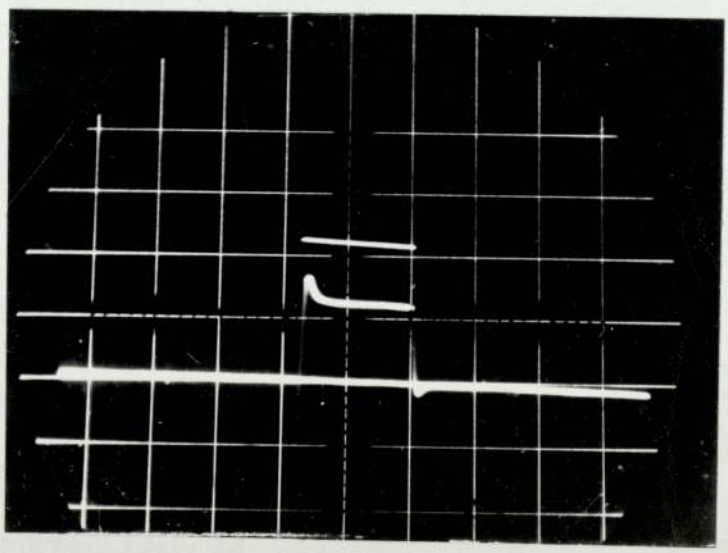

PHOTOGRAPH FOUR: electrode separation = 0.85cm

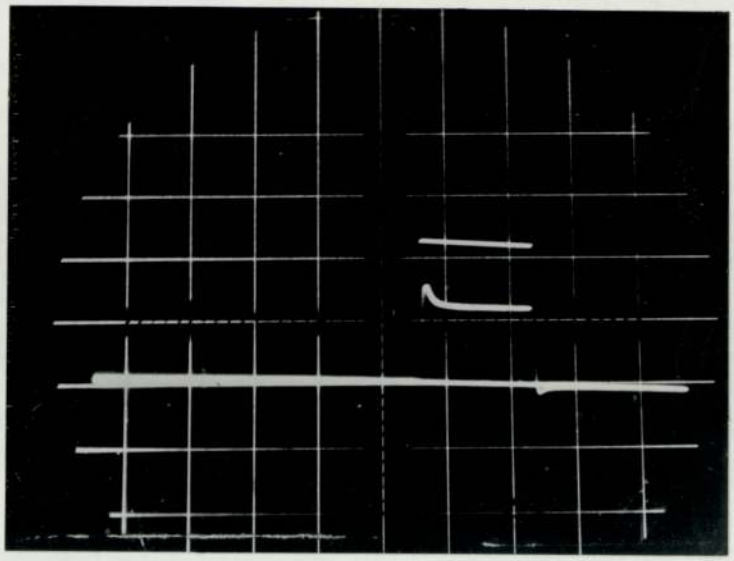

PHOTOGRAPH FIVE: electrode separation = I.05cm

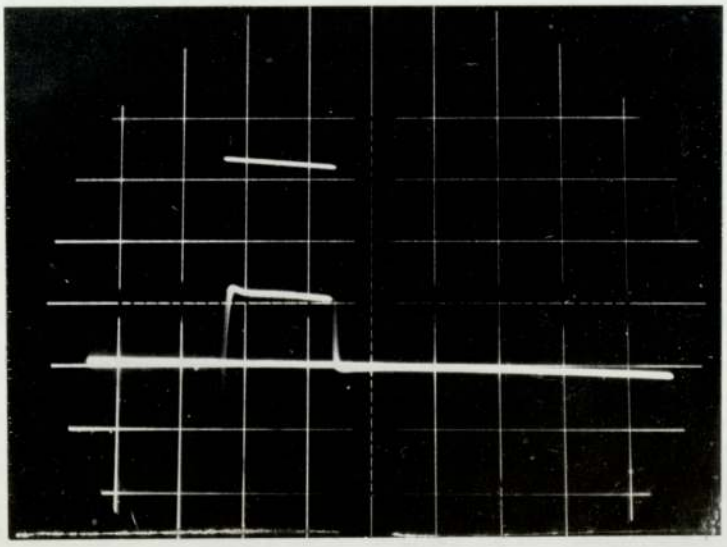

PHOTOGRAPH SIX: electrode separation = I.45cm

1.45 cm. The gas flowing through the cells was nitrogen at a flow rate of 3.6 cm^3 s^{-1}. The Y - base was set at 5 mV cm^{-1} and the time-base sweep was 5 ms cm^{-1} for all cell separations except l = 0.2 cm where the Y-base was 10 mV cm^{-1}.

The effect of decreasing the pulse width from 8 to 1.9 ms was to shorten the width of the output pulse. The initial peak was not affected. The height of the observed pulse began to decrease when the pulse amplitude was lower than 20 Volts (at l = 0.85 cm).

The height of the pulse represents the current flowing through the circuit. Table 8 compares the measured current with that calculated from the pulse height at various inter-electrode separations. The input resistance of the oscilloscope was 10 MΩ . The height cannot be measured accurately when the top of the pulse is not horizontal and consequently there is a small difference in the magnitudes of the two currents.

The photographs indicate a very short delay time and a rise time of about 0.26 ms. This is quite small (3.2%) when compared with the applied pulse time. Hence, the current pulse can be said to be rectangular indicating that the electrons collected are of similar energy. The top of the pulse represents the time of arrival of the slowest electrons. A more rounded pulse would have indicated a broad energy spectrum for the electrons in the cell. The time constant of the circuit, calculated from photograph 2 is about 1.8 ms which is sufficiently long to allow collection of slow electrons. The oscilloscope traces show that the electrons have a reasonably narrow energy distribution; the average energy is likely to be about thermal.

As stated earlier, the width of the current pulse decreased as the applied pulse time was made shorter. Only at very small pulse

TABLE 8

COMPARISION OF THE MEASURED CURRENT WITH THAT CALCULATED FROM THE PULSE HEIGHT IN PHOTOGRAPHS 1 – 6

PHOTOGRAPH NUMBER	PULSE HEIGHT	CURRENT ($X10^{-10}$ A)	
		CALCULATED	MEASURED
1	0.55 cm	1.40	1.40
2	1.05 cm	5.25	5.20
3	1.23 cm	6.15	5.85
4	1.10 cm	5.50	5.60
5	1.05 cm	5.25	5.40
6	0.95 cm	4.75	4.95

width (< 1ms), did the height of the current pulse decrease. This would seem to indicate that all electrons present in the cell are collected as they only require a few microseconds to traverse the cell. As a first approximation, electrons farthest from the anode (10 mm. away) would only take about three times the time taken by electrons closest to the electrode to be collected. Hence, the collection of charged particles is completed in the initial upsurge of the observed current pulse.

Output pulses from a circuit consisting of a coupling capacitor and an input impedance (Fig. 49) have similar characteristics to the current pulses observed in the present study. The tail of the electron pulse represents the natural decay of the RC network at the amplifier input.[73] The coupling capacitor determines the tilt or droop of the horizontal section of the waveform, seen in the photographs. If the input voltage pulse is Vi and the output voltage Vo, then the two are related by,

$$\frac{dVi}{dt} - \frac{dVo}{dt} = \frac{Vo}{RC}$$

For a rectangular pulse input, the solution of the above equation is $Vo = V \cdot \exp - (W / RC)$ where V is the applied pulse amplitude and W it the pulse width.[74] The above equation predicts a larger output voltage with increasing values of RC. Consequently, the tilt of the decay curve becomes increasingly horizontal. Hence, photographs of the electron pulse taken at small cell separations (0.2 and 0.45 cm) exhibit steeper decay curves than those taken at longer electrode spacings (0.65, 0.85 and 1.05 cm) where the charge density is high.

The oscilloscope traces have provided further data on the state of the electrons in the detector and have also aided in the interpretation of the measured current.

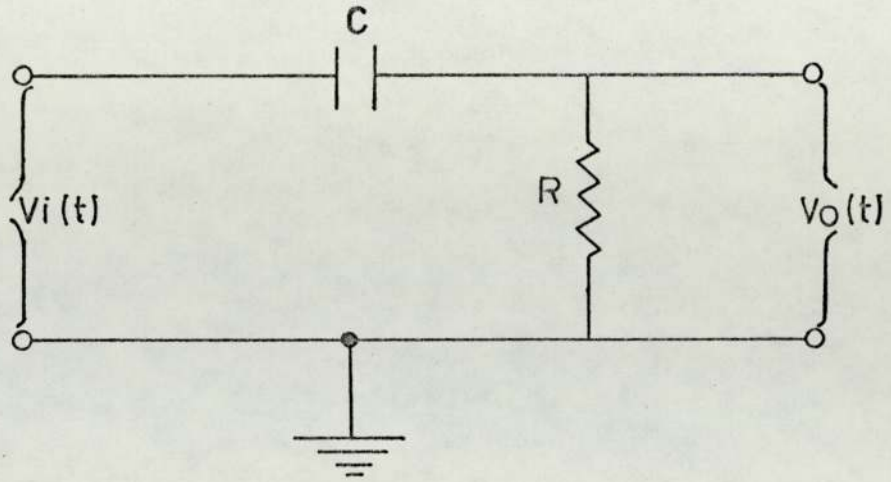

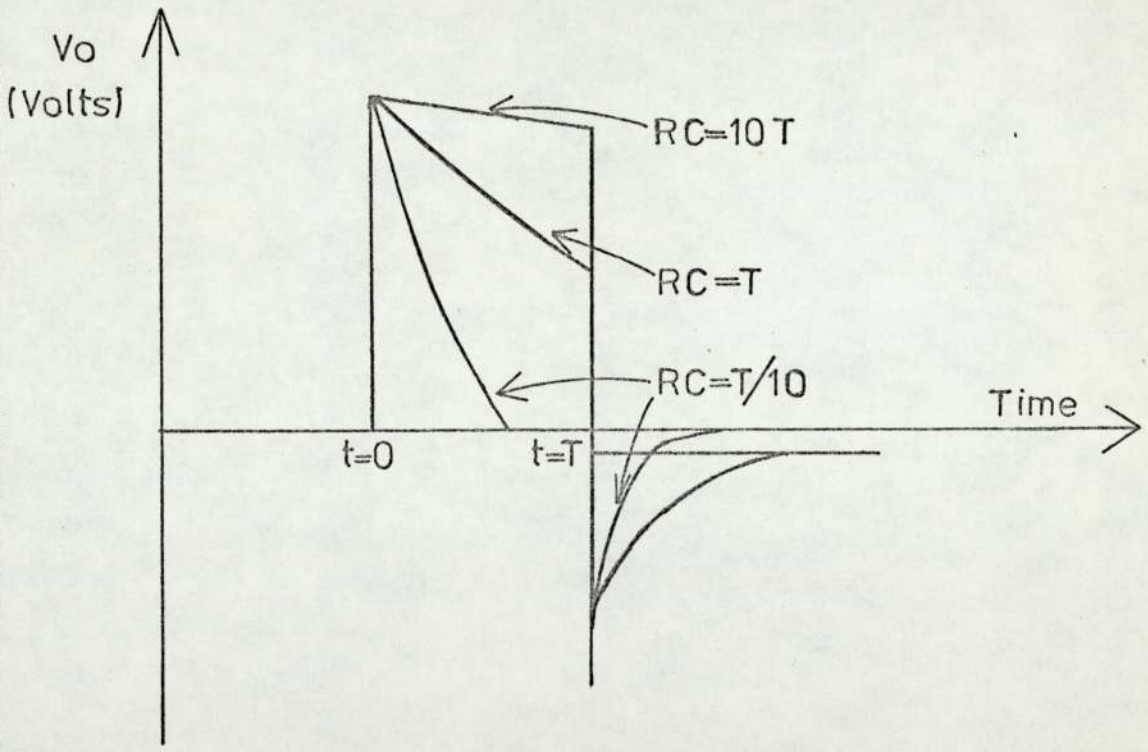

FIG. 49

DIFFERENTIATING CIRCUIT AND OUTPUT PULSE

5.2 PROBE STUDIES

The difference in electron and ion mobilities has been held responsible for the large excess of positive ions in the ECD. Kinetic analysis of the processes occurring in the cell becomes meaningful only when the concentration of positive species is considered to be about a thousand times greater than the free electron concentration. An attempt was thus made to determine the positive ion density in the cell using electrostatic probes.

Experimentally, electrostatic probes are simple devices consisting merely of an insulated wire (platinum) used with a d.c. power supply and an ammeter (Fig. 50). However, the theory of probes is extremely complicated. The difficulty stems from the fact that probes are boundaries to a plasma, and near the boundary the equations governing the motion of the ions in the plasma change their character.

The current drawn by a probe is a function of the charged species, the number density, the applied potential and local conditions around the probe surface. Fig. (51) shows the current-voltage graph obtained with a double-probe system. It has three distinct regions :

a) REGION AB

At large negative voltages, the current is relatively insensitive to the applied voltage and corresponds to positive ion saturation on probe 2. All electrons are repelled and an ion sheath surrounds the probe.

b) REGION BC

A transition region close to zero applied potential where the current changes rapidly with voltage due to the ability of electrons to approach both probes.[75] As the probe voltage is made less negative, some of the high energy electrons penetrate the ion sheath and reach the probe. The less negative the voltage relative to the

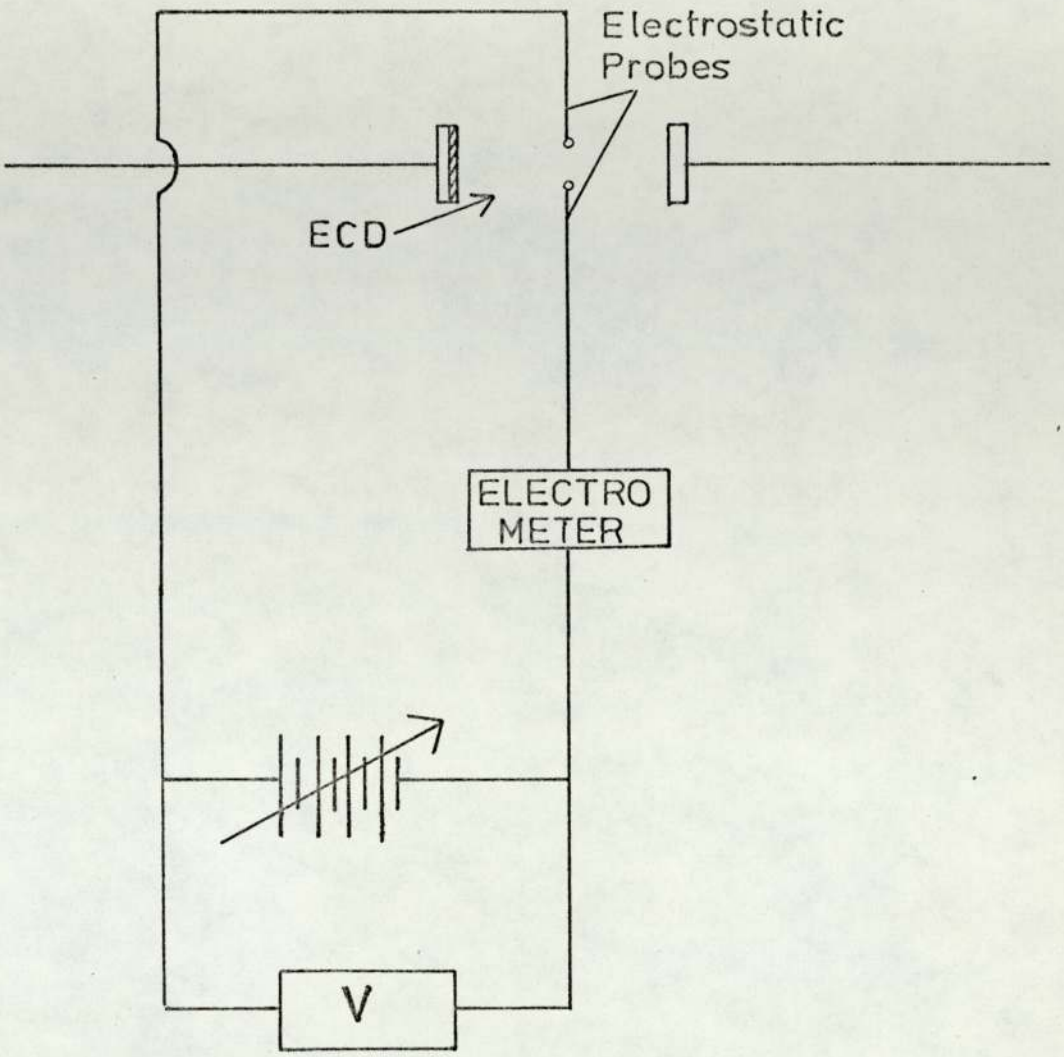

FIG.50

CIRCUIT DIAGRAM FOR A DOUBLE PROBE SYSTEM

plasma, the more electrons will have sufficient energy to overcome the retarding field. Thus, the current steadily increases.

c) REGION CD

A region at large positive voltages where the current is relatively independent of the applied voltage and corresponds to negative charge saturation on probe 1. If the probe voltage is made positive relative to the plasma, electrons are accelerated towards the probe. Near the probe surface there is therefore an excess of negative charge, which builds up until the total charge is equal to the positive charge on the probe.(76)

Johnson and Malter(77) developed the double probe technique. The operation of a double probe system is governed by two factors :

i. Kirchhoff's law that the total net current drawn by the probes is zero, ie. the electron current collected by the probes is always equal to the total positive ion current collected by them.

ii. The electron current to each probe is governed by the Boltzmann Law.

At high pressures ($>$ 1 mm Hg) a positive ion experiences many collisions with neutral molecules within the sheath surrounding the probe. Under these conditions the mean free path for the charged species is very much smaller than either the Debye length or the probe diameter. The effect istwo fold : first, the motion of the ions within the sheath becomes mobility controlled and secondly, a fraction of the ions entering the sheath is lost from the sheath due to the scattering.

The theoretical treatment of Su and Lam(78) has probably had the widest application to probe theory in high pressure, collision dominated plasmas. They determined the charge distribution

about a spherical probe using the continuity equations together with Poisson's equation making no assumptions regarding the presence of a boundary layer sheath.

A quantitative analysis of the results obtained has been made, using three different theories developed by workers[79] using electrostatic probes to measure positive ion concentrations in flames. Conclusions reached have to be treated with caution as it is assumed that the theories are generally applicable.

The circuit for the double probe system used is shown in Fig. (50). Current was measured on an AVO 1388 B d.c. amplifier. The ECD was not part of the probe circuit. Each probe consisted of a platinum wire enclosed in a glass tube (0.128 in. in diameter). The end of the wire was turned into a sphere of radius 2.9×10^{-4} m. Care had to be taken to ensure that the two probes had very similar areas. Studies were made with a slow flow of nitrogen through the cell and a fixed inter-electrode separation of 0.5 cm. Fig. (51) shows the current-voltage plot obtained. Analysis of results is as follows :

1) TRAVERS AND WILLIAMS APPROACH[75]

One assumption needs to be made; at high pressures, the positive ion current density reaching the edge of the sheath layer surrounding the probe is equal to the positive ion random current density in the plasma.

Within the sheath, the positive ion current, ip, at a radius r is given by,

$$ip = -4\pi r^2 N_+ e \mu_+ X$$

where, N+ is the positive ion density (m^{-3}) and μ_+ is the mobility of the positive ion. Substitution of Poisson's equation for charge density gives,

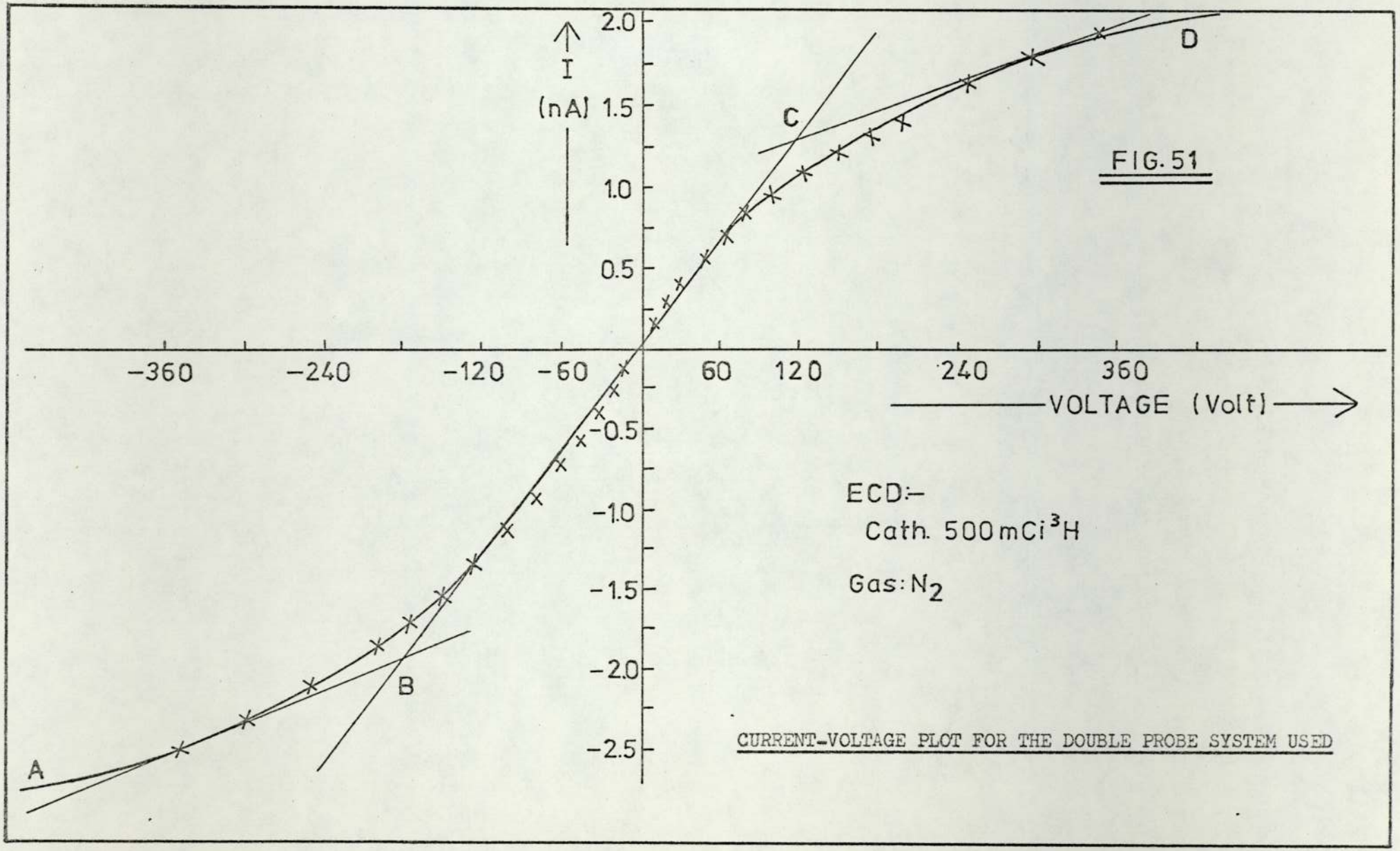

FIG. 51

CURRENT-VOLTAGE PLOT FOR THE DOUBLE PROBE SYSTEM USED

$$\frac{d^2V}{dr^2} + \frac{2}{r}\frac{dV}{dr} = \frac{-ip}{4\pi\mu_+ \varepsilon_o r^2 (dV/dr)}$$

Integrating once and applying boundary conditions that $dV/dr = 0$ at $r = \bar{a}$ (the sheath radius) leads to,

$$V = \left[\frac{ip}{6\pi\mu_+ \varepsilon_o}\right]^{1/2} \int \frac{(\bar{a}^3 - r^3)^{1/2}}{r^2}\, dr \qquad [47]$$

As no analytical solution of the above integral has been found, a numerical integration was performed between the limits $r = \bar{a}$ and $r = r_p$ for a range of values of the ratio $\bar{a} / r_p$ where r_p is the probe radius. To facilitate this, the integral was made non-dimensional by means of the substitution $x = r/\bar{a}$. Making this substitution the above integral becomes,

$$\bar{a}^{1/2} \int_{1/n}^{1} \frac{(1 - x^3)^{1/2}}{x^3}\, dx$$

where $n = \bar{a} / r_p$. Equation [47] can now be written as,

$$Vp = \left(\frac{ip}{6\pi\mu_+ \varepsilon_o}\right)^{1/2} (\bar{a}^{1/2} I) \qquad [48]$$

where Vp is onset potential for saturation currents and

$$I = \int_{1/n}^{1} \frac{(1 - x^3)^{1/2}}{x^3}\, dx$$

At Vp = 130 Volts, the positive ion current, ip, is the sum of the currents to probe 1 and 2, ie.

$$ip = ip_1 + ip_2 = (1.10 + 1.38)\ nA$$

$$= 2.48\ nA$$

Hence $(I\, \bar{a}^{1/2}) = 0.54$, calculated from Eq. [48]. The value of

$\bar{a}$ can be obtained from a graph of $(\bar{a}^{1/2} I)$ versus $\bar{a}$. Table 9 gives the values of I and $\bar{a}$, calculated from the probe radius. The value of $\bar{a}$ when $(I\bar{a}^{1/2}) = 0.54$ is 3.18×10^{-3} m. The time for an unscattered positive ion to cross the sheath is given by,

$$t_+ = \frac{1}{\mu_+} \left[\frac{2}{3} (\bar{a}^3 - r_p^3) \right]^{1/2} \frac{(\bar{a}^{1/2} I)}{V_p}$$

$$= 2.38 \times 10^{-3} \text{ s.}$$

The positive ion current, ip, can be expressed by,

$$ip = \frac{6\pi \bar{a}^2}{2\alpha} \frac{Jr}{P} \qquad [49]$$

where Jr is the positive ion random current density; α is the scattering coefficient ($torr^{-1}$) and P is the gas pressure. The value of α calculated from the collision frequency, ν_c and t_+ is,

$$\alpha = \frac{\nu_c t_+}{P} = 2.29 \times 10^{-4} \text{ torr}^{-1}$$

at atmospheric pressure. The random ion current density, Jr, calculated from Eq.[49] is 2.27×10^2 Am^{-2}. Jr can alternatively be expressed by

$$Jr = e N_+ \left(\frac{K T_+}{2\pi M_+} \right)^{1/2}$$

where T_+ is ion temperature (equal to the gas temperature) and M_+ is the mass of positive ion (N_4^+). Hence,

$$N_+ = \left(\frac{2\pi M_+}{K T_+} \right)^{1/2} \frac{Jr}{e}$$

$$N_+ = 1.70 \times 10^{13} \text{ cm}^{-3}$$

2) SU AND LAM APPROACH

The theory allows the determination of positive ion concent-

TABLE 9

NUMERICAL VALUES OF THE INTEGRAL I FOR VARIOUS VALUES OF $\bar{a}/r_p$

n	I	$\bar{a} = nr_p$	$I\ \bar{a}^{-1/2}$
1	0	2.90×10^{-4} m	0
2	0.770	5.80×10^{-4} m	1.86×10^{-2}
3	1.734	8.70×10^{-4} m	5.12×10^{-2}
4	2.722	11.60×10^{-4} m	9.28×10^{-2}
5	3.716	14.50×10^{-4} m	1.42×10^{-1}
6	4.713	17.40×10^{-4} m	1.97×10^{-1}
8	6.715	23.20×10^{-4} m	3.24×10^{-1}
10	8.716	29.0×10^{-4} m	4.70×10^{-1}

ration from the measurement of positive ion current drawn by a spherical probe operated at plasma potential. This is the potential where no sheath exists and hence the probe is at the same potential as the plasma. In the absence of any electric field at this point, charged particles migrate to the probe purely because of their thermal velocities. The plasma potential corresponds to that point on the graph (Fig. 51) where the regions BC and CD meet. The relation that expresses the positive ion concentration is,

$$N^+ = I^+ / (4 \pi r_p D^+ e) \qquad [50]$$

where D^+ is the positive ion diffusion coefficient and I^+ is the positive ion current at plasma potential. The values are :

$D^+ = 6.2 \times 10^{-6}$ m^2 s^{-1} (for N_2^+)[11] and $I^+ = 1.65$ nA at $V = -162$ Volts. Hence, the ion density is 4.56×10^{11} cm^{-3}.

3) BOHM, BURHOP AND MASSEY'S APPROACH[76,80]

In the case of spherical probes and in the limit $\lambda \ll r_p$.

$$I^+ = \frac{n+ \bar{v} Ap}{4} \quad \frac{3 \lambda e}{4 r_p} \qquad [51]$$

The mean free path, λ, ($\simeq 10^{-6}$ cm) is very much smaller than the probe radius, $r_p \simeq 10^{-2}$ cm. $\bar{v}$ is the average magnitude of the thermal velocity and is calculated from the kinetic theory. The probe area, $Ap = 4 \pi r_p^2$. I^+ is as defined previously. The positive ion concentration is given by,

$$N+ = \frac{4 I^+}{3 \bar{v} \pi r_p \lambda e}$$

$$N+ = 4.9 \times 10^{11} \text{ cm}^{-3}$$

The Travers and Williams approach has been found to give a value of N+ one or two orders of magnitude higher than that obtain-

ed with other theories.[79] There is very good agreement between the other two values obtained and hence the positive ion concentration in the detector (for nitrogen) can be said to be about 4.7 x 10^{11} cm^{-3}. A typical current density of about 10^{-10} A gives an electron concentration of 1.6 x 10^{9} cm^{-3}. Hence, the Gaines factor, as the ratio of positive ions to electrons is 3 x 10^{2}; this is comparable to the mean value of R (3.4 x 10^{2}) calculated from the values given in Table (6).

5.3 FLOW OUTLET CURRENT

Carrier gas flow has been considered to be a plausible mode of loss for positive ions in the cell. It would lead to an increase in free electron concentration as losses through volume recombination diminish. The time constant for removal of ions through flow is comparable to that of other processes responsible for the loss of positive ions from the cell (as shown in section 4.6). Wentworth et al.,[18] assumed that there was slow removal of material from the detector by flow of the carrier gas. They attributed the observed peak in the graph of (Ne versus s) to a change in the mechanism by which positive ions were removed from the detector. Lyons et al.,[39] suggested that the concentration of positive ions was inversely proportional to the gas flow rate. However, no experimental evidence was presented in either of these studies and so an attempt was made to verify experimentally whether carrier gas flow was a possible mode of loss for positive ions in the cell.

An electrometer was connected to the gas outlet which as described in section 4.1, was a brass tubing threaded half way through the cell body. The electrical contact was insulated by a PTFE sleeve. An external source of potential was not included as this would have introduced additional difficulties in interpretat-

ing the current. The electrometer was thus floating, ie. it could assume a potential positive or negative with respect to the cell potential. The ECD was operated in the normal way and its response was not affected by the current measured on the gas outlet.

Figures (52) and (53) show the variation in this current with d.c voltage as applied to the detector. The cell length was also varied. It is to be noted that a high gas flow rate (4.7 cm^3 s^{-1}) was used in these experiments. The current measured on the gas outlet is a function of the applied potential as an electric field exists between one of the cell electrodes and the gas outflow tube. Hence, at low potentials, the current increases and when at high potentials the current flowing in the ECD circuit reaches its plateau value (indicating the collection of all charged species in the cell), the current measured on the gas outlet decreases. The decrease in the field intensity between one of the cell electrodes and the gas outflow tube is also responsible for the observed decrease in current (at a given voltage) with increasing inter-electrode spacing. At cell separations greater than 1 cm, the polarity of the electrodes seems to be reversed and consequently the sign of the current changes.

The current measured on the gas outlet also varied with the carrier gas flow rate (Fig. 54). The graph shows that at low flow rates (20 cm^3 min^{-1}) the current measured is very small but it increases ten fold when the gas flow is 180 cm^3 min^{-1}. In the pulsed mode, at short pulse periods, the current increases steeply to a maximum; thereafter it declines gradually to a steady level at long pulse interval.

The current measured on the outflow tube could either be due to electrons or positive ions being removed from the cell by carrier gas flow. It cannot be the former because, as Lovelock[42] has

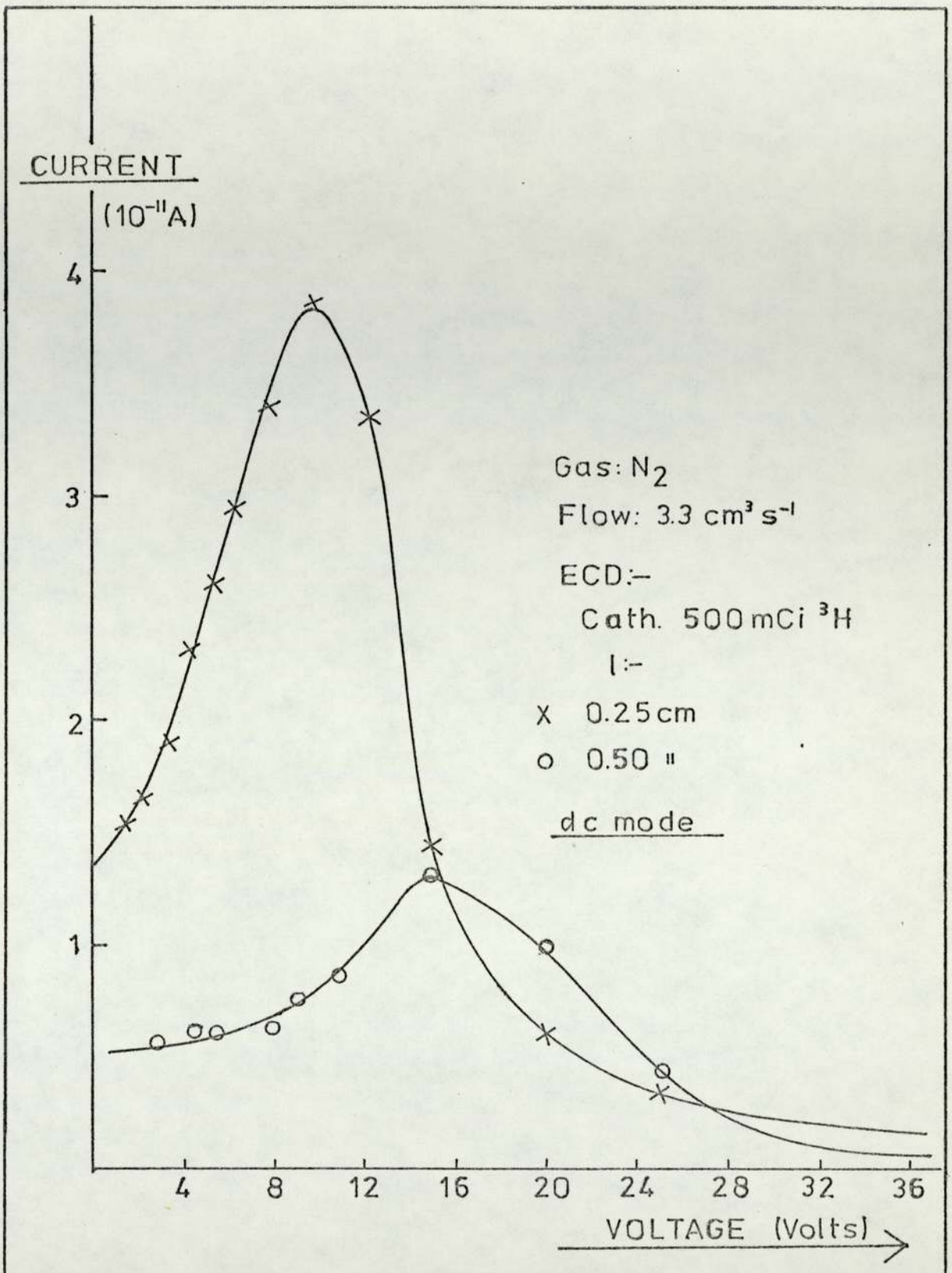

FIG. 52

VARIATION OF CURRENT (MEASURED ON GAS OUTLET) WITH DETECTOR VOLTAGE

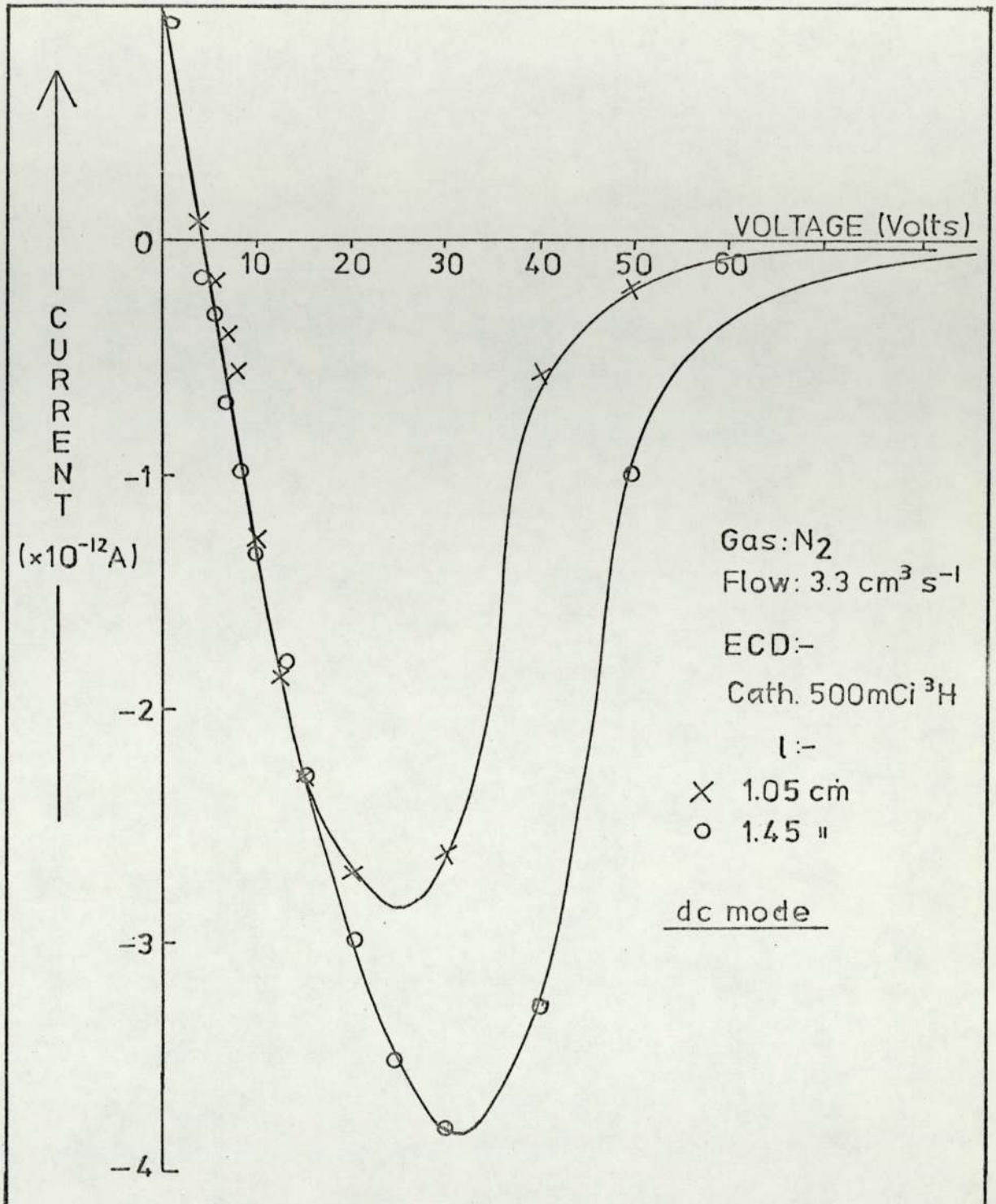

FIG. 53

VARIATION OF CURRENT (MEASURED ON GAS OUTLET) WITH DETECTOR VOLTAGE

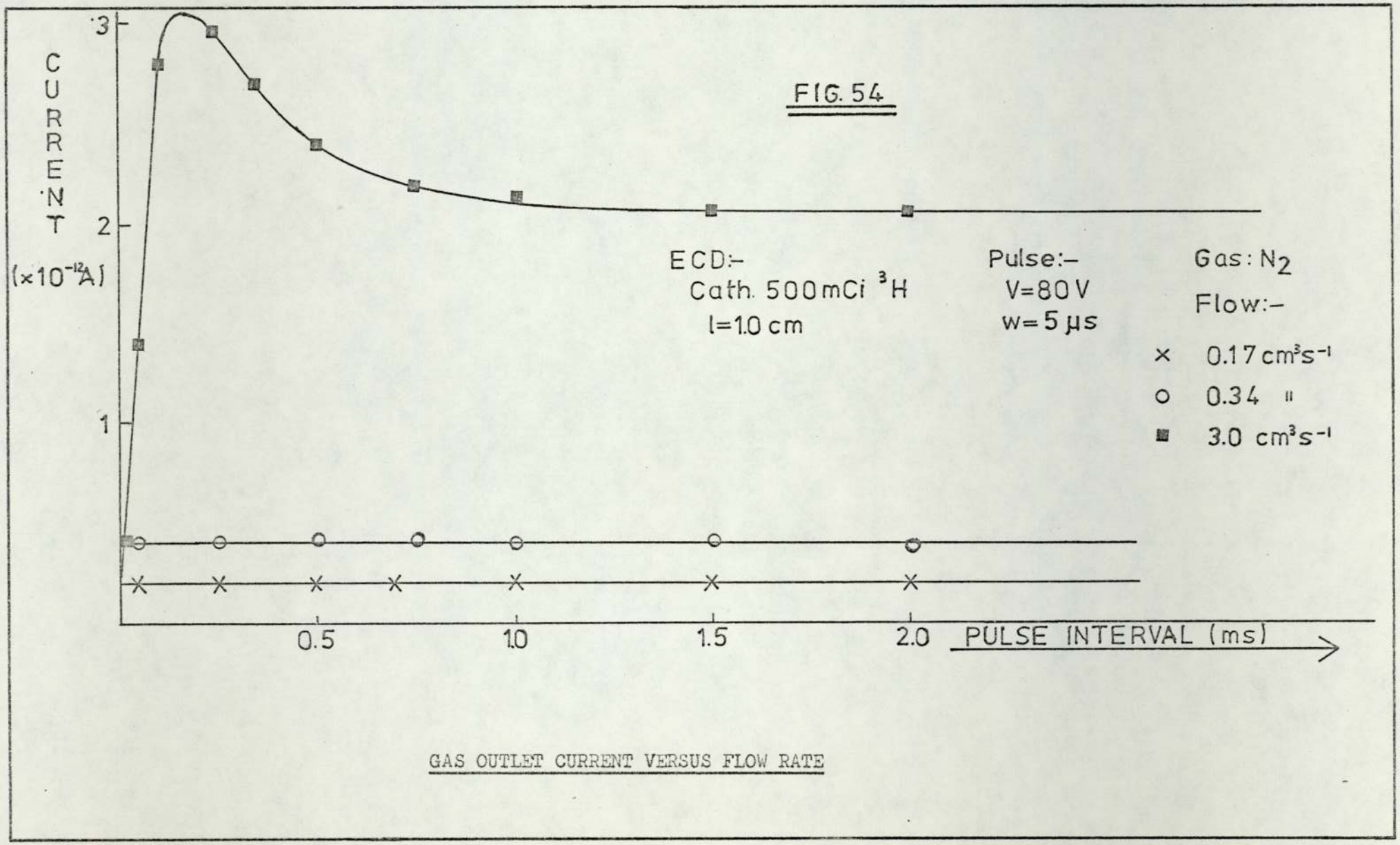

GAS OUTLET CURRENT VERSUS FLOW RATE

pointed out, the residence time of electrons within the detector is too short for a sensible proportion of them to leave the cell in the carrier gas stream. The magnitude of the measured current (10^{-12} to 10^{-11} A) is also rather large for it to be an 'electron current.

The directional drift imposed on the positive ions by the applied field does not significantly alter the residence time of the ions. Their velocity will be comparable to that of gas molecules and hence, the observed current is probably due to the removal of positive species from the cell by gas flow. It can also be concluded from Fig. (54) that at short pulse periods and in the d.c. mode both negative and positive species contribute to the ECD current and at long pulse periods there seems to be a steady removal of positive ions from the cell when the gas flow rate is high.

CHAPTER SIX - CONCLUSION

During the past fifteen years, a fundamental understanding of electron capture detection has been gradually developing. This study has been a further attempt to relate the detector's response to operating parameters and also to detector characteristics. The instrument's potential use as a means of investigating electron-ion processes at normal temperature and pressure has also been put to test. A theory of the detector has been developed to assist in this account and to generally predict the observed signal.

A detector of cylindrical geometry with variable electrode spacing enabled the depth of the reaction zone to be determined. Results obtained with a ^{63}Ni source supported the normally accepted value of about 9 mm. for the range of β^- particles. With ^{3}H sources, the reaction zone seems to extend to about 6.5 mm. from the source and hence does not support the value of 2mm. quoted by Wentworth et. al.,[18] The range-energy relationship showed that the range of average energy β^- particles is about 2 mm. However, in the ECD, it appears that high energy Beta particles are responsible for ionisation, thereby extending the reaction zone to about 6.5 mm. with the normal carrier gases flowing through the cell.

The gas pressure is expected to alter the range of β^- particles and consequently the plasma volume and the degree of ionisation. Results obtained confirmed theoretical predictions that the current should vary linearly with gas pressure when the range of β^- particles is greater than the cell length (at very low pressures) and be independent of pressure when the electrode spacing exceeds the path length.

Studies carried out with two sources of different activities (500 mCi and 150 mCi ^{3}H) showed that the ratio of the observed currents for the two foils depended very much on the characteristics

of the applied potential. In the pulsed mode of operation, at long pulse interval, the ratio was nearly the same as that of the two activities but at short pulse period and in the d.c. mode, the current ratio was about one half the theoretical ratio of the activities. Strong space charge effects, under the latter conditions, could probably be responsible for reducing the current from the 500 mCi source.

The carrier gas flow has been shown to have two effects on the processes occurring in the cell. Firstly, a high gas flow rate tends to diffuse the plasma and hence effect better mixing; secondly, it seems to remove positive ions from the cell at a steady rate. The current variation with electrode spacing in a cell of assymmetric configuration showed that even at large electrode separations ($>$ 1 cm), the current remained very close to its maximum value. This would seem to indicate that the vortices in the flow pattern have dispersed the charged species over a much larger volume than the space in the vicinity of the cathode and consequently more charges were collected during the applied pulse time (w).

The residence time for gas molecules, at high gas flow rates, has been shown to be comparable to the time constants for processes removing positive ions from the cell, ie. volume recombination and surface recombination at the cathode. Experimental evidence included the measurement of a current on the gas outlet. This current was inferred to be due to positive ions since electrons could not be removed from the cell as their residence time is too short for a sufficient number to leave the detector and thus account for the measured current. At long pulse interval the current on the outflow tube reached a steady level, possibly indicating a constant removal of material in the high flow region, where the ECD standing current is independent of carrier gas flow.

Analysis of the current variation with flow of carrier gas is complicated by the presence of a capturing impurity in the gas line. Besides enhancing the diffusion of the plasma and removal of positive species from the cell, a higher gas flow also decreases the concentration of the contaminant, leading to an increase in current. Large changes in standing current with gas flow seem to indicate a predominant effect of the latter as a gas line suspected of leakage showed.

The ECD was used in both the d.c. and pulsed modes of operation. In the former mode, the standing current has been shown to be proportional to V^2 and inversely proportional to l^3 at reasonably high gas flow rates ($> 1\ cm^3\ s^{-1}$).

Kinetic analysis of the detector's response in the d.c. mode, based on the proposed model, has been attempted; however, the agreement was not very good. It is difficult to make reasonable assumptions concerning the various processes occurring in the cell under this mode as it has inherent sources of error: the electron energy distribution is likely to be higher than thermal; a relatively dense space charge may oppose applied potential and absorption of material on electrodes gives rise to contact potentials. The detector could also respond to other parameters of the sample besides electron attachment. The use of the detector in the d.c. mode, at least for routine chemical analysis, is to be avoided.

The pulsed mode of operation was suggested by Lovelock[12] to avoid many of the problems faced in the d.c. mode. In literature reviews,[7,61] the interpretation of the detector response and the physical state in the cell under the pulsed mode, are often not clearly stated or even on occasions erroneous.

The observed current is attributed to the collection of free electrons only and the contribution of positive ions is said

to be negligible. Results obtained in the present study show that the current at small pulse periods does approach the d.c. saturation current. Hence, both electrons and positive ions are removed from the cell by the applied potential. If the pulse width is sufficiently long (1 to 5 μs, depending on detector geometry and size), all the free electrons in the cell are collected and an equal number of positive ions are neutralised by surface recombination at the cathode. Under these conditions, the observed current is a measure of the electron concentration in the cell. The current variation with pulse width and also with the applied voltage, exhibit a plateau after an initial increase. This would seem to indicate that all free electrons are being collected. Oscillographic traces of the current pulse tend to support this conclusion as well. They also show that the electrons have a narrow energy distribution. It seems likely that the average energy is about thermal, ie. $\simeq$ 0.03 eV.

With the use of electrostatic probes, the positive ion density has been shown to be very much greater than that of the electrons. In the pulsed mode, space charge effects are said to be minimised since charge separation occurs only during the short time the pulse is applied for. Studies of the pulse amplitude required for saturation current at various cell separations showed a potential trough similar to that observed under the d.c. mode. It seems that a space charge of positive ions is evident even under the pulsed mode.

Measurement of current at various pulse widths allowed the electron deift velocity to be determined. Wentworth et. al.,[18] also found this to be the case. Velocities obtained in various gases have been tabulated. Agreement with literature values is good and hence it can be concluded that the ECD has a potential use as a means of determining electron drift velocities in various polyatomic gases at low values of X/P.

A theoretical model for the ECD is presented. The analysis is based on treating the detector as a system of rate processes. The significance and the necessary inclusion of a parameter for the build up of positive ions in the cell has been pointed out. The model also makes use of known values of electron-ion recombination coefficients and positive ion mobilities to predict the observed response. The theory developed so far shows an improvement on simpler approaches but still does not conform completely to experiment, notably in not predicting the maximum observed when Ne is plotted against the pulse interval.

In the presence of small molecules, electron attachment leads to a decrease in free electron concentration in the cell. Studies investigating the stability of negative ions have shown that electron detachment is not a very likely process to occur at ordinary temperatures. Small concentrations of UF_6 were introduced in helium as carrier gas in an attempt to study this phenomenon. The detector response, however, was difficult to interpret as dissociative attachment seem to have occurred.

To study the effect of water vapour on the ECD response, small amounts of H_2O were introduced in the carrier gas stream with the help of anhydrous and hydrated $Na_2 SO_4$. The current decreases with increasing concentrations of H_2O and the effect is more pronounced at long pulse periods. The electron attachment coefficient has been evaluated, basing the calculation on Lovelock's stirred reactor model.[42] Also, the electron-ion recombination coefficient for the most likely positive ion (H_3O^+) has been calculated from the proposed model. The rate constant's temperature dependency has also been discussed.

Electron capture detection is a continuously growing field. Recently the ECD has undergone structural changes designed to make

the detector response absolute and independent of the ambient variables of temperature and pressure for strongly electron capturing compounds. The coulometric ECD[42,84] consists of a metal tube about 5 cm. in length and a fine wire running down the centre of the tube, forming the anode. The radio-active source is ^{3}H giving a saturation current of between 30 and 50 nA. An extremely high ionisation efficiency (about 93%) is achieved under the following experimental conditions :

i) high electron concentration in the cell, well in excess of sample concentration.

ii) operation of the cell under the pulsed mode with $s > 150\mu s$.

iii) low gas flow rate and a cell with a large volume.

The limit of detection has been found to be 1×10^{-13} g of SF_6 injected.[85] Atmospheric halocarbons, CCl_3F, CCl_4 and $CCl_2 = CCl_2$ have been determined by this technique.[86]

Other developments have been the drift tube detector by Karasek and Kane,[68] the photo-electron capture detector[87] (using an external photon source instead of the traditional radio-active source) and Horning et. al.,[88] have coupled the ECD to a mass-spectometer. These developments emphasise the need to identify the species involved in various reactions taking place in the cell.

This study has attempted to solve some of the pressing problems faced in the normal use of the ECD. Assumptions made in previous theoretical models concerning the physical state inside the detector have been further justified on the basis of experimental evidence obtained. The detector's behaviour is not yet fully understood but because it is an indispensible instrument in today's trace analysis, further attempts have to be made to domesticate the detector completely.

REFERENCES

1. Lovelock J. E. and Lipsky S.R. J.Am.Chem. Soc., 82, (1960), 431.

2. Lovelock J. E. "Physical Processes in Radiation Biology", Academic Press, Inc., N.Y. (1964).

3. Lovelock J. E., Zlatkis A. and Becker R.S., Nature 193, (1962) 540.

4. Lovelock J. E., Fenimore D.C. and Zlatkis A. J. Gas Chromatogr., (1967), 392.

5. Wentworth W. E., Becker R. S. and Tung R., J. Phys. Chem., 71, (1967), 1652.

6. Smith R. V. Amer. Lab., 3, Nov. (1971), 58.

7. Aue W. A. and Kapila S. J. Chromat. Sci. 2, (1973), 255.

8. Halász I. Anal. Chem., 36, (1964), 1428.

9. Scolnick M. J. Chromat. Sci. 7, (1969), 300.

10. Morrison M. E. and Corcoran W. H. Anal. Chem., 39, (1967), 255.

11. Von Engel A. "Ionised Gases" Oxford University Press (1965)

12. Lovelock J. E. Anal. Chem., 35, (1963), 474.

13. Seymour J. "Physical Electronics", Pitman Press, (1972).

14. Sharpe J. "Nuclear Radiation Detectors", p. 130-4, Methuens, London (1955).

15. Friedlander G, Kennedy J. W. and Miller J. M. "Nuclear and Radiochemistry", John Wiley, (1964).

16. Wang C. H. and Willis D. L. (Editors) "Radiotracer Methodology in Biological Science" Prentice Hall, Englecliffs, N. J., (1965) p.68.

17. Warman J. M. and Sauer M. C. J. Chem. Phys., 52, (1970), 6428.

18. Wentworth W. E., Chen. E. and Lovelock J. E. J. Phys. Chem., 70, (1966), 455.

19. J. E. Lovelock and N. L. Gregory, "3rd Int. Symp. Gas Chromatogr.," Academic Press, N.Y. (1962), p. 219.

20. Landowne R. A. Anal. Chem., 42, (1970) 1468.

21. Maggs R. J., Joynes P. L. Davis A. J. and Lovelock J. E. Anal. Chem. 43, (1971), 1966.

22. Hasted J. B. "Physics of Atomic Collisions", Butterworths, London (1972).

23. Farragher A. L., Page F. M. and Wheeler R. C. Disc. Faraday Soc., 37, (1964), 203.

24. Wentworth W. E., Becker R. S., and Tung R. J. Phys. Chem. 71, (1967) 1652.

25. Lyons L. E., Morris G. C., and Warren L. J. J. Phys. Chem., 72, (1968) 3677.

26. Page F. M. and Goode G. C. "Negative Ions and the Magnetron", John Wiley & Sons, London (1968).

27. Stanton H. E. J.Chem. Phys. 32, (1960) 1348.

28. Ferguson E. E., Fehsenfeld F. C., and Schmeltekopf A. L., J.Chem. Phys. 47, (1967) 3085.

29. Massey H. S. W. "Electronic and Ionic Impact Phenomena" Vol.II. Clarendon Press, Oxford (1969).

30. Massey H. S. W. "Electronic and Ionic Impact Phenomena" Vol.III. Clarendon Press, Oxford (1971).

31. Blaunstein R. P. and Christoporou L. G. Radiat. Res. Rev., 3, (1971) 69.

32. Burdett M. Ph.D. Thesis, University of Aston in Birmingham, (1968).

33. Zlatkis A. and Lovelock J. E. Clin. Chem., 11, (1965), 259.

34. Zielinski W. L., Fishbein L. and Thomas R. O. J. Chromatogr., 30, (1967), 77.

35. Thomson J. J. Phil. Mag. 47, (1924), 337.

36. Loeb L. B. "Basic Processes of Gaseous Electronics" p. 205, University of California Press, (1955).

37. Lovelock J. E. Anal. Chem. 33, (1961) 162.

38. Healy R. H. and Reed J. W. "The Behaviour of Slow Electrons in Gases", Amalgated Wireless Limited, Sydney, (1941).

39. Lyons L. E., Morris G. C. and Warren L. J. Aust. J. Chem., 21, (1968), 853.

40. Meisels G. G. J. Am. Chem. Soc., 87, (1965), 950.

41. Sullivan J. J. and Burgett C. A. Cromatographia 8, (1975) 176.

42. Lovelock J. E. J. Chromatogr. 99, (1974), 3.

43. Ramey R. L. "Physical Electronics", Prentice-Hall, London (1961).

44. Page F. M. Unpublished work, University of Aston.

45. Frank-Kamenetskii D. A. "Plasma - The Fourth State of Matter", Macmillan Press, N.Y. (1972).

46. Scolnick M. E. M.Sc. Thesis, University of Aston in Birmingham (1969).

47. Vlcek A. A. Nature, 180, (1957), 753.

48. Lovelock J. E. Seventh International Symposium on Gas Chromatography, Copenhagen, (1968).

49. Wang Y. (Editor) "Handbook of Radioactive Nuclides", Chemical Rubber Co. (1969).

50. Radiochemical Centre Limited, Amersham, England. Private communication.

51. Hucks E. B.Sc. project, University of Aston in Birmingham (1966).

52. Lubkowitz J. A. and Parker W. C. J. Chromatogr., 62, (1971), 53.

53. Shoemake G. R., Fenimore D. C. and Zlatkis A. J. Gas Chromatogr., August, (1965), 285.

54. Kahn L and Goldberg M. C. J. Gas Chromatogr., Ibid, August (1965), 287.

55. Taylor, M.P. J. Chromatog. 9, (1962), 28.

56. Chamberlain A. T. Pye Unicam Limited, Cambridge. Private communication.

57. Devaux P. and Guiochon G. J. Chromatogr. Sci. 7, (1969) 561.

58. Lovelock J. E. Bowerchalke, Salisbury. Private communication.

59. Van de Wiel H. J. and Tommassen P. J. Chromat. 71, (1972) 1 - 7.

60. Brown S. C. "Basic Data of Plasma Physics", Technology Press, N.Y. (1961).

61. Pellizzari E. D. J. Chromatogr., 98, (1974), 323.

62. Oskam M. and Middlestadt V. Phys. Rev., 132, (1963), 1445.

63. Stockdale J., Compton R. N and Schweinler H. C. J.Chem. Phys. 53, (1970), 1502.

64. Mellor J. W. 'Comprehensive Treatise on Inorganic and Theoretical Chemistry' Vol. II. Longmans, London (1961).

65. Glasstone S. 'Textbook of Physical Chemistry', Macmillan and Co. Limited, London (1960) p. 783.

66. Moruzzi J. L. and Phelps A. V. J.Chem. Phys. 45, (1966), 4617.

67. Devaux P. and Guiochon G. Bull. Soc. Chim. Fr., (1966) 1404.

68. Karasek F. W. and Kane D. M. Anal. Chem. 45, (1973), 576.

69. Good D., Durden D. A. and Kebarle P. J.Chem.Phys. 52, (1970) 212.

70. King I. R. J. Chem. Phys. 24, (1957), 817.

71. Calcote H. F. 8th International Symposium on Combustion, Baltimore. Williams and Wilkins Co. (1962), p. 184.

72. Green J. A. and Sugden T. M. 9th International Symposium on Combustion, New York, Academic Press Inc. (1963) p. 607.

73. Lovelock J. E. Private communication to F. M. Page, University of Aston in Birmingham.

74. Nicholson P. W. "Nuclear Electronics", Wiley - Interscience, London (1974).

75. Travers B. L. and Williams H. Report: The use of electrical probes in low pressure flames", Rocket Propulsion Establishment, Wescott, (1963).

76. Huddlestone R. H. and Leonard S. L. "Plasma Diagnostic Techniques", Academic Press, New York (1965).

77. Johnson E. O. and Malter L. Phys. Rev., 80, (1950) 58.

78. Su C. H. and Lam S. H. Phys. Fluids 6, (1963), 1479.

79. Carabetta R. and Porter R. P. "Twelfth International Symposium on Combustion" Combustion Institute, Pittsburgh, Pennsylvania. (1969).

80. Bohm D., Burhop E. H. S. and Massey H. S. W. "The Characteristics of Electrical Discharges in Magnetic Fields", McGraw-Hill (1949).

81. Page F. M. "Physical Chemistry of Fast Reactions", edited by Levitt B. Plenum Press, London (1973), p. 214.

82. Jensen D. E. and Padley P. J. Trans. Faraday Soc., 62, (1966) 2140.

83. Langevin P. Annals. Chim. Phys. 28, (1903), 289, 433.

84. Lovelock J. E., Maggs R. J. and Adlard E. R. Anal. Chem., 43, (1971), 1962.

85. Bros. E., Chamberlain A.T., Page F. M. and Patel S. P. Int. Sym. on Development of Nuclear - Based Techniques for Measurement, Detection and Control of Environmental Pollutants, I. A. E. A., Vienna (1976).

86. Lillian D. and Singh H. B. Anal. Chem. 46, (1974), 1060.

87. Wentworth W., Tishbee A, Batten C. and Zlatkis A. J. Chromatogr., 112, (1975), 229.

88. Horning et. al., Anal. Chem., 45, (1973), 936.